Differential mechanisms for TRIM32-mediated muscle tissue growth and homeostasis

by

Simranjot Bawa

B.S., Panjab University, 2009
M.S., Panjab University, 2011
M.S., Kansas State University, 2017

AN ABSTRACT OF A DISSERTATION

submitted in partial fulfillment of the requirements for the degree

DOCTOR OF PHILOSOPHY

Department of Biochemistry and Molecular Biophysics
College of Arts and Sciences

KANSAS STATE UNIVERSITY
Manhattan, Kansas

2020

Abstract

The decision of a cell or tissue to undergo growth or maintain homeostasis requires a delicate balance between signaling pathways. In situations that require rapid growth, metabolism may be rewired to increase cell size. One such pathway, termed glycolysis, utilizes glucose to generate energy and metabolic intermediates to produce cellular constituents, including proteins, sugars, and lipids, necessary for building biomass. This is similar to the 'Warburg effect,' whereby cancer cells redirect the availability of energetic substrates to generate building blocks required for the uncontrolled growth and proliferation of cells. However, mechanisms that control and promote the utilization of metabolic intermediates for the accumulation of cellular material are not fully understood. The unifying theme of this dissertation is to understand how the E3 ubiquitin ligase TRIM32 mediates the regulation and maintenance of muscle tissue in *Drosophila melanogaster*, where it is well-established that larval muscles alter their metabolic profile towards glycolysis to allow for a 200-fold increase in growth during development.

Previous studies in our lab found that loss of *Drosophila* TRIM32, orthologous to the gene mutated in patients with Limb-girdle muscular dystrophy type 2H (LGMD2H), exhibit smaller muscles with progressive tissue degeneration. It was assumed that this reduced cell size was a secondary consequence of muscle deterioration. However, we made the surprising discovery that TRIM32 physically interacts with two enzymes that function in glycolysis. Furthermore, loss of TRIM32 reduces glycolytic flux, thus limiting the ability of muscle cells to produce cellular building blocks required for growth. Mutations in TRIM32 also cause a reduction in the overall size of the developing larval brain, another tissue with high glycolytic activity. This 'Warburg-like' elevated glycolytic rate that operates in larval muscle and brain tissue is analogous to the altered metabolism in rapidly proliferating cancer or stem cells. Since TRIM32 is upregulated in

multiple types of cancer, we hypothesized that TRIM32 could be a general regulator of highly glycolytic tumor cells. Using a *Drosophila* wing disc tumor model, we found that Pvr-induced epithelial tumors are reduced in size upon removal of TRIM32. These findings suggest that TRIM32 directly controls cell growth, not just in muscle tissue, but in other cell types that exhibit altered metabolism to increase cell size.

The pathological alleles present in LGMD2H patients vary in origin, consisting of point mutations (R394H, D487N), a single amino acid deletion (D588Δ), frameshift deletions (A422fs, T520fs, L535fs, I590fs), and a stop codon (R613*). It is not clear how these conserved mutations alter TRIM32 function. We hypothesized that similar to loss of TRIM32, LGMD2H mutations also reduce muscle size, contributing to disease pathogenesis. However, we found that transgenic expression of some of these myopathic alleles (R394H, D487N and 520fs) exhibit normal muscle growth, but rather induce myofibril abnormalities, altered nuclear morphology, and reduced TRIM32 protein levels. These results mimic phenotypes in patients afflicted with LGMD2H. We further uncovered that levels of the transmembrane proteins βPS integrin and Sarcoglycan δ (Scgδ), both core components of costameres, are elevated in Drosophila muscles expressing TRIM32 disease alleles and in mouse C2C12 muscle cells expressing an inactive version of TRIM32. These studies, taken together, have identified two independent roles of TRIM32 in the growth and maintenance of muscle tissue. TRIM32 stabilizes glycolytic enzymes to stimulate muscle growth and likely controls protein turnover of costamere components essential for myofibril stability and integrity.

Differential mechanisms for TRIM32-mediated muscle tissue growth and homeostasis

by

Simranjot Bawa

B.S., Panjab University, 2009
M.S., Panjab University, 2011
M.S., Kansas State University, 2017

A DISSERTATION

submitted in partial fulfillment of the requirements for the degree

DOCTOR OF PHILOSOPHY

Department of Biochemistry and Molecular Biophysics
College of Arts and Sciences

KANSAS STATE UNIVERSITY
Manhattan, Kansas

2020

Approved by:

Major Professor
Erika R. Geisbrecht

Copyright

Abstract

The decision of a cell or tissue to undergo growth or maintain homeostasis requires a delicate balance between signaling pathways. In situations that require rapid growth, metabolism may be rewired to increase cell size. One such pathway, termed glycolysis, utilizes glucose to generate energy and metabolic intermediates to produce cellular constituents, including proteins, sugars, and lipids, necessary for building biomass. This is similar to the 'Warburg effect,' whereby cancer cells redirect the availability of energetic substrates to generate building blocks required for the uncontrolled growth and proliferation of cells. However, mechanisms that control and promote the utilization of metabolic intermediates for the accumulation of cellular material are not fully understood. The unifying theme of this dissertation is to understand how the E3 ubiquitin ligase TRIM32 mediates the regulation and maintenance of muscle tissue in *Drosophila melanogaster*, where it is well-established that larval muscles alter their metabolic profile towards glycolysis to allow for a 200-fold increase in growth during development.

Previous studies in our lab found that loss of *Drosophila* TRIM32, orthologous to the gene mutated in patients with Limb-girdle muscular dystrophy type 2H (LGMD2H), exhibit smaller muscles with progressive tissue degeneration. It was assumed that this reduced cell size was a secondary consequence of muscle deterioration. However, we made the surprising discovery that TRIM32 physically interacts with two enzymes that function in glycolysis. Furthermore, loss of TRIM32 reduces glycolytic flux, thus limiting the ability of muscle cells to produce cellular building blocks required for growth. Mutations in TRIM32 also cause a reduction in the overall size of the developing larval brain, another tissue with high glycolytic activity. This 'Warburg-like' elevated glycolytic rate that operates in larval muscle and brain tissue is analogous to the

altered metabolism in rapidly proliferating cancer or stem cells. Since TRIM32 is upregulated in multiple types of cancer, we hypothesized that TRIM32 could be a general regulator of highly glycolytic tumor cells. Using a *Drosophila* wing disc tumor model, we found that Pvr-induced epithelial tumors are reduced in size upon removal of TRIM32. These findings suggest that TRIM32 directly controls cell growth, not just in muscle tissue, but in other cell types that exhibit altered metabolism to increase cell size.

The pathological alleles present in LGMD2H patients vary in origin, consisting of point mutations (R394H, D487N), a single amino acid deletion (D588Δ), frameshift deletions (A422fs, T520fs, L535fs, I590fs), and a stop codon (R613*). It is not clear how these conserved mutations alter TRIM32 function. We hypothesized that similar to loss of TRIM32, LGMD2H mutations also reduce muscle size, contributing to disease pathogenesis. However, we found that transgenic expression of some of these myopathic alleles (R394H, D487N and 520fs) exhibit normal muscle growth, but rather induce myofibril abnormalities, altered nuclear morphology, and reduced TRIM32 protein levels. These results mimic phenotypes in patients afflicted with LGMD2H. We further uncovered that levels of the transmembrane proteins βPS integrin and Sarcoglycan δ (Scgδ), both core components of costameres, are elevated in *Drosophila* muscles expressing TRIM32 disease alleles and in mouse C2C12 muscle cells expressing an inactive version of TRIM32. These studies, taken together, have identified two independent roles of TRIM32 in the growth and maintenance of muscle tissue. TRIM32 stabilizes glycolytic enzymes to stimulate muscle growth and likely controls protein turnover of costamere components essential for myofibril stability and integrity.

Table of Contents

List of Figures

List of Tables

Acknowledgments

There are many who helped me along the way on this journey.

I want to take a moment to thank them.

First and foremost, I am deeply indebted to my Ph.D. advisor **Dr. Erika Geisbrecht** for supporting me during these past five years; you have been a tremendous mentor. Erika provided me with every bit of guidance, assistance, and expertise that I needed during my first few semesters; and when I felt ready to venture into research on my own and branch out into new research areas, Erika gave me the freedom to pursue my ideas, at the same time continuing to provide valuable feedback, advice, and encouragement. Thank you for being my mentor, teacher, and friend. I am very fortunate to have Erika as my advisor and the experience has been very valuable to me and I will treasure it for the rest of my life.

Thank you, **Dr. Michal Zolkiewski**, **Dr. Timothy Durrett,** and **Dr. Jocelyn McDonald,** for serving on my advisory committee. I am extremely grateful to **Dr. Zolkiewski** for his constant encouragement and support throughout my graduate study. A special thanks to **Dr. Durrett** and **Dr. McDonald,** for your advice, recommendations, and comments over the years. I am very thankful to **Dr. Brian Geisbrecht** for helping in research and allowing me to use his laboratory facilities as required. A special acknowledgment goes to my lab mates of many years: **David,** for assisting and providing valuable suggestions throughout my research. To **Samantha**, **JP,** and **Joseph** for being supportive and moving the project forward.

Last but not least, I would like to thank my family and friends (**Swati**, **Shruti,** and **Cherry**) for being supportive, persistent, and patient all these years. Thank you for being my constant cheerleaders.

Dedication

In loving memory of my grandparents

(Surjit Kaur Bawa & Narinder Singh Bawa,

Manmohan Kaur & Mohan Singh)

I dedicate this thesis to my family. I am grateful to my parents ***Surinder Singh Bawa*** *and* ***Avinder Kaur,*** *and my brother* ***Ajit Singh Bawa*** *for their moral support and constant encouragement. Thank you for your unconditional love; this work would not have been possible without your faith in my abilities.*

Chapter 1 - Muscle Development in *Drosophila*

1.1 Introduction

Drosophila melanogaster, or the fruit fly, provides a powerful *in vivo* model system to dissect complex genetic questions and to study diverse biological mechanisms that contribute to the formation and maintenance of muscle tissue. Genes and signaling pathways that regulate and control myogenesis are well conserved from *Drosophila* to vertebrates (FERRÚS *et al.* 2000). Hence the fly model has been instrumental in understanding the molecular basis of human muscle disease. Of particular interest, the absence of an adaptive immune response in *Drosophila* prevents the infiltration of additional cell types that promote disease progression. This innate feature, combined with the lack of muscle stem cells throughout most of *Drosophila* muscle development, provide an excellent opportunity to uncover muscle intrinsic properties that contribute to muscle health. Using *Drosophila* as a model to study muscle development has provided valuable insights into muscle specification, myoblast fusion, muscle differentiation, and myofibril assembly.

1.2 Drosophila larval muscle development

The life cycle of *Drosophila* is comprised of four distinct stages: embryo, larva, pupal, and adult. During this life cycle, two sets of muscles are generated to compliment required functions during each stage of development (**Fig 1.1**). Larvae have 54 distinct muscle groups, while adult flies present with 152 muscle types that ensure various locomotor behaviors such as crawling, walking, jumping, and flying (DE JOUSSINEAU et al. 2012). In *Drosophila,* muscle formation occurs in two waves: one during embryonic development, which produces larval body wall or somatic muscles, followed by a second wave of myogenesis post larval muscle histolysis to generate adult flight muscles. The embryonic and subsequent larval somatic musculature consists of a

stereotypical pattern of 30 muscles per abdominal hemisegment (A2-A7), that can be distinguished based on the size, shape, orientation, number of nuclei, and tendon attachment sites.

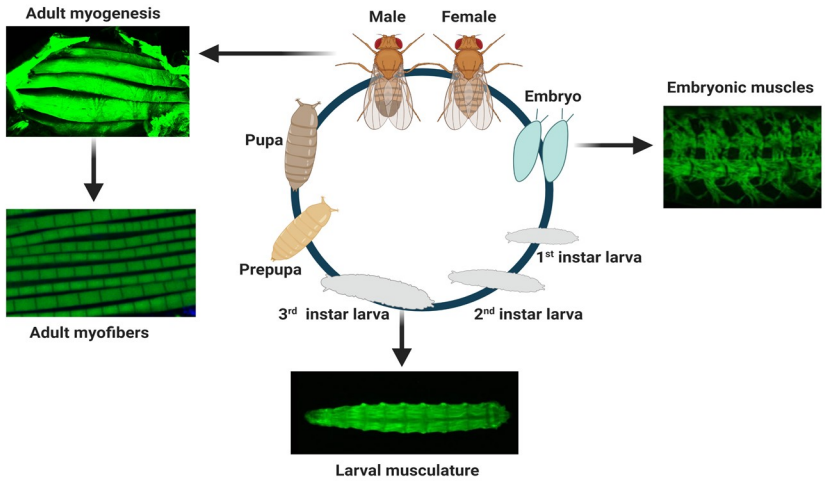

Figure 1.1: The *Drosophila* life cycle.

The *Drosophila* life cycle is marked by four distinct stages. The embryonic muscles develop to generate set of larval muscles that continue to grow during each of the three larval instars. Third instar larvae transition into pupae and undergo metamorphosis to form adults. Wing-disc associated myoblasts and persistent larval muscles serve as templates to form the adult thoracic musculature.

Somatic larval muscle formation begins with the invagination of the mesoderm (BATE *et al.* 1999). The anterior-posterior and dorsal-ventral compartmentalization in the mesoderm is achieved by modulating the expression of transcription factor Twist in each hemisegment (LEPTIN 1991; BUFF *et al.* 1998). Following post somatic mesoderm arrangements, myoblasts are formed. The formation of muscle founder cells (FC) and adult muscle precursors (AMP) is dependent on Notch signaling (BAKER and SCHUBIGER 1996). AMPs remain undifferentiated and until the mid-second larval instar. The FC's and fusion competent myoblasts (FCM) form embryonic body wall muscles. Founder and muscle progenitor cells express specific transcription factors (Kruppel, Slouch, and Ladybird) together known as "muscle identity genes" essential to activate the muscle specific gene expression (BOURGOUIN *et al.* 1992; RUIZ-GÓMEZ *et al.* 1997; JAGLA *et al.* 1998;

KNIRR *et al.* 1999). In addition, the zinc finger transcription factor Lame duck (Lmd) and Myocyte enhancer factor 2 (Mef2) are crucial for differentiation and specification of FCs (TAYLOR 1995; BLACK and OLSON 1998).

Myoblast fusion, or the generation of syncytial muscle cells, requires the expression of a specific class of immunoglobulin (Ig) superfamily transmembrane proteins. Genetic studies have shown that genes that encode for two of these Ig-containing proteins, *Drosophila dumbfounded (duf)* and *sticks and stones (sns),* mediate the interaction between FC and FCMs (DUAN *et al.* 2001; DUTTA *et al.* 2004). Following reiterative myoblast fusion, muscle fibers attach to the tendon cells at both ends and establish myotendinous junctions (MTJ). These attachments are necessary to anchor the larval musculature and maintain the contractile apparatus. For this attachment process, the proper migration of myotubes towards tendon precursor cells is critical. The formation of tendon precursor cells is dependent on the expression of Egr-like transcription factor Stripe (FROMMER *et al.* 1996). Myotubes elongate towards the direction of tendon precursor cells and involve the interaction between Robo and EGF-like ligand Slit (SCHWEITZER *et al.* 2010). The stability of the MTJ is mediated through integrin and extracellular matrix (ECM) proteins. Integrins are transmembrane proteins and form heterodimers of two alpha and beta subunits (CHARVET *et al.* 2012) **(Fig 1.3**). The βPS subunit is encoded by the *myosephroid* (*mys*) gene in *Drosophila (*BROWER et al. 1995). In the absence of βPS subunit (*mys* mutants), muscles detach from the tendon cells and round up, suggesting βPS subunit is indispensable for muscle attachment (NEWMAN and WRIGHT 1981). Likewise, αPS1 equivalent of vertebrate subunits α3, α6, and α7 is encoded by *multiple edematous wings* (*mew*), and αPS2 subunit from *inflated (if)* locus is similar to α5, α8, αV, and αIIb (BROWER *et al.* 1995).

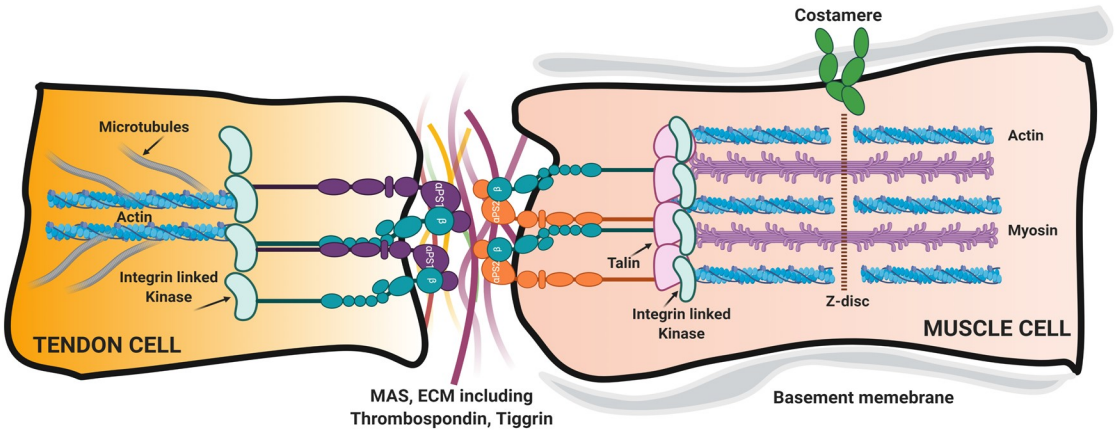

Figure 1.2: Overview of the MTJ interface between muscle and tendon cells.

The tendon cells link actin filaments and microtubules to tendon specific integrins (αPS1) and ECM molecules. Thrombospondin, Tiggrin components of ECM are secreted from the myotendinous junction. In muscle cells integrins (αPS2 and βPS) and actin filaments are stabilized by talin and Integrin linked kinase (ILK). The integrins are also connected to Z-disc along with the other proteins that together form costamere complex at the sarcolemma. (Created using BioRender.com).

The functional musculature assembly depends on the integration of muscles with their corresponding tendon cells. These adhesions are stabilized by integrin receptors and ECM components. Therefore, mutations associated with the attachment proteins results in severe muscle adhesion defects. Muscle specific loss of αPS1 results in muscle detachment; however, tendon-specific loss of *αPS2* does not lead to detached muscles. The tendon specific αPS2βPS specifically interacts with ECM ligand Laminin and αPS1βPS binds to Thrombospondin (Tsp) and Tiggrin (Tig) at the muscle attachment site (FOGERTY *et al.* 1994; SUBRAMANIAN *et al.* 2007). Tiggrin is secreted from the muscle cells, and *tig* mutants exhibit muscle detachment phenotypes, whereas Thrombospondin (Tsp) and laminin secreted from the tendon cells. Tsp is a key ECM component, and in *tsp* mutant embryos, somatic muscles fail to attach to the tendon cells (SUBRAMANIAN *et al.* 2007). *Laminin* mutants are embryonic lethal with prominent defects in somatic muscles, dorsal vessel (heart) and endoderm (HENCHCLIFFE *et al.* 1993; YARNITZKY and VOLK 1995). Talin is

another major cytoplasmic scaffold protein recruited at the integrin adhesion site and crucial for establishing a stable link between sarcomeric cytoskeleton and tendon matrix (NAYAL *et al.* 2004). Embryos deficient in *Talin* also show detached muscles, similar to *mys* mutants (PROUT *et al.* 1997; WALSH and BROWN 1998). These genetic analyses have revealed that Talin is essential for the maintenance of the integrin adhesion complex.

Drosophila larva and their muscle fibers grow enormously from first to third larval instar stage. This increase in muscle fiber length is without the addition of new myoblasts and is regulated by the insulin/Tor pathway followed by nuclear growth by endoreplication (DEMONTIS and PERRIMON 2009; WEITKUNAT and SCHNORRER 2014). The dramatic increase in muscle size during larval development is regulated by Estrogen related (ERR) transcription factor. ERR triggers glycolytic gene expression to promote larval growth by converting carbohydrates to biomass (TENNESSEN *et al.* 2011; TENNESSEN *et al.* 2014). With increased muscle growth, new sarcomeres are added close to the muscle attachment sites; however, the molecular mechanism behind sarcomere assembly still remains unclear. (BAI *et al.* 2007; CONTOMPASIS *et al.* 2010; ORFANOS *et al.* 2015).

1.3 *Drosophila* adult myogenesis

At the end of the larval stage, larvae crawl out of the food source and find a dry place to pupate. During pupal morphogenesis, larval muscles undergo histolysis, and persistent muscles are remodeled to form an adult set of muscles. *Drosophila* thoracic segment is categorized into fibrillar and tubular muscles. The fibrillar muscles are also known as indirect flight muscles (IFMs) form the bulk of the thoracic musculature. IFMs comprise of two sets of muscles: dorsal ventral muscles

(DVM) and dorsal longitudinal muscles (DLM) based on the orientation in the thorax (LAURICHESSE and SOLER 2020) (**Fig 1.3**).

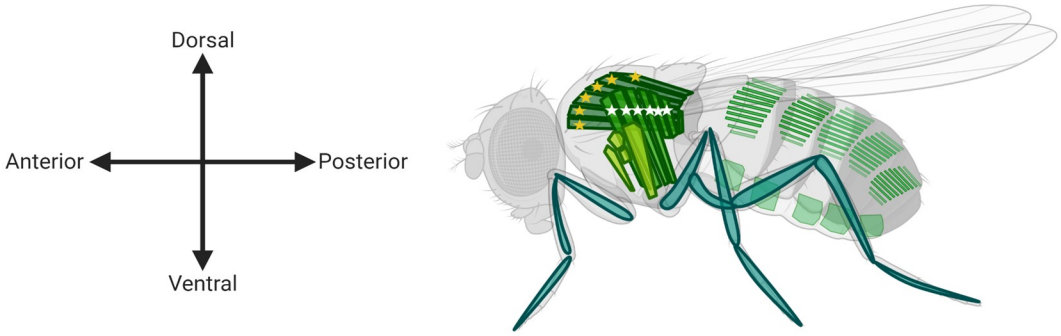

Figure 1.3: IFM organization in *Drosophila* thorax.

The cartoon representation of *Drosophila* DLM (dorsal longitudinal muscle) and DVM (dorsal ventral muscle (DVM). The yellow star shows DLM fibers running along anterior-posterior axis. The DVMs are marked by white star. (Created using BioRender.com)

The ultrastructural assembly of IFMs is similar to vertebrate skeletal muscle (SCHEJTER 2016) (**Fig 1.4**). A set of AMPs are set aside during embryogenesis and remain silent in the wing imaginal disc during the larval stage (LAWRENCE 1982). These AMPs proliferate during late second larval instar, leave the imaginal disc and migrate and fuse with the persistent larval muscles (WEITKUNAT and SCHNORRER 2014). The partially histolyzed larval lateral oblique muscles (LOM) fuse with adult myoblasts to develop DLMs; however, DMVs are formed *de novo* via myoblast fusion (FARRELL *et al.* 1996). During the first 12h of pupal development, LOMs undergo longitudinal cleavage. At 20h after puparium formation (APF), three LOMs split longitudinally into six DLMs. The myoblasts continue to be incorporated into the developing muscles by fusion, and IFMs continue to grow and elongate to attain the appropriate mass and size until the fly ecloses out of the pupal case (FERNANDES *et al.* 1991).

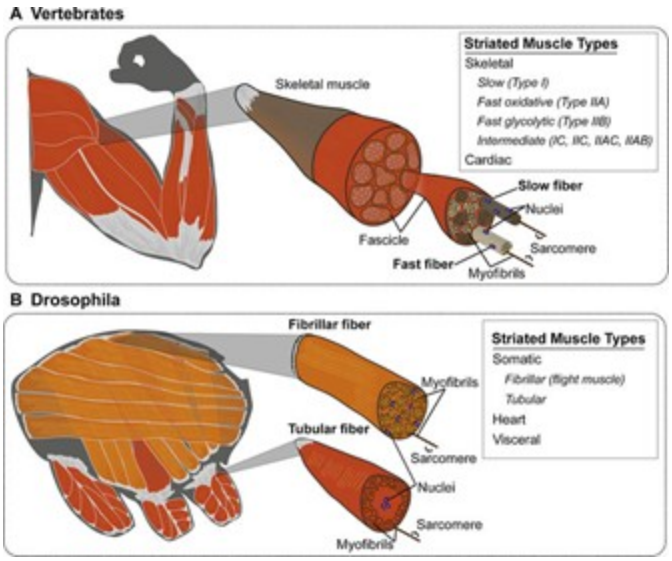

Figure 1.4: Vertebrate and *Drosophila* striated muscle structure.

(A) Diagram of the human arm illustrating basic vertebrate skeletal muscle structure. Muscles, red; tendons, light grey. The slow and fast muscle fibers that form a muscle. Nuclei (blue) are present at the fiber periphery. B) Diagram of the *Drosophila* thorax illustrating fibrillar flight muscle (orange) and tubular jump and leg muscle (red). Nuclei (blue) are dispersed throughout the flight muscle fiber sarcoplasm between myofibril bundles, which are separated by internal membranes. (Reused with permission from Elsevier , NIKONOVA *et al.* 2020).

The differentiated and functional IFMs require the integration of specific genes during development. Myoblasts expressing *twi* and *notch* fuse to form IFMs, and at 36h APF, *twi* expression is lost (**Fig 1.5**). The constitutive expression of *twist* and *notch* post myoblast fusion results in failed muscle differentiation (FERNANDES *et al.* 1996; ANANT *et al.* 1998). Unlike, larval muscles consist of single myofiber, adult muscles are multifiber. The adult multinuclear myofibers attach to the tendon cells and mature into contractile myofibrils. Cell-specific integrin molecules mediate the interaction between the muscle cells and the myotendinous junction. Interestingly, not all cells associated with mature DLMs undergo terminal differentiation. A recent investigation identified the unfused cells found at the surface of the muscle fibers in adult fly corresponds to muscle stem cells, also known as satellite cells (CHATURVEDI *et al.* 2017). These satellite cells are generally quiescent during development; however, upon injury, the cells undergo a proliferation

process in *Notch-delta* dependent manner and generate myoblast competent cells that fuse with the injured muscle fibers as a repair mechanism (MAURO 1961). The *Drosophila* and vertebrate satellite cells show remarkable similarities and provide a concrete platform to study muscle repair, damage in case of injury, aging, and myopathies using the fly as a genetic model (CONBOY and RANDO 2002; CHATURVEDI *et al.* 2017; BOUKHATMI and BRAY 2018).

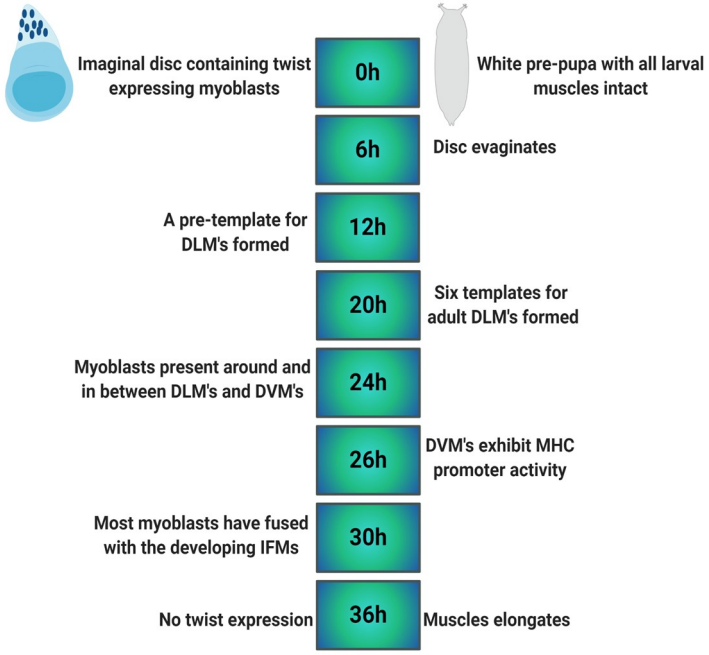

Figure 1.5: IFM development timeline.

Schematic of early events during pupal remodeling leading to IFM development. (Created using BioRender.com)

1.4 Assembly of sarcomeres

Sarcomeres are force producing machines within muscle tissue, whose protein composition and structural features are conserved across the vertebrates and invertebrates. In myofibers, sarcomeres are the smallest contractile unit arranged in a repetitive linear fashion throughout the muscle. The thick (myosin) and thin filaments (F-actin) form the major contractile components along with the Tropomyosin and Troponin proteins. The Z-disc borders the sarcomere and appears

as a series of dark lines that anchors the actin filaments. Surrounding the Z-line, the I-band corresponds to the region where thick filaments do not superimpose with thin filaments. The anisotropic A-band spans the entire length of a single thick filament. The M-line anchors the thick filaments and the associated proteins. The H-zone is the region adjacent to the M-line, where myosin is not superimposed by actin (**Fig 1.6**) and during contraction H-band shortens. The interaction between actin and myosin results in muscle contraction.

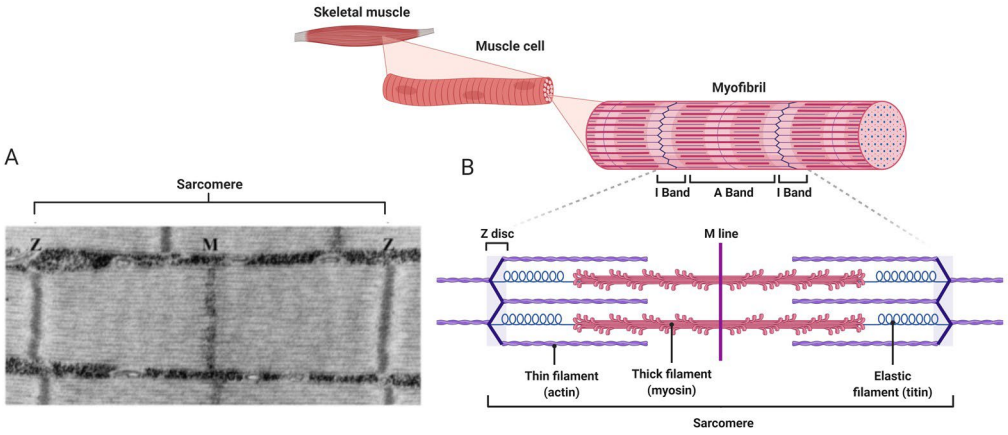

Figure 1.6: Structure of the sarcomere.

(A) EM picture of IFM *Drosophila* showing sarcomere structure with Z-disc and M-line. (B) Muscle cell consists of numerous myofbirils. Each myofibril has organized actin (thin) and myosin (thick) filaments arranged in a linear order called sarcomeres. The Z-disc anchors the actin molecules and M-line provides scaffold for myosin filaments. Z-disc borders the sarcomere, I-band represents region without actin and A-band spans the entire myosin length. (Created using BioRender.com)

Sarcomere assembly is initiated at the embryo stage, where the individual components of the sarcomere are assembled and interdigitated into mature sarcomeres through integrin-mediated adhesion complexes. Initiation starts with the formation of Z-body aggregates at the membrane and localization of α-actinin and Titin proteins within the bodies, which further matures into Z-discs (McKenna *et al.* 1986; Rhee *et al.* 1994). Genetic studies have shown the requirement of integrin molecules for Z-disc assembly. Integrin adhesion sites, also termed as protocostameres,

result in the accumulation of α-actinin, which serves as a nucleation site for forming thin filaments (SPARROW and SCHÖCK 2009). The actin filaments elongate to the M-line. Premyofibrils accumulate muscle myosin II as they mature into myofibrils and form thick filaments (FYRBERG *et al.* 1990; LANGE *et al.* 2005). Microtubules serve as scaffold essential for cytoskeletal elements and myofibrillar arrangement (DHANYASI *et al.* 2020). Post assembly myofibrils are surrounded by a specialized membrane known as sarcolemma, which forms a physical barrier against the external environment and provides a structure to the muscle. The protocostamere matures into costameres, forming protein assemblies that circumferentially align in register with Z-disk (SPARROW and SCHÖCK 2009). Similar to integrins, dystrophin-associated complex is integrated at the costameres and stabilizes the sarcolemma during muscle contraction (BLAKE *et al.* 2002).

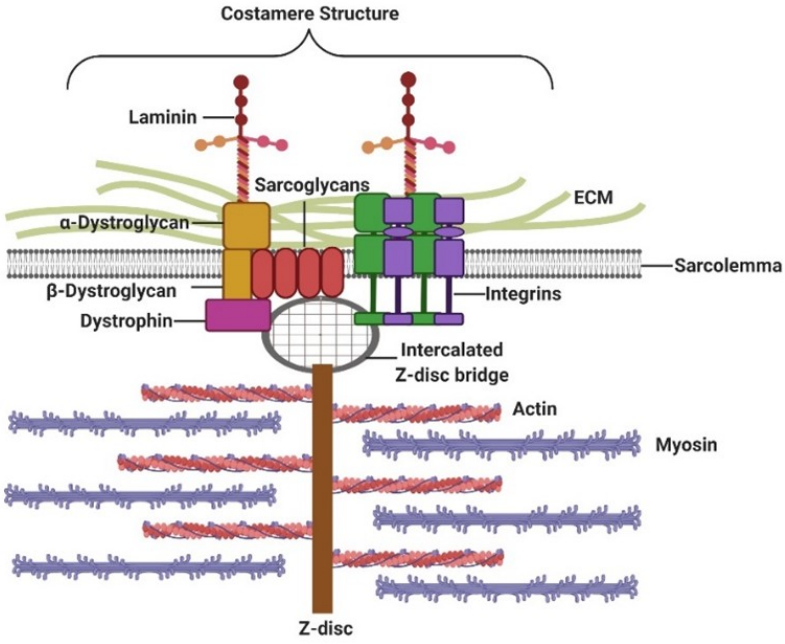

Figure 1.7: Graphical representation of costamere assembly and structure.

Costameres connect the contractile apparatus at the Z-disc and sarcolemma to the ECM. (Created using BioRender.com)

1.5 *Drosophila* as a model of skeletal muscle growth and aging

Sarcopenia is a debilitating characteristic feature of aged humans, resulting in a progressive loss of skeletal muscle mass, strength, and function. Multiple extrinsic and intrinsic factors such as immobility, poor nutrition, and age-related changes are recognized as potential causative factors that drive changes in muscle tissue during aging. While sarcopenia is not fully reversible, muscle atrophy that occurs in response to the activated proteolytic system results in the shrinkage of muscle fibers is generally reversible (THOMAS 2007). Apart from aging, excessive muscle mass loss is often associated with cancer, myopathies, and muscular dystrophies. In case of sarcopenia and cancer cachexia, preferentially glycolytic type IIb muscle fibers are affected (SCHIAFFINO and REGGIANI 2011), whereas in obese individuals, oxidative type I fibers are commonly lost (HICKEY *et al.* 1995). Therefore, it is crucial to understand the signaling pathways that control protein turnover and regulate nutrient availability essential for maintaining muscle mass and healthy aging.

Drosophila provides an ideal system to study muscle function because the fruit fly and mammalian skeletal muscle fibers share similar structural and metabolic properties. *Drosophila* genes that encode for Myosin heavy chain (Mhc), Actin88F (Act88F), Flightin (Fln), and Kettin, essential for muscle structure, assembly, and maintenance, are similar to mammalian Titin and Elastin (KOANA and HOTTA 1978; BERNSTEIN *et al.* 1993; VIGOREAUX *et al.* 1993; AN and MOGAMI 1996; HAIGH *et al.* 2010; SALVI *et al.* 2012). Like vertebrates, *Drosophila* myofibers appear to be either glycolytic or oxidative. The flight muscles (direct and indirect) are known to possess oxidative properties necessary to sustain flight (DEMONTIS *et al.* 2013). Conversely, larval muscles are highly glycolytic, used intermittently for crawling (TENNESSEN *et al.* 2014).

Mechanisms regulating skeletal muscle growth and atrophy are conserved between *Drosophila* and mammals. The rapid larval muscle growth in fruit fly is largely dependent on

insulin/Akt/TOR pathway, similar to vertebrates. In contrast, overexpression of transcription factors like FOXO and Myc inhibit muscle growth (DEMONTIS and PERRIMON 2009). In mammals, denervation, muscle disuse, starvation, and aging can induce atrophy of skeletal muscle. However, in *Drosophila*, developmental atrophy is observed during histolysis. During muscle morphology changes, most of the larval muscles are histolyzed, and the persistent muscles serve as a template for the development of adult skeletal muscles. Taken together, myogenic signals essential for regulating muscle size and atrophy are mostly similar between *Drosophila* and mammals, thereby making fruit flies suitable for examining factors regulating muscle hypertrophy and atrophy.

Consequently, dramatic age-related muscle deterioration is also prominent in the short-life span of *Drosophila*. The muscle ultrastructure analysis of old flies exhibits accumulated misfolded proteins, mitochondrial degeneration followed by disorganized sarcomeres and sarcoplasmic reticulum (HUNT and DEMONTIS 2013). These features mimic the defects observed in mammalian models of sarcopenia (TOMONAGA 1977). Contrary to humans, age-related loss of muscle mass has not been reported in flies before; however, *Drosophila* provides an excellent system to understand the intrinsic events that occur during sarcopenia (PICCIRILLO *et al.* 2014). The availability of a broad array of genetic tools in *Drosophila* allows for muscle specific or genome-wide analysis based on changes in nutrition, environment, or preexisting condition to study muscle function during aging.

References

1. An, H. S., and K. Mogami, 1996 Isolation of 88F actin mutants of Drosophila melanogaster and possible alterations in the mutant actin structures. J Mol Biol 260**:** 492-505.
2. Anant, S., S. Roy and K. VijayRaghavan, 1998 Twist and Notch negatively regulate adult muscle differentiation in Drosophila. Development 125**:** 1361-1369.
3. Bai, J., J. H. Hartwig and N. Perrimon, 2007 SALS, a WH2-domain-containing protein, promotes sarcomeric actin filament elongation from pointed ends during Drosophila muscle growth. Dev Cell 13**:** 828-842.
4. Baker, R., and G. Schubiger, 1996 Autonomous and nonautonomous Notch functions for embryonic muscle and epidermis development in Drosophila. Development 122**:** 617-626.
5. Bate, M., M. Landgraf and M. Ruiz Gómez Bate, 1999 Development of larval body wall muscles. Int Rev Neurobiol 43**:** 25-44.
6. Bernstein, S. I., P. T. O'Donnell and R. M. Cripps, 1993 Molecular genetic analysis of muscle development, structure, and function in Drosophila. Int Rev Cytol 143**:** 63-152.
7. Black, B. L., and E. N. Olson, 1998 Transcriptional control of muscle development by myocyte enhancer factor-2 (MEF2) proteins. Annu Rev Cell Dev Biol 14**:** 167-196.
8. Blake, D. J., A. Weir, S. E. Newey and K. E. Davies, 2002 Function and genetics of dystrophin and dystrophin-related proteins in muscle. Physiol Rev 82**:** 291-329.
9. Boukhatmi, H., and S. Bray, 2018 A population of adult satellite-like cells in. Elife 7.
10. Bourgouin, C., S. E. Lundgren and J. B. Thomas, 1992 Apterous is a Drosophila LIM domain gene required for the development of a subset of embryonic muscles. Neuron 9**:** 549-561.
11. Brower, D. L., T. A. Bunch, L. Mukai, T. E. Adamson, M. Wehrli *et al.*, 1995 Nonequivalent requirements for PS1 and PS2 integrin at cell attachments in Drosophila: genetic analysis of the alpha PS1 integrin subunit. Development 121**:** 1311-1320.
12. Buff, E., A. Carmena, S. Gisselbrecht, F. Jiménez and A. M. Michelson, 1998 Signalling by the Drosophila epidermal growth factor receptor is required for the specification and diversification of embryonic muscle progenitors. Development 125**:** 2075-2086.
13. Charvet, B., F. Ruggiero and D. Le Guellec, 2012 The development of the myotendinous junction. A review. Muscles Ligaments Tendons J 2**:** 53-63.
14. Chaturvedi, D., H. Reichert, R. D. Gunage and K. VijayRaghavan, 2017 Identification and functional characterization of muscle satellite cells in. Elife 6.
15. Conboy, I. M., and T. A. Rando, 2002 The regulation of Notch signaling controls satellite cell activation and cell fate determination in postnatal myogenesis. Dev Cell 3**:** 397-409.
16. de Joussineau, C., L. Bataillé, T. Jagla and K. Jagla, 2012 Diversification of muscle types in Drosophila: upstream and downstream of identity genes. Curr Top Dev Biol 98**:** 277-301.
17. Demontis, F., and N. Perrimon, 2009 Integration of Insulin receptor/Foxo signaling and dMyc activity during muscle growth regulates body size in Drosophila. Development 136**:** 983-993.

18. Demontis, F., R. Piccirillo, A. L. Goldberg and N. Perrimon, 2013 Mechanisms of skeletal muscle aging: insights from Drosophila and mammalian models. Dis Model Mech 6**:** 1339-1352.
19. Duan, H., J. B. Skeath and H. T. Nguyen, 2001 Drosophila Lame duck, a novel member of the Gli superfamily, acts as a key regulator of myogenesis by controlling fusion-competent myoblast development. Development 128**:** 4489-4500.
20. Dutta, D., S. Anant, M. Ruiz-Gomez, M. Bate and K. VijayRaghavan, 2004 Founder myoblasts and fibre number during adult myogenesis in Drosophila. Development 131**:** 3761-3772.
21. Farrell, E. R., J. Fernandes and H. Keshishian, 1996 Muscle organizers in Drosophila: the role of persistent larval fibers in adult flight muscle development. Dev Biol 176**:** 220-229.
22. Fernandes, J., M. Bate and K. Vijayraghavan, 1991 Development of the indirect flight muscles of Drosophila. Development 113**:** 67-77.
23. Fernandes, J. J., S. E. Celniker and K. VijayRaghavan, 1996 Development of the indirect flight muscle attachment sites in Drosophila: role of the PS integrins and the stripe gene. Dev Biol 176**:** 166-184.
24. Ferrús, A., A. Acebes, M. C. Marín and A. Hernández-Hernández, 2000 A genetic approach to detect muscle protein interactions in vivo. Trends Cardiovasc Med 10**:** 293-298.
25. Fogerty, F. J., L. I. Fessler, T. A. Bunch, Y. Yaron, C. G. Parker *et al.*, 1994 Tiggrin, a novel Drosophila extracellular matrix protein that functions as a ligand for Drosophila alpha PS2 beta PS integrins. Development 120**:** 1747-1758.
26. Frommer, G., G. Vorbrüggen, G. Pasca, H. Jäckle and T. Volk, 1996 Epidermal egr-like zinc finger protein of Drosophila participates in myotube guidance. EMBO J 15**:** 1642-1649.
27. Fyrberg, E., M. Kelly, E. Ball, C. Fyrberg and M. C. Reedy, 1990 Molecular genetics of Drosophila alpha-actinin: mutant alleles disrupt Z disc integrity and muscle insertions. J Cell Biol 110**:** 1999-2011.
28. Haigh, S. E., S. S. Salvi, M. Sevdali, M. Stark, D. Goulding *et al.*, 2010 Drosophila indirect flight muscle specific Act88F actin mutants as a model system for studying congenital myopathies of the human ACTA1 skeletal muscle actin gene. Neuromuscul Disord 20**:** 363-374.
29. Henchcliffe, C., L. García-Alonso, J. Tang and C. S. Goodman, 1993 Genetic analysis of laminin A reveals diverse functions during morphogenesis in Drosophila. Development 118**:** 325-337.
30. Hickey, M. S., J. O. Carey, J. L. Azevedo, J. A. Houmard, W. J. Pories *et al.*, 1995 Skeletal muscle fiber composition is related to adiposity and in vitro glucose transport rate in humans. Am J Physiol 268**:** E453-457.
31. Hunt, L. C., and F. Demontis, 2013 Whole-mount immunostaining of Drosophila skeletal muscle. Nat Protoc 8**:** 2496-2501.
32. Jagla, T., F. Bellard, Y. Lutz, G. Dretzen, M. Bellard *et al.*, 1998 ladybird determines cell fate decisions during diversification of Drosophila somatic muscles. Development 125**:** 3699-3708.
33. Knirr, S., N. Azpiazu and M. Frasch, 1999 The role of the NK-homeobox gene slouch (S59) in somatic muscle patterning. Development 126**:** 4525-4535.

34. Koana, T., and Y. Hotta, 1978 Isolation and characterization of flightless mutants in Drosophila melanogaster. J Embryol Exp Morphol 45**:** 123-143.
35. Lange, S., I. Agarkova, J. C. Perriard and E. Ehler, 2005 The sarcomeric M-band during development and in disease. J Muscle Res Cell Motil 26**:** 375-379.
36. Laurichesse, Q., and C. Soler, 2020 Muscle development : a view from adult myogenesis in Drosophila. Semin Cell Dev Biol 104**:** 39-50.
37. Lawrence, P. A., 1982 Cell lineage of the thoracic muscles of Drosophila. Cell 29**:** 493-503.
38. Leptin, M., 1991 twist and snail as positive and negative regulators during Drosophila mesoderm development. Genes Dev 5**:** 1568-1576.
39. MAURO, A., 1961 Satellite cell of skeletal muscle fibers. J Biophys Biochem Cytol 9**:** 493-495.
40. McKenna, N. M., C. S. Johnson and Y. L. Wang, 1986 Formation and alignment of Z lines in living chick myotubes microinjected with rhodamine-labeled alpha-actinin. J Cell Biol 103**:** 2163-2171.
41. Nayal, A., D. J. Webb and A. F. Horwitz, 2004 Talin: an emerging focal point of adhesion dynamics. Curr Opin Cell Biol 16**:** 94-98.
42. Newman, S. M., and T. R. Wright, 1981 A histological and ultrastructural analysis of developmental defects produced by the mutation, lethal(1)myospheroid, in Drosophila melanogaster. Dev Biol 86**:** 393-402.
43. Piccirillo, R., F. Demontis, N. Perrimon and A. L. Goldberg, 2014 Mechanisms of muscle growth and atrophy in mammals and Drosophila. Dev Dyn 243**:** 201-215.
44. Prout, M., Z. Damania, J. Soong, D. Fristrom and J. W. Fristrom, 1997 Autosomal mutations affecting adhesion between wing surfaces in Drosophila melanogaster. Genetics 146**:** 275-285.
45. Rhee, D., J. M. Sanger and J. W. Sanger, 1994 The premyofibril: evidence for its role in myofibrillogenesis. Cell Motil Cytoskeleton 28**:** 1-24.
46. Ruiz-Gómez, M., S. Romani, C. Hartmann, H. Jäckle and M. Bate, 1997 Specific muscle identities are regulated by Krüppel during Drosophila embryogenesis. Development 124**:** 3407-3414.
47. Salvi, S. S., R. P. Kumar, N. B. Ramachandra, J. C. Sparrow and U. Nongthomba, 2012 Mutations in Drosophila myosin rod cause defects in myofibril assembly. J Mol Biol 419**:** 22-40.
48. Schejter, E. D., 2016 Myoblast fusion: Experimental systems and cellular mechanisms. Semin Cell Dev Biol 60**:** 112-120.
49. Schiaffino, S., and C. Reggiani, 2011 Fiber types in mammalian skeletal muscles. Physiol Rev 91**:** 1447-1531.
50. Schweitzer, R., E. Zelzer and T. Volk, 2010 Connecting muscles to tendons: tendons and musculoskeletal development in flies and vertebrates. Development 137**:** 2807-2817.
51. Sparrow, J. C., and F. Schöck, 2009 The initial steps of myofibril assembly: integrins pave the way. Nat Rev Mol Cell Biol 10**:** 293-298.
52. Subramanian, A., B. Wayburn, T. Bunch and T. Volk, 2007 Thrombospondin-mediated adhesion is essential for the formation of the myotendinous junction in Drosophila. Development 134**:** 1269-1278.
53. Taylor, M. V., 1995 Muscle development. Making Drosophila muscle. Curr Biol 5**:** 740-742.

54. Tennessen, J. M., K. D. Baker, G. Lam, J. Evans and C. S. Thummel, 2011 The Drosophila estrogen-related receptor directs a metabolic switch that supports developmental growth. Cell Metab 13**:** 139-148.
55. Tennessen, J. M., N. M. Bertagnolli, J. Evans, M. H. Sieber, J. Cox *et al.*, 2014 Coordinated metabolic transitions during Drosophila embryogenesis and the onset of aerobic glycolysis. G3 (Bethesda) 4**:** 839-850.
56. Thomas, D. R., 2007 Loss of skeletal muscle mass in aging: examining the relationship of starvation, sarcopenia and cachexia. Clin Nutr 26**:** 389-399.
57. Tomonaga, M., 1977 Histochemical and ultrastructural changes in senile human skeletal muscle. J Am Geriatr Soc 25**:** 125-131.
58. Vigoreaux, J. O., J. D. Saide, K. Valgeirsdottir and M. L. Pardue, 1993 Flightin, a novel myofibrillar protein of Drosophila stretch-activated muscles. J Cell Biol 121**:** 587-598.
59. Walsh, E. P., and N. H. Brown, 1998 A screen to identify Drosophila genes required for integrin-mediated adhesion. Genetics 150**:** 791-805.
60. Weitkunat, M., and F. Schnorrer, 2014 A guide to study Drosophila muscle biology. Methods 68**:** 2-14.
61. Yarnitzky, T., and T. Volk, 1995 Laminin is required for heart, somatic muscles, and gut development in the Drosophila embryo. Dev Biol 169**:** 609-618.

Chapter 2 - TRIM32: A multifunctional protein involved in muscle homeostasis, tumorigenesis, and glucose metabolism

2.1 TRIM family proteins

The Tripartite motif family of proteins (TRIM) are characterized by the presence of N-terminal RING (Really Interesting New Gene) finger followed by one or two B-box domains (BB1 and BB2) and Coiled-Coil region with a variable C-terminus (SARDIELLO *et al.* 2008; TOCCHINI and CIOSK 2015). The TRIM family consists of approximately 70 protein members involved in a plethora of biological processes, such as apoptosis, cell cycle regulation, muscle homeostasis, and the innate immune response (WULCZYN *et al.* 2011; LAZZARI and MERONI 2016). Each domain has independent functions, and the variability in the C-terminal region defines the structural and biochemical properties of the protein and imparts target specificity (**Fig 2.1A**.). The TRIM family of proteins are sorted into nine categories classified as CI-CIX based on the composition of the C-terminal domain (TOCCHINI and CIOSK 2015). The CVII subclass of TRIM includes proteins with five or six NHL (NCL-1, HT2A, LIN-41) repeats, which folds into β-propeller structure (**Fig 2.1B**). TRIM-NHL proteins bind RNAs and are key regulators of cell growth, proliferation, and differentiation. There are four TRIM-NHL proteins encoded in *Drosophila melanogaster*, *Mus musculus,* and *Homo sapiens* followed by five in *Caenorhabditis elegans* (WULCZYN et al. 2011) (**Fig 2.1C**).

One of the TRIM-NHL proteins, TRIM32, was initially identified as a protein that binds HIV-1 Tat (a key transactivator of viral transcription) (FRIDELL *et al.* 1995) . TRIM32, an E3 ligase contains an N-terminal signature tripartite motif (TRIM) , implicated in muscle physiology, cell differentiation, growth, and tumorigenesis (ALBOR *et al.* 2006; COHEN *et al.* 2012; IZUMI and KANEKO 2014). Human TRIM32 is expressed in a variety of tissues, including skeletal muscle,

with elevated levels eminent in brain and heart (FROSK *et al.* 2002). Another b-box affiliate (abba) protein encoded by *Drosophil*a (*tn*) gene was identified as an orthologue of human TRIM32 and is highly expressed in larval and adult muscle tissue and demonstrates structural and functional conservation across species (LABEAU-DIMENNA *et al.* 2012; DOMSCH *et al.* 2013; BAWA *et al.* 2020). This review focuses on highlighting the role of TRIM32 as a multifunctional protein in regulating a multitude of developmental and physiological functions and summarizing its current involvement in regulating glycolytic enzymes to promote growth in both normal and cancerous tissues.

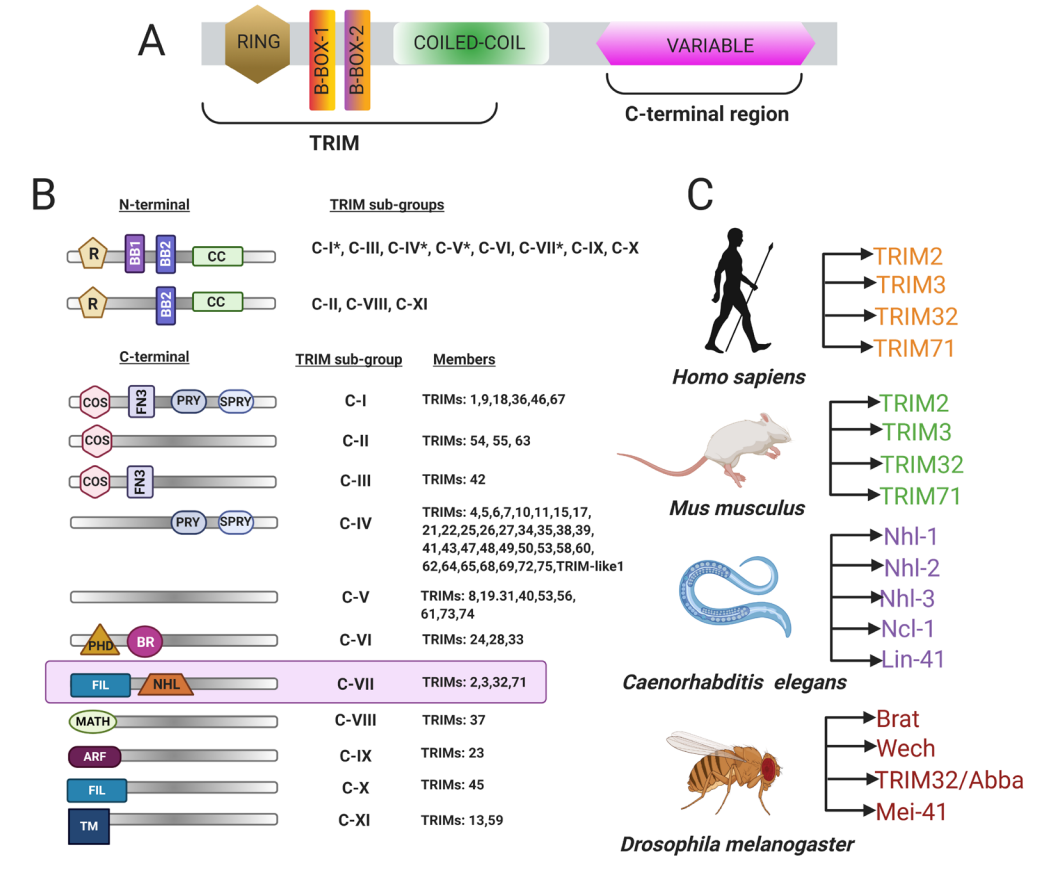

Figure 2.1: Classification of TRIMNHL family proteins.

(A) Schematic of TRIMNHL protein. The N-terminus comprises of RING domain, one or two B-box region and Coiled -coil domain followed by variable C-terminus. (B) Table representing different categories of TRIMNHL proteins. (C) Different NHL proteins encoded in vertebrates and invertebrates.
(Fig 2.1B adapted from WILLIAMS *et al.* 2019, created with BioRender.com)

2.1.1 Structural and functional organization of TRIM32

TRIM32 is a part of the largest subfamily of RING E3 ligases involved in regulating multifaceted post-translational modifications of cellular proteins through ubiquitination. The N-terminal consists of a catalytic RING domain, a B-box domain (Type II), Coiled-Coil region, and its C-terminal comprises of six NHL repeats (**Fig 2.2A**). Mammalian and *Drosophila* TRIM32 overall share modest amino acid sequence identity (~40%) (LABEAU-DIMENNA *et al.* 2012; BAWA *et al.* 2020) (**Fig 2.2B,C**). The RING domain consists of conserved cysteine and histidine residues spaced out in the core of the domain for the binding of zinc ions, which is essential for the RING domain structural maintenance and biological activity (BORDEN and FREEMONT 1996; SAURIN *et al.* 1996). Furthermore, the RING domain coordinates two zinc ions in a cross bridged fashion, which binds with the thiol group (S^-) of the cysteine and a nitrogen atom from the side chain of histidine (BERG 1990). For a protein to exhibit E3 ligase activity, the RING domain must possess proline after cysteine at 7^{th} position, this residue is missing in nematode LIN-41and the protein lacks the catalytic activity. (BUDHIDARMO *et al.* 2012; TOCCHINI *et al.* 2014) (**Fig 2.2D**).

A combination of structural, biophysical, and biochemical approaches has determined the role of individual domains in self-association, substrate ubiquitination, and protein-protein interactions. The crystal structure solved for TRIM32 RING domain is reported as a dimer of four alpha helices where both N and C termini are located to the proximity of the core (KOLIOPOULOS *et al.* 2016) (**Fig 2.3A**). The dimerization promotes the association of E2-Ub conjugates and enhances the ubiquitin transfer. Another zinc-binding region is the B-box domain type II, and similar to the RING domain, B-box II also coordinates two zinc ions in a similar cross-brace manner (**Fig 2.3B**). Typically, the B-box domain type II presents a two-turn α-helix followed by two short β-strands

separated by a type-2 β-turn with two structured loops adjacent to the helix (MASSIAH *et al.* 2006) (**Fig 1.3C**).

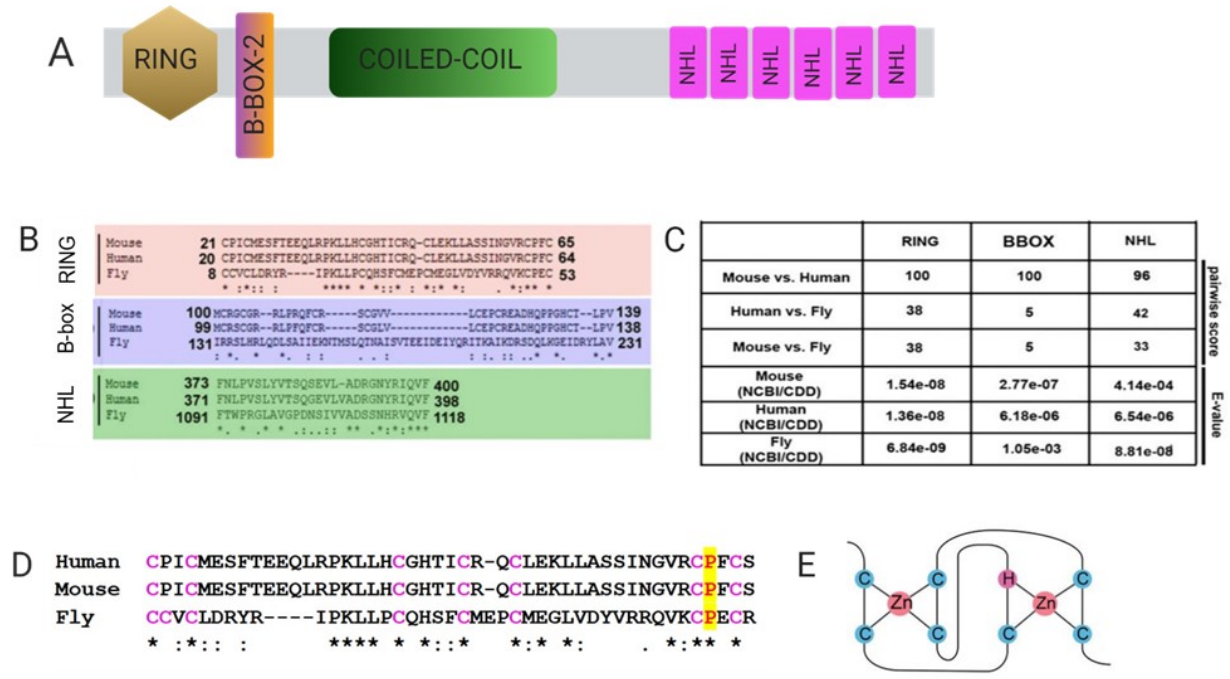

Figure 2.2 TRIM32 protein is conserved across species.

(A) Schematic of TRIM32 protein. (B) Clustlaw sequence alignment comparison of human, mouse and fly TRIM32 domains. RING and NHL domain shows the highest conservation across the species. (C) Table of pairwise alignment scores (calculated by the number of identities in the best-match alignment divided by the length of the compared residues, not including gap spaces and expressed as a percentage) as well as the E-values generated by the CDD that were used to identify the domains within each ortholog. (D) The sequence alignment of RING domain of human, mouse and fly TRIM32 protein shows conserved proline residue after cysteine essential for the catalytic activity of the protein. (E) The cross-bridged arrangement of Cys/His rich sequences in RING domain essential for the Zn binding. (Fig 2.2 B,C and E reused with permission from PNAS and The EMBO Journal, LABEAU-DIMENNA *et al.* 2012, KOLIOPOULOS *et al.* 2016)

Functional studies have shown that both the RING and B-box domain determines the subcellular localization of TRIM32 (LAZZARI *et al.* 2019). The B-box2 domain, together with the antiparallel Coiled-coil region, forms high order complexes crucial for the catalytic activity. The C-termini presents NHL repeats that are short stretches of about 40 amino acids. The X-ray structure of *Drosophila* TRIM32 NHL motif revealed a β propeller where each NHL repeat folds

into four antiparallel β sheets arranged toroidally around a central axis (BAWA *et al.* 2020) (**Fig 2.3D**). These NHL repeats are essential for mediating protein-protein interaction and provides substrate specificity (TOCCHINI and CIOSK 2015).

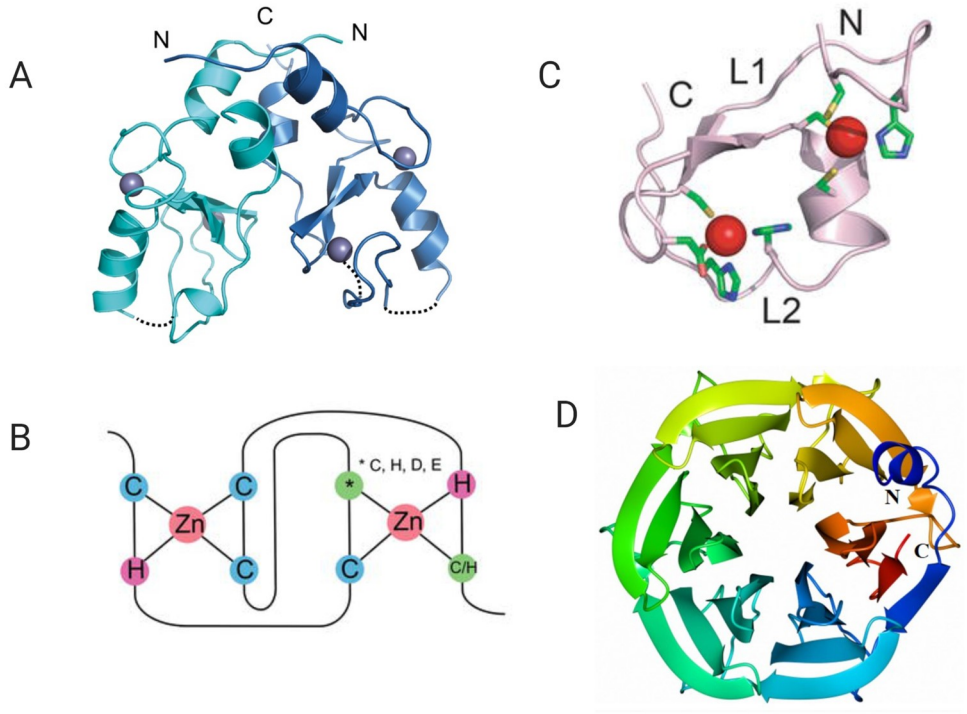

Figure 2.3: TRIM32 domain structural analysis.

(A) Ribbon structure presentation TRIM32 RING domain as dimer with each ring monomer colored in cyan and blue with Zn^{2+} ions represented as grey spheres. (B) The coordination of Zn^{2+} ions in diagonal manner in B-box II domain. (C) Ribbon drawing of MID1 B-box II domain shows canonical ββα fold coordinating Zn^{2} ions in red spheres. (D) *Drosophila* TRIM32 NHL crystal structure is a β-propeller with six NHL repeats. Each repeat consists of four antiparallel β sheets arranged toroidally around a central axis. (Fig 2.3 A-D reused with permission from The EMBO Journal and eLife. KOLIOPOULOS *et al.* 2016 , BAWA *et al.* 2020)

The investigation led by Marios G Koliopoulos and group has reported that TRIM32 RING domain independently mediates the dimerization of protein and promotes tetramer formation. The model suggests that the oligomerization provides four substrate-recognition NHL domains that could enhance substrate binding and/or bring different substrates together (KOLIOPOULOS *et al.* 2016).

However, a biochemical approach is required to validate the model and evaluate the functional consequence of this structural arrangement.

2.1.2 E3 ligase activity and TRIM32 substrates

Ubiquitination is a biochemical process that mediates numerous protein functions such as protein turnover, subcellular protein localization, and protein-protein interaction (PICKART and EDDINS 2004). Ubiquitin is a small 8 kilodalton (kDa) molecule that covalently attaches to the target protein and implements post-translational modifications. The different types of ubiquitin labeling on the substrate leads to versatile fates (SADOWSKI and SARCEVIC 2010) (**Fig 2.4A**). Protein modification can either be a single ubiquitin molecule (monoubiquitylation) or a chain of ubiquitin (polyubiquitylation). The first ubiquitin molecule covalently binds to the substrate through an isopeptide bond between the α-carboxyl group of the ubiquitin backbone and the ε-amino group of lysine in the substrate. Secondary ubiquitin molecules attach to one of the seven lysine (K) residues of the previous ubiquitin molecule. This process requires the unification of three classes of enzymes: E1-ubiquitin activating enzyme, E2-ubiquitin conjugating enzyme, and an E3 ligase. E3 ligases consist of the catalytic domain that transfers the ubiquitin moieties to the substrate protein through a coordinated two-step enzyme reaction (WEISSMAN 2001) (**Fig 2.4B**).

To clear out damaged, toxic and misfolded proteins from the tissues, cells undergo protein degradation mechanism specifically performed by 26S proteasome complex (LECKER *et al.* 2006). TRIM32 was identified as an E3 ligase and can self-ubiquitinate and other substrates to regulate protein turnover and activity (ALBOR *et al.* 2006). K48 polyubiquitin chains on the target proteins are sensed by the proteasome machinery, where the substrates are cleaved proteolytically into peptides and degraded (THROWER *et al.* 2000). Many muscle-specific substrates of TRIM32 like

actin, tropomyosin, desmin, and dysbindin have been identified (LOCKE *et al.* 2009; COHEN *et al.* 2012; LABEAU-DIMENNA *et al.* 2012; DOMSCH *et al.* 2013). TRIM32 is also known to ubiquitinate proteins involved in cell cycle pathway regulation such as Abi2, p53, c-Myc, MYCN, and p53 (KANO *et al.* 2008; IZUMI and KANEKO 2014; LIU *et al.* 2014). Other substrates of TRIM32 include anti-apoptotic component XIAP, an E3 SUMO ligase Piasy; the cytoplasmic enzyme NDRG2; the RAR nuclear receptor; the PB1 viral RNA polymerase.

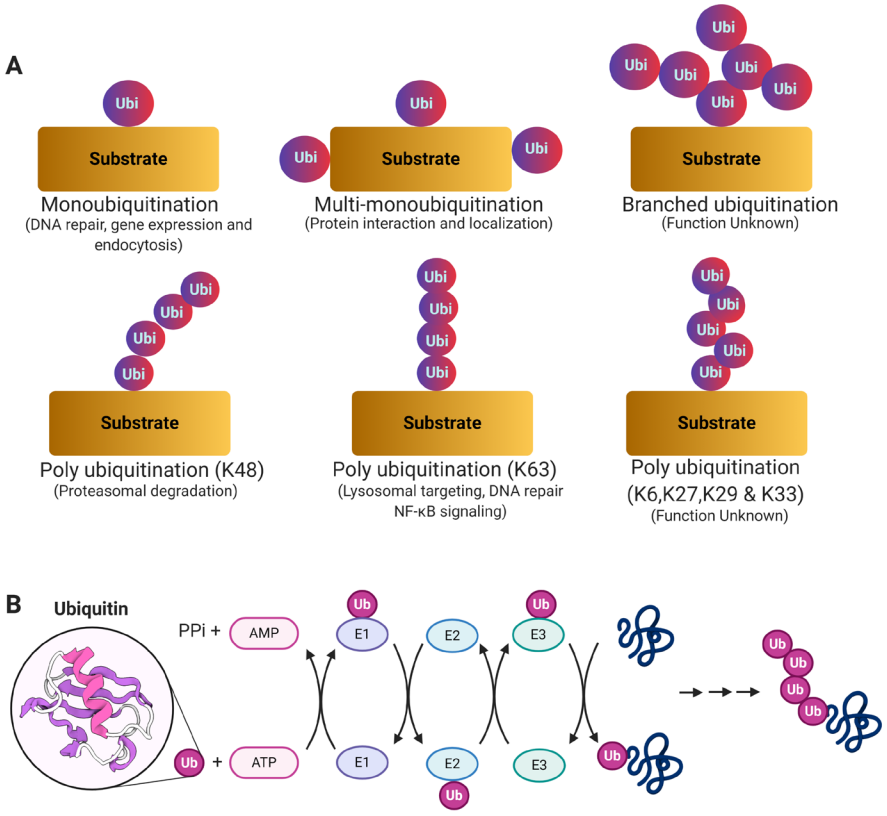

Figure 2.4: Different types of ubiquitination leads to diverse fates.

(A) The ubiquitin molecules can attach to the substrate/proteins as monomers (Monoubiquitination) or multiple lysines on subsrate (Multi-monoubiquitination) followed by sequential addintion of polyubiquitin moieties (Polyubiquitination). The polyubiquitination can lead to linear (K6, K27, K29, K33 K48 and K63) or branched chain arrangements. Mono and multi-monoubiquitination regulates processes like DNA repair, gene expression, protein interaction and localization. Polyubiquitination through K48, K63 linkages results in protein degradation and signaling transduction. (B) Schematic diagram illustrating the conjugation of

ubiquitin molecules to the substrate performed by ubiquitin-activating enzymes (E1s), ubiquitin-conjugating enzymes (E2s), and ubiquitin ligases (E3s). (Schematic created using BioRender.com)

Recent studies have shown TRIM32 induces autophagy in muscle cells by activating ULK1 through K63 polyubiquitin linkages (DI RIENZO *et al.* 2019). TRIM32 mediated K63 linkages on MITA, Glis2, and innate adaptor protein STING results in innate immune signaling and protein trafficking (ZHANG *et al.* 2012; RAMACHANDRAN *et al.* 2014). Based on the broad substrate specificity, it is not surprising that TRIM32 has versatile biological activities.

2.2 Pathomechanism of TRIM32 in Limb-Girdle Muscular Dystrophy type 2H

Limb-Girdle Muscular dystrophies (LGMDs) are a heterogeneous group of rare genetic disorders that are characterized by progressive muscle weakness and degeneration (GUGLIERI *et al.* 2008; MAHMOOD and JIANG 2014). Patients with LGMDs display mild to severe phenotypes with variable onset. The clinical features associated with LGMDs include difficulties in walking, climbing stairs, and scapular winging (MURPHY and STRAUB 2015; TOCCHINI and CIOSK 2015). In some cases, the disease progression is accompanied with respiratory and cardiac dysfunction. LGMDs can be inherited as dominant (LGMD1) and recessive (LGMD2) traits. At present, 31 subtypes of LGMDs have been reported (MURPHY and STRAUB 2015; TOCCHINI and CIOSK 2015). Currently, there are no treatments available to reverse the muscle weakness however, supportive therapies can enhance quality of life.

2.2.1 Mutations associated with LGMD2H

Mutations in the B-box and NHL region of TRIM32 results in two clinically diverse diseases: Bardet–Biedl syndrome, a genetically complex non-myopathic disorder involving retinal dystrophy, obesity, kidney abnormalities, and polydactyly and Limb-Girdle Muscular Dystrophy

type 2H or sarcotubular myopathy (STM) that specifically affects proximal limb musculature and causes progressive muscle degeneration (**Fig 2.5A**) (CHIANG *et al.* 2006; SARDIELLO *et al.* 2008).

LGMD2H, a mild autosomal recessive disorder, was first described in the Hutterite population of Manitoba, with *TRIM32* identified as a causative gene associated with the dystrophy. The homozygous mutation p.D487N in the third NHL repeat was found in 41 Hutterite families resulting in LGMD2H (SHOKEIR and KOBRINSKY 1976; FROSK *et al.* 2002; FROSK *et al.* 2005). Later the same mutation was found in patients with sarcotubular myopathy (STM), indicating these two disorders are subtle variants of each other. Additional mutations in TRIM32 (p.R394H, p.T520TfsX13, and p.D588del) were found in the European population (LOCKE *et al.* 2009). Patients with these mutations exhibit distinct clinical features, such as proximal muscle weakness, respiratory weakness, chronic keratitis, mild ankle contractions, and calf pseudohypertrophy (FROSK *et al.* 2005; SCHOSER *et al.* 2005).

The biochemical studies performed on TRIM32 protein carrying disease-causing mutations inhibit the self-association property of the protein (LOCKE *et al.* 2009). It is evident that the Coiled-coil region is essential for forming higher-order complexes; however, the inability of the mutant protein to dimerize implies that NHL repeats are equally crucial for the oligomerization of TRIM32 (CENTNER *et al.* 2001; SHORT and COX 2006; LI *et al.* 2007; KAR *et al.* 2008; LANGELIER *et al.* 2008; NAPOLITANO and MERONI 2012). Further, the interaction of the E2N enzyme (ubiquitin-conjugating enzyme) with E3 ligase is essential to catalyze the transfer of the ubiquitin molecule to the substrate. In addition, the binding ability of TRIM32 protein with E2N enzyme was also abolished upon introducing D487N, and R394H point mutations, strongly providing evidence that these mutations perturb protein interaction properties (SACCONE *et al.* 2008).

Recently, four new mutations in Spanish and Australian families were identified in RING, NHL, and Coiled-coil domains of TRIM32. A homozygous point mutation p.V59M in the fourth NHL repeat, compound heterozygous for c.650 A > G (p.N217S) and c.1701_1703del (p.F568del) mutations, involving the coiled-coil and fourth NHL repeat, respectively, and mutation in RING domain (SERVIÁN-MORILLA *et al.* 2019) (**Fig 2.5B**). Patients with newly identified mutations show variable clinical features such as ankle contractions, paravertebral muscle atrophy, and foot drop with proximal upper limb weakness. Muscle MRI (magnetic resonance imaging) revealed fatty degeneration in thighs and lower leg, degeneration of gluteus muscles, and gastrocnemius muscles in the lower leg. Muscle biopsies from the patients exhibit reduced TRIM32 protein levels (SERVIÁN-MORILLA *et al.* 2019). Increased autophagic flux was also reported in patients with TRIM32 mutations. This suggests that the mutations have a crippling effect on TRIM32 protein. The variable phenotypes observed in the patients highlights the importance of employing model organisms to dissect the mechanisms behind the pathologies.

A

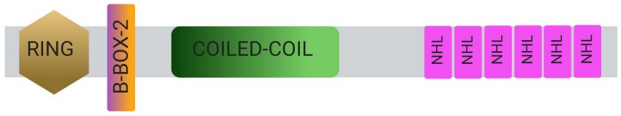

B

Mutations	Domain
c.115_116insT (p.C39LfsX17)	RING
c.650 A > G(p.N217S)	Coiled-coil
p.R394H	First NHL repeat
p.D487N	Third NHL repeat
p.V59M	Fourth NHL repeat
p.T520TfsX13	Fourth NHL repeat
c.1701_1703del (p.F568del)	Fourth NHL repeat
p.D588del	Fifth NHL repeat

Figure 2.5: Mutations in different region of TRIM32 results in LGMD2H.

(A) Schematic of TRIM32 protein. (B) Table illustrating mutations causative of muscular dystrophy. (Created using BioRender.com)

2.2.2 Mouse model for Limb-Girdle Muscular Dystrophy type 2H

TRIM32KO mice was the first in vivo model generated to study pathology associated with Limb-Girdle Muscular Dystrophy Type 2H (KUDRYASHOVA *et al.* 2009). Disruption of *TRIM32* resulted in animals with impaired muscle strength and reduced muscle weight. Ultrastructural and histological analysis in *TRIM32* deficient muscles confirmed the presence of myopathic features like centralized nuclei and fiber splitting (**Fig 2.6A,B**). Transmission electron microscopy (TEM) analysis unveiled extensive muscle damage such as Z-line streaming, autophagic vacuoles, myofibrillar degeneration, and dilated sarcotubular system with prominent sarcoplasmic reticulum and mitochondrial defects (FROSK *et al.* 2005; KUDRYASHOVA *et al.* 2009). The phenotypes recapitulated the clinical profile associated with LGMD2H and sarcotubular myopathy patients. mRNA profiling detected elevated expression of *TRIM32* in the brain as compared to skeletal muscle, indicating a potential role for TRIM32 in the nervous system. In addition, neurofilament proteins were decreased in *TRIM32KO* brains with reduced myelinated axon diameter. Along with muscle defects, the murine model also exhibits a neurogenic phenotype not observed in patients with muscular dystrophy (KUDRYASHOVA *et al.* 2009).

To gain further insight into the myopathy mechanisms, a *TRIM32* knock-in mouse was created that mimics the LGMD2H disease-causing D487N point mutation. Similar to *TRIM32*-null mice, *TRIM32KI* mice also presented mild myopathic and neurogenic phenotype. The D487N point mutation reduced TRIM32 protein level, suggesting that the mutation destabilizes the protein. However, the neurogenic element present in both LGMD2H mice model complicates the analysis (KUDRYASHOVA *et al.* 2011).

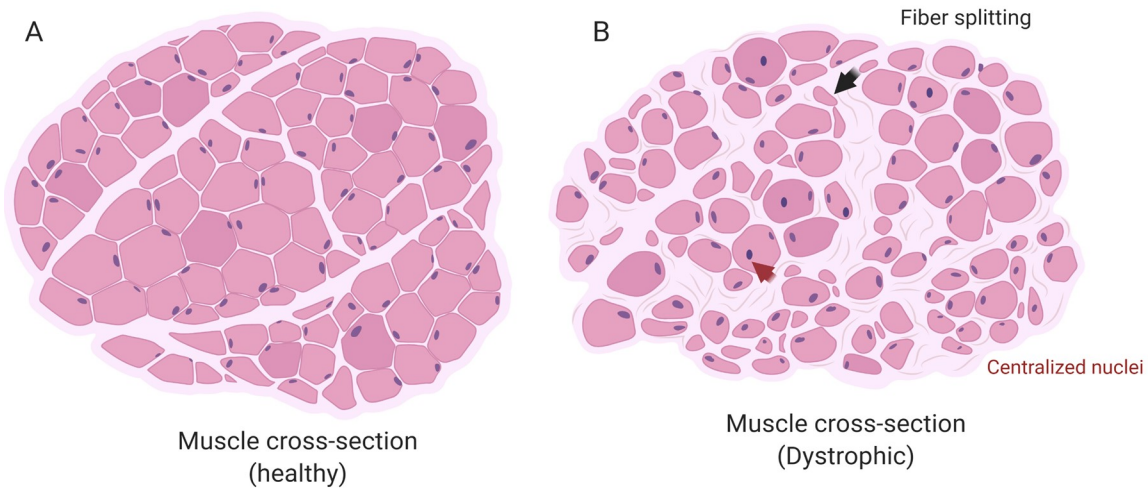

Figure 2.6: Schematic representation of dystrophic muscle-cross section.

(A) Healthy muscle cross-section where the fibers are closely packed, and nuclei are found at the periphery of the fibers. (B) An example of dystrophic muscle biopsy exhibiting common features such as internalized nuclei (magenta arrowhead) and fiber splitting (black arrowhead). (Created using BioRender.com).

2.2.3 *Drosophila* model for Limb-Girdle Muscular Dystrophy type 2H

In an EMS screen, *lethal (2)thin* was identified as a recessive mutation with mutants exhibiting muscle defects and characteristic long "thin" puparium (**Fig 2.7A**). To further study the muscle specific function of *l(2)tn*, the mutation was mapped to the second chromosome using deficiency mapping. Phenotypic analysis revealed *l(2)tn* mutants with degenerative myofibrils. The mapped region contained eleven candidate genes, with *CG15105/another b-box affiliate (abba)* an orthologue of human TRIM32 as one of them. Further genetic analysis confirmed *tn* is allelic to *abba* and is highly expressed in muscle. *In situ* hybridization assay showed robust *tn* mRNA expression in the embryo stage, and protein expression was observed in skeletal muscle precursor cells (**Fig 2.7B-F**). Immunostaining with Z-disk associated muscle LIM protein 84B (Mlp84B) exhibited colocalization between TRIM32 and Mlp84B, providing evidence that TRIM32 is a Z-disk associated protein (**Fig 2.7F**). TRIM32 was also found localized at Z-disc and M-line in the adult myofibers (DOMSCH *et al.* 2013). Loss of *TRIM32* (*tn-/-)* or muscle specific

knockdown of *tn (mef>tnRNAi)* results in progeny undergoing normal embryonic myogenesis, with severe muscle defects observed in L2 and L3 larvae (**Fig 2.7G,H**). The overexpression of full length TRIM32 protein in the mutant background reverted the muscle morphology to *WT,* emphasizing the importance of TRIM32 in myofibrillar stability (LABEAU-DIMENNA *et al.* 2012; DOMSCH *et al.* 2013).

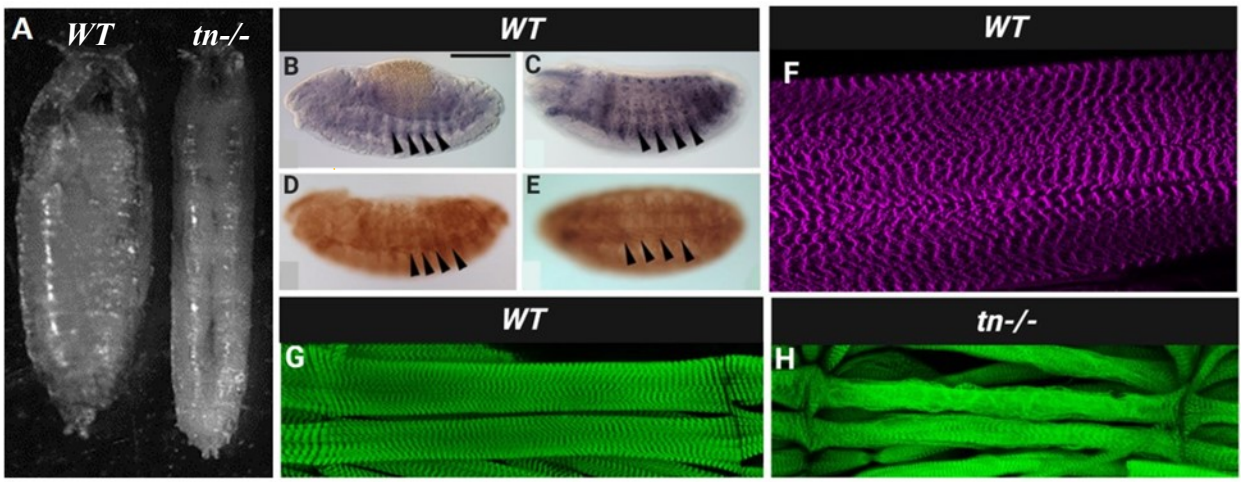

Figure 2.7: Phenotypic analysis of loss of *TRIM32* mutants.

(A) *TRIM32* mutants exhibit long thin elongated pupae as compared to *WT* (control). *tn* mRNA expression in *WT* embryos stage 13 (B) and 16 (C). TRIM32 protein accumulates in developing embryonic muscles stage 13 (D) ans 16 (E). (F) *WT* L3 larval muscles stained with anti-TRIM32 shows TRIM32 localizes to the Z-disc of the sarcomere. (G) Snapshot of *WT* and *tn-/-* (H) larval muscles stainied with phalloidin. *WT* VL3 and VL4 muscles show highly organized sarcomeres. In contrast tn-/- mutant larval muscles appear thinner, looser with prominent striation defects and myofibrillar unbundling. (Fig 2.7 B-E, reused with permission from PNAS, LABEAU-DIMENNA *et al.* 2012)

A genetic assay employed to study the influence of TRIM32 domain(s) on *Drosophila* muscle function and architecture uncovered important information. The deletion of either N-terminal domains (RING, B-box2, and Coiled-coil) or NHL repeats caused severe F-actin striation defects and progressive muscle degeneration, emphasizing the requirement of each domain for normal TRIM32 function in muscle. Most of the myopathies involve defects in sarcomere-related proteins, which are critical components of muscle architecture (FIELITZ *et al.* 2007). We and others reported

abnormal accumulation of sarcomeric proteins tropomyosin, myosin heavy chain in the *tn* mutant degenerative myofibers; however, Mlp84B, α-actinin, and actin remained relatively well localized (LABEAU-DIMENNA *et al.* 2012b). The data signifies TRIM32 is crucial for the assembly of sarcomeric proteins.

Loss of *mlp84b* and *α-actinin* in *tn* mutant background produced larvae with muscle defects indicating a genetic interaction between TRIM32 and Z-disc proteins (DOMSCH *et al.* 2013). Costameres are Z-line associated structures associated with sarcolemma essential for maintaining muscle integrity (HENDERSON *et al.* 2017). *Drosophila* also possesses orthologs of the costameric proteins β-Integrin, Talin, Spectrin, and Vinculin, suggesting conserved structure and function (LABEAU-DIMENNA *et al.* 2012). Microscopic analysis of these costameric proteins in *WT* muscle showed localization at the sarcolemma and Z-disc confirming the existence of costameres in flies. Loss of *tn* disturbed the spatial organization of β-integrin, Talin, Spectrin, and Vinculin in mutant larvae; these proteins were no longer retained at the Z-disc and sarcolemma (LABEAU-DIMENNA *et al.* 2012a). Additionally, δ-Sarcoglycan another component of the costamere complex was abnormally accumulated in the *tn* mutants. These data strongly imply that TRIM32 is inevitable for costamere stability. However, additional experiments are required to understand TRIM32 mediated catalytic activity on regulation of these costameric proteins. In **chapter 3** and **chapter 4,** we further show that abnormal protein levels of Tropomyosin, δ-Sarcoglycan and β-integrin in *TRIM32* loss of function mutants and LGMD2H pathological alleles likely contributes to muscle defects.

A comprehensive genetic analysis in the vertebrate model is complicated by the ubiquitous expression of TRIM32 and non-muscle defects in *TRIM32* mutant mice that are independent of the muscle pathology associated with LGMD2H (KUDRYASHOVA *et al.* 2009;

KUDRYASHOVA *et al.* 2011). Our *Drosophila* model allows for the autonomous evaluation of TRIM32 muscle function. First, abnormal locomotor ability and muscle degeneration are only present upon RNAi knockdown of TRIM32 in muscle, but not in neurons (**discussed in Chapter 4**) (LABEAU-DIMENNA *et al.* 2012). The absence of an adaptive immune system in *Drosophila* prevents the infiltration of additional cell types that generally promote inflammation and drive disease progression in muscular dystrophies. The lack of muscle stem cells in *Drosophila* larvae presents an opportunity to observe TRIM32-driven disease progression without the complications of muscle repair (PICCIRILLO *et al.* 2014). The abnormal muscle histology and mobility defects present in *tn-/-* mutants recapitulate phenotypes present in LGMD2H patients and provide a platform to study pathogenesis associated with LGMD2H.

2.2.4 In vitro model system for examining TRIM32 function

Multiple in vitro systems have been extensively employed to study distinct biochemical characteristics of TRIM32 and understand biological changes associated with the pathological mutations. A yeast two-hybrid experiment (Y2H) revealed important information on how mutations alter TRIM32 function. The p.D487N, p.R394H, and p.1559delC mutations in yeast abolished the ability of TRIM32 to self-interact and homodimerize (SACCONE *et al.* 2008). However, BBS mutation p.P130S and LGMD2H mutation p.D588del retained the dimeric property of the protein. The binding of E2 enzyme is critical for the E3 ligase activity of the protein. E2N enzyme encoded by UBE2N gene specifically binds TRIM32 however, p.D487N, p.R394H and p.1559delC mutations perturbed the ability of protein to associate with E2N enzyme (SACCONE *et al.* 2008). The data suggests that these mutations in the NHL domain impair interaction properties of the protein. In addition, dysbindin a member of the dystrophin-associated complex was found to bind TRIM32 in yeast and mammalian HEK293 cells. TRIM32 polyubiquitinate

dysbindin in HEK293 cells and target it for degradation. However, LGMD mutants D487N, R394H failed to interact and ubiquitinate dysbindin. We can anticipate from the data that these mutations abrogate the ligase activity of TRIM32 (LOCKE *et al.* 2009). Conversely, Matthew Locke and colleagues reported LGMD D487N and R394H mutants were able to self-associate in yeast. In mammalian cells, the D487N mutant is able to bind E2 ubiquitin-conjugating enzyme UbcM3. However, D487N mutant transfected in HEK293T cells failed to monoubiquitinate TRIM32 (LOCKE *et al.* 2009). The results differ from the analysis performed in yeast and highlight the importance of implementing multiple systems to validate the findings.

In response to stress and during physiological conditions, tuning and maintaining autophagy flux is fundamental for muscle homeostasis. Ubiquitin modification controls multiple steps in autophagy signaling and many autophagy regulators are found to be substrates of E ubiquitin ligases. TRIM32 function in regulating autophagy was recently identified (DI RIENZO *et al.* 2019; SERVIÁN-MORILLA *et al.* 2019). Elevated levels of TRIM32 were prominent in starved HEK293 cells treated with bafilomycin A1 (BafA1), a lysosome inhibitor. Moreover, in vitro GST pulldown assay also confirmed the binding of TRIM32 with ATG8 family proteins. In addition, a duoLink proximity ligation assay showed TRIM32 cells colocalize with autophagic protein markers p62 and LC3B. Similar to WT_TRIM32, the D487N, and P130S disease mutants weakly bind p62. Further, in C2C12 cells, WT_TRIM32 and P130S localized within acidic compartments to undergo autophagic degradation in muscle cells. However, LGMD2H disease mutants (D487N, R394H, and V591M) failed to undergo autophagy. In vitro ubiquitination confirmed TRIM32 ability to mono-ubiquitinate p62. This modification was lost upon introducing LGMDH disease-causing mutations in the NHL domain. The study manifests that TRIM32 can undergo selective autophagy and regulate p62 activity (SERVIÁN-MORILLA *et al.* 2019). The dystrophic mutants defective in

autophagy provides a new mechanism associated with the pathology of LGMD2H yet to be explored in more detail.

2.2.5 Function of TRIM32 in muscle atrophy and regeneration

Skeletal muscle fibers undergo physiological changes as consequence of metabolism, age, and pathological conditions. A prominent feature of dystrophic muscle is progressive muscle wasting (atrophy), often result of altered myogenic signals (DASTUR and RAZZAK 1973). Regulation of muscle mass is essentially an equilibrium between skeletal protein synthesis and degradation within myofibers. The two major pathways that strike a balance in protein turnover is the ubiquitin-proteasome system (UPS) and the autophagy-lysosome system (ALS).

Insulin/Akt-PI3K is one of the important signaling pathways responsible for muscle growth. The activation of phosphatidylinositol-3-kinase (PI3K) generates the membrane phospholipid phosphoinositide-3,4,5-triphosphate (PIP3). PIP3 acts as a docking site for phosphoinositide-dependent kinase 1 (PDK1) and Akt. PDK1 phosphorylates Akt and leads to its activation. Further activated Akt represses the transcription factor FoXO and stimulates protein synthesis essential for muscle growth. Conversely, FoXO during fasting induces the expression of atrophy-related genes and ubiquitin ligases (MURF-1, Atrogin), which controls the rapid degradation of myofibrillar components during atrophy (SANDRI *et al.* 2004).

The Stitt and Cohen groups recognized the role of TRIM32 in regulating insulin–PI3K–Akt–FoxO signaling in both normal and atrophying muscles (STITT *et al.* 2004; COHEN *et al.* 2014). Plakoglobin, a component of the desmosome adhesion complex, was identified as one of the substrates of TRIM32 in muscle extracts. In epithelia, plakoglobin regulates cell motility, growth, and differentiation (JAMORA and FUCHS 2002; CALAUTTI *et al.* 2005). During fasting, TRIM32

reduced the association of plakoglobin with p85–PI3K that negatively influenced Akt-PI3K signaling. However, plakoglobin levels were not affected in fasting/atrophying muscles, proposing a mechanism of regulation different then proteasomal degradation. Downregulation of plakoglobin levels in normal muscles led to decreased phosphorylation of PI3K, Akt, and FoxO3, and atrophy of the muscles. PI3K-Akt signaling involving TRIM32 and plakoglobin provides a new mechanism of muscle growth (**Fig 2.8**) (COHEN *et al.* 2014). Furthermore, *TRIM32* deficient mice also exhibit both reduced muscle and body size. However, upon fasting, *TRIM32KO* muscles undergo atrophy similar to *WT* mice (KUDRYASHOVA *et al.* 2012). Moreover, the selective downregulation of TRIM32 in adult muscles and/or myotubes undergo atrophy, indicating additional E3 ligases account for rapid fiber atrophy and trigger muscle wasting (COHEN *et al.* 2014).

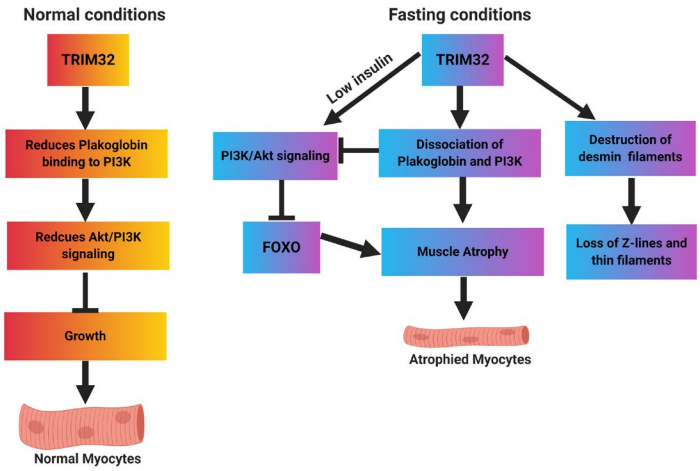

Figure 2.8: Mechanism for regulation by TRIM32 in muscle atrophy.

(A) In normal cellular conditions TRIM32 reduces Plakloglobin binding to PI3K–p85 complex and regulates normal growth. (B) Under fasting condition, TRIM32 results in disassembly and ubiquitination of desmin filaments followed by degradation of thin filaments and perturbs PI3K/Akt signaling and plakoglobin function and contributes to atrophy. (Adapted from STITT *et al.* 2004). (Created using BioRender.com.)

Acute muscle atrophy induces rapid degradation of sarcomeric proteins by several E3 ubiquitin ligases such as muscle ring finger 1 (MURF1) and muscle atrophy F box (MAFbx, also called atrogin1) (LECKER *et al.* 2004). Previous investigations uncovered a function for TRIM32 in muscle atrophy. Goldberg and colleagues reported shRNA mediated knockdown of TRIM32 in HEK293 cells during fasting attenuated muscle wasting and loss of actin, tropomyosin, and troponin; however, TRIM32 expression was induced at the normal level unlike other atrophy related E3s, Atrogin1/MAFBx, and MuRF1 (LECKER *et al.* 2004; COHEN *et al.* 2012). In an effort to identify new substrates of TRIM32, muscle extracts incubated with TRIM32 precipitated thin filament components (actin, tropomyosin) and Z-disc associated proteins (Desmin and α-actin). In vitro ubiquitination assays performed on muscle extracts provide evidence that TRIM32 ubiquitinates actin and tropomyosin (COHEN *et al.* 2012). Further analysis demonstrates, TRIM32 also regulates the Z-disc associated protein desmin, an intermediate filament protein crucial for the integrity of thin filaments. It was observed that during fasting, desmin filaments undergo rapid phosphorylation, which promotes ubiquitylation by TRIM32 and disassembly of thin filaments. On the contrary, in starved *TRIM32* deficient muscles, degradation of desmin filaments and disassembly of thin filament components were observed. Presumably, additional E3 ligases can catalyze the breakdown of desmin filaments and can initiate the breakdown of thin filament assembly. The data implies an alternative mechanism that regulates desmin turnover in fasting conditions.

The involvement of TRIM32 in atrophy is quite complicated. TRIM32 degrades Z-disc associated elements during fasting and causes the breakdown of myofibrillar filaments and negatively regulates growth (COHEN *et al.* 2012). However, another set of data demonstrates that TRIM32 induces autophagy as a protective mechanism to attenuate muscle damage during

atrophy. AMBRA1 Activating molecule in BECN1-regulated autophagy protein 1 (AMBRA1), a positive regulator of autophagy, was found in a proteomic screen with TRIM32. The coimmunoprecipitation assay confirmed the association between TRIM32 and AMBRA1. Further domain analysis showed that AMBRA1 binds to the catalytic RING domain of TRIM32 (**Fig 2.9**). Downregulation of AMBRA1 levels in C2C12 myoblasts reduced the basal autophagy flux (Di Rienzo *et al.* 2019). However, TRIM32 seems dispensable for sustaining basal autophagy. Since autophagy is upregulated in atrophic muscles and TRIM32 function in atrophy has been defined before, G. M. Fimia and group further explored TRIM32 dynamics with autophagy under the atrophic stimulus. *TRIM32* deficient myotubes treated with dexamethasone, a synthetic analog of glucocorticoids, an atrophy inducer caused impaired autophagy. Immunoblot analysis revealed reduced protein levels of LC3-II, NBR1 indicative of defects in autophagic flux. In comparison to in vitro model, *TRIM32KO* mice were used to assess the efficiency of autophagy under atrophic conditions *in vivo*. *TRIM32KO* mice treated with dexamethasone, and quadricep muscles blotted for LC3, NBR1, and p62 reported decreased protein levels as compared to *TRIM32WT*. Both in vitro and in vivo data confirmed impaired autophagy in *TRIM32KO* atrophic muscle cells.

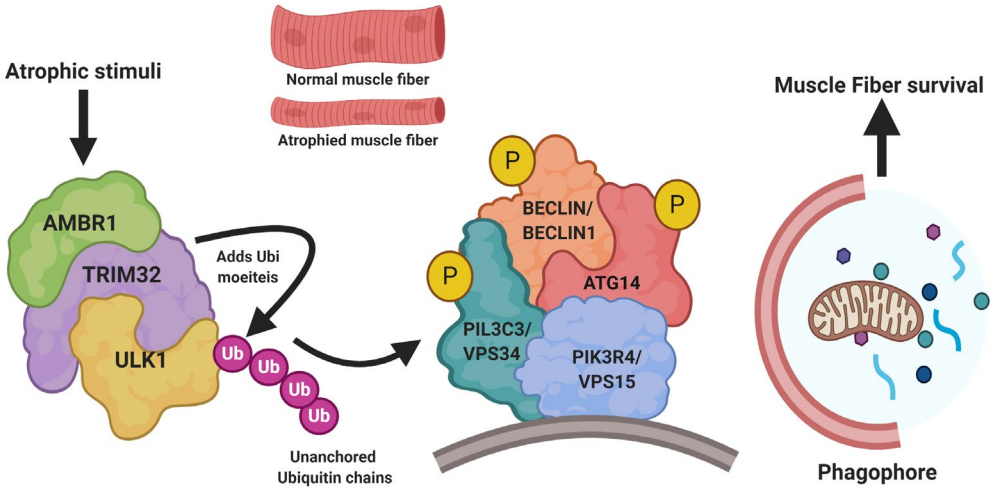

Figure 2.9: TRIM32 regulates autophagy in atrophic condition in muscle cells.

TRIM32 binds AMBR1 and ULK1 under atrophic stimuli and activates ULK1 through anchored polyubiquitination. ULKI initiates autophagosome formation by phosphorylating components of autophagy pathway. The autophagy induces a protective mechanism for muscle fibers in atrophic condition by promoting mitochondrial degradation and preventing accumulation of ROS. (Adapted from DI RIENZO *et al.* 2019). Created using BioRender.com.

Further coimmunoprecipitation experiments performed on 293T cells showed TRIM32 binds ULK1, an autophagy regulator in complex with AMBR1 through the RING domain. In vitro ubiquitination assays prove that TRIM32 modifies ULKI and adds K63 linked polyubiquitin chains essential for the kinase activity of ULK1. Lastly, the autophagic response in TRIM32 pathogenic mutants were evaluated. The D487N and R394H mutants expressing cells treated with dexamethasone depicted the inability of ULK1 to phosphorylate BECLIN 1 and ATG14 confirming the impaired autophagic activity. Similarly, cells obtained from LGMD2H patients also showed defects in autophagy upon atrophic stimulation (DI RIENZO *et al.* 2019). This likely reflects that deregulation in autophagy potentially correlates with disease progression.

Impaired muscle growth in *TRIM32* deficient mice associated with satellite cell senescence and premature sarcopenia prompted to investigate the function of TRIM32 in muscle regeneration and regrowth. Model of hindlimb suspension-induced skeletal muscle atrophy in rodents was employed to study changes in TRIM32 expression during muscle remodeling. TRIM32 expression increase about 2-fold during muscle unloading and 4.5-fold during muscle reloading. Western blot analysis reported TRIM32 induction during C2C12 differentiation (KUDRYASHOVA *et al.* 2005). Clearly, increased protein expression suggests that TRIM32 plays an essential role during muscle growth and remodeling.

Adult skeletal muscle has a remarkable regenerative capacity in response to injury, damage, aging and or inflammation. Muscle stem cells also known as satellite cells are indispensable for muscle regeneration. Skeletal satellite cells are quiescent myogenic cells associated with the

sarcolemma of the myofibers and get activated in response to trauma and facilitate muscle repair. Since TRIM32 function in atrophy and muscle growth has been defined before, Nicklas and group evaluated the regenerative activity of TRIM32 in cardiotoxin-induced myofibers. Cardiotoxin caused extensive myofiber damage, followed by a period of recovery with satellite cell proliferation and differentiation. *In situ* RNA hybridization showed upregulated TRIM32 mRNA in regenerating myofibers (NICKLAS *et al.* 2012). Additionally, *TRIM32* null mice presented delayed myogenic differentiation and a significant increase in apoptosis. Also, *TRIM32* deficient C2C12 myoblasts inhibited the differentiation of the muscle cells, and the myoblasts showed elevated concentration of cell senescence markers p53, Senescence-associated beta-galactosidase (SA-β-gal), and Human heterochromatin protein 1γ (HP1γ). Moreover, increased protein levels of E3 SUMO ligase PIAS4 substrate of TRIM32 and regulator of cell senescence was also reported. This increase in the PIAS4 protein levels in *TRIM32-/-* myoblasts and myotubes was primarily due to defective sumoylation (KAHYO *et al.* 2001; ALBOR *et al.* 2006). 2D fluorescence difference gel electrophoresis (2D-DIGE) utilized to determine binding partners of TRIM32 in skeletal muscle identified NDGR2 (N-myc downstream-regulated gene) as one of the substrates. *TRIM32KO* myoblasts exhibited accumulation of NDGR2 and in vitro studies demonstrated TRIM32 could polyubiquitinate NDGR2. Of note, overexpressing NDGR2 in myoblasts slowed the rate of cell proliferation, suggesting TRIM32 regulates NDGR2 protein turnover through proteasomal degradation. Taken together, the findings demonstrate that TRIM32 is induced in activated satellite cells, implemented in myoblast senescence, and is crucial for myoblast differentiation and regeneration.

2.3 TRIM32, glucose metabolism and link to cancer

Glycolysis is a universal central metabolic pathway involved in energy production required for cellular activities. Although glycolysis is less efficient than oxidative phosphorylation in yielding net ATP, metabolic intermediates of the glycolytic pathway are essential for synthesizing macromolecules necessary for cell survival, signal transduction, and biomolecular interactions. The reprogramming of the glycolysis controls carbohydrate metabolism in both skeletal muscle and various cancer types. Likewise, TRIM32 is ubiquitously expressed and recognizes proteins that are implicated in muscle function, tumor suppression, and or progression. This section summarizes the role of glycolysis and TRIM32 in muscle development and tumorigenesis and establishes a functional relationship between TRIM32 and metabolism.

2.3.1 Glucose metabolism in muscle physiology

The primary function of the skeletal muscle is to ensure movement, oxygen consumption, nutrient storage, and regulating whole-body metabolism. Therefore, maintaining skeletal muscle strength and structure is vital for the quality of life and to ensure proper musculoskeletal function. Skeletal muscle health is regulated by multiple signaling pathways essential for protein synthesis and turnover. The muscle mass adapts to the pathophysiological changes in the body, and defects in anabolic signaling are prominent in aging, disuse, malignancy, and injury, which promotes loss of muscle mass and strength (GREEN *et al.* 1992). Various genetic models (mice, flies, and worms) have been employed to study mechanisms associated with skeletal muscle growth and regeneration.

Skeletal muscle comprises ~ 40% of the total body weight and mainly derives energy from glucose and fatty acids (KIM *et al.* 2016). To ensure efficient muscle performance, a constant

supply of ATP is crucial. Vertebrate muscle fibers are categorized into three main types based on their ability to produce ATP. Fast glycolytic fibers primarily feed on anaerobic glycolysis as their source of ATP and have fast contractions. These fibers store a large amount of glycogen used in glycolysis to generate ATP quickly. Other types of fibers are slow oxidative (SO) and fast oxidative (FO), where SO fibers primarily have a slow contraction and utilize aerobic respiration (glucose and oxygen) to meet the demands of contracting muscle. In contrast, fast oxidative fibers use aerobic respiration but can switch to glycolysis for energy and can fatigue more quickly than SO fibers. However, the glycolytic fibers produce less ATP and are prone to fatigue faster than the oxidative fibers (SZENT-GYÖRGYI 2004; SCHIAFFINO and REGGIANI 2011).

A highly conserved Akt-mTOR signaling pathway plays a significant role in regulating skeletal muscle growth and controls cell size (PHILP *et al.* 2011; GOODMAN *et al.* 2012). The study performed by Goodman and group demonstrated glycolytic flux mediated coordination between the mTOR pathway in controlling cell size. GAPDH, one of the key enzymes in the glycolytic pathway, was shown to bind Rheb (Ras homolog enriched in brain), an activator of mTOR signaling. It was found that siRNA mediated knockdown of GAPDH in HEK293 cells under high glucose conditions increased the phosphorylation of S6K and 4EBP1. However, in cells with low glucose, attenuating the expression of GAPDH suppressed S6K1 phosphorylation. Rheb binds mTOR and promotes cell growth under high glycolytic flux. In contrast, the cells with low glucose concentration, GAPDH interacts with Rheb, and inhibits mTOR signaling. The data supports the idea that GAPDH is a vital regulator of mTOR activity in response to glucose availability and regulates protein synthesis essential for cell growth (GOODMAN *et al.* 2012).

Studies performed in *Drosophila* highlight the importance of glycolytic genes in normal muscle development. The components of the glycolytic pathway provide ATP critical for

contractile apparatus within the muscle fibers. Antibody staining in adult myofibers showed localization of glycolytic enzymes, Glyceraldehyde-3-phosphate dehydrogenase (GAPDH), Aldolase, Triosephosphate isomerase (TPI), and Phosphoglycerate kinase (PGK) at M-line and Z-disc within the sarcomere. *Drosophila Gpdh* mutants are defective in flight, signifying the requirement of glycolytic enzymes in-flight maintenance. Further, myofibrils from *Gpdh* null mutants did not show localization of glycolytic enzymes (GAPDH, aldolase, TPI, and PGK) at the M-line and Z-disc, providing evidence that these enzymes are interdependent and form complexes at the sarcomere (SULLIVAN *et al.* 2003). However, the mechanism behind the colocalization of these enzymes within the sarcomere is not clear. Additional experiments are required to understand how these enzymes localize at the M-line and Z-disc and provide ATP for muscle contraction.

Apart from serving as a source of energy, recent studies have identified a critical role for carbohydrate metabolism in normal larval development. Tennessen and group identified *dERR* (Estrogen related receptor) as a key regulator of glycolysis during the larval stages. *dERR* mutants exhibit elevated levels of circulating sugar trehalose and are ATP deficient. Microarray analysis performed on *dERR* mutants revealed glycolytic genes were downregulated, suggestive of altered carbohydrate metabolism. Furthermore, the metabolomic analysis depicted a reduction in lactate levels in the mutants, confirming reduced glycolytic flux (TENNESSEN *et al.* 2011). The authors show that glycolytic genes are activated during mid-embryogenesis and ERR accumulates through embryo development. Northern blot analysis in *dERR* mutants showed this metabolic switch was disrupted. This ERR regulated transcriptional switch is essential to regulate and support the dramatic growth of the larvae. Taken together, the data provides evidence that glycolytic intermediates serve as precursors for the synthesis of amino acids, fatty acids, and nucleotides to

support the dramatic growth of larvae post embryogenesis. (TENNESSEN *et al.* 2011; TENNESSEN *et al.* 2014).

Jagla and colleagues screened for orthologous genes in *Drosophila* and zebrafish expressed in muscle to study their function in muscle homeostasis. The gene ontology analysis represented enrichment of proteins encoding metabolic genes, including the ones involved in the glycolytic pathway. *Pglym78* mutants exhibited altered embryonic muscle architecture. The muscles were reduced in size with lesser nuclei indicative of myoblast fusion defects. Actin foci formation, a prominent feature of fusion-competent myoblasts, was also affected in *Pglym78* mutants. Similarly, attenuating the expression of vertebrate orthologue *Pgam2 in* zebrafish showed reduced birefringence and perturbed muscle architecture. Additionally, muscle specific reduction of other glycolytic genes *Pfk*, *Tpi*, *Gapdh1*, *Pgk*, *PyK,* and *Impl3* presented embryos with thinner muscles. Further, expressing a dominant negative form of insulin receptor (InR^{DN}) in muscles reduced pyruvate kinase activity. Also, reducing muscle specific expression of *Akt*, presented embryos with thinner muscle and defects in myoblast fusion similar to the phenotype observed in glycolytic gene deficient embryos. Together, the *in vivo* genetic data affirms the idea of involvement of glycolytic genes in promoting myogenic function in coordination with the Insulin/Akt-Tor pathway. The study concludes that insulin acts upstream of glycolysis and promotes biomass accumulation essential for muscle growth (TIXIER *et al.* 2013) (**Fig 2.10**).

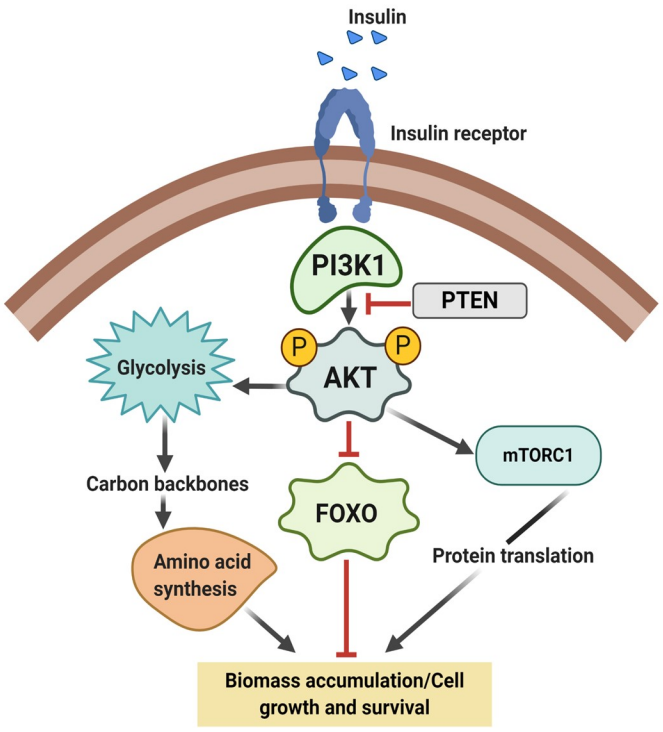

Figure 2.10: Insulin pathway regulates glycolysis and promotes muscle growth.
Insulin acts upstream of glycolysis and mTOR pathway, stimulates amino acid synthesis essential for protein translation and promotes muscle growth by fusion. (Adapted from TIXIER *et al.* 2013). Schematic created using BioRender.com.

In context to skeletal muscle, altered metabolism is often associated with myopathies and muscular dystrophies (LAURETANI *et al.* 2003). Integration of metabolomics and proteomics has revealed dramatic metabolic changes in the diseased muscles. Proteomic profiling on mice hindlimb suspension model of immobilization- induced atrophy showed elevated levels of phosphoglycerate kinase, enolase, aldolase, triosephosphate isomerase, and lactate dehydrogenase (GANNON *et al.* 2008). In Duchenne muscular dystrophy (DMD, glycolytic type II fibers are preferentially affected over oxidative type I fibers with significant cardiac dysfunction that suggests cardiac atrophy and remodeling (CICILIOT *et al.* 2013; EREZ and DEBERARDINIS 2015). Further, patients with Duchene muscular dystrophy exhibit dysregulated glycolytic metabolism with reduction in Phosphoglycerate mutase (PYGM), Aldolase A (ALDOA), cytoplasmic

Glycerol-3-phosphate dehydrogenase [NAD(+)] (GPD1), Triosephosphate isomerase (TPI1), Phosphoglycerate kinase (PGK1), Beta enolase (ENO3), and Pyruvate kinase M1/M2 (PKM2) enzymes (HEYDEMANN 2018). Moreover, proteomic characterization performed on muscle biopsy specimens of patients with Inclusion body myositis also showed perturbed abundance of glycolytic enzymes (LI *et al.* 2006; PARKER *et al.* 2009). Notably, several glycolytic proteins are also downregulated in muscle tissue derived from *Trim32KO* (MOKHONOVA *et al.* 2015). The unbiased proteomics approach signifies that the glycolytic pathway is compromised in various myopathies and, these changes are likely to exacerbate muscle damage. In **chapter 3**, we show that *TRIM32* deficient muscles also show reduced glycolytic flux and contributes to loss of muscle mass.

2.2.2 TRIM32 and its oncogenic role in tumor growth

TRIM32 overexpression has been reported in benign and malignant tumors suggesting a potential role for this E3 ligase in tumor progression. Initially, p53 was identified as a novel target of TRIM32. In response to stress, p53 induces the expression of TRIM32 transcriptionally. TRIM32 binds p53 through its NHL domain and negatively regulates p53 protein turnover through the proteasomal degradation pathway. TRIM32 inhibits p53 mediated apoptosis and promotes xenograft tumors (LIU *et al.* 2014). Elevated TRIM32 mRNA levels were also observed in the tumorigenic epidermal model of study. Further, studies confirmed that TRIM32 induces epidermal thickening *in vivo* and negatively regulates apoptosis in TNFα/UVB mediated oncogenic response in keratinocytes and promotes cell survival through degradation of PIASY (HORN *et al.* 2004). Under normal cellular conditions, another protein, Ab1 interactor 2 (Abi2) is known to suppress cell growth and reduce cell motility. Later, Kano and group demonstrated that TRIM32 also ubiquitinates and degrades Abi2, and promotes cell growth and proliferation (KANO *et al.* 2008).

Qingyu Luo and colleagues found TRIM32 mRNA levels elevated in head and neck squamous carcinomas. Squamous cell carcinomas (SCC) are aggressive, and patients with SCC have low ARID1A (AT-Rich Interaction Domain 1A) expression resulting in poor prognosis. Screening of E3 ligases in 293T cells identified TRIM32 regulates ARID1A protein levels. The investigation identified that TRIM32 promotes SCC proliferation and chemoresistance by degrading ARID1A (LUO *et al.* 2020). Additionally, TRIM32 overexpression is also associated with lung cancer tissues. The experiments suggested that TRIM32 can promote the proliferation of lung cancer cells by activating the JAK2/STAT3-signaling pathway, further solidifying the oncogenic role of TRIM32 (YIN *et al.* 2019). The elevated expression of TRIM32 observed in non-small cell lung cancer (NSCLC) cell lines induced cisplatin chemoresistance in cells. Cell-based assays exhibit TRIM32 upregulates mitochondrial membrane potential, increases cell proliferation, and reduced cisplatin-induced ROS accumulation. Further, an increase in expression of Bcl2, a known suppressor of mitochondrial apoptosis, was observed upon TRIM32 induction (DU *et al.* 2018).

Tumor cells rewire their metabolism, exhibit aerobic glycolysis and favor glucose metabolism to generate energy and metabolic intermediates to produce cellular constituents, including proteins, sugars, and lipids, required to support cell proliferation and growth. This metabolic reprogramming to increase glucose uptake is termed as Warburg effect (LIBERTI and LOCASALE 2016a; LU 2019). The PI3K/Akt pathway is shown to enhance glycolysis in various cancer cells and is shown to affect apoptosis and cell proliferation in gastric cancer cells (OKI *et al.* 2005; LI *et al.* 2009; YOSHIZAWA *et al.* 2010; XU *et al.* 2011; WANG *et al.* 2016b). TRIM32 upregulation poorly coordinates with the overall survival of patients with gastric cancer. Jianjun Wang and colleagues identified a potential link between TRIM32 and Akt signaling in gastric

cancer cells. Knockdown of TRIM32 inhibited phosphorylation of Akt in NCI-N87 and MKN74 cells and suppressed the growth of the cells. GLUT1 and HKII protein levels were also reduced upon TRIM32 silencing. In contrast, overexpression of TRIM32 improved the phosphorylation of Akt and inhibited apoptosis. TRIM32 is expressed in all cells of the human body and, therefore, may be a general regulator of growth in normal and cancerous tissues that require a rapid increase in cell size (WANG *et al.* 2020). A better understanding of TRIM32 function may lead to therapeutic interventions to either increase cell size in patients with mutations in TRIM32 or to limit the growth of cancers that overexpress TRIM32. We further show in **chapter 3** that TRIM32 regulates uncontrolled cell growth in epithelial tumors. TRIM32 negatively impacts glycolysis, resulting in reduced tumor growth.

2.3.3 TRIM32 function as a tumor suppressor

Tumor cells evade apoptosis and continue to proliferate uncontrollably. Programmed cell death is a major targeted pathway for tumor suppression, and various chemotherapeutic agents induce apoptosis to slow the spread of cancerous tissues. TRIM32 is an intriguing protein that regulates both cell death and survival pathways. XIAP (X-linked inhibitor of apoptosis protein) one of the components of anti-apoptotic machinery, is often overexpressed in malignant tumors and is an attractive target for cancer therapy (FERREIRA *et al.* 2001; SELIGSON *et al.* 2007; SHI *et al.* 2008; WANG *et al.* 2010; YIM *et al.* 2014; DIZDAR *et al.* 2018). Yeung Sook Ryu and group reported TRIM32 an E3 ligase for XIAP and downregulates anti-apoptotic pathway. Overexpression of TRIM32 in HEK 293 cells decreased the levels of XIAP. More importantly, TRIM32 facilitates TNFα sensitized cell death through the ubiquitination of XIAP (RYU *et al.* 2011). Recently, we reported *Drosophila TRIM32* (dTRIM32) genetically interacts with *death-*

associated inhibitor of apoptosis (*DIAP1*) vertebrate orthologue of *XIAP*, *Dronc*, and death-associated APAF1-related killer (*Dark*) and regulates apoptosis in muscle tissue. We show that loss of *dTRIM32* elevates DIAP protein levels and inhibits Dronc processing essential for degradation of larval abdominal muscles (dorsal external oblique muscles (DEOMs). The in vivo genetic data suggests dTRIM32 regulates DIAP activity through ubiquitination mediated degradation. Our results mimic the apoptotic regulation via vertebrate TRIM32 confirming functional conservation between two species (VISHAL *et al.* 2018). It will be interesting to test TRIM32 mediated regulation of other components of the anti-apoptotic pathway for a better therapeutic approach.

The tumor suppressor function of TRIM32 was more defined in its ability to facilitate the proteasomal degradation of MYCN in neuroblastoma cells. The asymmetric cell division maintains a critical balance between self-renewing and differentiating the ability of the cells. The inability to maintain ACD homeostasis can lead to neuroblastomas. Amplification of *MYCN* oncogene has been observed in retinoblastoma, glioblastoma, and medulloblastoma. Izumi and Kaneko reported the accumulation of MYCN at the spindle poles during mitosis. It was found that TRIM32 recruitment at the spindle poles promotes MYCN degradation, essential for the establishment of asymmetric cell division. TRIM32 also suppressed the self-renewal division of cancer progressing /stem cells and maintained homeostatic conditions in the neuroblastoma cells (IZUMI and KANEKO 2014). Interestingly, TRIM32 also ubiquitinates and degrades c-myc necessary for muscle stem cell differentiation (NICKLAS *et al.* 2012). Taken together, the data suggests targeting TRIM32/myc complex in stem cell differentiation and regulation will provide new avenues for stem cell cancer drug therapy.

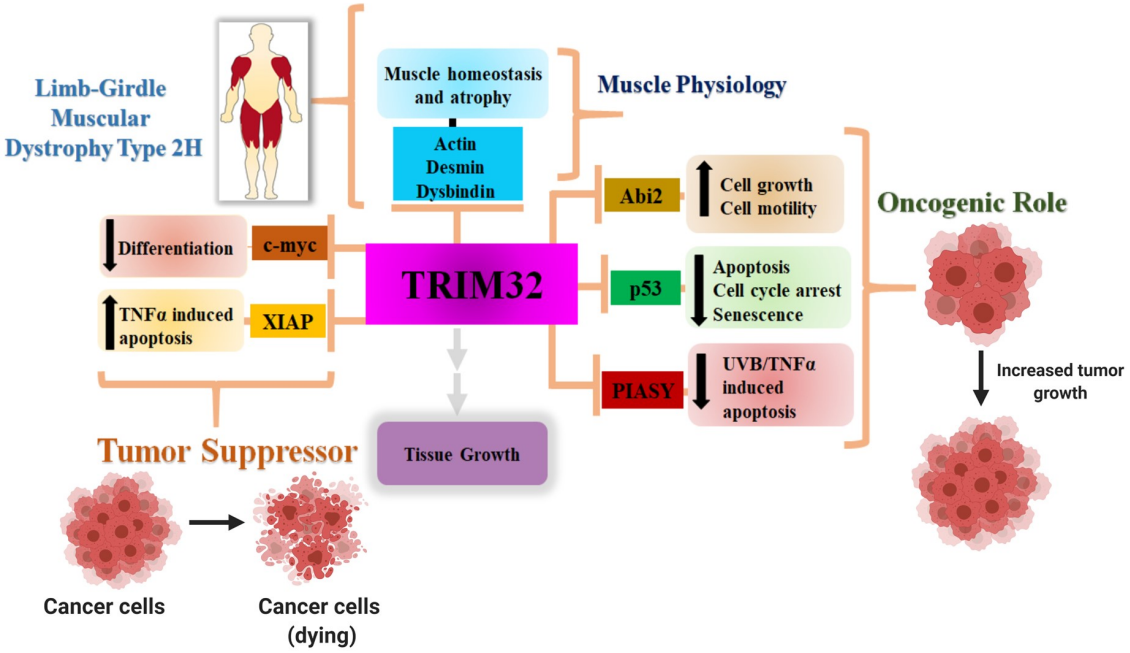

Figure 2.11: Schematic illustration summarizing TRIM32 function in muscle homeostasis, tumor growth and suppression. (Adapted from LAZZARI and MERONI 2016). Schematic created using BioRender.com

References

1. Albor, A., S. El-Hizawi, E. J. Horn, M. Laederich, P. Frosk *et al.*, 2006 The interaction of Piasy with Trim32, an E3-ubiquitin ligase mutated in limb-girdle muscular dystrophy type 2H, promotes Piasy degradation and regulates UVB-induced keratinocyte apoptosis through NFkappaB. J Biol Chem 281**:** 25850-25866.
2. Bawa, S., D. S. Brooks, K. E. Neville, M. Tipping, M. A. Sagar *et al.*, 2020 TRIM32 cooperates with glycolytic enzymes to promote cell growth. Elife 9.
3. Berg, J. M., 1990 Zinc fingers and other metal-binding domains. Elements for interactions between macromolecules. J Biol Chem 265**:** 6513-6516.
4. Borden, K. L., and P. S. Freemont, 1996 The RING finger domain: a recent example of a sequence-structure family. Curr Opin Struct Biol 6**:** 395-401.
5. Budhidarmo, R., Y. Nakatani and C. L. Day, 2012 RINGs hold the key to ubiquitin transfer. Trends Biochem Sci 37**:** 58-65.
6. Calautti, E., J. Li, S. Saoncella, J. L. Brissette and P. F. Goetinck, 2005 Phosphoinositide 3-kinase signaling to Akt promotes keratinocyte differentiation versus death. J Biol Chem 280**:** 32856-32865.
7. Centner, T., J. Yano, E. Kimura, A. S. McElhinny, K. Pelin *et al.*, 2001 Identification of muscle specific ring finger proteins as potential regulators of the titin kinase domain. J Mol Biol 306**:** 717-726.
8. Chiang, A. P., J. S. Beck, H. J. Yen, M. K. Tayeh, T. E. Scheetz *et al.*, 2006 Homozygosity mapping with SNP arrays identifies TRIM32, an E3 ubiquitin ligase, as a Bardet-Biedl syndrome gene (BBS11). Proc Natl Acad Sci U S A 103**:** 6287-6292.
9. Ciciliot, S., A. C. Rossi, K. A. Dyar, B. Blaauw and S. Schiaffino, 2013 Muscle type and fiber type specificity in muscle wasting. Int J Biochem Cell Biol 45**:** 2191-2199.
10. Cohen, S., D. Lee, B. Zhai, S. P. Gygi and A. L. Goldberg, 2014 Trim32 reduces PI3K-Akt-FoxO signaling in muscle atrophy by promoting plakoglobin-PI3K dissociation. J Cell Biol 204**:** 747-758.
11. Cohen, S., B. Zhai, S. P. Gygi and A. L. Goldberg, 2012 Ubiquitylation by Trim32 causes coupled loss of desmin, Z-bands, and thin filaments in muscle atrophy. J Cell Biol 198**:** 575-589.
12. Dastur, D. K., and Z. A. Razzak, 1973 Possible neurogenic factor in muscular dystrophy: its similarity to denervation atrophy. J Neurol Neurosurg Psychiatry 36**:** 399-410.
13. Di Rienzo, M., M. Antonioli, C. Fusco, Y. Liu, M. Mari *et al.*, 2019 Autophagy induction in atrophic muscle cells requires ULK1 activation by TRIM32 through unanchored K63-linked polyubiquitin chains. Sci Adv 5**:** eaau8857.
14. Dizdar, L., L. M. Jünemann, T. A. Werner, P. E. Verde, S. E. Baldus *et al.*, 2018 Clinicopathological and functional implications of the inhibitor of apoptosis proteins survivin and XIAP in esophageal cancer. Oncol Lett 15**:** 3779-3789.
15. Domsch, K., N. Ezzeddine and H. T. Nguyen, 2013 Abba is an essential TRIM/RBCC protein to maintain the integrity of sarcomeric cytoarchitecture. J Cell Sci 126**:** 3314-3323.
16. Du, Y., W. Zhang, B. Du, S. Zang, X. Wang *et al.*, 2018 TRIM32 overexpression improves chemoresistance through regulation of mitochondrial function in non-small-cell lung cancers. Onco Targets Ther 11**:** 7841-7852.
17. Erez, A., and R. J. DeBerardinis, 2015 Metabolic dysregulation in monogenic disorders and cancer - finding method in madness. Nat Rev Cancer 15**:** 440-448.

18. Ferreira, C. G., P. van der Valk, S. W. Span, J. M. Jonker, P. E. Postmus *et al.*, 2001 Assessment of IAP (inhibitor of apoptosis) proteins as predictors of response to chemotherapy in advanced non-small-cell lung cancer patients. Ann Oncol 12**:** 799-805.
19. Fielitz, J., M. S. Kim, J. M. Shelton, S. Latif, J. A. Spencer *et al.*, 2007 Myosin accumulation and striated muscle myopathy result from the loss of muscle RING finger 1 and 3. J Clin Invest 117**:** 2486-2495.
20. Frosk, P., M. R. Del Bigio, K. Wrogemann and C. R. Greenberg, 2005 Hutterite brothers both affected with two forms of limb girdle muscular dystrophy: LGMD2H and LGMD2I. Eur J Hum Genet 13**:** 978-982.
21. Frosk, P., T. Weiler, E. Nylen, T. Sudha, C. R. Greenberg *et al.*, 2002 Limb-girdle muscular dystrophy type 2H associated with mutation in TRIM32, a putative E3-ubiquitin-ligase gene. Am J Hum Genet 70**:** 663-672.
22. Gannon, J., L. Staunton, K. O'Connell, P. Doran and K. Ohlendieck, 2008 Phosphoproteomic analysis of aged skeletal muscle. Int J Mol Med 22**:** 33-42.
23. Goodman, C. A., J. A. Kotecki, B. L. Jacobs and T. A. Hornberger, 2012 Muscle fiber type-dependent differences in the regulation of protein synthesis. PLoS One 7**:** e37890.
24. Green, H. J., R. Helyar, M. Ball-Burnett, N. Kowalchuk, S. Symon *et al.*, 1992 Metabolic adaptations to training precede changes in muscle mitochondrial capacity. J Appl Physiol (1985) 72**:** 484-491.
25. Guglieri, M., V. Straub, K. Bushby and H. Lochmüller, 2008 Limb-girdle muscular dystrophies. Curr Opin Neurol 21**:** 576-584.
26. Henderson, C. A., C. G. Gomez, S. M. Novak, L. Mi-Mi and C. C. Gregorio, 2017 Overview of the Muscle Cytoskeleton. Compr Physiol 7**:** 891-944.
27. Heydemann, A., 2018 Skeletal Muscle Metabolism in Duchenne and Becker Muscular Dystrophy-Implications for Therapies. Nutrients 10.
28. Horn, E. J., A. Albor, Y. Liu, S. El-Hizawi, G. E. Vanderbeek *et al.*, 2004 RING protein Trim32 associated with skin carcinogenesis has anti-apoptotic and E3-ubiquitin ligase properties. Carcinogenesis 25**:** 157-167.
29. Izumi, H., and Y. Kaneko, 2014 Trim32 facilitates degradation of MYCN on spindle poles and induces asymmetric cell division in human neuroblastoma cells. Cancer Res 74**:** 5620-5630.
30. Jamora, C., and E. Fuchs, 2002 Intercellular adhesion, signalling and the cytoskeleton. Nat Cell Biol 4**:** E101-108.
31. Kahyo, T., T. Nishida and H. Yasuda, 2001 Involvement of PIAS1 in the sumoylation of tumor suppressor p53. Mol Cell 8**:** 713-718.
32. Kano, S., N. Miyajima, S. Fukuda and S. Hatakeyama, 2008 Tripartite motif protein 32 facilitates cell growth and migration via degradation of Abl-interactor 2. Cancer Res 68**:** 5572-5580.
33. Kar, A. K., F. Diaz-Griffero, Y. Li, X. Li and J. Sodroski, 2008 Biochemical and biophysical characterization of a chimeric TRIM21-TRIM5alpha protein. J Virol 82**:** 11669-11681.
34. Kim, K. M., H. C. Jang and S. Lim, 2016 Differences among skeletal muscle mass indices derived from height-, weight-, and body mass index-adjusted models in assessing sarcopenia. Korean J Intern Med 31**:** 643-650.

35. Koliopoulos, M. G., D. Esposito, E. Christodoulou, I. A. Taylor and K. Rittinger, 2016 Functional role of TRIM E3 ligase oligomerization and regulation of catalytic activity. EMBO J 35**:** 1204-1218.
36. Kudryashova, E., I. Kramerova and M. J. Spencer, 2012 Satellite cell senescence underlies myopathy in a mouse model of limb-girdle muscular dystrophy 2H. J Clin Invest 122**:** 1764-1776.
37. Kudryashova, E., D. Kudryashov, I. Kramerova and M. J. Spencer, 2005 Trim32 is a ubiquitin ligase mutated in limb girdle muscular dystrophy type 2H that binds to skeletal muscle myosin and ubiquitinates actin. J Mol Biol 354**:** 413-424.
38. Kudryashova, E., A. Struyk, E. Mokhonova, S. C. Cannon and M. J. Spencer, 2011 The common missense mutation D489N in TRIM32 causing limb girdle muscular dystrophy 2H leads to loss of the mutated protein in knock-in mice resulting in a Trim32-null phenotype. Hum Mol Genet 20**:** 3925-3932.
39. Kudryashova, E., J. Wu, L. A. Havton and M. J. Spencer, 2009 Deficiency of the E3 ubiquitin ligase TRIM32 in mice leads to a myopathy with a neurogenic component. Hum Mol Genet 18**:** 1353-1367.
40. LaBeau-DiMenna, E. M., K. A. Clark, K. D. Bauman, D. S. Parker, R. M. Cripps *et al.*, 2012a Thin, a Trim32 ortholog, is essential for myofibril stability and is required for the integrity of the costamere in Drosophila. Proceedings of the National Academy of Sciences of the United States of America 109**:** 17983-17988.
41. LaBeau-DiMenna, E. M., K. A. Clark, K. D. Bauman, D. S. Parker, R. M. Cripps *et al.*, 2012b Thin, a Trim32 ortholog, is essential for myofibril stability and is required for the integrity of the costamere in Drosophila. Proc Natl Acad Sci U S A 109**:** 17983-17988.
42. Langelier, C. R., V. Sandrin, D. M. Eckert, D. E. Christensen, V. Chandrasekaran *et al.*, 2008 Biochemical characterization of a recombinant TRIM5alpha protein that restricts human immunodeficiency virus type 1 replication. J Virol 82**:** 11682-11694.
43. Lauretani, F., C. R. Russo, S. Bandinelli, B. Bartali, C. Cavazzini *et al.*, 2003 Age-associated changes in skeletal muscles and their effect on mobility: an operational diagnosis of sarcopenia. J Appl Physiol (1985) 95**:** 1851-1860.
44. Lazzari, E., M. S. El-Halawany, M. De March, F. Valentino, F. Cantatore *et al.*, 2019 Analysis of the Zn-Binding Domains of TRIM32, the E3 Ubiquitin Ligase Mutated in Limb Girdle Muscular Dystrophy 2H. Cells 8.
45. Lazzari, E., and G. Meroni, 2016 TRIM32 ubiquitin E3 ligase, one enzyme for several pathologies: From muscular dystrophy to tumours. Int J Biochem Cell Biol 79**:** 469-477.
46. Lecker, S. H., A. L. Goldberg and W. E. Mitch, 2006 Protein degradation by the ubiquitin-proteasome pathway in normal and disease states. J Am Soc Nephrol 17**:** 1807-1819.
47. Lecker, S. H., R. T. Jagoe, A. Gilbert, M. Gomes, V. Baracos *et al.*, 2004 Multiple types of skeletal muscle atrophy involve a common program of changes in gene expression. FASEB J 18**:** 39-51.
48. Li, D., X. Qu, K. Hou, Y. Zhang, Q. Dong *et al.*, 2009 PI3K/Akt is involved in bufalin-induced apoptosis in gastric cancer cells. Anticancer Drugs 20**:** 59-64.
49. Li, J., C. Yin, H. Okamoto, H. Jaffe, E. H. Oldfield *et al.*, 2006 Proteomic analysis of inclusion body myositis. J Neuropathol Exp Neurol 65**:** 826-833.
50. Li, X., B. Gold, C. O'hUigin, F. Diaz-Griffero, B. Song *et al.*, 2007 Unique features of TRIM5alpha among closely related human TRIM family members. Virology 360**:** 419-433.

51. Liberti, M. V., and J. W. Locasale, 2016 The Warburg Effect: How Does it Benefit Cancer Cells? Trends Biochem Sci 41**:** 211-218.
52. Liu, J., C. Zhang, X. L. Wang, P. Ly, V. Belyi *et al.*, 2014 E3 ubiquitin ligase TRIM32 negatively regulates tumor suppressor p53 to promote tumorigenesis. Cell Death Differ 21**:** 1792-1804.
53. Locke, M., C. L. Tinsley, M. A. Benson and D. J. Blake, 2009 TRIM32 is an E3 ubiquitin ligase for dysbindin. Hum Mol Genet 18**:** 2344-2358.
54. Lu, J., 2019 The Warburg metabolism fuels tumor metastasis. Cancer Metastasis Rev 38**:** 157-164.
55. Luo, Q., X. Wu, Y. Nan, W. Chang, P. Zhao *et al.*, 2020 TRIM32/USP11 Balances ARID1A Stability and the Oncogenic/Tumor-Suppressive Status of Squamous Cell Carcinoma. Cell Rep 30**:** 98-111.e115.
56. Mahmood, O. A., and X. M. Jiang, 2014 Limb-girdle muscular dystrophies: where next after six decades from the first proposal (Review). Mol Med Rep 9**:** 1515-1532.
57. Massiah, M. A., B. N. Simmons, K. M. Short and T. C. Cox, 2006 Solution structure of the RBCC/TRIM B-box1 domain of human MID1: B-box with a RING. J Mol Biol 358**:** 532-545.
58. Mokhonova, E. I., N. K. Avliyakulov, I. Kramerova, E. Kudryashova, M. J. Haykinson *et al.*, 2015 The E3 ubiquitin ligase TRIM32 regulates myoblast proliferation by controlling turnover of NDRG2. Hum Mol Genet 24**:** 2873-2883.
59. Murphy, A. P., and V. Straub, 2015 The Classification, Natural History and Treatment of the Limb Girdle Muscular Dystrophies. J Neuromuscul Dis 2**:** S7-S19.
60. Napolitano, L. M., and G. Meroni, 2012 TRIM family: Pleiotropy and diversification through homomultimer and heteromultimer formation. IUBMB Life 64**:** 64-71.
61. Nicklas, S., A. Otto, X. Wu, P. Miller, S. Stelzer *et al.*, 2012 TRIM32 regulates skeletal muscle stem cell differentiation and is necessary for normal adult muscle regeneration. PLoS One 7**:** e30445.
62. Oki, E., H. Baba, E. Tokunaga, T. Nakamura, N. Ueda *et al.*, 2005 Akt phosphorylation associates with LOH of PTEN and leads to chemoresistance for gastric cancer. Int J Cancer 117**:** 376-380.
63. Parker, K. C., S. W. Kong, R. J. Walsh, M. Salajegheh, B. Moghadaszadeh *et al.*, 2009 Fast-twitch sarcomeric and glycolytic enzyme protein loss in inclusion body myositis. Muscle Nerve 39**:** 739-753.
64. Philp, A., D. L. Hamilton and K. Baar, 2011 Signals mediating skeletal muscle remodeling by resistance exercise: PI3-kinase independent activation of mTORC1. J Appl Physiol (1985) 110**:** 561-568.
65. Piccirillo, R., F. Demontis, N. Perrimon and A. L. Goldberg, 2014 Mechanisms of muscle growth and atrophy in mammals and Drosophila. Dev Dyn 243**:** 201-215.
66. Pickart, C. M., and M. J. Eddins, 2004 Ubiquitin: structures, functions, mechanisms. Biochim Biophys Acta 1695**:** 55-72.
67. Ramachandran, H., T. Schäfer, Y. Kim, K. Herfurth, S. Hoff *et al.*, 2014 Interaction with the Bardet-Biedl gene product TRIM32/BBS11 modifies the half-life and localization of Glis2/NPHP7. J Biol Chem 289**:** 8390-8401.
68. Ryu, Y. S., Y. Lee, K. W. Lee, C. Y. Hwang, J. S. Maeng *et al.*, 2011 TRIM32 protein sensitizes cells to tumor necrosis factor (TNFα)-induced apoptosis via its RING domain-

dependent E3 ligase activity against X-linked inhibitor of apoptosis (XIAP). J Biol Chem 286**:** 25729-25738.
69. Saccone, V., M. Palmieri, L. Passamano, G. Piluso, G. Meroni *et al.*, 2008 Mutations that impair interaction properties of TRIM32 associated with limb-girdle muscular dystrophy 2H. Hum Mutat 29**:** 240-247.
70. Sadowski, M., and B. Sarcevic, 2010 Mechanisms of mono- and poly-ubiquitination: Ubiquitination specificity depends on compatibility between the E2 catalytic core and amino acid residues proximal to the lysine. Cell Div 5**:** 19.
71. Sandri, M., C. Sandri, A. Gilbert, C. Skurk, E. Calabria *et al.*, 2004 Foxo transcription factors induce the atrophy-related ubiquitin ligase atrogin-1 and cause skeletal muscle atrophy. Cell 117**:** 399-412.
72. Sardiello, M., S. Cairo, B. Fontanella, A. Ballabio and G. Meroni, 2008 Genomic analysis of the TRIM family reveals two groups of genes with distinct evolutionary properties. BMC Evol Biol 8**:** 225.
73. Saurin, A. J., K. L. Borden, M. N. Boddy and P. S. Freemont, 1996 Does this have a familiar RING? Trends Biochem Sci 21**:** 208-214.
74. Schiaffino, S., and C. Reggiani, 2011 Fiber types in mammalian skeletal muscles. Physiol Rev 91**:** 1447-1531.
75. Schoser, B. G., P. Frosk, A. G. Engel, U. Klutzny, H. Lochmüller *et al.*, 2005 Commonality of TRIM32 mutation in causing sarcotubular myopathy and LGMD2H. Ann Neurol 57**:** 591-595.
76. Seligson, D. B., F. Hongo, S. Huerta-Yepez, Y. Mizutani, T. Miki *et al.*, 2007 Expression of X-linked inhibitor of apoptosis protein is a strong predictor of human prostate cancer recurrence. Clin Cancer Res 13**:** 6056-6063.
77. Servián-Morilla, E., M. Cabrera-Serrano, E. Rivas-Infante, A. Carvajal, P. J. Lamont *et al.*, 2019 Altered myogenesis and premature senescence underlie human TRIM32-related myopathy. Acta Neuropathol Commun 7**:** 30.
78. Shi, Y. H., W. X. Ding, J. Zhou, J. Y. He, Y. Xu *et al.*, 2008 Expression of X-linked inhibitor-of-apoptosis protein in hepatocellular carcinoma promotes metastasis and tumor recurrence. Hepatology 48**:** 497-507.
79. Shokeir, M. H., and N. L. Kobrinsky, 1976 Autosomal recessive muscular dystrophy in Manitoba Hutterites. Clin Genet 9**:** 197-202.
80. Short, K. M., and T. C. Cox, 2006 Subclassification of the RBCC/TRIM superfamily reveals a novel motif necessary for microtubule binding. J Biol Chem 281**:** 8970-8980.
81. Stitt, T. N., D. Drujan, B. A. Clarke, F. Panaro, Y. Timofeyva *et al.*, 2004 The IGF-1/PI3K/Akt pathway prevents expression of muscle atrophy-induced ubiquitin ligases by inhibiting FOXO transcription factors. Mol Cell 14**:** 395-403.
82. Sullivan, D. T., R. MacIntyre, N. Fuda, J. Fiori, J. Barrilla *et al.*, 2003 Analysis of glycolytic enzyme co-localization in Drosophila flight muscle. J Exp Biol 206**:** 2031-2038.
83. Szent-Györgyi, A. G., 2004 The early history of the biochemistry of muscle contraction. J Gen Physiol 123**:** 631-641.
84. Tennessen, J. M., K. D. Baker, G. Lam, J. Evans and C. S. Thummel, 2011 The Drosophila estrogen-related receptor directs a metabolic switch that supports developmental growth. Cell Metab 13**:** 139-148.

85. Tennessen, J. M., N. M. Bertagnolli, J. Evans, M. H. Sieber, J. Cox *et al.*, 2014 Coordinated metabolic transitions during Drosophila embryogenesis and the onset of aerobic glycolysis. G3 (Bethesda) 4**:** 839-850.
86. Thrower, J. S., L. Hoffman, M. Rechsteiner and C. M. Pickart, 2000 Recognition of the polyubiquitin proteolytic signal. EMBO J 19**:** 94-102.
87. Tixier, V., L. Bataillé, C. Etard, T. Jagla, M. Weger *et al.*, 2013 Glycolysis supports embryonic muscle growth by promoting myoblast fusion. Proc Natl Acad Sci U S A 110**:** 18982-18987.
88. Tocchini, C., and R. Ciosk, 2015 TRIM-NHL proteins in development and disease. Semin Cell Dev Biol 47-48**:** 52-59.
89. Tocchini, C., J. J. Keusch, S. B. Miller, S. Finger, H. Gut *et al.*, 2014 The TRIM-NHL protein LIN-41 controls the onset of developmental plasticity in Caenorhabditis elegans. PLoS Genet 10**:** e1004533.
90. Vishal, K., S. Bawa, D. Brooks, K. Bauman and E. R. Geisbrecht, 2018 Thin is required for cell death in the Drosophila abdominal muscles by targeting DIAP1. Cell Death Dis 9**:** 740.
91. Wang, J., Y. Fang and T. Liu, 2020 TRIM32 Promotes the Growth of Gastric Cancer Cells through Enhancing AKT Activity and Glucose Transportation. Biomed Res Int 2020**:** 4027627.
92. Wang, J., Y. Liu, R. Ji, Q. Gu, X. Zhao *et al.*, 2010 Prognostic value of the X-linked inhibitor of apoptosis protein for invasive ductal breast cancer with triple-negative phenotype. Hum Pathol 41**:** 1186-1195.
93. Wang, L., F. Ouyang, X. Liu, S. Wu, H. M. Wu *et al.*, 2016 Overexpressed CISD2 has prognostic value in human gastric cancer and promotes gastric cancer cell proliferation and tumorigenesis via AKT signaling pathway. Oncotarget 7**:** 3791-3805.
94. Weissman, A. M., 2001 Themes and variations on ubiquitylation. Nat Rev Mol Cell Biol 2**:** 169-178.
95. Williams, F. P., K. Haubrich, C. Perez-Borrajero and J. Hennig, 2019 Emerging RNA-binding roles in the TRIM family of ubiquitin ligases. Biol Chem 400**:** 1443-1464.
96. Wulczyn, F. G., E. Cuevas, E. Franzoni and A. Rybak, 2011 miRNAs Need a Trim : Regulation of miRNA Activity by Trim-NHL Proteins. Adv Exp Med Biol 700**:** 85-105.
97. Xu, X., Y. Zhang, D. Qu, T. Jiang and S. Li, 2011 Osthole induces G2/M arrest and apoptosis in lung cancer A549 cells by modulating PI3K/Akt pathway. J Exp Clin Cancer Res 30**:** 33.
98. Yim, J. H., W. G. Kim, M. J. Jeon, J. M. Han, T. Y. Kim *et al.*, 2014 Association between expression of X-linked inhibitor of apoptosis protein and the clinical outcome in a BRAF V600E-prevalent papillary thyroid cancer population. Thyroid 24**:** 689-694.
99. Yin, H., Z. Li, J. Chen and X. Hu, 2019 Expression and the potential functions of TRIM32 in lung cancer tumorigenesis. J Cell Biochem 120**:** 5232-5243.
100. Yoshizawa, A., J. Fukuoka, S. Shimizu, K. Shilo, T. J. Franks *et al.*, 2010 Overexpression of phospho-eIF4E is associated with survival through AKT pathway in non-small cell lung cancer. Clin Cancer Res 16**:** 240-248.
101. Zhang, J., M. M. Hu, Y. Y. Wang and H. B. Shu, 2012 TRIM32 protein modulates type I interferon induction and cellular antiviral response by targeting MITA/STING protein for K63-linked ubiquitination. J Biol Chem 287**:** 28646-28655.

Chapter 3 - *Drosophila* TRIM32 cooperates with glycolytic enzymes to promote cell growth

Simranjot Bawa[1], David S. Brooks[1], Kathryn E. Neville[2], Marla Tipping[2], Md Abdul Kader Sagar[3], Joseph A. Kollhoff[1], Geetanjali Chawla[4,5], Brian V. Geisbrecht[1], Jason M. Tennessen[5], Kevin W. Eliceiri[3], and Erika R. Geisbrecht[1]

This chapter has been published as a journal article in eLife.

Abstract

Cell growth and/or proliferation may require the reprogramming of metabolic pathways, whereby a switch from oxidative to glycolytic metabolism diverts glycolytic intermediates towards anabolic pathways. Herein we identify a novel role for TRIM32 in the maintenance of glycolytic flux mediated by biochemical interactions with the glycolytic enzymes Aldolase and Phosphoglycerate mutase. Loss of *Drosophila* TRIM32, encoded by *thin (tn)*, shows reduced levels of glycolytic intermediates and amino acids. This altered metabolic profile correlates with a reduction in the size of glycolytic larval muscle and brain tissue. Consistent with a role for metabolic intermediates in glycolysis-driven biomass production, dietary amino acid supplementation in *tn* mutants improves muscle mass. Remarkably, TRIM32 is also required for ectopic growth - loss of TRIM32 in a wing disc-associated tumor model reduces glycolytic metabolism and restricts growth. Overall, our results reveal a novel role for TRIM32 for controlling glycolysis in the context of both normal development and tumor growth.

Introduction

The metabolism of all cells must adapt to meet the energetic and biosynthetic needs of growth and homeostasis (LLOYD 2013; ZHU and THOMPSON 2019). For example, tissues composed of non-dividing, differentiated cells must strike a balance between catabolic pathways that provide energy for cellular homeostasis and anabolic pathways that repair the cell and generate cell type-specific molecules (LLOYD 2013). In contrast, the metabolic requirements of cell growth and proliferation often require a shift towards anabolic pathways that favors the synthesis of macromolecules, such as proteins, lipids, nucleic acids, and complex carbohydrates (ZHU and THOMPSON 2019). Striking this delicate balance between degradative and biosynthetic processes requires the integration of extracellular and intracellular information by complex signaling networks.

The mechanisms by which cell proliferation and tissue growth rewire metabolism to enhance biosynthesis are diverse and complex (LUNT and VANDER HEIDEN 2011). These changes in metabolic flux involve pathways such as the pyrimidine and purine biosynthesis, one carbon metabolism, and the interplay between the citric acid cycle and amino acids pools. However, the pathway most commonly associated with enhanced biosynthesis is glycolysis, where in biological systems ranging from yeast to human T-cells, glycolytic flux is often elevated in the context of cell growth and proliferation (ZHU and THOMPSON 2019). This observation is particularly apparent in the fruit fly *Drosophila melanogaster*, where the onset of larval development is preceded by a metabolic switch that induces the coordinate up-regulation of genes involved in glycolysis, the pentose phosphate pathway, and lactate dehydrogenase (LDH) (TENNESSEN *et al.* 2011). The resulting metabolic program allows larvae to use dietary carbohydrates for both energy production and biomass accumulation. Moreover, studies of *Drosophila* larval muscles reveal that this metabolic transition is essential for muscle growth and development, suggesting that glycolysis

serves a key role in controlling growth (TENNESSEN *et al.* 2014b). The mechanisms that control glycolysis specifically in larval muscle, however, remain relatively unexplored. As a result, *Drosophila* larval development provides an excellent model for understanding how glycolysis and biomass production are regulated in a rapidly growing tissue. Moreover, since larval muscle increases in size without cell divisions, larval muscle provides an unusual opportunity to understand how glycolytic metabolism promotes growth independent of cell division.

Of the known factors that promote muscle development, TRIM32 is an intriguing candidate for coordinating metabolism with cell growth. This protein is a member of the Tripartite motif (TRIM)-containing family of proteins defined by an N-terminal RING domain, one or two B-boxes, a coiled-coil domain, and a variable C-terminal region (TOCCHINI and CIOSK 2015; WATANABE and HATAKEYAMA 2017). In TRIM32, six Ncl-1, HT2A, Lin-41 (NHL) repeats comprise the C-terminus and are proposed to mediate the diverse functions of TRIM32, including cell proliferation, neuronal differentiation, muscle physiology and regeneration, and tumorigenesis (TOCCHINI and CIOSK 2015; LAZZARI and MERONI 2016; WATANABE and HATAKEYAMA 2017). A single mutation in the B-box region of TRIM32 causes the multisystemic disorder Bardet-Biedl syndrome (BBS) (CHIANG *et al.* 2006), while multiple mutations that cluster in the NHL domains result in the muscle disorders Limb-girdle muscular dystrophy type 2H (LGMD2H) and Sarcotubular Myopathy (STM) (FROSK *et al.* 2005; SCHOSER *et al.* 2005; BORG *et al.* 2009; NERI *et al.* 2013; NECTOUX *et al.* 2015; LAZZARI *et al.* 2019; SERVIÁN-MORILLA *et al.* 2019).

A complete understanding of TRIM32 function is confounded by its ubiquitous expression and multitude of potential substrates for E3 ligase activity via the RING domain. Many known TRIM32 target substrates include proteins implicated in muscle physiology (KUDRYASHOVA *et al.* 2005; ALBOR *et al.* 2006; LOCKE *et al.* 2009; COHEN *et al.* 2012; COHEN *et al.* 2014; VOLODIN *et*

al. 2017) or the prevention of satellite cell senescence (KUDRYASHOVA *et al.* 2012; MOKHONOVA *et al.* 2015; SERVIÁN-MORILLA *et al.* 2019), consistent with a role for TRIM32 in LGMD2H. However, additional polyubiquitinated substrates, including p53, Abi2, Piasy, XIAP, and MYCN, are implicated in tumorigenesis (ALBOR *et al.* 2006; KANO *et al.* 2008; RYU *et al.* 2011; IZUMI and KANEKO 2014; LIU *et al.* 2014). Importantly, TRIM32 protein levels are upregulated in multiple tumor types, suggesting that TRIM32 is a key player in growth regulation (HORN *et al.* 2004; ITO *et al.* 2017; ZHAO *et al.* 2018). There is precedence for NHL function in controlling cell proliferation as two other *Drosophila* NHL-containing proteins, Brat and Mei-P26, act as tumor suppressors in the larval brain and female germline, respectively (ARAMA *et al.* 2000; EDWARDS *et al.* 2003).

Here we provide a novel mechanism for TRIM32 in cell growth. Our data show that TRIM32 promotes glucose metabolism through the stabilization of glycolytic enzyme levels. This increased rate of TRIM32-mediated glycolytic flux generates precursors that are utilized for biomass production. Surprisingly, this mechanism operates in both non-dividing muscle cells as well as in proliferating larval brain cells, demonstrating a universal metabolic function for TRIM32 in growth control.

Materials and methods

Fly genetics

Fly stocks were reared on standard cornmeal media at 25 °C unless otherwise indicated. The *WT* control strain was w^{1118} [Bloomington (BL) *Drosophila* Stock Center; BL3605). The *tnΔA* mutation (LABEAU-DIMENNA *et al.* 2012b) was maintained over the *CyO, Tb/Sco* (BL36335) balancer chromosome. Non-Tb individuals from the *tnΔA/CyO,* Tb^{1} stock were used for *tn-/-*

analysis. The following Gal4 and/or RNAi lines were used: *mef2*-Gal4 (BL27390), *elav*-Gal4 (BL458), *5053*-Gal4 (BL2702), UAS-*tn RNAi-A* [Vienna *Drosophila* Resource Center (VDRC); v19290), UAS-*tn RNAi-B* (BL31588), and UAS-*tn RNAi-C* (v19291). UAS-*TRIM32* was previously described (LABEAU-DIMENNA *et al.* 2012b). The *UAS-2XFLAG-dERR* transgene was generated by amplifying the *dERR* cDNA using the oligos listed in the Key Resources Table. The resulting PCR product was sequenced, inserted into the NotI site of pUAST-attP, and injected to a strain containing the attP40 site by BestGene Inc (Chino Hills, CA, USA). The transgenic *dpp-Gal4, UAS-mCherry, LDH-GFP* and *UAS-Pvr^{act}* flies were a kind gift from U. Banerjee (WANG *et al.* 2016a). The *LDH-GFP* line (**Fig. 6 –figure supplement 1A**) was generated using a previously described *pLdh* genomic rescue construct (LI *et al.* 2017). Briefly, GFP was inserted at the 3' end of the *Ldh* coding region using a PCR based method. The plasmid was injected into the strain attP40w by Rainbow Transgenics (Camarillo, CA) and the F1 generation was screened for transgene integration at the attP40 docking site. This transgene is capable of rescuing the *Ldh* mutant larval lethal phenotype (Chawla and Tennessen, in preparation).

Immunostaining and microscopy

Muscle. Synchronized L2 or wandering L3 larvae were rinsed with 0.7% (w/v) NaCl/0.1% Triton, filleted in ice cold 1X PBS on Sylgard plates, and fixed in 4% (v/v) formaldehyde (Fisher) followed by three washes with 0.5% PBT. Phalloidin 488 or 594 was used to label F-actin (1:400, Molecular Probes). *Other tissues*. Wing discs, larval brains, or midguts were isolated from wandering L3 larvae and fixed for 25 minutes in 4% formaldehyde in PBS. Both discs and brains were stained overnight with DAPI (1:400) at 4°C. Midguts were stained with Phalloidin 488 (1:400, Molecular Probes). Anti-Caspase-3 (1:100, Cell Signaling Technology,

Danvers, MA, USA) staining on brains was performed overnight at 4°C followed by labeling with Alexa Fluor anti-rabbit 568 secondary antibody (1:400). Either muscle fillets, isolated brains or wing discs were mounted in anti-fade mounting medium (190% glycerol, 0.5% n-propyl gallate in 20mM Tris buffer, pH=8.0) and imaged using a Zeiss 700 confocal microscope.

Molecular Biology

The NHL region of *Drosophila* TRIM32 (nucleotides 3231-4062) was PCR amplified using Phusion polymerase (ThermoFisher Scientific), digested with EcoRI and NotI, and ligated into the pGEX-5X-2 expression vector containing an N-terminal GST tag. Tm2, Ald, and Pglym were amplified by PCR and subcloned into the pT7HMT protein expression vector with either SalI/NotI or BamHI/NotI. Primers used for PCR amplification are included in the Key Resources Table.

Protein Expression and Purification

Protein expression was performed in *E.coli* BL21 cells. A single colony was inoculated into 100mL of LB media supplemented with the appropriate antibiotic at 37°C, incubated overnight and then diluted into 1L of Terrific Broth. Protein expression was induced at $OD_{600} = 0.6$ after the addition of Isopropyl β-D-1-thiogalactopyranoside (IPTG) to a final concentration of 1mM (GEISBRECHT *et al.* 2006). After 18 hours of incubation at 18°C, cells were centrifuged and were lysed using a microfluidizer for cell lysis. After centrifugation, the GST_TRIM32_NHL tagged protein was purified using GST affinity chromatography (GE Healthcare), further purified using size exclusion and ion-exchange Chromatography, and concentrated using 30K Amicon centrifuge columns (Millipore). The large scale expression and purification of Tm2, Ald, and Pglym was similar but used Ni^{2+} column for the initial purification step for His-tag binding. The purified proteins were stored at -80°C until use.

Crystallization, X-ray Diffraction, Structure Solution, and Refinement

Crystals of a recombinant form of the NHL-repeat region of *Drosophila* TRIM32 were obtained by vapor diffusion of hanging drops. Briefly, a sample of purified protein was buffer exchanged into double-deionized water and concentrated to 5 mg/ml. Crystals were obtained from 2 µl droplets that had been established by mixing 1 µl of protein with 1 µl of precipitant solution [0.1M HEPES (pH 7.8), 0.2 M NaCl, and 25% (v/v) PEG-3350] and incubating over 500 µl of precipitant solution at 20 °C. Rod-shaped crystals appeared within 2-3 days and grew to their full size within 1-2 weeks. Single crystals were harvested and briefly soaked in a cryopreservation buffer consisting of precipitation solution supplemented with an additional 20% (v/v) glycerol. Monochromatic X-ray diffraction data were collected at beamline 22-BM of the Advanced Photon Source at Argonne National Laboratory using incident radiation of λ=1.000 Å. Reflections were indexed, integrated, and scaled using the HKL2000 software suite (OTWINOWSKI and MINOR 1997). Initial phases were obtained by molecular replacement using program PHASER (MCCOY *et al.* 2007a) and a poly-alanine model derived from chain A of PDB entry 1Q7F. The model was constructed and refined through an iterative process consisting of automated building and refinement in PHENIX (ADAMS *et al.* 2002; ZWART *et al.* 2008), coupled with manual inspection and modifications. The final model consists of 292 protein residues, 85 ordered solvent molecules, and 6 ligand molecules. 94% of the protein residues occupy favored regions in the Ramachandran plot, with an additional 4% in allowed regions. Additional information on data collection and model statistics may be found in **Fig. 1-source data 1**. The final model and structure factors have been deposited in the PDB under accession code 6D69.

Mass spectrometry (MS) analysis

L3 larvae were homogenized in lysis buffer [50 mM Tris-HCl (pH 7.5), 100 mM NaCl, 10% (v/v) glycerol and 1 mM EDTA] plus inhibitors [1 mM Na3VO4, 5 mM NPPS, 2 mM PMSF, 2 ug/ml Leupeptin, 10 µM MG132, 1x Halt Pro inhibitor cocktail (Roche)]. 10 µg of purified TRIM32_NHL protein was coupled to Cyanogen bromide-activated-Sepharose 4B beads (Sigma-Aldrich), incubated for 2 hrs at 4°C with 100 mg of lysates prepared from L3 larvae. Bead-protein complexes were washed 3X with wash buffer (50 mM Tris-HCl (pH 7.5), 150 mM NaCl, 1 mM EDTA and 1% (v/v) Triton]. Control pulldowns were performed using beads alone. Beads containing protein complexes were sent to Oklahoma State University for MS analysis. Statistical analysis was performed using Perseus MaxQuant (COX and MANN 2012; TYANOVA *et al.* 2016).

In vitro binding assay

To assess the interaction with TRIM32_NHL, 10 µg of purified candidate proteins (Tm2, Ald or Pglym) or the negative control (SCIN) were immobilized on Ni^{2+}-NTA magnetic beads (ThermoFisher Scientific) for 1.5 h followed by incubation with 10 µg of dTRIM32 NHL for 30 min at 4 °C on a rotating platform. The complexes were washed 6x [300 mM NaCl, PBS (pH = 7.0) + 1% (v/v) Triton]. The bound proteins were eluted by boiling at 100 °C in 6X Laemmli buffer for 10 minutes. The binding was analyzed on 12% sodium dodecyl sulfate polyacrylamide gel electrophoresis (SDS-PAGE) under reducing conditions followed by Coomassie Blue Staining.

Co-Immunoprecipitation

For lysate preparation, *WT* third-instar larvae were homogenized in lysis buffer (50mM Tris-HCl pH 7.5, 100mM NaCl, 10% glycerol, 1% Triton, 1mM EDTA) containing 1X Halt Protease Inhibitor (Thermo fisher Scientific) and 10 µM MG132. The lysate was precleared via

centrifugation at 13,000 x for 20 minutes at 4°C and the resulting protein concentration was measured using the Bradford Assay (Biorad, Hercules, CA). 500µg of the lysate was set aside for input analysis. For immunoprecipitations, 20µL of Protein A Sepharose 4b beads (Thermo Fisher Scientific) were washed twice with the lysis buffer. The beads were then incubated with 15ug of *Drosophila* anti-TRIM32 antibody overnight at 4°C. The antibody conjugated beads were then mixed with 2 mg of lysate and incubated for 2 hours at 4°C on a rotating wheel. Post incubation, the resin was centrifuged at 1000 x g for 3 minutes washed 5 times with wash buffer (1M NaCl, 1%Triton, PBS). 30uL of 6X Laemmli buffer was used to elute bound proteins off the resin and these samples were denatured by heating at 100°C for 10 minutes. Eluted protein samples were subjected to 10% SDS PAGE gel electrophoresis and transferred to polyvinyl difluoride (PVDF) membranes (Pierce Biotechnology, Inc., Waltham, MA) for Western blotting with the following primary antibodies: rabbit anti-*Drosophila* Ald [1:1000, (SULLIVAN *et al.* 2003)], rabbit anti-*Drosophila* Pglym [1:1000, (SULLIVAN *et al.* 2003)], guinea pig anti-*Drosophila* TRIM32 [1:500, (LaBeau-Dimenna, et al., 2012)], rabbit anti-human ALD [1:1000, Biorad, Hercules, CA], rabbit anti-human PGAM1 [1:1000, Cell Signaling, Danvers, MA]. Post treatment with the primary antibodies, blots were washed thoroughly with the wash buffer (TBS+ 0.1%Tween) and incubated with HRP conjugated and fluorescent secondary antibodies (dilution 1:5000) for 2 hours at room temperature. Protein detection was performed using the Prometheus ProSignal™ Pico western blotting detection kit (Genesee Scientific).

Metabolomics Analysis

Pooled *WT* or *tn-/-* L3 larvae (25 each) were selected and washed with NaCl/0.1% Triton to remove food or debris. Each batch of pooled larvae were flash frozen in liquid nitrogen and sent to the

University of Utah Metabolomics Core. Metabolites were extracted and derivatized before gas chromatography-mass spectrometry (GC-MS) analysis with an Agilent 5977B GC-MS. Data was collected using MassHunter software and metabolite identity was determined using MassHunter Quant. The metabolite data was normalized to standards, parsed, and Metaboanalyst 3.0 was used for statistical analysis and data processing. Independently, groups of 10 larvae were weighed on an analytical scale to determine the difference in body mass between *WT* and mutant cohorts before analysis. Six biological replicates were performed for each genotype.

In vivo feeding assays

To assess the impact of amino acid supplements on muscle mass in *WT* and *tn-/-,* embryos were reared from hatching until analysis at the L3 stage at 25 °*C* on three different food conditions in 60 mm petri dishes: (1) Agar only control: 2.25% (w/v) agar in distilled water; (2) Yeast extract powder (mixture of amino acids, carbohydrates, peptides and soluble vitamins): 15% (w/v) yeast extract powder added to 2.25% (w/v) agar; or (3) Amino acids: 20 individual amino acids were individually weighed and added to 2.25% (w/v) agar (LEE and MICCHELLI 2013). Both *WT* and *tn-/-* L3 larvae were dissected, stained with phalloidin, and analyzed using confocal microscopy for each condition. Note that agar contains two polysaccharides, agarose and agaropectin. Thus, the larvae are starved, but not completely devoid of nutrients.

ATP Assay

25 L3 larvae were pooled and homogenized in 100µl of extraction buffer [6 M guanidine HCL, 100 mM Tris (pH 7.8), 4 mM EDTA], boiled for 5 minutes, and centrifuged at 13,000 x g for 5 minutes at 4°C. Protein concentrations were measured using the Bradford Assay kit (Biorad,

Hercules, CA). ATP levels were determined using an ATP Determination Kit (Molecular Probes) as described in (TENNESSEN *et al.* 2014a). 100 µl assays were performed in a 96 well plate and the luminescence was measured using Perkin Elmer EnSpire Multimode plate reader. Each sample was processed in triplicate and read in triplicate. The amount of ATP was normalized to total protein concentration.

Quantitation and statistical analysis

Muscle diameter measurements. Z-stack images for each fillet were converted to a maximum intensity projection. The Polylines plugin from ImageJ was used to measure the muscle width of all VL3 muscles from dissected L2 and L3 individuals. *Pupal case axial ratio determination.* Pupa of the appropriate genotype were removed from vials, oriented dorsal side up, and attached to slides using a small drop of nail polish. Images were taken with a Leica M165 FC Stereomicroscope. Length and width measurements for each pupae were performed in ImageJ using the line and measure functions. Values were put into an Excel spreadsheet and the axial ratio (length/width) was calculated for each individual. The raw data was imported into Graphpad Prism 6.0 and graphed as a box and whiskers plot. N≥10 for each genotype. *Brain and midgut analysis.* Z-stack images of isolated brain or midgut tissue areas were measured in ImageJ using the outline and measure functions N≥8 for each genotype. Brain lobe cell size was determined using the analyze particle function after thresholding in ImageJ. N>300 cells in 10 individual brain lobes for each genotype. *Larval mass measurements.* For each genotype and condition tested, pools of 10 larvae weighed on a digital scale. The average of each pool (N=3) was plotted. *Wing disc-associated tumor analysis*. Z-stack images of each wing disc were used to measure the area and volume. For area measurements, the single plane that contained the maximum area for each disc

was fully outlined using the free draw tool followed by the measure command in ImageJ. For volume quantitation, each disc in each Z-section was outlined, subjected to thresholding, and the stack command was used to measure the stacked volume. *Statistics.* Raw data was imported to GraphPad Prism 6.0 for statistical analysis and graph generation. All error bars represent mean ± standard deviation (SD). Statistical significances were determined using either student t-tests, Mann-Whitney tests or one-way ANOVA. Differences were considered significant if $p < 0.05$ and are indicated in each figure legend.

Western blots

Five whole L3 larvae were homogenized in 3X SDS sample buffer [188 mM Tris-HCl (pH 6.8), 3% (w/v) SDS, 30% (v/v) glycerol, 0.01% (w/v) bromophenol-blue, and 15% (v/v) β-mercaptoethanol], boiled at 95°C for 10 min, and centrifuged at 15,000 x g to remove cellular debris. To analyze overall protein levels, lysates were subjected to SDS–PAGE, transferred to polyvinyl difluoride (PVDF) membranes (Pierce Biotechnology, Inc., Waltham, MA), and probed with the appropriate primary antibodies: rabbit-Pglym [1:1000, (SULLIVAN *et al.* 2003)], rabbit-Ald, [1:1000, (SULLIVAN *et al.* 2003)], rat-Tm (1:500, Babraham Institute, Cambridge, UK) and mouse anti-ATPase 5α (1:10000, Abcam, Cambridge, MA). Horseradish Peroxidase (HRP) conjugated secondary antibodies (1:3000–1:5000, GE Healthcare, Chicago, IL) were used to detect primary antibodies. Protein detection was carried out using the ECL Plus western blotting detection kit (ThermoFisher Scientific, Waltham, MA). Densitometry analysis was performed by calculating the relative band intensities of candidate proteins to ATPase 5α loading control using ImageJ software.

Quantitative PCR (qPCR)

RNA was isolated from a pool of five whole L3 larvae for each genotype using the RNAeasy Mini Kit (QIAGEN, Valencia, CA). After elution, RNA concentrations were determined and single strand complementary DNA (cDNA) was synthesized from 100ng of RNA using the SuperScript VILO cDNA Synthesis Kit (Invitrogen, Carlsbad, CA). For qPCR, each cDNA sample was diluted to 1:50 and mixed with Power UP SYBR Green Master mix also mixed with the appropriate primers (Applied Biosystems, Foster City, CA). *rp49* was used as the reference gene. Primers were synthesized by Integrated DNA Technologies (IDT):

rp49: F5';-GCCCAAGGGTATCGACAACA-3', R5'-GCGCTTGTTCGATCCGTAAC-3'

Ald: F5'- GGCCGCCGTCTACAAGGC-3', R5'-GTTCTCCTTCTTGCCAGC-3'

Pglym78: F5-AGTCCGAGTGGAACCAGAAGA-3', R5'-GGCTTGAAGTTCTCGTCCAG-3'

Three independent biological replicates were processed for each genotype and reactions were run in triplicate using the Quant Studio 3 Applied Biosystem with Quant studio design and analysis software. The average of the triplicates was used to calculate the 2-ΔΔCt values (normalized fold expression). Quantification of mRNA levels between different genotypes at the same time point was performed using the student t-test.

Agilent Seahorse XFe96 Analyzer experiments

Larval brain, muscle, and wing disc preparation. The Agilent Seahorse XFe96 metabolic analyzer was placed in an incubator set to 12°C, and analyzer was set to 25°C with the heat on (running Wave software version 2.4). An Agilent Seahorse XFe96 cartridge (Agilent, Santa Clara, CA) was hydrated with 200 µl of calibrant solution (Agilent, Santa Clara, CA) overnight at 25°C. The next day, brains, muscles, or discs were dissected in phosphate buffered solution (PBS) and added to

an Agilent 96-well cell plate (Agilent, Santa Clara, CA) containing 50 µl of Agilent Seahorse assay media with supplements required for specific assay (see glycolytic rate assay method). Tissue was sunk to the bottom of the well and centered in the middle between the three raised spheres. Forceps were used to lower the tissue restraint such that the plastic ring is facing towards the bottom of the well and the nylon screen is facing the top of the well. A probe was used to gently push the edge of the tissue restraint down toward the bottom of the well until the restraint did not move or float in the well. 130 µl of assay media was added to each well; resulting in a total of 180 µl final in each well. The cell plate was placed on the tray of the XFe96 analyzer. The instrument was for basal and glycolytic rate assays with all cycle procedures consisting of one-minute mixing, zero-minutes waiting, and three-minutes measuring. *Basal ECAR measurements using the XFe96.* Basal levels of extracellular acidification (ECAR) were measured for a minimum of six cycles. Tissue restraints were measured without tissue as a control. Agilent Seahorse XF assay medium (Agilent, Santa Clara, CA) supplemented with 10mM glucose, and 10mM sodium pyruvate was used for all basal measurement assays. A minimum of 4 biological replicates were used to analyze the basal rate of *WT* and *tn-/-* larval muscle. Standard error of the mean (SEM) was used in analyzing metabolic measurement levels. Statistical significance was determined using the Holm-Sidak method with alpha=0.05. *Glycolytic Rate Assay.* Analysis of glycolytic rate with mitochondrial-produced acidification subtracted was conducted using base medium without phenol red (Agilent, Santa Clara, CA), supplemented with 5mM Hepes (Agilent, Santa Clara, CA), 2 mM glutamine, 10mM glucose and 1mM sodium pyruvate. 20 µl of 50 µM rotenone and antimycin-A was added to port A and injected at the 7th cycle, resulting in a final concentration of 5 µM rotenone and antimycin-A. 22 µl of 1M 2-deoxyglutarate (2-DG) was added to port B and injected at the 12th cycle, resulting in a final concentration of 100mM 2-DG. The software package included with this

kit analyzes the oxygen consumption and extracellular acidification rates, while factoring in the buffer capacity of the media. It also calculates the acidification caused by the mitochondria and subtracts this from the data. This method produces the proton efflux rate (PER). A minimum of 4 biological replicates were used to analyze the glycolytic rate of *WT* and *tn-/-* larval brains. Standard error of the mean (SEM) was used in analyzing metabolic measurement levels. Statistical significance was determined using the Holm-Sidak method with alpha=0.05. *Normalization of XFe96 measurements by protein concentration*. XFe96 analysis data was normalized by protein concentration. Protein normalization was conducted using the Pierce 660nm protein assay reagent (Thermo Fisher Scientific, Waltham, MA). Each sample was homogenized in default lysis buffer (50 mM Tris (pH 7.5), 125 mM NaCl, 5% glycerol, 0.2% IGEPAL, 1.5 mM $MgCl_2$, 1 mM DTT, 25 mM NaF, 1 mM Na_3VO_4, 1 mM EDTA and 2 × Complete protease inhibitor (Roche, Indianapolis, IN) on ice, incubated on ice for 15 minutes, and centrifuged at full speed for 15 minutes at 4°C. Supernatant was collected and measured as indicated in the Pierce 660nm protein assay reagent manual. Samples were assayed using a Biotek Cytation 3 plate reader. PER and muscle ECAR values were divided by µg amount of protein measured to determine the normalized pmol/min/µg rate of proton efflux and mpH/min/µg rate of extracellular acidification. Standard error of the mean (SEM) was used in analyzing metabolic measurement levels. Statistical significance was determined using the Holm-Sidak method with alpha=0.05.

Respirometry

Larval metabolic rates were assessed by indirect calorimetry, measuring CO2 production with flow-through respirometry using the Multiple Animal Versatile Energetics platform for metabolic phenotyping (MAVEn, Sable Systems International, Las Vegas, NV, USA). Baseline ultra zero

air was provided from a compressed air cylinder and regulated at approximately 20 mL/min through each of 16 respirometry chambers simultaneously. Larvae were measured in groups of five in each chamber. The MAVEn automated flow switching between chambers and baseline (interleave ratio 16:1; dwell time per chamber 2 minutes). Differential carbon dioxide concentration was measured with a LiCor 7000 infrared gas analyzer. The wet mass of insects prior to and following respirometry was measured to the nearest 0.01 mg (Mettler Toledo XS22SDU Analytical Balance). N = 6 chambers with 5 larvae in each chamber for each genotype.

FLIM

The multiphoton based (DENK *et al.* 1990) lifetime and intensity imaging was performed on a custom multiphoton laser scanning system built around an inverted Nikon Eclipse TE2000U at the Laboratory for Optical and Computational Instrumentation (YAN *et al.* 2006). A 20x air immersion objective (Nikon Plan Apo VC, 0.75 NA) (Melville, NY, USA) was used for all imaging. For NADH imaging, data was collected using an excitation wavelength of 740 nm, and the emission was filtered at 457 ± 50 nm (Semrock, Rochester, NY) for the spectral peak for NADH/NADPH. For intensity imaging, the excitation was set at 980 nm, and an emission 520 ± 35 filter was used (Semrock, Rochester, NY). The FLIM fitting process was done according to the methods sections describing FLIM analysis performed for the same scope (GHANBARI *et al.* 2019). For each sample, around eight neighboring fields were randomly selected, and the average value of lifetime and free NADH ratio were calculated.

L-lactate assays

L-lactate levels in the brain and muscle were measured in the indicated genotypes. L3 larval brains and muscle carcasses were dissected and placed in ice-cold 1X PBS. Brains (n=20 each, total 60 brains per genotype) or muscle tissue (N=8, total 24 carcasses per genotype) were pooled together

and homogenized in 50µL 1X PBS. Bradford Assay was used to quantitate protein concentrations. Each lysate was transferred to a 96 well plate and incubated with lactate dehydrogenase and NAD/MTT for 2 hours at room temperature (EnzyChrom™ Glycolysis Assay Kit, BioAssay Systems). The intensity of the reduced dye was measured at 565nm, which is directly proportional to the concentration of the L-Lactate in the sample.

EdU incorporation assay

Dissected larval brains were incubated in *Drosophila* Schneider's medium containing 10uM EdU (ThermoFisher Scientific, Waltham, MA) for 2 hours at room temperature. Tissues were fixed and Click-iT EdU staining was performed according to the manufacturer's protocol. For quantification, images of the whole larval brain were captured using a Zeiss 700 confocal microscope. ImageJ was used to manually count the number of EdU positive cells.

Glucose Uptake Assay

Wandering L3 larvae of the following genotypes (*dpp*-Gal4 UAS-mCherry, UAS-*LDH*GFP >UAS-Pvr^{act,} *tn-/-*; *dpp*-Gal4 UAS-mCherry, UAS-*LDH*GFP> UAS-Pvr^{act}) were placed in *Drosophila* HL3 buffer (NaCl 70mM, KCl 5mM, $CaCl_2$ 1.5mM, $MgCl_2$ 20mM, $NaHCO_3$ 10mM, trehalose 5mM, sucrose 115mM, and Hepes 5mM (pH 7.2) on ice. Wing discs were dissected in ice cold PBS followed by incubation with 2-NBDG (2.5mg/mL, Cayman Chemical, Ann Arbor, MI) for 15 minutes at room temperature. The tissues were washed with 1X PBS twice, fixed and imaged. Similarly, for analyzing glucose uptake in larval brain, *WT* and *tn-/-* mutant brains were dissected and incubated with 2-NBDG as indicated above.

Food intake assay

Approximately 15-35 early L3 larvae of the indicated genotypes were fed on yeast paste with 0.16% Erioglaucine dye for 24 hours (ADITI *et al.* 2016). Post feeding larvae were pooled together and washed 3 times with distilled water. The pooled larvae were homogenized in 250 µL of ddH_2O, centrifuged at 15000rpm for 20 minutes. 225 µL of supernatant was carefully transferred to a 1.5mL tube containing 50 µL 100% ethanol and centrifuged for 10 minutes. 250 µL of the supernatant was placed in a new tube and centrifuged again for 5 minutes. Following centrifugation, 200 µL of the supernatant was placed in a 96 well crystal plate and the OD was measured at 633nm. Three groups of 15 larvae of each genotype were analyzed.

TUNEL Assay

For TUNEL labeling, fixed brains were treated with 20µg/mL Proteinase K in PBS for 20 minutes. For positive control, *WT* brains were incubated with 100µl of DNase (1U/ µl) for 10 minutes at room temperature post Proteinase K treatment. The tissues were rinsed three times with PBT, followed by a wash in 100µl terminal deoxynucleotidyltransferase (TdT) equilibration buffer (from the Kit, DeadEnd™ Fluorometric TUNEL System Promega). For the enzymatic reaction, a working solution of TdT enzyme (30%) with the reaction buffer (70%) was made and added to the tissues. The samples were then incubated for 2 hours in a 37◦C incubator and flickered every 30 minutes to mix the contents. The reaction was terminated by immersing the tissues in stop buffer (0.3 M NaCl/0.03 M sodium citrate) for 15 minutes at room temperature. DAPI (1:400) was used as a counterstain.

Results

TRIM32 binds to glycolytic enzymes

While NHL domain-containing proteins can interact with both RNAs and proteins (TOCCHINI and CIOSK 2015; WATANABE and HATAKEYAMA 2017), few bona fide TRIM32 binding partners have been identified. Causative mutations in human LGMD2H cluster in the NHL repeats (Fig. 1A) (FROSK *et al.* 2005; SCHOSER *et al.* 2005; BORG *et al.* 2009; COSSÉE *et al.* 2009; NERI *et al.* 2013; NECTOUX *et al.* 2015; LAZZARI *et al.* 2019), suggesting that this region may mediate protein-protein interactions important in disease prevention. We previously showed that mutations in *Drosophila* TRIM32 also show progressive larval muscle degeneration, despite modest sequence identity (~42%) across the NHL domains (LABEAU-DIMENNA *et al.* 2012b). To gain molecular-level insight into the functional conservation between the NHL regions in fly and mammalian TRIM32, we obtained a crystal structure of TRIM32_NHL at 2.6 Å resolution (Rwork/Rfree = 18.2/22.8%) (**Fig. 3.1 –figure supplement 3.1A-C; Fig. 1 –source data 1**). The structure was solved by molecular replacement, using the NHL-repeat region of the *Drosophila* Brat protein as a search model (PDB Code 1Q7F) (EDWARDS *et al.* 2003). This structure features a six-bladed β-propeller, where each NHL repeat is comprised of four antiparallel β-strands (**Fig. 3.1B; Fig. 1 – figure supplement 1C**). We then used the TRIM32_NHL structure to construct a model for mouse TRIM32_NHL using SWISS-MODEL. Indeed, the superimposition of these two structures demonstrate that the NHL region of *Drosophila* TRIM32 is a faithful model to understand NHL function (**Fig. 3.1B**).

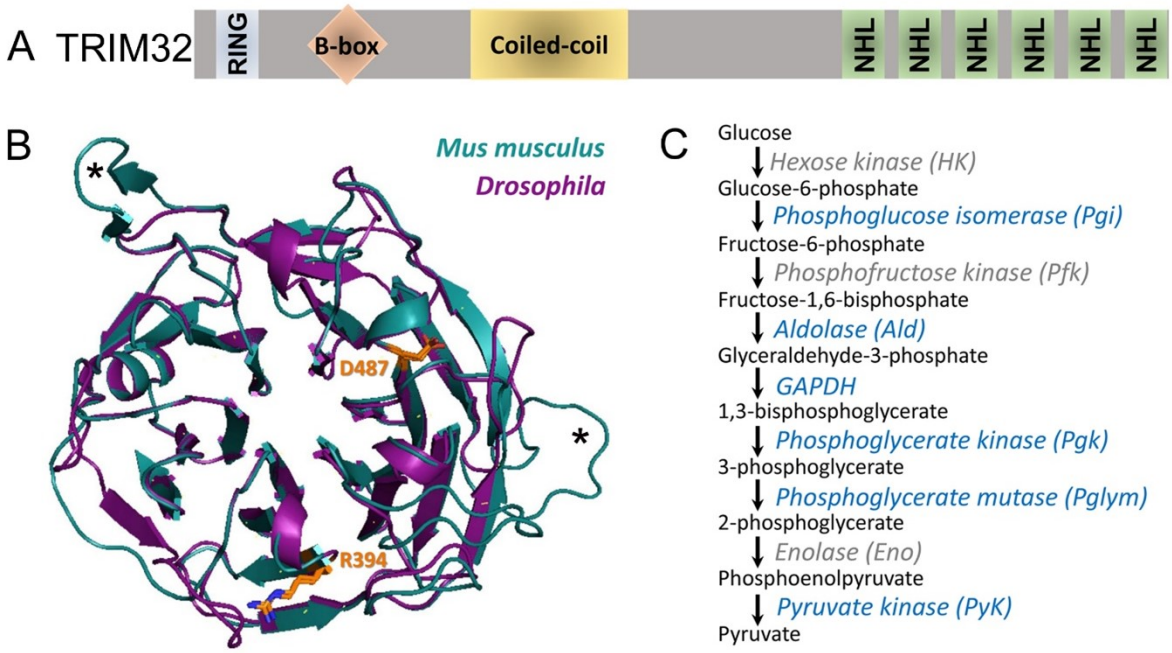

Figure 3.1: The NHL region of *Drosophila* TRIM32 is structurally conserved.

(A) Schematic showing the RING, B-box, coiled-coil, and NHL domains in TRIM32. (B) Superimposed protein structures of the six NHL repeats in *Drosophila* (magenta) and *Mus musculus* (blue) TRIM32. Each NHL repeat consists of four antiparallel beta sheets that are arranged toroidally around a central axis. Mouse NHL has two additional loops (asterisks) not present in the fly protein. The positions and orientation of both R394/R1114 and D487/D1211 are identical between *Mus musculus* and *Drosophila* (orange). (C) The glycolytic pathway. Peptides corresponding to enzymes that co-purified with TRIM32_NHL are shown in blue. See also Fig. 1 –figure supplement 1, Fig. 1–source data 1, and Fig. 1–source data 2.

To identify TRIM32_NHL-interacting proteins, we performed in vivo pulldowns followed by mass spectrometry (MS) to uncover associated peptides. Briefly, the C-terminal region of *Drosophila* TRIM32 containing all six NHL domains (AA 1061-1353) was fused in-frame with an N-terminal Glutathione S-transferase (GST) tag. This GST_TRIM32_NHL protein was expressed, purified, and incubated with third instar larval (L3) lysates. These resulting protein complexes were subjected to MS to detect peptide fragments that co-purify with TRIM32_NHL. In addition to the recovery of our bait protein, we detected peptides corresponding to Tropomyosin (Tm) and Troponin T (TnT) (**Fig. 3.1 –source data 2**), which are both known polyubiquitinated

substrates of mammalian TRIM32 (COHEN *et al.* 2012). Surprisingly, glycolytic enzymes were also enriched in the list of possible NHL binding proteins (**Fig. 3.1C; Fig. 3.1 –source data 2**) and were further evaluated for physical interactions with TRIM32.

We utilized two independent methods to validate candidate protein interactions with TRIM32. First, an *in vitro* binding assay using purified proteins was developed with Tropomyosin 2 (Tm2) as a positive control. Indeed, incubation of TRIM32_NHL together with His-tagged Tm2 confirmed a physical interaction between these two proteins (Fig. 2 –figure supplement 1A). This assay was then used to test for physical interactions with candidate glycolytic enzymes. To this end, we expressed and purified His-tagged Aldolase (Ald) or His-tagged Phosphoglycerate mutase 78 (Pglym), both of which were low or absent in control pulldowns. Both Ald and Pglym were found to directly interact with the NHL domains of TRIM32 (**Fig. 3.2A,B**). Note that no binding was detected between TRIM32_NHL and the His-tagged control protein SCIN, ruling out non-specific binding of the His tag. To extend these findings, we utilized immunoprecipitation experiments to test for in vivo interactions with full length TRIM32. As expected, immunoprecipitation of TRIM32 successfully pulled down Tm as an interacting protein at the predicted molecular weight of ~ 37 kD (**Fig. 3.2 –figure supplement 1B**). We also confirmed that both Ald and Pglym co-immunoprecipitate with anti-TRIM32 antibody. Interestingly, the bands corresponding to these proteins migrated at a higher molecular weight than the expected size present in input lysates (**Fig. 3.2C,D; asterisk**), suggestive of a post-translational modification. Two approaches were taken to confirm the specificity of the slower migrating bands that correspond to Ald or Pglym. First we concentrated L3 lysates before SDS-PAGE analysis. After overexposure of the Western blots, faint bands corresponding to the higher molecular weight forms of Ald or Pglym were present (**Fig. 3.2C,D; asterisk**). We also immunoprecipitated TRIM32 from

larval lysates and probed for Ald or Pglym using antibodies raised against the orthologous human proteins (ALD or PGAM1). While these antibodies did not cross react well in input lysates, there was an obvious band corresponding to the higher molecular weight forms of both Ald and Pglym after pulling down TRIM32 (**Fig. 3.2 –figure supplement 1D,E**). Collectively, these data demonstrate that Ald and Pglym interact with the NHL domain of TRIM32 and in vivo, a subpopulation of these post-translationally modified glycolytic enzymes can be found in a complex with TRIM32.

The majority of TRIM32 studies have focused on the biological impact of polyUb chain addition onto substrates (KUDRYASHOVA *et al.* 2005; LOCKE *et al.* 2009; COHEN *et al.* 2012; LIU *et al.* 2014; MOKHONOVA *et al.* 2015). This modification targets a protein for proteasomal degradation and usually increases protein substrate levels in the absence of its E3 counterpart. Indeed, the known mammalian substrate Tm binds to TRIM32_NHL (COHEN *et al.* 2012) and accordingly, *Drosophila* Tm was modestly increased in larvae mutant for *tn* (**Fig. 3.2 –figure supplement 1C**). Strikingly, this same loss of TRIM32 resulted in a ~50% decrease in the protein levels of Ald or Pglym78 (**Fig. 3.2E,F**). This downregulation was not due to a decrease in TRIM32-mediated transcription as mRNA levels of *Ald* or *Pglym* were not altered in *tn-/-* (**Fig. 3.2 –figure supplement1F,G**). Taken together, these data highlight a unique role for TRIM32 in the stabilization of glycolytic enzyme levels.

Loss of TRIM32 disrupts glycolytic metabolism in larval muscles

To understand the biological implications for the physical interaction between TRIM32 and the glycolytic enzymes Ald and Pglym, we profiled 85 metabolites present in *WT* or *tn-/-* L3 larvae.

Principal component analysis (PCA) revealed a distinct separation between *WT* and *tn-/-* experimental groups (**Fig. 3.3 –figure supplement 1A**). Examination of individual metabolites

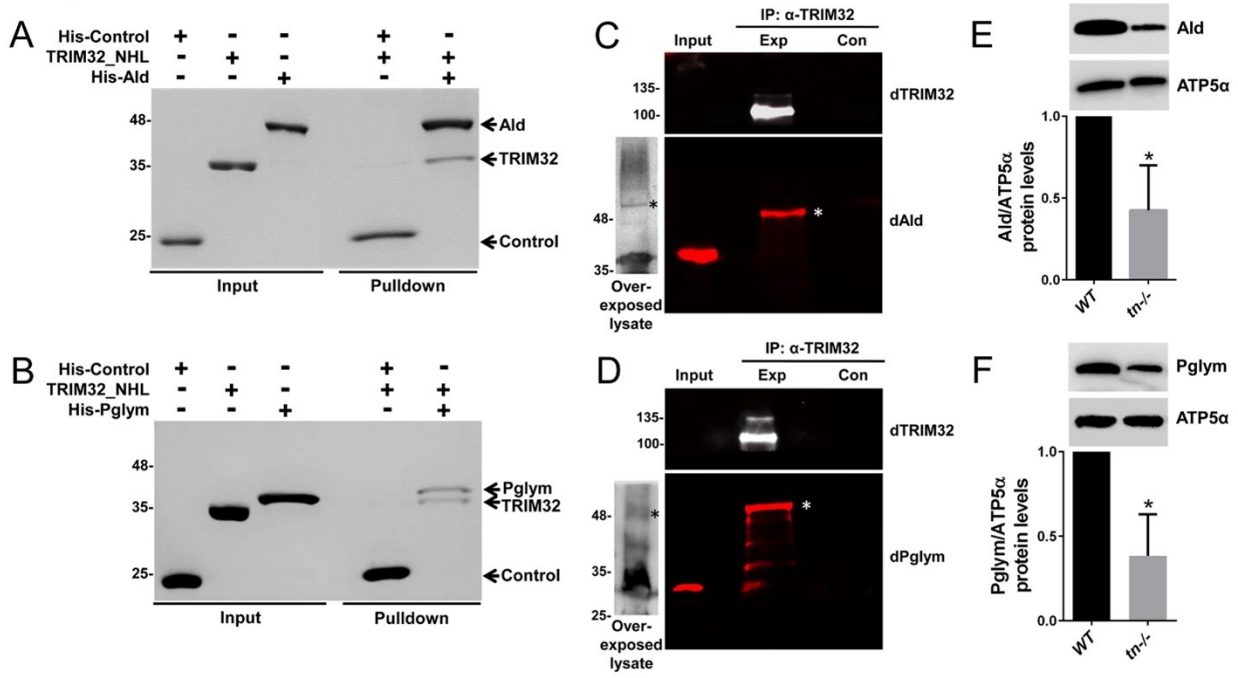

Figure 3.2: Drosophila TRIM32 physically interacts with the glycolytic enzymes Ald and Pglym78.

(A,B) *In vitro* binding assays. Untagged TRIM32_NHL was incubated with either the His-tagged SCIN control protein or the His-tagged candidate proteins Ald (A) or Pglym (B). After washing in 300mM NaCl and 0.1% Triton, each of these protein complexes was separated by SDS-PAGE followed by Coomassie staining. Ald and Pglym proteins directly bind the NHL region of TRIM32, while no interaction with the His-SCIN control protein is observed. (C,D) Western blotting with antibodies against *Drosophila* Ald (dAld; C) or *Drosophila* Pglym (dPglym; D) detects higher molecular weight bands (asterisk) upon immunoprecipitation of *Drosophila* TRIM32, but not in control lanes. The observed molecular weights of Ald or Pglym in input larval lysates (~30 µg) is predominant over a higher migrating form that can be visualized after overexposure of blots with concentrated lysate (~300 µg). (E,F) Western blots showing that mutations in *tn* reduce Ald (E) or Pglym (F) protein levels ~50% quantitated relative to ATP5α in L3 larvae. N=3. Mean +/- SD (*, $p < 0.05$). See also Fig. 2–figure supplement 1.

upon loss of TRIM32 showed a decrease in the terminal glycolytic products pyruvate and lactate as well as significant depletion of the glucose-derived metabolites glycerol-3-phosphate and 2-

hydroxyglutarate (**Fig. 3.3A,B**). These metabolic changes suggest that TRIM32 is required for sustaining the conversion of glucose to pyruvate and lactate in L3 larvae.

The production of pyruvate at the end of glycolysis has two fates, either a reduction to lactate or oxidation to CO_2 in the mitochondrion (TESLAA and TEITELL 2014; MOOKERJEE *et al.* 2015). To determine if reduced lactate levels in *tn-/-* results in increased respiration and therefore elevated ATP synthesis, we assessed these two outputs of overall energy metabolism in control or mutant whole larvae. Respirometry analysis revealed a modest increase in CO_2 production upon loss of TRIM32 (**Fig. 3.3 –figure supplement 1B**). However, ATP levels were significantly decreased in *tn-/-* larvae (**Fig. 3.3 –figure supplement 1C**). Given that different larval tissues may have altered metabolic profiles that influence outputs of whole body metabolism, we sought to assess glycolytic activity in individual tissues.

A unique aspect of *Drosophila* larval development is the 200-fold increase in body size from first instar (L1) larvae through the L3 stage. In order to support high levels of biomass accumulation, glycolytic metabolism is increased prior to larval growth (TENNESSEN *et al.* 2011; TENNESSEN *et al.* 2014b). One larval tissue that requires high glycolytic activity is the somatic musculature, where *WT* body wall muscles undergo dramatic growth as development proceeds from second instar larvae (L2) **(Fig. 3.3C,G**) to the L3 stage **(Fig. 3.3D,G**). We, and others, previously reported a loss of structural integrity in TRIM32-deficient muscles (LABEAU-DIMENNA *et al.* 2012b; DOMSCH *et al.* 2013) and assumed that the associated reduction in muscle size was a secondary consequence of progressive tissue degeneration. While multiple independent alleles of *tn* have been shown to produce smaller muscles (LABEAU-DIMENNA *et al.* 2012b; DOMSCH *et al.* 2013), quantification of $tn^{\Delta A}$/ $tn^{\Delta A}$ mutants (*tn-/-*) confirmed a decrease in larval muscle diameter in both

L2 (**Fig. 3.3E,G**) and L3 individuals (**Fig. 3.3F,G**). Thus, loss of TRIM32 compromises the glycolytic-driven growth of muscles during larval development.

As an initial assessment of glycolytic activity, we measured the extracellular acidification rate (ECAR) in *WT* or *tn-/-* muscle carcasses using the Agilent Seahorse XFe96 Analyzer. Since a major contributor to extracellular acidification is lactate excretion into medium during glycolysis (TESLAA and TEITELL 2014; MOOKERJEE and BRAND 2015), we anticipated, and indeed, observed a reduction in ECAR upon loss of TRIM32 (**Fig. 3.3H**). While quantitative, end-point assays such as ECAR, only measure a population of muscles at a single time point. For real-time measurements of glycolytic flux, the Xe96 Analyzer was used to calculate the proton efflux rate (PER). This assay specifically provides a measurement of protons derived from glycolysis by correcting for both the production of protons derived from mitochondrial reactions and for the buffering capacity of the assay medium. Briefly, the assay measures ECAR of the system under three conditions: (1) without manipulation, (2) following addition of the electron transport chain inhibitors rotenone and antimycin A, and (3) after addition of the glycolytic inhibitor 2-deoxy-D-glucose (2-DG). The end result of the assay is a measurement of acidification rate largely due to glycolytic sources. Our analysis revealed that glycolytic metabolism produces fewer protons in *tn-/-* muscle carcasses as compared with *WT* controls (**Fig. 3.3I**), thus supporting our hypothesis that TRIM32 is required to support glycolytic flux.

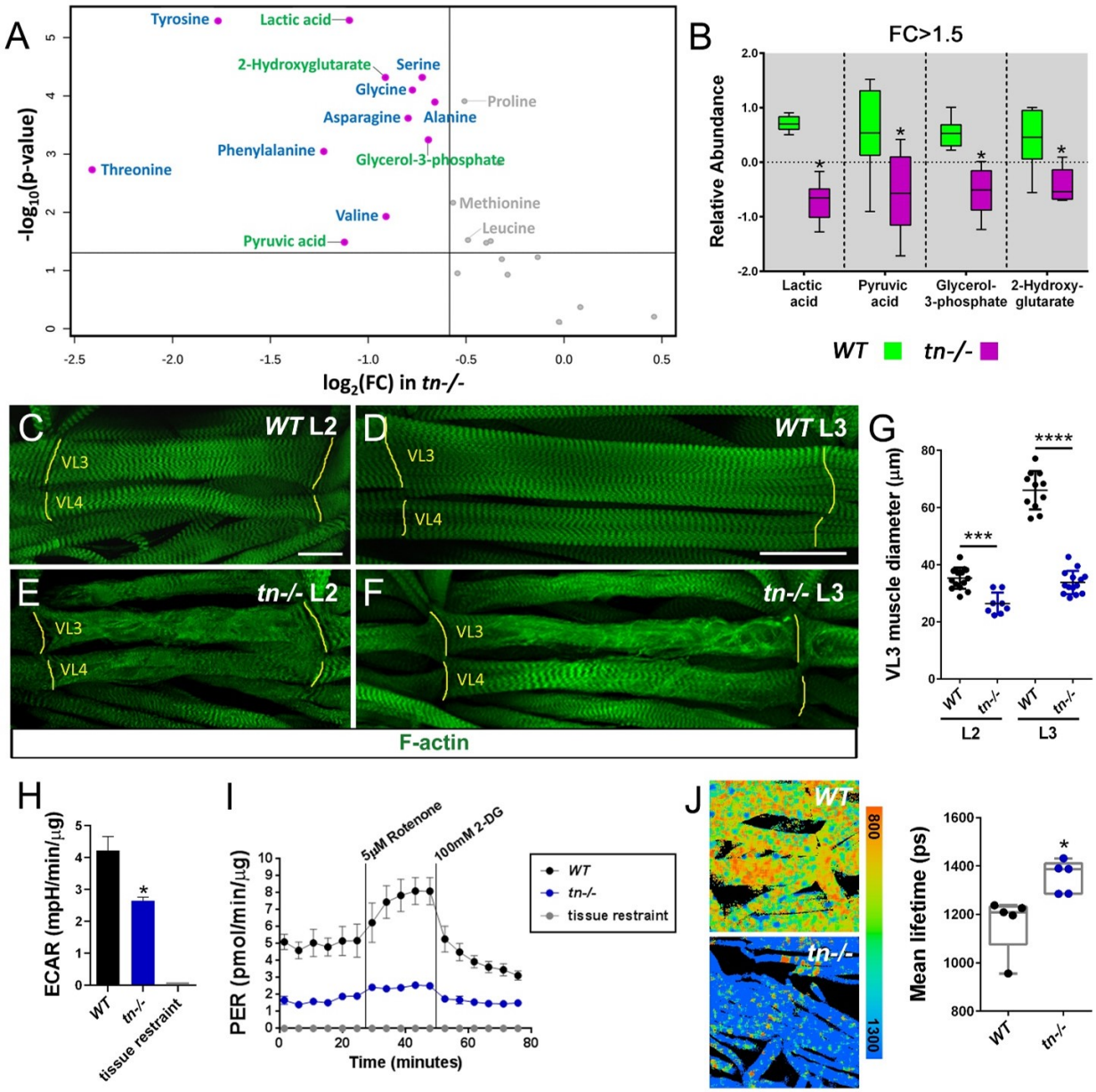

Figure 3.3: *Loss of* TRIM32 decreases glycolytic flux and reduces muscle tissue size.

(A) Volcano plot illustrating fold change (FC) (log base 2) compared with p-value (- log base 10) between *WT* and *tn-/-* L3 larvae. Vertical line represents FC>1.5. Horizontal line depicts a significance level $p<0.05$. Metabolites that are reduced in *tn-/-* larvae include indicators of glycolytic flux (green) and amino acids (blue). Metabolites in gray are significant, but exhibit a FC < 1.5. (B) Box and whisker plot of terminal glycolytic metabolites significantly reduced upon loss of TRIM32. N=6. (C-F) Ventral longitudinal muscles 3 (VL3) and 4 (VL4) stained with phalloidin to visualize F-actin (green). (C,D) The stereotypical morphology of *WT* muscles is not altered as overall muscle size increases from the L2 (C) to the L3 (D) stage. (E,F) In addition to sarcomeric disorganization, the VL3 and VL4 muscles are noticeably smaller in *tn-/-* larvae during L2 (E) and L3 (F) development. Muscle attachment sites (MASs) are denoted by yellow lines. (G)

Scatter plot depicting VL3 muscle diameter. The diameter of *WT* muscles increase from the L2 to the L3 stage. This cell size increase is abolished in *tn-/-*. N≥8. (H) Bar graph shows that ECAR measurements are decreased in isolated *tn-/-* muscle carcasses compared to *WT*. N≥4. (I) Analysis of the glycolytic rate in *WT* or *tn-/-* muscle tissue after subtraction of mitochondrial-produced acidification. This PER is diminished upon loss of TRIM32. N=4. (J) NADH lifetime image comparison of *WT* and *tn-/-* muscles. Box and whisker plot shows *WT* muscles have significantly lower NADH lifetime, indicative of higher glycolytic flux, than *tn-/-*. N=5. Mean +/- SD. (****, $p < 0.001$; ***, $p < 0.01$; *, $p < 0.05$; n.s., not significant). Scale bars: 25μm (C,E), 50μm (D,F). See also **Fig. 3–figure supplement 1.**

To independently validate that loss of TRIM32 results in decreased glycolytic flux, we directly measured NADH levels within muscle tissues using fluorescence lifetime imaging (FLIM), which exploits the fluorescent characteristic of this cofactor to visualize NADH levels in cellular microenvironments (PROVENZANO *et al.* 2009; SZASZÁK *et al.* 2011; YASEEN *et al.* 2017; MARTIN *et al.* 2018). Since the fluorescent lifetime of NADH (the time required for NADH to decay when exposed to 740 nm wavelength light) is longer when NADH is bound to mitochondrial enzymes than in the free state, this assay can distinguish intracellular NADH pools (BIRD *et al.* 2005; SKALA *et al.* 2007). This analysis revealed that *WT* muscles analyzed by FLIM showed a markedly shorter lifetime than *tn-/-* muscles (**Fig. 3.3J**). Since free, unbound NADH is predominate in highly glycolytic cells, here we confirm a reduction in the glycolytic profile upon loss of TRIM32. These data, taken together, strongly support the hypothesis that TRIM32 maintains glycolytic flux in larval muscle tissue.

One consequence of analyzing *tn* mutant alleles is the possibility that the observed muscle defects result from loss of TRIM32 in other tissues. To rule out TRIM32-mediated systemic defects, we utilized tissue-specific RNAi approaches (BRAND and PERRIMON 1993). First, we reconfirmed that induction of three independent RNAi constructs targeting *tn mRNA* transcripts with the *mef2*-Gal4 muscle driver produced smaller muscles (**Fig. 3.4A,B,D**) (LABEAU-DIMENNA *et al.* 2012b; DOMSCH *et al.* 2013; BROOKS *et al.* 2016). Knockdown of TRIM32 in a single muscle (5053-

Gal4>*tn RNAi*, asterisk) within each hemisegment was sufficient to reduce muscle cell size (**Fig. 3.4C**). As a proxy to monitor glycolytic activity, we assayed L-lactate levels in muscle carcasses. Consistent with our metabolomics data, the relative concentration of lactate levels was decreased in *tn-/-* muscles (**Fig. 3.4E**). Induction of *tn RNAi* in muscle tissue (*mef2>tn RNAi*) decreased lactate levels, while this same reduction did not occur upon TRIM32 knockdown in neurons (*elav>tn RNAi*). Here we conclude that TRIM32-mediated regulation of glycolysis in muscle tissue is cell autonomous.

Estrogen-related receptor (ERR) is a nuclear hormone receptor that acts as a transcriptional switch in embryogenesis to induce genes required for aerobic glycolysis during larval growth (TENNESSEN *et al.* 2011). Therefore, we posited that genetic upregulation of carbohydrate metabolism genes via ERR may improve muscle growth and function. As a positive control, we expressed a cDNA encoding for TRIM32 in *tn-/-* muscle tissue (*tn-/-; mef>TRIM32*) and found that the muscle diameter was restored to *WT* (**Fig. 3.4F**). This result also confirmed the cell autonomy of TRIM32. Overexpression of ERR in *tn-/-* muscles not only improved muscle size (**Fig. 3.4F**), but also corrected the functional deficit associated with the inability of *tn-/-* to contract body wall muscles during pupal morphogenesis (**Fig. 3.4G,H**) (LABEAU-DIMENNA *et al.* 2012b; DOMSCH *et al.* 2013). Importantly, protein levels of Ald and Pglym were stabilized upon expression of ERR in *tn-/-* muscles (**Fig. 3.4I,J**), indicating that restoration of glycolytic protein levels is sufficient to recover TRIM32-mediated growth defects.

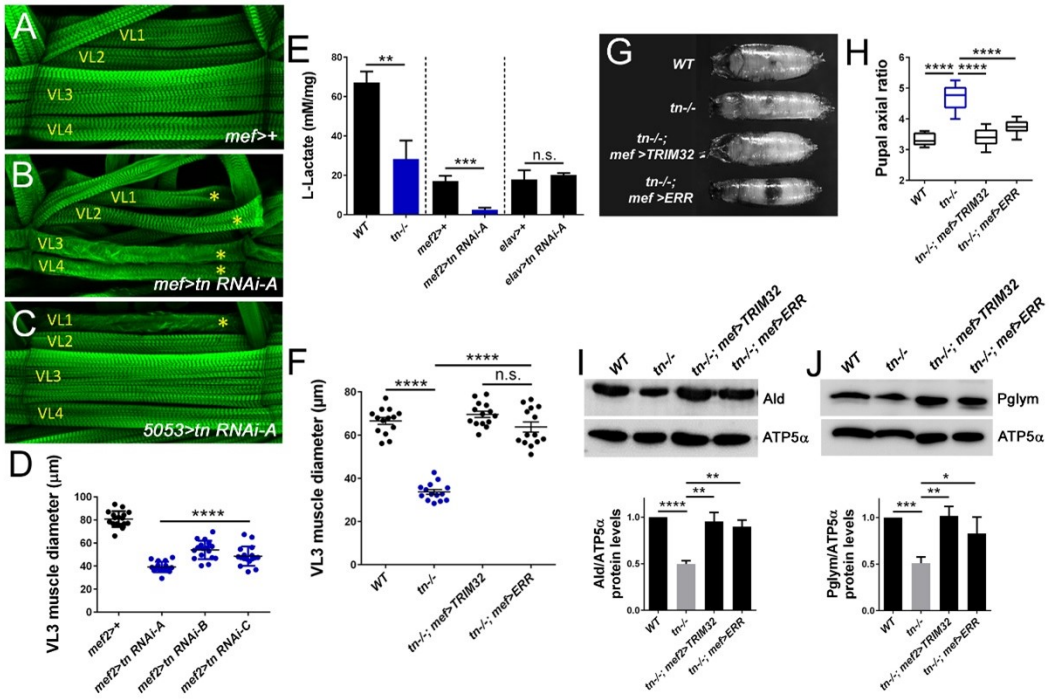

Figure 3.4: Muscle defects are cell autonomous and can be rescued upon stabilization of glycolytic enzyme levels.

(A-E) Knockdown of TRIM32 in muscle tissue decreases muscle size and reduces lactate levels. (A-C) Phalloidin-labeled VL1-4 muscles in a representative hemisegment of the indicated genotypes. (A) *mef2*>+ control muscles appear *WT*. (B,C) RNAi knockdown of *tn* in all muscles with *mef2*-Gal4 (B) or only muscle VL1 using the *5053*-Gal4 driver (C) show a reduction in muscle size (asterisk). (D) Knockdown of *tn* mRNA transcripts with three independent UAS-*tn RNAi* constructs in muscle tissue under control of the *mef2* promoter (*mef2>tn RNAi*) show reduced VL3 muscle diameter compared to *mef2/+* VL3 muscles. N≥10. (E) Bar graph reveals a cell autonomous role for TRIM32 in muscle tissue. L-lactate levels in muscle carcasses are decreased upon loss of TRIM32 in all tissues. Induction of *tn RNAi* in muscle, but not neuronal tissue, reduces the concentration of muscle-derived lactate. N>8. (F-J) Muscle-specific expression of TRIM32 (*tn-/-, mef>TRIM32*) or ERR (*tn-/-, mef>ERR*) in a *tn-/-* background attenuates the loss of muscle size, muscle contraction, and stabilizes glycolytic protein levels. (F) Scatter plot shows that the reduced VL3 muscle diameter upon loss of TRIM32 is restored upon expression of TRIM32 or ERR in muscle tissue. N≥10. (G,H) The inability to contract body wall muscles in *tn-/-* causes elongated pupae. Muscle-specific expression of TRIM32 or ERR restores muscle contraction. (G) Representative pupal cases of the indicated genotypes. (H) Quantitation of pupal axial ratios represented by a box and whisker plot. N=10. (I,J) Western blots showing the relative amounts of Ald or Pglym protein relative to the ATP5α loading control. Both Ald and Pglym protein levels are stabilized upon TRIM32 or ERR expression in muscle tissue compared to *tn-/-*. N=3. Mean +/- SD (****, p<0.001; ***, p< 0.01; **, p< 0.05; *, p< 0.01; n.s., not significant).

TRIM32 maintains amino acid pools

Our metabolomics analysis revealed that loss of TRIM32 not only disrupts the production of glycolytic intermediates, but also induces a significant decrease in eleven of the twenty amino acids (**Fig. 3.5A**). These changes in amino acid abundance are likely due to both decreased synthesis and increased catabolism (**Fig. 3.3 –figure supplement 1D**), as we observed that *tn-/-* exhibited a >1.5 decrease in not only serine and glycine levels which are normally synthesized from glucose, but also a reduction in the anaplerotic amino acids proline and aspartic acid. Moreover, loss of TRIM32 also induced a significant depletion of alanine, which is both synthesized from and catabolized into pyruvate. Overall, the metabolomic profile of *tn-/-* indicates that disruption of glucose catabolism results in depletion of larval amino acid pools, raising the possibility that decreased amino acid availability contributes to the *tn-/-* muscle defects. We tested this possibility by supplementing the diets of both mutant and control larvae with amino acid sources. As an initial approach, we first determined if the *tn-/-* larval phenotype exhibited enhanced sensitivity to nutrient deprivation. Indeed, when reared on starvation media, the muscle diameter of *tn* mutants was smaller than muscles of control larvae raised on the same media (**Fig. 3.5B,C,F**). In contrast, mutant larvae fed a diet consisting of only yeast extract or supplemented with all 20 amino acids exhibited no decrease in muscle diameter (**Fig. 3.5D,E,F**). We observed similar results in the context of L3 body mass and muscle contraction during the larval to pupal transition, whereby *tn-/-* raised on an agar only diet exhibited dramatically more severe phenotypes compared with *WT* control larvae (**Fig. 3.5G,H,I**). Supplementation of the larval diet with yeast extract or amino acids, however, suppressed both phenotypes in *tn-/-* (**Fig. 3.5G,H,I**). These results suggest that *tn-/-* mutants are uniquely sensitive to dietary amino acids, consistent with the smaller amino acid pool size observed upon loss of TRIM32.

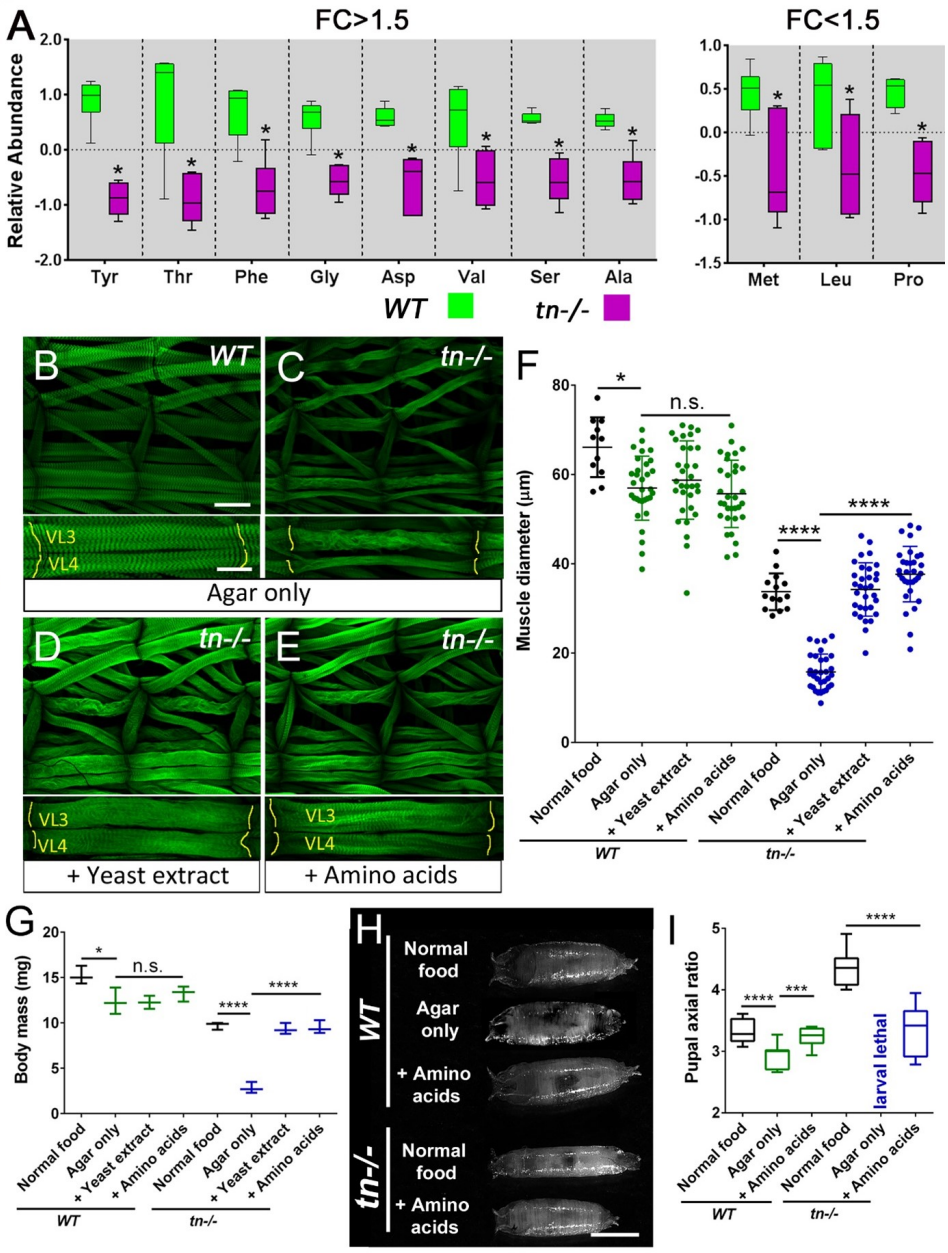

Figure 3.5: Amino acid supplementation is sufficient to improve *tn-/-* muscle mass.

(A) Box and whisker plots showing the relative abundance of individual amino acids in L3 larvae with a FC>1.5 (left panel) or FC<1.5 (right panel) that are significantly reduced upon loss of TRIM32. N=6. (B-E) Maximum intensity projections of *WT* (B) or *tn-/-* (C-E) L3 muscles stained for F-actin. Upper panel depicts two complete hemisegments and lower panel focuses on the VL3 and VL4 muscles. Muscle attachment sites (MASs) are denoted by yellow lines. (B) An example of thinner *WT* musculature reared on agar as a sole nutritional source. (C) Muscles in larvae deficient for TRIM32 are substantially thinner when raised on agar alone. (D,E) Suppression of the reduced muscle diameter is observed in *tn-/-* muscles supplemented with total yeast extract (D) or amino acids (E) compared to *tn-/-* muscles alone. (F) Scatter plot showing the diameter of muscle VL3 in *WT* or *tn-/-* exposed to the indicated nutritional diets. N≥32. (G) Average body

mass measurements of *WT* or *tn-/-* L3 larvae. Ten individuals were weighed for each biological replicate that was performed in triplicate. (H) Representative pupal cases grown on the indicated diets. (I) The axial ratio (length/width) of pupal cases represented by box and whisker plots. N≥10. Mean +/- SD. (****, p< 0.001; *, p< 0.05; n.s., not significant). Scale bars: 100 μm (A-D, upper panel), 50 μm (A-D, lower panel), 1 mm (G)

TRIM32 regulates glycolysis in a diversity of tissues

LDH expression generally correlates with LDH activity and increased glycolytic flux (ŽDRALEVIĆ *et al.* 2017; TANNER *et al.* 2018). Only a few larval tissues show high LDH activity and exhibit elevated glycolytic rates (LI *et al.* 2017; EICHENLAUB *et al.* 2018), including muscle and the larval brain (Fig. 3.6 –figure supplement 1A). Since we already established that *tn-/-* muscles were smaller, we wondered if growth of the larval brain also requires TRIM32. The overall size of larval brains dissected from *WT* (Fig. 3.6A) or *tn-/-* (**Fig. 3.6B**) L3 individuals showed a dramatic size difference, whereby loss of TRIM32 reduced the average area of the larval brain by ~40% (Fig. 3.6G). To determine if a brain-specific reduction in TRIM32 is cell autonomous, we induced two independent *tn RNAi* lines in both neuronal (*elav>tn RNAi*) and muscle tissue (*mef2>tn RNAi*). As expected, reduced larval brain size was observed upon RNAi knockdown of TRIM32 with *elav*-Gal4 (**Fig. 3.6C,D,G**), but not with the *mef2* driver (**Fig. 3.6E-G**).

Increased biomass accumulation is a primary mechanism for the hypertrophic growth of post-mitotic larval muscles (DEMONTIS and PERRIMON 2009), while larval brain development requires both cell growth and cell proliferation (HARTENSTEIN *et al.* 2008). Thus, we wondered whether the TRIM32-mediated reduction in brain size was associated with altered glycolytic activity that reduced cell growth. Two experiments were performed to assess the glycolytic state in larval brain tissue. PER analysis (NEVILLE *et al.* 2018) of individual larval brains isolated from *tn-/-* showed a reduced glycolytic rate compared to their *WT* counterparts (**Fig. 3.6H**). Consistent with reduced substrate flux through the glycolytic pathway, L-lactate levels were also lower in dissected *tn-/-*

larval brains (Fig. 3.6I). Tissue-specific knockdown experiments verified that decreased lactate levels in larval brains resulted from inducing *tn RNAi* in neuronal, but not muscle tissue (Fig. 3.6I). Next we assessed how lower glycolytic activity affects overall larval brain size. Defective cell proliferation (assayed by EdU incorporation) or increased cell death (assessed using TUNEL labeling and cleaved-Caspase3 immunoreactivity) did not account for the overall brain size reduction (Fig. 3.6 –figure supplement 1B-I). Quantitation of individual brain cell size revealed a marked reduction upon loss of TRIM32 (**Fig. 3.6 –figure supplement 1J-M**) consistent with an increase in cell size as the primary mechanism for TRIM32-mediated tissue growth.

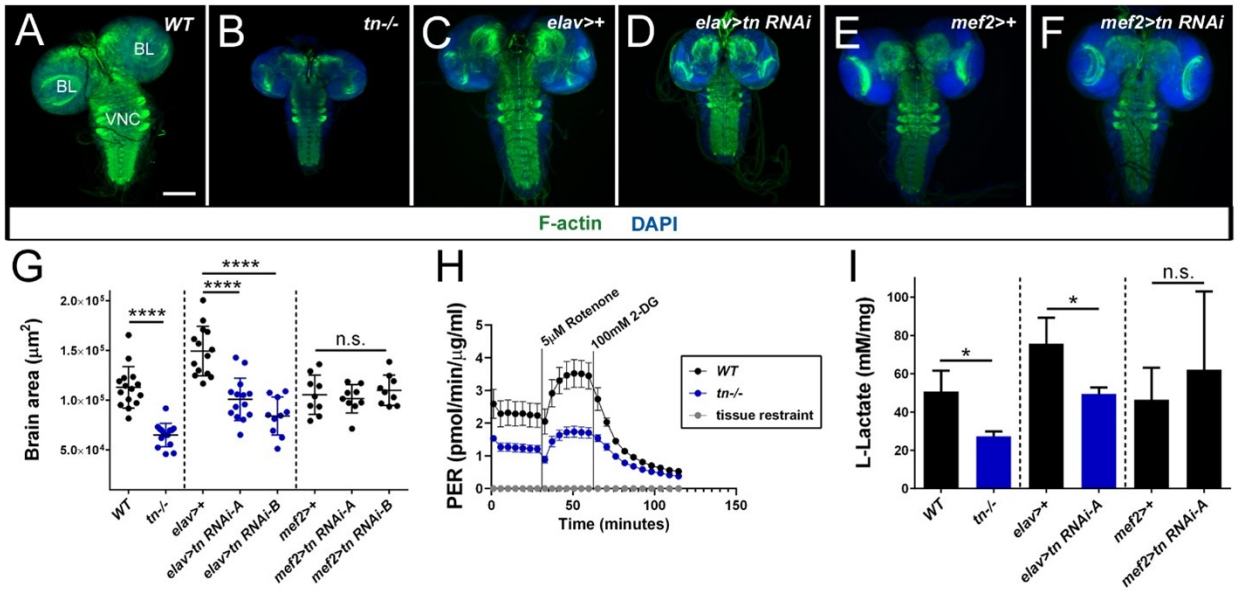

Figure 3.6: TRIM32 maintains glycolytic-mediated growth in the larval brain.

(A-F) L3 larval brains labeled with DAPI (blue) and F-actin (green). (A) A representative micrograph of a *WT* larval brain showing the individual brain lobes (BL) and the ventral nerve cord (VNC). (B) The overall size of *tn-/-* brains is reduced due to mutations in *tn*. (C) Control brains expressing the pan-neuronal *elav*-Gal4 driver. (D) RNAi knockdown of *tn* in neurons under control of the *elav* promoter causes smaller brains. (E,F) Expression of *mef2*-Gal4 alone (E) or *mef2>tn RNAi* in muscle tissue does not alter brain size (F). (G) Scatter plot depicting the entire brain area (including the BL and VNC) of *WT*, *tn-/-,* Gal4 driver controls, or tissue-specific *tn RNAi* knockdown brains. N≥9. (H) Glycolytic rate assay shows a reduction in the proton efflux rate (PER) upon loss of TRIM32 in isolated L3 larval brains. The glycolytic rate is calculated after subtraction of mitochondrial-produced acidification. N=4. (I) Bar graph representing L-lactate levels in isolated larval brain tissue. Only loss of TRIM32 in brain, but not muscle tissue, caused

a reduction in L-lactate levels. N≥15. Scale bar: 100 μm (A-F). Mean +/- SD. (****, p< 0.001; ***, p < 0.01; n.s., not significant). See also **Fig. 6 –figure supplement 1.**

The elevated glycolytic rate that operates in larval muscle and brain tissue is analogous to the Warburg effect in rapidly proliferating cancer cells (TENNESSEN *et al.* 2014b; LI *et al.* 2017), whereby glucose metabolism is used to synthesize amino acids and other metabolites required for cell growth (LUNT and VANDER HEIDEN 2011; LIBERTI and LOCASALE 2016b). Thus, we hypothesized that TRIM32 could be a general regulator of highly glycolytic tumor cells. Unlike muscle or brain tissue, neither LDH activity (WANG *et al.* 2016a) nor LDH-GFP expression (**Fig. 3.7A**) were detectable in control wing discs, suggesting that this tissue does not exhibit elevated glycolytic activity. Accordingly, loss of TRIM32 did not alter the volume (**Fig. 3.7D**) or area (**Fig. 3.7 –figure supplement 1A-C**) of mutant discs compared to *WT* control discs. Moreover, measurements of glycolytic flux using either PER assays (**Fig. 3.7 –figure supplement 1D**) or FILM analysis confirmed that TRIM32-deficient wing discs (**Fig. 3.7F,G**) did not show altered glycolytic activity. To examine the possibility that TRIM32 regulates the growth of highly glycolytic tumor cells, we confirmed that overexpression of the activated platelet PDGF/VEGF receptor (Pvr^{act}) in *dpp*-expressing wing disc cells increased LDH-GFP expression and promoted tissue overgrowth (**Fig. 7B,D; Fig. 7 –figure supplement 1C**) (WANG *et al.* 2016a). Remarkably, removal of TRIM32 caused smaller tumors, effectively reducing the overall size of the wing disc (**Fig. 7C,D; Fig 7– figure supplement 1C**). Analysis of LDH-GFP expression revealed biological variability as ~50% of TRIM32-deficient wing discs lost LDH-GFP expression (**Fig 7E**). FILM analysis validated a decrease in the glycolytic activity of tumors grown in *tn-/-* larvae compared to Pvr-induced tumors in both normal and tumorous glycolytic tissues, thus providing a novel molecular explanation for the upregulation of TRIM32 in multiple types of cancer cells.

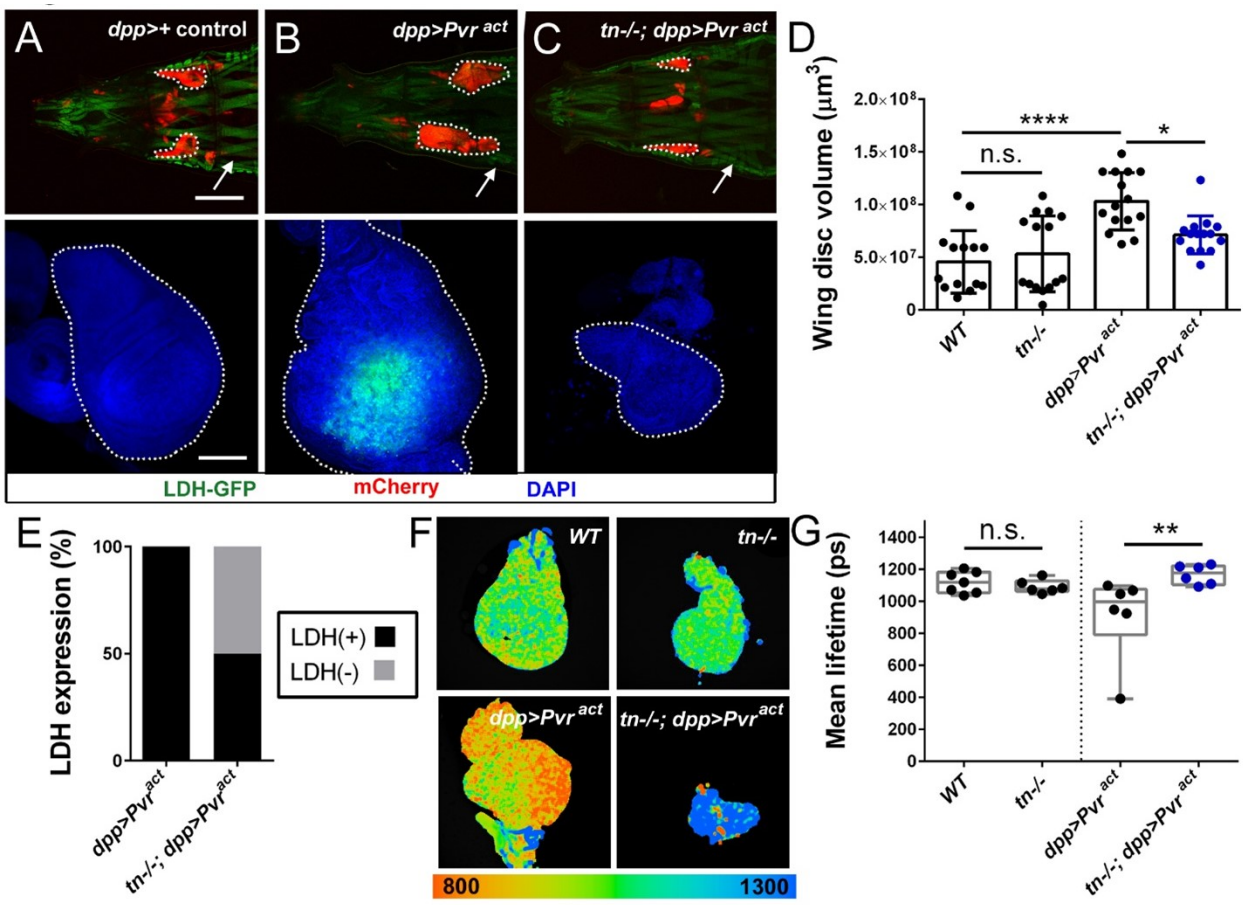

Figure 3.7: Loss of *TRIM32* reduces *Pvr*-induced glycolytic tumor growth.

(A-C) Either intact (upper panel; red) or isolated (lower panel, blue) wing discs from L3 larvae of the indicated genotypes. LDH-GFP is high in somatic muscles (white arrow). Wing discs are outlined (white dotted outlines). (A) The normal size and shape of control *dpp-Gal4/+* wing discs. (B) Overexpression of the activated Pvr receptor (*dpp>Pvr^{act}*) causes tissue overgrowth and an increase in LDH-GFP expression (green). (C) Tumor growth in a *tn-/-* host is dramatically reduced in size. (D) Overall wing disc volumes are represented in this column plot. N≥15. (E) Approximately 50% of LDH-GFP(+) cells induced by activated Pvr expression is reduced upon loss of TRIM32. N=20. (F) Representative fluorescence lifetime micrographs of control (*WT* or *tn-/-*) or tumorous (*dpp>Pvr^{act}* or *tn-/-; dpp>Pvr^{act}*) wing discs. (G) Box and whisker plot confirms no difference in the glycolytic profile between *WT* or *tn-/-* discs. The decreased lifetime in *dpp>Pvr^{act}* discs, indicative of higher glycolytic flux, is reduced upon loss of TRIM32. N=6. Mean +/- SD. (****, $p < 0.001$; *, $p < 0.05$; n.s., not significant). Scale bars: 0.5 mm (A-C, upper panels), 100 µm (A-C, lower panels). See also **Fig. 7 –figure supplement 1** and **Fig. 7 –figure supplement 2.**

DISCUSSION

A unique feature of *Drosophila* larval development is the inherent glycolytic nature of muscle and brain tissue (TIXIER *et al.* 2013; TENNESSEN *et al.* 2014b; LI *et al.* 2017), which promotes biomass synthesis during this stage of rapid organismal growth. Maintenance of such a high metabolic rate predicts that enzymes are present at sufficient concentrations in the cell to mediate the rapid shunting of intermediates through the pathway (MENARD *et al.* 2014). We show here that TRIM32 directly interacts with and maintains the levels of two glycolytic enzymes. Decreased protein levels of both Ald and Pglym (and possibly other glycolytic enzymes) cripple this rapid flux, effectively blunting the generation of metabolic intermediates that contribute to anabolic synthesis necessary to sustain cell growth (**Fig. 8**).

An alternative mechanism that limits cell and tissue growth is nutrient deprivation (AHMAD *et al.* 2018). In many organisms, the insulin/target of rapamycin (TOR) pathways integrate nutritional signals to physiologically control body size (HYUN 2013). Implicit in this mechanism is the scaling of individual organs. Four pieces of evidence refute nutritional status as a mechanism for TRIM32-mediated tissue growth. First, the overall body size of *tn* mutant pupae is not smaller than their *WT* counterparts under starvation conditions, but instead elongated due to defective muscle contraction (LABEAU-DIMENNA *et al.* 2012b; DOMSCH *et al.* 2013) (**Fig. 3.4G,H; Fig. 3.5H,I**). Second, the size of the wing disc and midgut, both tissues that show reduced growth in poorly fed larvae, is not altered upon loss of TRIM32 (**Fig. 3.7D; Fig 3.7 –figure supplement 1A-C; Fig 3.7 –figure supplement 2F-H**). Surprisingly, cellular glucose uptake assayed by the non-metabolizable fluorescent glucose analog 2-[*N*-(7-nitrobenz-2-oxa-1,3-diazol-4-yl)amino]-2-deoxyglucose (2-NBDG), was normal in *tn-/-* larval brains and wing disc-derived tumors (**Fig. 3.7 –figure supplement 2A-D**), demonstrating that glucose is not a limiting substrate for glycolysis in isolated

tn-/- tissues. Finally, even though systemic effects compromise feeding in *tn-/-* whole larvae (**Fig. 3.7 –figure supplement 2E**), food intake remained constant upon tissue-specific knockdown of TRIM32 in muscle or brains that show reduced tissue growth (**Fig. 3.7 –figure supplement 2I,J**). Collectively, these data demonstrate that TRIM32 functions in a cell autonomous manner to regulate tissue growth, independent of systemic nutritional status.

Li, et al., recently reported that pathways controlling lactate and glycerol-3-phosphate metabolism function redundantly in larval growth (LI *et al.* 2019). Removal of LDH and hence lactate production caused an increase in glycerol-3-phosphate, which was sufficient to maintain larval redox balance. Since both LDH and GPDH1 regulate redox balance necessary for maintaining high glycolytic flux to promote biomass accumulation, *Ldh, Gpdh1* double mutants exhibit severe growth defects with reduced brain size. Our results show that loss of TRIM32 decreases both lactate and glycerol-3-phosphate levels (**Fig. 3.3A,B**), thus mimicking the reduced carbohydrate metabolism in *Ldh, Gpdh1* double mutants.

It is not clear how mutations in a ubiquitously expressed protein such as TRIM32 result in tissue-specific diseases. One prediction is that TRIM32 differentially interacts with proteins in diverse cell types to elicit distinct biological outputs. There is strong evidence to support this hypothesis in the context of LGMD2H. TRIM32 is upregulated in proliferating satellite cells and loss of this protein prevents myotube regeneration, partially through the misregulation of NDRG and c-Myc (KUDRYASHOVA *et al.* 2012; NICKLAS *et al.* 2012; MOKHONOVA *et al.* 2015; SERVIÁN-MORILLA *et al.* 2019). Muscle-specific targets that contribute to disease progression are less clear. TRIM32-mediated deregulation of key muscle substrates, including actin, α-actinin, tropomyosin, and desmin, contribute to muscle atrophy (KUDRYASHOVA *et al.* 2005; LOCKE *et al.* 2009; COHEN *et al.* 2012; COHEN *et al.* 2014), but studies have not been performed to directly test this model in the

context of LGMD2H. Interestingly, mammalian glycolytic type II fibers are preferentially affected over oxidative type I fibers in muscle atrophy induced by aging/starvation, as well as in Duchenne's and Becker muscular dystrophies (DMD) (CICILIOT *et al.* 2013; PANT *et al.* 2015). *TRIM32 KO* muscles also show a decrease in the glycolytic proteins GAPDH and PyK (MOKHONOVA *et al.* 2015), just as we observe a reduction in Ald and Pglym levels in *tn-/-* muscles, suggesting that TRIM32-mediated regulation of glycolysis may be a general mechanism that underlies some muscular dystrophies.

The multi-faceted roles exhibited by TRIM32 in muscle physiology and cancer seem quite different on the surface. However, control of glycolytic flux may be a common mode of regulation that has been overlooked. As in muscle tissue, the majority of studies on TRIM32 and cancer have focused on identifying substrates that are subject to poly-ubiquitination and subsequent proteasomal degradation. Piasy, p53 and Abi2 are known targets of TRIM32 E3 activity that regulate the proliferative balance in cancer cells (ALBOR *et al.* 2006; KANO *et al.* 2008; LIU *et al.* 2014). The proteolytic turnover of these proteins may affect signaling pathways independent of glycolytic TRIM32 regulation or may be a compensatory mechanism in response to metabolic shifts in which normal cells can transiently adopt cancer-like metabolism during periods of rapid proliferation.

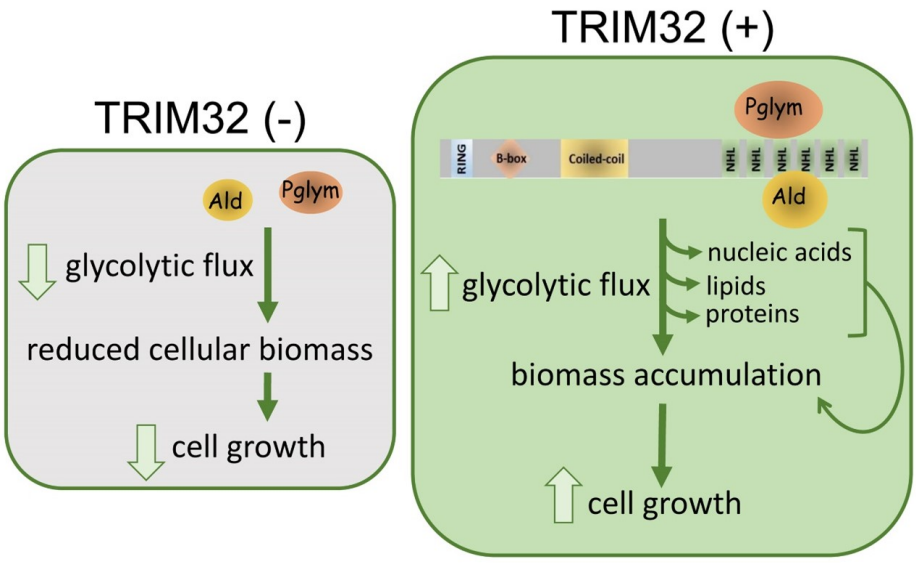

Figure 3.8: Model for TRIM32 function in the regulation of cell size.

Biochemical interactions between TRIM32 and glycolytic enzymes such as Ald or Pglym cooperate in maintaining glycolytic activity for the synthesis of macromolecules required for cell growth. Loss of TRIM32 results in reduced levels of glycolytic enzymes, reduced glycolytic pathway intermediates, and compromises cell growth.

Limitations of this study

How does this loss of TRIM32 lead to a reduction in glycolytic enzymes? Glycolytic proteins may be substrates for TRIM32 E3 ligase activity. It seems unlikely that TRIM32 polyubiquitinates Ald or Pglym for proteasomal degradation as protein levels are not elevated upon loss of this putative E3 activity. Furthermore, co-immunoprecipitaion of higher molecular weight forms of Ald or Pglym with TRIM32 suggests a yet unidentified post-translational modification. Another possibility, which we favor, is that the NHL domain of TRIM32 serves as a scaffold for the subcellular localization of glycolytic proteins to limit diffusion of substrates during glycolysis. This does not negate, but rather expands the repertoire of TRIM32 functions.

ACKNOWLEDGEMENTS

We thank Jim Vigoreaux for sharing antibodies and Kasra X. Ramyar, Joe McWhorter, and Samantha Gameros for technical assistance. We also thank James Cox for services at the University of Utah Metabolomics Core as well as Steve Hartson and Janet Rogers for services and guidance at the Oklahoma State University Proteomics and Mass Spectrometry Core. Special appreciation to the VDRC and BDSC for fly lines used in this study. This work was supported by grant through **the National Institute of Arthritis and Musculoskeletal and Skin Diseases (NIAMS)** to E.R.G (R21AR073373, R01AR060788, and R56AR060788). J.M.T. is supported by a MIRA award from NIGMS (R35GM119557). X-ray diffraction data were collected at Southeast Regional Collaborative Access Team 22-BM beamline at the Advanced Photon Source, Argonne National Laboratory. Supporting institutions may be found at www.ser-cat.org/members.html. Use of the Advanced Photon Source was supported by the US Department of Energy, Office of Science, Office of Basic Energy Sciences, under Contract W-31-109-Eng-38*.

References

1. Adams, P.D., Grosse-Kunstleve, R.W., Hung, L.-W., Ioerger, T.R., McCoy, A.J., Moriarty, N.W., Read, R.J., Sacchettini, J.C., Sauter, N.K., and Terwilliger, T.C. (2002). PHENIX: Building New Software for Automated Crystallographic Structure Determination. Acta Cryst *D58*, 1948-1954.
2. Aditi, K., Shakarad, M.N., and Agrawal, N. (2016). Altered lipid metabolism in Drosophila model of Huntington's disease. Sci Rep *6*, 31411.
3. Ahmad, M., Keebaugh, E.S., Tariq, M., and Ja, W.W. (2018). Evolutionary responses of. Front Ecol Evol *6*.
4. Albor, A., El-Hizawi, S., Horn, E.J., Laederich, M., Frosk, P., Wrogemann, K., and Kulesz-Martin, M. (2006). The interaction of Piasy with Trim32, an E3-ubiquitin ligase mutated in limb-girdle muscular dystrophy type 2H, promotes Piasy degradation and regulates UVB-induced keratinocyte apoptosis through NFkappaB. J Biol Chem *281*, 25850-25866.
5. Arama, E., Dickman, D., Kimchie, Z., Shearn, A., and Lev, Z. (2000). Mutations in the beta-propeller domain of the Drosophila brain tumor (brat) protein induce neoplasm in the larval brain. Oncogene *19*, 3706-3716.
6. Bird, D.K., Yan, L., Vrotsos, K.M., Eliceiri, K.W., Vaughan, E.M., Keely, P.J., White, J.G., and Ramanujam, N. (2005). Metabolic mapping of MCF10A human breast cells via multiphoton fluorescence lifetime imaging of the coenzyme NADH. Cancer Res *65*, 8766-8773.
7. Borg, K., Stucka, R., Locke, M., Melin, E., Ahlberg, G., Klutzny, U., Hagen, M., Huebner, A., Lochmüller, H., Wrogemann, K.*, et al.* (2009). Intragenic deletion of TRIM32 in compound heterozygotes with sarcotubular myopathy/LGMD2H. Hum Mutat *30*, E831-844.
8. Brand, A.H., and Perrimon, N. (1993). Targeted gene expression as a means of altering cell fates and generating dominant phenotypes. Development *118*, 401-415.
9. Brooks, D.S., Vishal, K., Kawakami, J., Bouyain, S., and Geisbrecht, E.R. (2016). Optimization of wrMTrck to monitor Drosophila larval locomotor activity. J Insect Physiol *93-94*, 11-17.
10. Chiang, A.P., Beck, J.S., Yen, H.J., Tayeh, M.K., Scheetz, T.E., Swiderski, R.E., Nishimura, D.Y., Braun, T.A., Kim, K.Y., Huang, J.*, et al.* (2006). Homozygosity mapping with SNP arrays identifies TRIM32, an E3 ubiquitin ligase, as a Bardet-Biedl syndrome gene (BBS11). Proc Natl Acad Sci U S A *103*, 6287-6292.
11. Ciciliot, S., Rossi, A.C., Dyar, K.A., Blaauw, B., and Schiaffino, S. (2013). Muscle type and fiber type specificity in muscle wasting. Int J Biochem Cell Biol *45*, 2191-2199.
12. Cohen, S., Lee, D., Zhai, B., Gygi, S.P., and Goldberg, A.L. (2014). Trim32 reduces PI3K-Akt-FoxO signaling in muscle atrophy by promoting plakoglobin-PI3K dissociation. J Cell Biol *204*, 747-758.
13. Cohen, S., Zhai, B., Gygi, S.P., and Goldberg, A.L. (2012). Ubiquitylation by Trim32 causes coupled loss of desmin, Z-bands, and thin filaments in muscle atrophy. J Cell Biol *198*, 575-589.
14. Cossée, M., Lagier-Tourenne, C., Seguela, C., Mohr, M., Leturcq, F., Gundesli, H., Chelly, J., Tranchant, C., Koenig, M., and Mandel, J.L. (2009). Use of SNP array analysis to identify a novel TRIM32 mutation in limb-girdle muscular dystrophy type 2H. Neuromuscul Disord *19*, 255-260.

15. Cox, J., and Mann, M. (2012). 1D and 2D annotation enrichment: a statistical method integrating quantitative proteomics with complementary high-throughput data. BMC Bioinformatics *13 Suppl 16*, S12.
16. Demontis, F., and Perrimon, N. (2009). Integration of Insulin receptor/Foxo signaling and dMyc activity during muscle growth regulates body size in Drosophila. Development *136*, 983-993.
17. Denk, W., Strickler, J.H., and Webb, W.W. (1990). Two-photon laser scanning fluorescence microscopy. Science *248*, 73-76.
18. Domsch, K., Ezzeddine, N., and Nguyen, H.T. (2013). Abba is an essential TRIM/RBCC protein to maintain the integrity of sarcomeric cytoarchitecture. J Cell Sci *126*, 3314-3323.
19. Edwards, T.A., Wilkinson, B.D., Wharton, R.P., and Aggarwal, A.K. (2003). Model of the brain tumor-Pumilio translation repressor complex. Genes Dev *17*, 2508-2513.
20. Eichenlaub, T., Villadsen, R., Freitas, F.C.P., Andrejeva, D., Aldana, B.I., Nguyen, H.T., Petersen, O.W., Gorodkin, J., Herranz, H., and Cohen, S.M. (2018). Warburg Effect Metabolism Drives Neoplasia in a Drosophila Genetic Model of Epithelial Cancer. Curr Biol *28*, 3220-3228.e3226.
21. Frosk, P., Del Bigio, M.R., Wrogemann, K., and Greenberg, C.R. (2005). Hutterite brothers both affected with two forms of limb girdle muscular dystrophy: LGMD2H and LGMD2I. Eur J Hum Genet *13*, 978-982.
22. Geisbrecht, B.V., Bouyain, S., and Pop, M. (2006). An optimized system for expression and purification of secreted bacterial proteins. Protein Expr Purif *46*, 23-32.
23. Ghanbari, L., Carter, R.E., Rynes, M.L., Dominguez, J., Chen, G., Naik, A., Hu, J., Sagar, M.A.K., Haltom, L., Mossazghi, N.*, et al.* (2019). Cortex-wide neural interfacing via transparent polymer skulls. Nat Commun *10*, 1500.
24. Hartenstein, V., Spindler, S., Pereanu, W., and Fung, S. (2008). The development of the Drosophila larval brain. Adv Exp Med Biol *628*, 1-31.
25. Horn, E.J., Albor, A., Liu, Y., El-Hizawi, S., Vanderbeek, G.E., Babcock, M., Bowden, G.T., Hennings, H., Lozano, G., Weinberg, W.C.*, et al.* (2004). RING protein Trim32 associated with skin carcinogenesis has anti-apoptotic and E3-ubiquitin ligase properties. Carcinogenesis *25*, 157-167.
26. Hyun, S. (2013). Body size regulation and insulin-like growth factor signaling. Cell Mol Life Sci *70*, 2351-2365.
27. Ito, M., Migita, K., Matsumoto, S., Wakatsuki, K., Tanaka, T., Kunishige, T., Nakade, H., Nakatani, M., and Nakajima, Y. (2017). Overexpression of E3 ubiquitin ligase tripartite motif 32 correlates with a poor prognosis in patients with gastric cancer. Oncol Lett *13*, 3131-3138.
28. Izumi, H., and Kaneko, Y. (2014). Trim32 facilitates degradation of MYCN on spindle poles and induces asymmetric cell division in human neuroblastoma cells. Cancer Res *74*, 5620-5630.
29. Kano, S., Miyajima, N., Fukuda, S., and Hatakeyama, S. (2008). Tripartite motif protein 32 facilitates cell growth and migration via degradation of Abl-interactor 2. Cancer Res *68*, 5572-5580.
30. Kudryashova, E., Kramerova, I., and Spencer, M.J. (2012). Satellite cell senescence underlies myopathy in a mouse model of limb-girdle muscular dystrophy 2H. J Clin Invest *122*, 1764-1776.

31. Kudryashova, E., Kudryashov, D., Kramerova, I., and Spencer, M.J. (2005). Trim32 is a ubiquitin ligase mutated in limb girdle muscular dystrophy type 2H that binds to skeletal muscle myosin and ubiquitinates actin. J Mol Biol *354*, 413-424.
32. LaBeau-DiMenna, E.M., Clark, K.A., Bauman, K.D., Parker, D.S., Cripps, R.M., and Geisbrecht, E.R. (2012). Thin, a Trim32 ortholog, is essential for myofibril stability and is required for the integrity of the costamere in Drosophila. Proc Natl Acad Sci U S A *109*, 17983-17988.
33. Lazzari, E., El-Halawany, M.S., De March, M., Valentino, F., Cantatore, F., Migliore, C., Onesti, S., and Meroni, G. (2019). Analysis of the Zn-Binding Domains of TRIM32, the E3 Ubiquitin Ligase Mutated in Limb Girdle Muscular Dystrophy 2H. Cells *8*.
34. Lazzari, E., and Meroni, G. (2016). TRIM32 ubiquitin E3 ligase, one enzyme for several pathologies: From muscular dystrophy to tumours. Int J Biochem Cell Biol *79*, 469-477.
35. Lee, W.C., and Micchelli, C.A. (2013). Development and characterization of a chemically defined food for Drosophila. PLoS One *8*, e67308.
36. Li, H., Chawla, G., Hurlburt, A.J., Sterrett, M.C., Zaslaver, O., Cox, J., Karty, J.A., Rosebrock, A.P., Caudy, A.A., and Tennessen, J.M. (2017). Drosophila larvae synthesize the putative oncometabolite L-2-hydroxyglutarate during normal developmental growth. Proc Natl Acad Sci U S A *114*, 1353-1358.
37. Li, H., Rai, M., Buddika, K., Sterrett, M.C., Luhur, A., Mahmoudzadeh, N.H., Julick, C.R., Pletcher, R.C., Chawla, G., Gosney, C.J.*, et al.* (2019). Lactate dehydrogenase and glycerol-3-phosphate dehydrogenase cooperatively regulate growth and carbohydrate metabolism during. Development *146*.
38. Liberti, M.V., and Locasale, J.W. (2016). The Warburg Effect: How Does it Benefit Cancer Cells? Trends Biochem Sci *41*, 211-218.
39. Liu, J., Zhang, C., Wang, X.L., Ly, P., Belyi, V., Xu-Monette, Z.Y., Young, K.H., Hu, W., and Feng, Z. (2014). E3 ubiquitin ligase TRIM32 negatively regulates tumor suppressor p53 to promote tumorigenesis. Cell Death Differ *21*, 1792-1804.
40. Lloyd, A.C. (2013). The regulation of cell size. Cell *154*, 1194-1205.
41. Locke, M., Tinsley, C.L., Benson, M.A., and Blake, D.J. (2009). TRIM32 is an E3 ubiquitin ligase for dysbindin. Hum Mol Genet *18*, 2344-2358.
42. Lunt, S.Y., and Vander Heiden, M.G. (2011). Aerobic glycolysis: meeting the metabolic requirements of cell proliferation. Annu Rev Cell Dev Biol *27*, 441-464.
43. Martin, S.A., Souder, D.C., Miller, K.N., Clark, J.P., Sagar, A.K., Eliceiri, K.W., Puglielli, L., Beasley, T.M., and Anderson, R.M. (2018). GSK3β Regulates Brain Energy Metabolism. Cell Rep *23*, 1922-1931.e1924.
44. McCoy, A.J., Grosse-Kunstleve, R.W., Adams, P.D., Winn, M.D., Storoni, L.C., and Read, R.J. (2007). Phaser crystallographic software. J Appl Crystallogr *40*, 658-674.
45. Menard, L., Maughan, D., and Vigoreaux, J. (2014). The structural and functional coordination of glycolytic enzymes in muscle: evidence of a metabolon? Biology (Basel) *3*, 623-644.
46. Mokhonova, E.I., Avliyakulov, N.K., Kramerova, I., Kudryashova, E., Haykinson, M.J., and Spencer, M.J. (2015). The E3 ubiquitin ligase TRIM32 regulates myoblast proliferation by controlling turnover of NDRG2. Hum Mol Genet *24*, 2873-2883.
47. Mookerjee, S.A., and Brand, M.D. (2015). Measurement and Analysis of Extracellular Acid Production to Determine Glycolytic Rate. J Vis Exp, e53464.

48. Mookerjee, S.A., Goncalves, R.L.S., Gerencser, A.A., Nicholls, D.G., and Brand, M.D. (2015). The contributions of respiration and glycolysis to extracellular acid production. Biochim Biophys Acta *1847*, 171-181.
49. Nectoux, J., de Cid, R., Baulande, S., Leturcq, F., Urtizberea, J.A., Penisson-Besnier, I., Nadaj-Pakleza, A., Roudaut, C., Criqui, A., Orhant, L.*, et al.* (2015). Detection of TRIM32 deletions in LGMD patients analyzed by a combined strategy of CGH array and massively parallel sequencing. Eur J Hum Genet *23*, 929-934.
50. Neri, M., Selvatici, R., Scotton, C., Trabanelli, C., Armaroli, A., De Grandis, D., Levy, N., Gualandi, F., and Ferlini, A. (2013). A patient with limb girdle muscular dystrophy carries a TRIM32 deletion, detected by a novel CGH array, in compound heterozygosis with a nonsense mutation. Neuromuscul Disord *23*, 478-482.
51. Neville, K.E., Bosse, T.L., Klekos, M., Mills, J.F., Weicksel, S.E., Waters, J.S., and Tipping, M. (2018). A novel ex vivo method for measuring whole brain metabolism in model systems. J Neurosci Methods *296*, 32-43.
52. Nicklas, S., Otto, A., Wu, X., Miller, P., Stelzer, S., Wen, Y., Kuang, S., Wrogemann, K., Patel, K., Ding, H.*, et al.* (2012). TRIM32 regulates skeletal muscle stem cell differentiation and is necessary for normal adult muscle regeneration. PLoS One *7*, e30445.
53. Otwinowski, Z., and Minor, W. (1997). Processing of X-ray Diffraction Data Collected in Oscillation Mode. Methods Enzymol *276*, 307-326.
54. Pant, M., Sopariwala, D.H., Bal, N.C., Lowe, J., Delfín, D.A., Rafael-Fortney, J., and Periasamy, M. (2015). Metabolic dysfunction and altered mitochondrial dynamics in the utrophin-dystrophin deficient mouse model of duchenne muscular dystrophy. PLoS One *10*, e0123875.
55. Provenzano, P.P., Eliceiri, K.W., and Keely, P.J. (2009). Multiphoton microscopy and fluorescence lifetime imaging microscopy (FLIM) to monitor metastasis and the tumor microenvironment. Clin Exp Metastasis *26*, 357-370.
56. Ryu, Y.S., Lee, Y., Lee, K.W., Hwang, C.Y., Maeng, J.S., Kim, J.H., Seo, Y.S., You, K.H., Song, B., and Kwon, K.S. (2011). TRIM32 protein sensitizes cells to tumor necrosis factor (TNFα)-induced apoptosis via its RING domain-dependent E3 ligase activity against X-linked inhibitor of apoptosis (XIAP). J Biol Chem *286*, 25729-25738.
57. Schoser, B.G., Frosk, P., Engel, A.G., Klutzny, U., Lochmüller, H., and Wrogemann, K. (2005). Commonality of TRIM32 mutation in causing sarcotubular myopathy and LGMD2H. Ann Neurol *57*, 591-595.
58. Servián-Morilla, E., Cabrera-Serrano, M., Rivas-Infante, E., Carvajal, A., Lamont, P.J., Pelayo-Negro, A.L., Ravenscroft, G., Junckerstorff, R., Dyke, J.M., Fletcher, S.*, et al.* (2019). Altered myogenesis and premature senescence underlie human TRIM32-related myopathy. Acta Neuropathol Commun *7*, 30.
59. Skala, M.C., Riching, K.M., Gendron-Fitzpatrick, A., Eickhoff, J., Eliceiri, K.W., White, J.G., and Ramanujam, N. (2007). In vivo multiphoton microscopy of NADH and FAD redox states, fluorescence lifetimes, and cellular morphology in precancerous epithelia. Proc Natl Acad Sci U S A *104*, 19494-19499.
60. Sullivan, D.T., MacIntyre, R., Fuda, N., Fiori, J., Barrilla, J., and Ramizel, L. (2003). Analysis of glycolytic enzyme co-localization in Drosophila flight muscle. J Exp Biol *206*, 2031-2038.

61. Szaszák, M., Steven, P., Shima, K., Orzekowsky-Schröder, R., Hüttmann, G., König, I.R., Solbach, W., and Rupp, J. (2011). Fluorescence lifetime imaging unravels C. trachomatis metabolism and its crosstalk with the host cell. PLoS Pathog *7*, e1002108.
62. Tanner, L.B., Goglia, A.G., Wei, M.H., Sehgal, T., Parsons, L.R., Park, J.O., White, E., Toettcher, J.E., and Rabinowitz, J.D. (2018). Four Key Steps Control Glycolytic Flux in Mammalian Cells. Cell Syst *7*, 49-62.e48.
63. Tennessen, J.M., Baker, K.D., Lam, G., Evans, J., and Thummel, C.S. (2011). The Drosophila estrogen-related receptor directs a metabolic switch that supports developmental growth. Cell Metab *13*, 139-148.
64. Tennessen, J.M., Barry, W.E., Cox, J., and Thummel, C.S. (2014a). Methods for studying metabolism in Drosophila. Methods *68*, 105-115.
65. Tennessen, J.M., Bertagnolli, N.M., Evans, J., Sieber, M.H., Cox, J., and Thummel, C.S. (2014b). Coordinated metabolic transitions during Drosophila embryogenesis and the onset of aerobic glycolysis. G3 (Bethesda) *4*, 839-850.
66. TeSlaa, T., and Teitell, M.A. (2014). Techniques to monitor glycolysis. Methods Enzymol *542*, 91-114.
67. Tixier, V., Bataillé, L., Etard, C., Jagla, T., Weger, M., Daponte, J.P., Strähle, U., Dickmeis, T., and Jagla, K. (2013). Glycolysis supports embryonic muscle growth by promoting myoblast fusion. Proc Natl Acad Sci U S A *110*, 18982-18987.
68. Tocchini, C., and Ciosk, R. (2015). TRIM-NHL proteins in development and disease. Semin Cell Dev Biol *47-48*, 52-59.
69. Tyanova, S., Temu, T., Sinitcyn, P., Carlson, A., Hein, M.Y., Geiger, T., Mann, M., and Cox, J. (2016). The Perseus computational platform for comprehensive analysis of (prote)omics data. Nat Methods *13*, 731-740.
70. Volodin, A., Kosti, I., Goldberg, A.L., and Cohen, S. (2017). Myofibril breakdown during atrophy is a delayed response requiring the transcription factor PAX4 and desmin depolymerization. Proc Natl Acad Sci U S A *114*, E1375-E1384.
71. Wang, C.W., Purkayastha, A., Jones, K.T., Thaker, S.K., and Banerjee, U. (2016). In vivo genetic dissection of tumor growth and the Warburg effect. Elife *5*.
72. Watanabe, M., and Hatakeyama, S. (2017). TRIM proteins and diseases. J Biochem *161*, 135-144.
73. Yan, L., Rueden, C.T., White, J.G., and Eliceiri, K.W. (2006). Applications of combined spectral lifetime microscopy for biology. Biotechniques *41*, 249, 251, 253 passim.
74. Yaseen, M.A., Sutin, J., Wu, W., Fu, B., Uhlirova, H., Devor, A., Boas, D.A., and Sakadžić, S. (2017). Fluorescence lifetime microscopy of NADH distinguishes alterations in cerebral metabolism. Biomed Opt Express *8*, 2368-2385.
75. Zhao, T.T., Jin, F., Li, J.G., Xu, Y.Y., Dong, H.T., Liu, Q., Xing, P., Zhu, G.L., Xu, H., Yin, S.C.*, et al.* (2018). TRIM32 promotes proliferation and confers chemoresistance to breast cancer cells through activation of the NF-κB pathway. J Cancer *9*, 1349-1356.
76. Zhu, J., and Thompson, C.B. (2019). Metabolic regulation of cell growth and proliferation. Nat Rev Mol Cell Biol *20*, 436-450.
77. Zwart, P.H., Afonine, P.V., Grosse-Kunstleve, R.W., Hung, L.W., Ioerger, T.R., McCoy, A.J., McKee, E., Moriarty, N.W., Read, R.J., Sacchettini, J.C.*, et al.* (2008). Automated Structure Solution with the PHENIX Suite. Methods Mol Biol *426*, 419-435.

78. Ždralević, M., Marchiq, I., de Padua, M.M.C., Parks, S.K., and Pouysségur, J. (2017). Metabolic Plasiticy in Cancers-Distinct Role of Glycolytic Enzymes GPI, LDHs or Membrane Transporters MCTs. Front Oncol *7*, 313.

Chapter 4 - Costameric Integrin and Sarcoglycan protein levels are altered in a *Drosophila* model for Limb Girdle Muscular Dystrophy type 2H

Simranjot Bawa[1], Samantha Gameros[1], Kenny Baumann[2], David S. Brooks[1], Joseph A. Kollhoff[1], Michal Zolkiewski[1], Andrea David Re Cecconi[5], Nicolò Panini[6], Massimo Russo[6], Rosanna Piccirillo[5], Maithri M. Kashipathy[3], Kevin P. Battaile[4], Scott Lovell[3], Samuel E. A. Bouyain[2], Jessica Kawakami[2], and Erika R. Geisbrecht[1,2]

This chapter has been submitted as a journal article to Molecular Biology of the Cell

Abstract

Mutations in two different domains of the ubiquitously expressed TRIM32 protein give rise to two clinically separate diseases, one of which is Limb-girdle muscular dystrophy type 2H (LGMD2H). Uncovering the muscle-specific role of TRIM32 in LGMD2H pathogenesis has proven difficult as neurogenic phenotypes, independent of LGMD2H pathology, are present in *TRIM32 KO* mice. We previously established a platform to study LGMD2H pathogenesis using *Drosophila melanogaster* as a model. Here we show that LGMD2H disease-causing mutations in the NHL domain are molecularly and structurally conserved between fly and human TRIM32. Furthermore, transgenic expression of these myopathic alleles (R394H, D487N and 520fs) induce myofibril abnormalities, altered nuclear morphology and reduced TRIM32 protein levels, mimicking phenotypes in patients afflicted with LGMD2H. Intriguingly, we also report for the first time that the protein levels of βPS integrin and Sarcoglycan δ (Scgδ), both core components of costameres, are elevated in TRIM32 disease-causing alleles. Similarly, murine myoblasts overexpressing a catalytically inactive TRIM32 mutant, aberrantly accumulate α- and β-Dystroglycan and α-Sarcoglycan. We

speculate that the stoichiometric loss of costamere components disrupts costamere complexes to promote muscle degeneration.

Introduction

LGMD represents a group of genetically inherited disorders characterized by progressive muscle degeneration that initially affects proximal limb muscles (GUGLIERI *et al.* 2008; MAHMOOD and JIANG 2014). Clinical examination and muscle biopsies of LGMD patients reveal heterogeneity in disease onset and severity, making treatment options difficult. The majority of mutated genes that result in over 31 subtypes of LGMD encode for muscle structural proteins (MURPHY and STRAUB 2015; TOCCHINI and CIOSK 2015). In contrast, patients diagnosed with LGMD2H have mutations in the E3 ubiquitin ligase TRIM32. The N-terminus of TRIM32 is characterized by a Really Interesting New Gene (RING) domain, B-box domain, and coiled-coil region, followed by six Ncl-1, HT2A, Lin-41 (NHL) repeats in the C-terminus (SARDIELLO *et al.* 2008; TOCCHINI and CIOSK 2015). A mutation in the B-box region gives rise to Bardet-Biedl Syndrome (BBS), a disease whose clinical presentation shares no muscle pathology. The pathogenic mechanism associated with BBS is not fully understood (CHIANG *et al.* 2006).

The LGMD2H causative mutation c.1459G>A (p.D487N) in *TRIM32* was first identified in the Manitoba Hutterite descendants of North America (SHOKEIR and KOBRINSKY 1976; FROSK *et al.* 2002; FROSK *et al.* 2005). Subsequently, the same mutation was also reported in patients with Sarcotubular Myopathy (STM), suggesting that STM and LGMD2H are allelic disorders with vacuolar pathology more prominent in STM (FROSK *et al.* 2005; SCHOSER *et al.* 2005). More recently, one reported mutation in the RING domain and additional mutations in the NHL repeats of TRIM32 have been documented in patients of non-Hutterite origins. Some of these mutations

result in complete or partial deletions of the gene, further complicating the analysis (SERVIÁN-MORILLA *et al.* 2019). Interestingly, the inception and pathophysiological conditions associated with LGMD2H disease progression is highly variable, with patients encompassing mild to severe muscle damage. The common characteristics of LGMD2H/STM include rounded muscle fibers with increased internalized nuclei and degenerative/atrophic myofibers, followed by Z-line streaming with a dilated and vacuolated sarcotubular system (FROSK *et al.* 2005; SCHOSER *et al.* 2005; KUDRYASHOVA *et al.* 2009; SERVIÁN-MORILLA *et al.* 2019).

TRIM32 localizes to the Z-disc in both mammalian and *Drosophila* skeletal muscle, suggesting a major function in maintaining sarcomeric structure and physiology (LOCKE *et al.* 2009; LABEAU-DIMENNA *et al.* 2012b; LABEAU-DIMENNA *et al.* 2012a; DOMSCH *et al.* 2013). Numerous muscle proteins such as actin, desmin, dysbindin, and tropomyosin have been identified as substrates of TRIM32 E3 ligase activity (LOCKE *et al.* 2009; COHEN *et al.* 2012). While the abnormal accumulation of sarcomeric proteins have been reported in various myopathies (FIELITZ *et al.* 2007), the relationship between altered myoprotein levels and/or localization and muscle degeneration remain elusive in LGMD2H disease progression. In healthy muscle tissue, the ubiquitin proteasome-system (UPS) is a pivotal component of protein quality control that regulates muscle protein turnover and preserves proteolytic homeostasis (CIECHANOVER 2006). Proteins destined for proteasomal degradation are covalently attached by K48 -linked polyubiquitin molecules (THROWER *et al.* 2000). The ubiquitination reaction requires functional cooperation between E1 (ubiquitin activating enzyme), E2 (ubiquitin-conjugating enzyme) and E3 (ubiquitin ligase) proteins (WEISSMAN 2001). The RING domain in TRIM E3 ligases confers enzymatic activity and transfers the ubiquitin molecules onto target proteins to specify their fate and/or function (METZGER *et al.* 2014). The C-terminal NHL domain is implicated in mediating protein-

protein interactions and in the recognition of substrates for E3 ligase activity (TOCCHINI and CIOSK 2015). Therefore, we predict the mutations that cluster in the TRIM32_NHL repeats could directly affect the ubiquitination and/or localization of substrate proteins, thereby exacerbating muscle degeneration. Hence, it is critical to study the dual coordination between the RING and NHL domains to improve our understanding of protein stability and function.

The generation of *TRIM32KO* knockout (KO) mice was a key advance in the muscular dystrophy field (KUDRYASHOVA *et al.* 2009). Both neurogenic and muscular defects are present in *TRIM32KO* mice, increasing the difficulty in uncovering the muscle-specific role of TRIM32 in LGMD2H pathogenesis. Two current models, which are not mutually exclusive, postulate roles for TRIM32 in LGMD2H disease progression. Strong evidence support a model whereby TRIM32-deficient satellite cells contribute to disease pathogenesis. TRIM32 is upregulated in proliferating satellite cells and loss of this protein prevents myotube regeneration, further promoting disease progression (KUDRYASHOVA *et al.* 2012; NICKLAS *et al.* 2012; ASSERETO *et al.* 2016). Second, the deregulation of muscle substrates, including actin, α-actinin, tropomyosin, and desmin, may influence muscle degeneration (COHEN *et al.* 2012). Data support a role for TRIM32 in mediating levels of these proteins in muscle atrophy, but studies have not been performed to directly test this model in the context of LGMD2H. Thus, understanding additional targets of TRIM32-mediated protein regulation may uncover additional mechanisms of TRIM32 pathogenesis.

The progressive muscle degeneration and weakness associated with myopathies and muscular dystrophies are often a result of compromised mechanical stability in the myofiber costameric apparatus (JAKA *et al.* 2015). The dystrophin-glycoprotein components (DGC) along with the sarcoglycan subcomplex (α, β, γ, δ, ε and ζ) and integrin–vinculin–talin network form costameric

complexes at the sarcolemma and Z-disc that are essential for the integrity of skeletal muscle (HENDERSON *et al.* 2017). The sarcoglycan transmembrane glycoproteins are predominantly expressed in striated muscle and form subcomplexes with sarcospan to provide DGC stability at the membrane (CAMPBELL and KAHL 1989; ERVASTI *et al.* 1990; CROSBIE *et al.* 1999). Mutations that affect sarcoglycan proteins α, β, γ, and δ are implicated in autosomal recessive LGMD types 2 (C-F) (NIGRO and SAVARESE 2014).

Similar to the sarcoglycans, integrins are also transmembrane cell surface receptors that mediate the interaction between cell adhesion molecules (CAMs) and extracellular matrix (ECM) proteins. Integrin heterodimers are composed of α and β subunits and this assembly is essential for ligand binding and signal transduction (HYNES 2004; BARCZYK *et al.* 2010). Integrin complex function is required in skeletal muscle for myogenic cell differentiation, migration, sarcomerogenesis, and satellite cell regeneration (VACHON *et al.* 1997; LIU *et al.* 2011). Mice deficient in $\alpha_7\beta1$ integrins in muscle exhibit altered muscle fiber morphology and are susceptible to exercise-induced injury (HAYASHI *et al.* 1998; SCHWANDER *et al.* 2003; BOPPART and MAHMASSANI 2019). The *Drosophila* genome encodes for five α integrin subunits (α_1- α_5) and 2 β subunits (βPS and βν), whereby fly βPS is the vertebrate orthologue of the β1 subunit (BROWN *et al.* 2000).

We previously reported that loss of *Drosophila thin (tn),* which encodes for TRIM32, compromises the integrity of integrin-associated complexes (LABEAU-DIMENNA *et al.* 2012a). Here we take advantage of innate features in the *Drosophila* LGMD2H model to determine how different LGMD2H pathological alleles (R394H, D487N and 520fs) contribute to disease progression. The lack of stem cells in *Drosophila* larval muscle presents an opportunity to observe disease progression without the complications of differentiation and repair (PICCIRILLO *et al.* 2014). Moreover, the absence of an adaptive immune system in flies prevents the infiltration of cell types

that promote inflammation and disease progression in mammalian muscular dystrophies. Here we show that the myogenic expression of human disease alleles results in *Drosophila* muscle degeneration, reduced TRIM32 protein levels, and the abnormal accumulation of βPS integrin and Scgδ. Extending these findings in mammals, the levels of costamere proteins such as α-and β-Dystroglycans and α-Sarcoglycan, are elevated in catalytically defective TRIM32-expressing murine cells, suggesting that costamere complex integrity is essential to prevent LGMD2H disease progression.

Materials and Methods

Drosophila fly stocks

All fly stocks were reared and maintained on standard cornmeal medium at 25°C unless otherwise indicated. The following *Drosophila* stocks were obtained from the Bloomington (BL) *Drosophila* Stock Center (BDSC) or the Vienna *Drosophila* Resource Center (VDRC): w^{1118} was used as the *WT* control (BL3605); *mef2*-Gal4 (BL27390); *elav*-Gal4 (BL458); and UAS-*tn RNAi* (v19290). The *tn*Δ*A* mutation was balanced over CyO, Tb/Sco (BL36335) balancer chromosome and non-Tb individuals were used for the *tn* mutant analysis (LaBeau-DiMenna *et al.* 2012a; Bawa *et al.* 2020). *UAS-TRIM32FL* flies were described in (LaBeau-DiMenna *et al.* 2012a; Bawa *et al.* 2020). All deletion and mutation *UAS-TRIM32* deletion or point mutations fly lines were recombined into the *tn*Δ*A* background for genetic analysis using standard techniques.

Generation of transgenic fly lines

UAS-TRIM32 deletion mutants

Clone GH06739 corresponding to full length *tn_RA* was obtained from the *Drosophila* Genomics Resource Center (DGRC). Fragments corresponding to deletions missing the RING domain

(TRIM32_ ΔRING) or the NHL domain (TRIM32_ΔNHL) were PCR amplified using the following primers:

TRIM32_ΔRING forward: 5'-AATAAGAATAGCGGCCGCATGAATCTGCGACGAGAGATCACG-3'

TRIM32_ΔRING reverse: 5'-CTAGTCTAGATCAGAAGACTTGGACGCGGTGATTC-3′

TRIM32_ΔNHL forward: 5'-AATAAGAATAGCGGCCGCATGGAGCAATTCGAGCAGCTGTTG-3'

TRIM32_ΔNHL reverse: 5'-CTAGTCTAGATCACTGCTGGCGCTTGCGCAGGTACACCTG-3'. Each amplified region was digested with NotI and XbaI restriction enzymes (RE site) and subcloned into the pUAST *Drosophila* transformation vector. After sequence verification, all constructs were injected by Genetic Services, Inc. to obtain transgenic flies.

UAS-TRIM32 human mutation alleles

UAST-TRIM32FL was used as a template to introduce the mutations using the QuikChange II XL Site-directed Mutagenesis kit (Agilent Technologies). The following primer sequences were used: TRIM32_R394H forward: 5'-CGACTCCAGCAACCACCACGTTCAGGTCTTCG-3' TRIM32_R394H reverse –5'-CGAAGACCTGAACGTGGTGGTTGCTGGAGTCG-3' TRIM32_D487N forward: 5'-GCTTCATTTACGTGTGCAATAAGGAGAACCACAGAGTGC-3'; TRIM32_D487N reverse: 5'-CACACGATTCGTGTTCGATCAGGCTATATAATGCGGATGCTC-3' TRIM32_520fs forward: 5'-GAGCATCCGCATTATATAGCCTGATCGAACACGAATCGTGTG-3' TRIM32_520fs reverse- 5'-CACACGATTCGTGTTCGATCAGGCTATATAATGCGGATGCTC-3' After sequence

verification, all constructs were injected by Genetic Services, Inc. for the creation of transgenic flies.

Immunostaining and microscopy

Wandering L3 larvae were heat killed, filleted on sylgard plates in ice cold 1X-PBS, and fixed using 4% formaldehyde (Fisher Scientific) at room temperature for 20 minutes (BAWA *et al.* 2020). The fixed larvae were washed 3 times with PBS + 0.5% Tween 20 and the tissues were stained overnight at 4°C with the following primary antibodies: rat anti-TM (1:50; Babraham Institute); guinea pig anti-TRIM32 (1:100)(LABEAU-DIMENNA *et al.* 2012a), mouse anti-Lamin Dm_0/ADL67.10 (1:100; Developmental Studies Hybridoma Bank), and mouse anti-βPS integrin/CF.6G11 (1:50; Developmental Studies Hybridoma Bank). Post incubation with the primary antibodies, larval preps were washed with PBS + 0.5% Tween 20 and stained with the following fluorescent secondary antibodies: Alexa Fluor anti-rabbit 488, Alexa Flour anti-rat 594 and Alexa Flour anti-guinea pig 488 (1:400, Molecular Probes). Phalloidin 488 (1:400, Molecular Probes) was used to label F-actin. The stained tissues were mounted in anti-fade mounting medium (10% glycerol, 0.5% n-propyl gallate in 20 mM Tris buffer, pH = 8.0). A Zeiss 700 confocal microscope was used to capture raw data. Image processing was performed using Photoshop.

Crystallization, data collection and molecular modeling

Purified TRIM32_NHL (BAWA *et al.* 2020) in 50 mM NaCl, 10 mM Hepes pH 7.5 was concentrated to 9.4 mg/mL for crystallization screening. All crystallization experiments were setup using an NT8 drop-setting robot (Formulatrix Inc.) and UVXPO MRC (Molecular Dimensions) sitting drop vapor diffusion plates at 18 ºC. 100 nL of protein and 100 nL crystallization solution

were dispensed and equilibrated against 50 uL of the latter. Prismatic crystals were obtained in 1-2 days from Index HT screen (Hampton Research) condition F7 (25% (w/v) PEG 3350, 100 mM Bis-Tris pH 6.5, 200 mM ammonium sulfate). Samples were transferred to a fresh drop composed of 80% crystallization solution and 20% (v/v) PEG 200 and stored in liquid nitrogen. X-ray diffraction data were collected at the Advanced Photon Source beamline 17-ID using a Dectris Pilatus 6M pixel array detector.

Structure solution and refinement

Intensities were integrated using XDS (KABSCH 1988; KABSCH 2010) via Autoproc (VONRHEIN *et al.* 2011) and the Laue class analysis and data scaling were performed with Aimless (EVANS 2011). Structure solution was conducted by molecular replacement with Phaser (MCCOY *et al.* 2007b) using a previously determined structure of Trim32 NHL (PDB 6D69) as the search model. The top solution was obtained in the space group $P2_12_12_1$ with a single molecular in the asymmetric unit. Structure refinement and manual model building were conducted with Phenix (ADAMS *et al.* 2010) and Coot (EMSLEY *et al.* 2010) respectively. Anisotropic atomic displacement parameters were refined for all atoms except water molecules. Disordered side chains were truncated to the point for which electron density could be observed. Structure validation was conducted with Molprobity (CHEN *et al.* 2010) and figures were prepared using the CCP4MG package (POTTERTON *et al.* 2004). Structure superposition was conducted with GESAMT (KRISSINEL 2012) via CCP4i (WINN *et al.* 2011). The coordinates and structure factors for Trim32_NHL were deposited to the Worldwide Protein Databank (wwPDB) with the accession code 6XG7.

Human TRIM32 structure prediction

The structure of human TRIM32_NHL was computed by applying the following amino acid sequence to the I-TASSER (ZHANG 2008; ROY *et al.* 2010) server (May 2020). The top model yielded a C-score of -0.14 and TM-score of 0.70 ±0.12.

LKKMGAKGSTPGMFNLPVSLYVTSQGEVLVADRGNYRIQVFTRKGFLKEIRRSPSGIDSF
VLSFLGADLPNLTPLSVAMNCQGLIGVTDSYDNSLKVYTLDGHCVACHRSQLSKPWGIT
ALPSGQFVVTDVEGGKLWCFTVDRGSGVVKYSCLCSAVRPKFVTCDAEGTVYFTQGLG
LNLENRQNEHHLEGGFSIGSVGPDGQLGRQISHFFSENEDFRCIAGMCVDARGDLIVADS
SRKEILHFPKGGGYSVLIREGLTCPVGIALTPKGQLLVLDCWDHCIKIYSYHLRRYSTP

TRIM32 NHL domain mutation analysis

The structure of the NHL repeat region of *Drosophila* TRIM32 was prepared for ddG prediction by relaxing into cartesian space using coordinate restraints via Rosetta (LEAVER-FAY *et al.* 2011) and the lowest energy structure was selected Rosetta's cartesian ddG protocol (PARK *et al.* 2016). Briefly, the cartesian ddG protocol runs for three iterations, and the energies amongst the three were averaged, with the predicted ddG being the difference between the WT and the mutant. For Rosetta relax computations to determine per residue energies, the mutants were generated using Maestro, and point mutants along with the WT protein were relaxed and minimized for 1,000 independent trajectories. The top 100 lowest scoring structures were furthered for subsequent analysis.

βPS integrin antibody production

The peptide QSMRLALRVNEKHNC, corresponding to AAs 159-172 of *Drosophila* βPS integrin (FlyBase ID FBpp0071061), was conjugated to keyhole limpet hemocyanin (KLH) and injected

in rabbits for antisera production. Antibodies specific for βPS integrin were affinity-purified using the antigen (Genscript).

Western blotting

Five to ten L3 larvae were homogenized in 4x Laemmli sample buffer (Bio-Rad). The resulting larval lysate was boiled at 100°C for 10 minutes and centrifuged at 15000 rpm for 20 minutes to separate cellular debris. Lysate was stored at -20°C until further use. Lysates were subjected to SDS-PAGE to analyze overall protein levels, transferred to polyvinyl difluoride (PVDF) membranes (Pierce Biotechnology, Inc.), and incubated with appropriate primary antibodies: guinea pig anti-TRIM32 (1:500)(LaBeau-DiMenna *et al.* 2012a), rat anti-TM (1:500; Babraham Institute), rabbit anti-βPS integrin (1:1000; see description above), rabbit anti-Scgδ (1:500; LSBio), and mouse anti-ATP5α (1:10,000; Abcam) as a loading control. For the C2C12 experiments, we used as primary antibodies: mouse anti-α-Dystroglycan (1:2000; Millipore), mouse anti-ß-Dystroglycan (1:100; Hybridoma Bank), mouse anti-α-Sarcoglycan (1:250; Monosan), and mouse anti-vinculin (1:5000; Sigma). To detect primary antibodies, horseradish peroxidase (HRP) conjugated secondary antibodies were used at a dilution of 1:5000 (GE Healthcare). Protein blots were developed suing Prometheus ProSignal Pico detection system (Genesee Scientific) and imaged using the FluorChem M system. For the C2C12 experiments, to detect primary antibodies, alkaline phosphatase (Promega) conjugated secondary antibodies were used at a dilution of 1:7500. Protein blots were developed using CDP-star substrate (ThermoFisher Scientific) detection system and imaged using Odyssey FC system. Densitometry analysis of protein levels performed using ImageJ software.

Quantitative RT-PCR

Total RNA was isolated from a pool of three wandering L3 larvae using the RNAeasy Mini Kit (QIAGEN) for each genotype. After elution, RNA concentrations were determined and single strand complementary DNA (cDNA) was generated from 150ng of RNA using the qScript XLT cDNA SuperMix kit (Quanta Biosciences). For the qPCR reactions, each cDNA sample was diluted to 1:50 and mixed with Power UP SYBR Green Master mix and the appropriate primers (Applied Biosystems). *rp49* was used as the reference gene. The following primers were synthesized by Integrated DNA Technologies (IDT):

tn: 5'F-GAGCTGCATATCGAAATCACCG-3'; 5'R-AGATAGGCTTTTTCCGAGCAAAC-3'

rp49: 5'F-GCCCAAGGGTATCGACAACA-3'; 5R'-GCGCTTGTTCGATCCGTAAC-3'.

Three independent biological replicates were processed for each genotype and reactions were run in triplicate using the Quant Studio 3 Applied Biosystem with Quant studio design and analysis software. The average of the triplicates was used to calculate the $2^{-\Delta\Delta Ct}$ values (normalized fold expression).

Cell culture and transfection

C2C12 (ATCC), a myoblast cell line from the C3H mouse strain, was grown in DMEM (Dulbecco's Modified Eagle's Medium, Gibco), supplemented with fetal bovine serum (FBS) (Euroclone) and 2 mM L-glutamine, and maintained in culture at 37 °C with 5% CO_2. The cells used were not contaminated by mycoplasma. C2C12 myoblasts were transfected with plasmids expressing GFP, TRIM32FL-GFP, and TRIM32ΔRING-GFP (kindly provided by M. Kules-Martin, Oregon Health and Science University, Portland, OR) using Lipofectamine 2000.

FACS analysis

48 hours after transfection, cells were gently detached and counted, so that $5*10^5$ cells per transfection were stained with 0.5 µg of antibody against α-Dystroglycan (Millipore) for 1 hour with rocking. After 2 washes with PBS-BSA 1%, cells were incubated for one hour with anti-mouse, IgG-Alexa 647 (Molecular Probes). Cells were then analyzed on a Gallios flow cytometer (Beckman Coulter). Each analysis was run on at least 10,000 cells and data were analyzed using Kaluza software. The dot plots show the percentage of cells resulting positive to immunostaining for α-Dystroglycan that were previously gated on the region of GFP-positive cells.

Phenotypic measurements and quantification

Muscle diameter measurements

The 'Distance between two polylines' ImageJ plugin was used to measure the average diameter of each VL3 muscle. Raw values were imported into GraphPad Prism 8.0 for statistical analysis and graph generation. Each data point represents the average diameter for a single muscle.

Locomotion assay

Staged wandering L3 larvae of the appropriate genotypes were placed on a fresh apple juice agar plate (35 mm diameter) for 15 min to acclimate to their surroundings. Larval locomotion studies were performed as described (BROOKS *et al.* 2016).

Pupal axial ratio determination

Pupa of the indicated genotypes were removed from the vial and placed dorsal side up. Images were taken with a Leica M165 FC Stereomicroscope. Using ImageJ, the line and measure command were used for length and width measurements and the length/width ratios were calculated for each genotype ($N \geq 10$). This raw data was imported in the Graphpad Prism 8.0 and plotted as a box and whiskers plot.

Internuclear distance measurements

To quantitatively measure the myonuclear distance in the LGMD2H disease-causing alleles, we analyzed the nuclei in VL3 larval muscles. Measurements were made using the segmented line tool in ImageJ. The shortest distance between the nuclei was reported and the internuclear distance between the nuclei that were clustered together was considered zero. Statistical analysis was performed using Graph pad Prism 8 software and each data point represents a single distance between two nuclei represented as a scatter plot.

Flight assay

One day after eclosion, individual flies of the indicated genotypes were anesthetized and placed into individual vials connected to a plexiglass flight chamber 17 cm (h) x 17 cm (w) x 27 cm (l). An illumination lamp was placed at the opposite end of the chamber. Flies were released from the vial after wakening and flight distance was recorded when the fly landed. Flies that showed normal take-off flight behavior covered either an average distance of 15 cm or 27 cm within the chamber. Flies that tried to fly, but ended up at the bottom of the chamber traveled 7 cm. Flies that were unable to fly fell to the bottom of the chamber immediately and were scored as 'no flight' with a distance of 0 cm. The same flies were collected and reanalyzed at day 12. Each recorded measurement was imported into Graph pad Prism 8 software for statistical analysis and represented as a bar graph based upon the percentage of flies who flew each distance.

Statistical analysis

Statistical analysis was performed by automated software in Graphpad Prism 8.0 to prevent bias. Normally distributed data between two samples was analyzed using a two-tailed unpaired student t-test. The Mann-Whitney U-test was used to compare two samples with nonparametric data. For multiple group comparisons, none of the data sets conformed to a Gaussian distribution and thus

were subjected to the Kruskal-Wallis test. Differences were considered significant if $p < 0.05$ and are indicated in each figure legend. A summary of all n values, statistical tests, and p-values are detailed in Table S3.

Differential scanning calorimetry (DSC)

The NHL region of *Drosophila* TRIM32 was PCR amplified (nucleotides 3231-4062) from either *UAS-TRIM32* or *UAS-TRIM32_R394H* using the following primers:

MBP_NHL forward: 5'-TAACGCGTCGACAGTAGTAGCAGCAGCAGTGGCAGCAGCC-3'

MBP_NHL reverse: 5'-AATAAGAATGCGGCCGCTCAGAAGACTTGGACGCGGTGCTTC-3'. The amplified product was digested with SalI and NotI restriction enzymes (RE site underlined) and ligated into the digested pT7_MBP_HMT expression vector, a derivative of pT7HMT designed to express polyhistidine-tagged Maltose-binding fusion proteins cleavable by TEV protease (GEISBRECHT *et al.* 2006). Protein expression and purification of the *Drosophila* TRIM32_NHL and TRIM32_NHL_R397H proteins were performed as described in (Bawa et al. 2020). To determine the thermal stability of the TRIM32NHL variants, purified protein (1 mg/mL) was dialyzed in PBS, degassed, and loaded into a VP-DSC MicroCalorimeter (MicroCalTM Inc.). The temperature was scanned at 1˚C/min from 20˚C to 80˚C. Heat Capacity, Cp (kcal/mol/K), was plotted after subtraction of a blank thermogram obtained without protein.

Results

Loss of *Drosophila tn* is a muscle-specific model to study LGMD2H

We and others previously showed that the progressive muscle degeneration in *tn* mutants *(tn-/-)* is initiated after embryogenesis and is concurrent with increased larval muscle activity (LABEAU-

DIMENNA *et al.* 2012a). This loss of muscle integrity is particularly apparent in the skeletal, or body wall muscles of third instar larvae (L3) stained with phalloidin to label F-actin. *Wild-type* (*WT)* L3 muscles reveal a striated pattern of sarcomeres (**Fig. 4.1A,A'**), whereby *tn-/-* muscles are thinner with a loss of structural integrity (**Fig. 4.1B,B'**). Since *TRIMKO* mice exhibit both neurological and myopathic phenotypes that likely contribute to altered muscle morphology (KUDRYASHOVA *et al.* 2009), we decided to utilize our *Drosophila* model to directly examine the tissues(s) affected upon a depletion of TRIM32. Thus, we reduced TRIM32 function in either muscles or neurons using the Gal4/UAS system. Consistent with previous results (LABEAU-DIMENNA *et al.* 2012a), the structural deficits associated with muscle-specific RNAi knockdown of TRIM32 (*mef2>tn RNAi*) (**Fig. 4.1C,D,G**) also reduced the locomotor ability of L3 larvae comparable to *tn-/-* larvae (**Fig. 4.1H.**). However, this same reduction of TRIM32 under control of a pan-neuronal promoter (*elav>tn RNAi*) did not alter muscle structure (**Fig. 4.1E,F,G**) or function (**Fig. 4.1H.**). These results are consistent with published data whereby the reintroduction of TRIM32 solely into muscle tissue rescues the *tn-/-* dystrophic muscle phenotype (LABEAU-DIMENNA *et al.* 2012a; DOMSCH *et al.* 2013; BAWA *et al.* 2020). Importantly, our *Drosophila* LGMD2H model can be used to assess the muscle-specific function of TRIM32, thus avoiding neurogenic phenotypes present in *TRIM32KO* mice that may indirectly contribute to disease pathology.

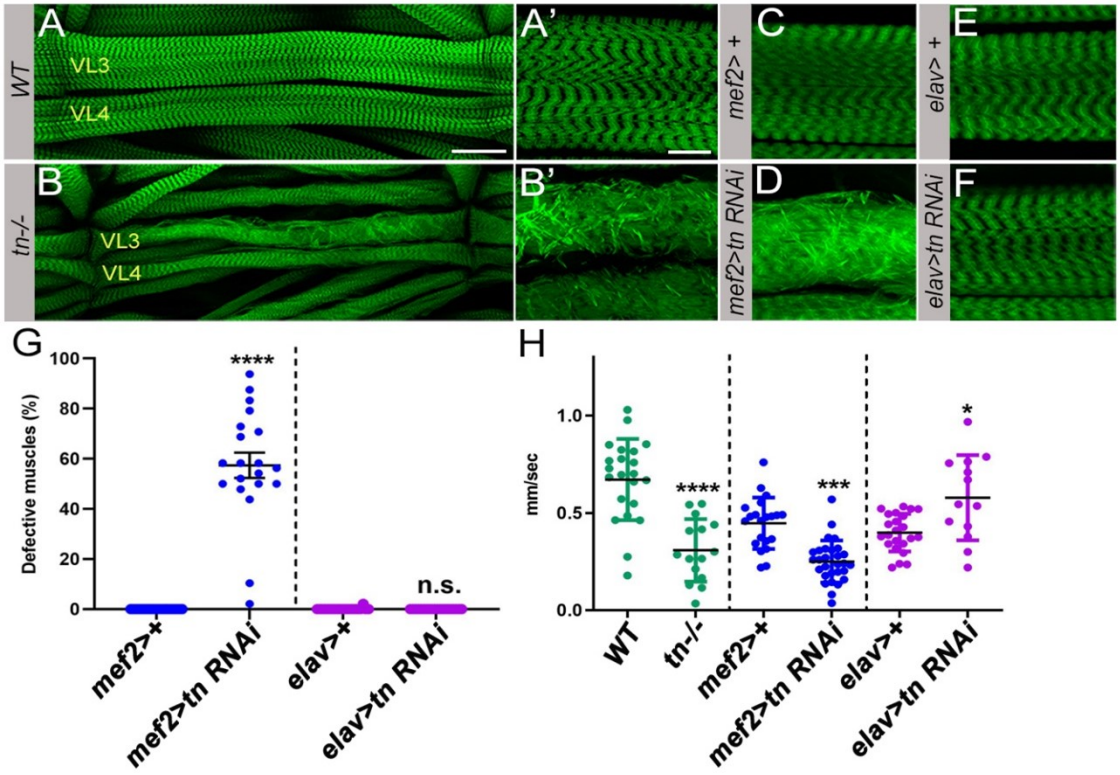

Figure 4.1: Muscle degeneration is neuronal-independent.

(A-B) L3 larval ventral longitudinal muscles 3 (VL3) and 4 (VL4) stained with phalloidin to visualize F-actin (green). (A,A') The stereotypical morphology of WT muscle with normal sarcomeric organization. (B,B') In addition to sarcomeric disorganization, the VL3 and VL4 muscles are noticeably smaller in *tn-/-* larvae. (C-F) Phalloidin labeling of VL3 muscles in L3 larvae. Muscle morphology is unaffected in *mef2*-Gal4 (C) or *elav*-Gal4 (E) driver controls. Dystrophic muscle is apparent upon muscle-specific *tn RNAi* (D), but not upon a decrease of TRIM32 in neurons (F). (G) Quantification shows that induction of *tn RNAi* in muscles, but not neurons, results in muscle defects. (H) Locomotion assay performed on L3 larvae shows a decrease in mobility upon loss of TRIM32 (*tn-/-*) or the induction of *tn RNAi* in muscle tissue (*mef2>tn RNAi*). The reduction in locomotion is minor upon neuronal-specific RNAi knockdown of TRIM32 (*elav>tn RNAi*). Mean +/- SD. (****, $p < 0.001$; *, $p < 0.05$; n.s., not significant). Scale bars: 50µm (A,B), 25µm (A'-B',C-F).

The RING domain and NHL repeats are indispensable for TRIM32 function

In addition to muscle degeneration, a unique feature of *tn-/-* muscles is the notable reduction in muscle size. We recently uncovered a mechanistic link between muscle growth and metabolism, whereby a loss of TRIM32 causes 'thinner muscles' due to defects in the glycolytic-driven accumulation of biomass. (BAWA *et al.* 2020). Therefore, to explore the role of the RING or NHL

domains in promoting muscle growth, we generated and analyzed transgenic flies expressing UAS-based *TRIM32FL*, *TRIM32_ΔRING* or *TRIM32_ΔNHL* constructs (**Fig. 4.2A**) under control of the *mef2* promoter in a *tn-/-* background (**Fig. 4.2B**). As expected, expression of full length TRIM32 in muscle tissue rescued the TRIM32-associated myofibrillar anomalies and muscle size defects (**Fig 4.2C,F**). Consistent with results reported by the Nguyen lab (DOMSCH *et al.* 2013), L3 muscle expression of TRIM32 devoid of either the RING domain (**Fig. 4.2D**) or NHL repeats (**Fig. 4.2E**) showed muscle degeneration similar to *tn* mutants. Quantification of the ventral longitudinal 3 (VL3) muscle diameter of both the *TRIM32_ΔRING* and *TRIM32_ΔNHL* deletions in a *tn-/-* background showed considerably reduced muscle size as compared to the *TRIM32FL* rescue animals (**Fig. 4.2F**). Taken together, our observations provide evidence that loss of either the RING domain or NHL repeats causes constraints in metabolic machinery resulting in smaller muscles.

We next investigated the functional consequences of the abnormal muscle morphology present in the *TRIM32_ΔRING* and *TRIM32_ΔNHL* deletion mutants. During fly metamorphosis, the transition from the larval to pupal stages requires abdominal muscles to contract. However, failure of this contraction results in an extended pupal case, serving as a proxy for muscle function (LABEAU-DIMENNA *et al.* 2012a; BAWA *et al.* 2020; BROOKS *et al.* 2020). We found that loss of either the RING or NHL domains resulted in longer pupae that failed to eclose. Quantitation of this pupal axial ratio (length/width measurements) was ~3 in *WT* individuals with a median of ~4 in *tn-/-* pupae (**Fig. 4.2G**). Restoration of normal pupal size was obtained after rescue by muscle-expressed *TRIM32FL.* In contrast, both TRIM32 deletion mutants when expressed in a *tn-/-* background, showed an axial ratio greater than 4, indicating defects in muscle contraction (**Fig.**

4.2H). Here we conclude that both RING domain and NHL repeats function together in promoting muscle growth and maintaining normal muscle function.

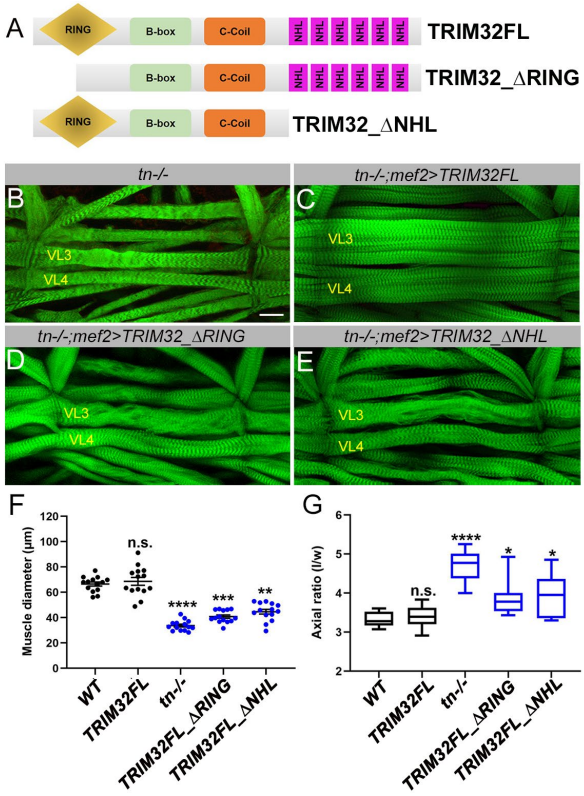

Figure 4.2: RING and NHL domain deletion mutants limit muscle growth and induce degeneration.

(A) Schematic representation of the RING, B-box, coiled-coil, and NHL domains in TRIM32FL and the TRIM32 deletion mutants. (B-E) VL3 and VL4 muscles stained for F-actin to visualize muscle fiber structure in L3 larvae. (B) *tn-/-* mutant muscles appear thinner with prominent sarcomere patterning defects. (C) Overexpression of TRIM32FL under control of the *mef2* promoter in a *tn-/-* background (*tn-/-; mef2*>TRIM32FL) rescued muscle morphology defects. (D,E) Deletion of either the RING (D) or NHL domain (E) mimics the loss of *TRIM32* function phenotype. In addition to muscle morphology defects, Δ*RING* and Δ*NHL* deletion mutants exhibited noticeably thinner VL3 and VL4 muscles similar to *tn* mutants. (F) A scatter plot showing VL3 muscle diameter in the indicated genotypes. Note that *TRIM32FL, TRIM32_ΔRING,* and *TRIM32_ΔNHL* are all expressed in a *tn-/-* background. Deletion of RING or NHL domains reduces VL3 muscle diameter, while muscle expression of TRIM32FL rescues this muscle loss. (G) Box and whisker plot of the pupal case axial ratios show Δ*RING* and Δ*NHL* deletion mutants are defective in muscle contraction, although not quite as severe as *tn* mutants. Note that *TRIM32FL, TRIM32_ΔRING,* and *TRIM32_ΔNHL* are all expressed in a *tn-/-* background. Mean +/- SD (****,***,** $p<0.005$, ****,* $p<0.0001$, n.s., non-significant). Scale bars: 50μm (B-E)

Human disease-causing mutations in *Drosophila* result in muscle degeneration and altered nuclear morphology

The identification of pathological mutations that cluster in the NHL repeats imply an essential role for this region in disease progression and, more fundamentally, in TRIM32 function Therefore, to understand the structural properties of the NHL repeats at the molecular level, we solved the structure of the C-terminal *Drosophila* TRIM32_NHL (dTRIM32_NHL) domain at improved resolution (1.3Å) using molecular replacement based upon our previously published structure of dTRIM32_NHL (PDB code 6D69) (BAWA *et al.* 2020). We found that both structures are nearly identical (**Fig. 4S1A,B**), featuring a six-bladed β propeller, where each NHL repeat consists of four strands of antiparallel β sheets arranged toroidally around a central axis. Superposition yielded an RMSD deviation of 0.51 Å between C□ atoms (288 residues) (**Table 4S1**). In an effort to model the equivalent human TRIM32_NHL (hTRIM32_NHL) region, a 3-dimensional model was obtained using the I-TASSER server. A high degree of similarity was predicted between these two structures despite the modest primary sequence homology (**Fig. 4S1C,D**). In addition, we observed that the conformation of the disease-causing amino acids R394H/R1114 and D487H/D1203 are conserved between human and fly proteins and may be accessible to mediate intermolecular contacts with the other proteins (**Fig. 4S1E,F**). Taken together, our approach provides strong evidence for structural and functional similarities between human and fly TRIM32, making our fly model well suited for studying molecular and cellular properties of human mutations associated with LGMD2H.

The pathological alleles present in the NHL domains of LGMD2H patients vary in origin, consisting of point mutations (R394H, D487N), a single amino acid deletion (D588Δ), frameshift deletions (A422fs, T520fs, L535fs, I590fs) and a stop codon (R613*) *) (SLACK and RUVKUN

1998; FROSK *et al.* 2002; SACCONE *et al.* 2008; BORG *et al.* 2009; COSSÉE *et al.* 2009). Since the molecular location of the two point mutations is identical between the human and fly TRIM32 protein, we assessed the cellular impact of these mutations and an additional frameshift mutation in the *Drosophila* musculature in mimicking LGMD2H pathology (**Fig. 4.3A**). To this end, we once again created transgenic *Drosophila* stocks that recapitulate the *TRIM32_R394H*, *TRIM32_D487N* and *TRIM32_520fs* myopathic mutations. Each of these pathological alleles was recombined into a *tn-/-* background and the resulting UAS-based proteins were expressed in muscle using *mef2*-Gal4 for the analysis of L3 larval muscle morphology. As expected, expression of TRIM32FL rescued the pupal lethality and reverted the muscle morphology defects present in *tn* mutants back to *WT* (**Fig. 4.3B**). Independent expression of the *TRIM32_R394H* (**Fig. 4.3C**), *TRIM32_D487N* (**Fig. 4.3D**), or *TRIM32_520fs* (**Fig. 4.3E**) alleles each showed substantial, although differential, muscle degeneration. Notably, the phenotypes of *TRIM32_D487N* and *TRIM32_520fs* appeared weaker than a complete loss of TRIM32 (**Fig. 4.3B**), suggesting that there is partial protein function in the pathogenic alleles. The dominant overexpression of *TRIM32FL*, *TRIM32_D487N* and *TRIM32_520fs* in a *WT* background did not affect muscle morphology (**Fig. 4S2A-C,E**). However, overexpression of *TRIM32_R394H* alone displayed myofibril defects (**Fig. 4S2D**), suggesting that the R394H mutation can function in a dominant manner in approximately 50% of the muscles examined (**Fig. 4S2E**). Interestingly and consistent with this observation, one patient diagnosed with LGMD2H is heterozygous for *R394H/+* mutation (SACCONE *et al.* 2008). Next we sought to determine the localization pattern of TRIM32 protein in the larval musculature of each mutant genotype. TRIM32 accumulated at the Z-disc in *TRIM32FL* muscles (**Fig. 4.3F**). Reduced TRIM32 expression levels were observed in *tn-/-, mef2>TRIM32_R394H* (**Fig. 4.3G**), *tn-/-, mef2>TRIM32_D487N* (**Fig. 4.3H**) and *tn-/-, mef2>TRIM32_520fs* (**Fig. 4.3I**) muscles. To

determine if changes in TRIM32 protein levels are concomitant with muscle degeneration in our fly model, we homogenized larvae for each of the myopathic mutants and investigated total protein levels. Western blot analysis showed comparatively reduced TRIM32 protein levels in all mutant alleles compared to *TRIM32FL* controls (**Fig. 4.3J,K**). Strikingly, muscle biopsies from LGMD2H patients also showed severe reduction in the TRIM32 protein levels (SERVIÁN-MORILLA *et al.* 2019), confirming that our *Drosophila* disease-causing alleles share specific pathophysiological characteristics with LGMD2H patients. To ensure that our transgenes indeed show comparable expression of *TRIM32*-expressing transcripts, we measured mRNA levels via qPCR (**Fig. 4.3L**). We found that the levels of *TRIM32 mRNA* transcripts were comparable in control (*mef2-Gal4/+*) or *TRIM32FL* rescue carcasses compared *to tn-/-* alone. Interestingly, mRNA levels of all *TRIM32* mutations showed a 4-fold to 6-fold increase, possibly suggesting that transcript levels are increased to compensate for reduced protein levels.

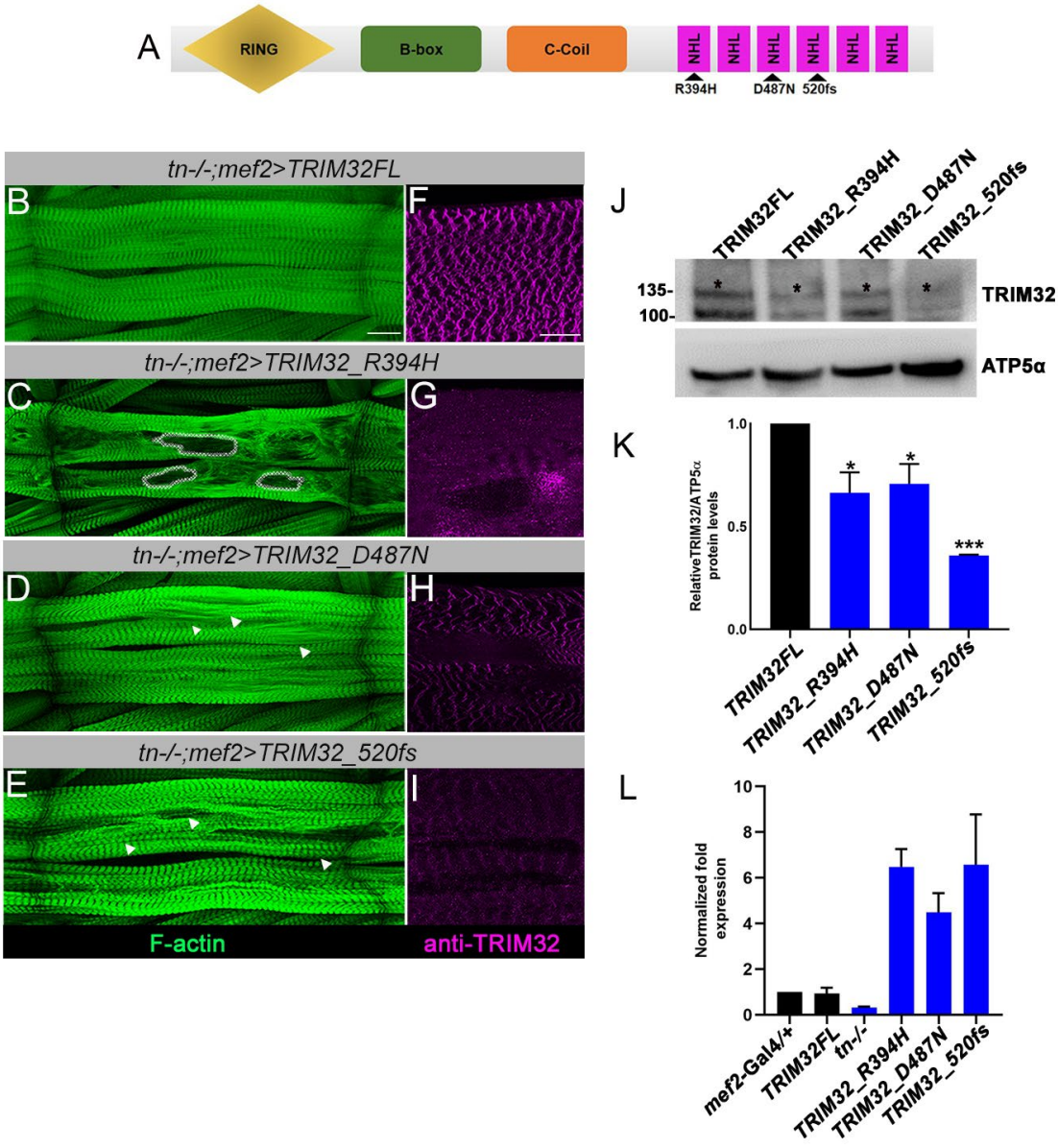

Figure 4.3: Expression of LGMD2H disease-causing alleles causes dystrophic muscle and reduces TRIM32 protein levels.

(A) Relative location of human TRIM32 mutations in NHL1 (R394H), NHL3 (D487N), or NHL4 (fs520). (B-E) Phalloidin-labeled body wall muscles in L3 larvae. (B) *TRIM32FL* control animals (*tn-/;mef2>TRIM32FL*) show *WT* muscle morphology. (C-E) Expression of human pathogenic mutations in a *tn* mutant background cause defects in muscle morphology. (C) Muscle expression of the *R394H* mutation (*tn-/-;mef2>TRIM32_R394H*) resulted in extensive muscle damage. Dotted lines indicate absence of sarcomeric structure. (D,E) The severity of the *D487N* (D) or *520fs* (E) mutations in larval musculature were milder than *R394H* mutant muscles (C), with myofibrillar abnormalities represented by white arrowheads. (F-I) TRIM32 protein localization in L3 muscle tissue upon transgene expression in a *tn-/-* background. (F) Z-disc expression of TRIM32 in *tn-/-;*

mef2>TRIM32FL muscle. (G-I) Z-disc localization appears normal yet reduced in protein amounts upon expression of pathogenic alleles. (J) Western blot analysis of whole larvae shows decreased TRIM32 protein levels in *R394H, D487N* or *520fs* mutants compared to *TRIM32FL* controls. ATP5α is used as a loading control. (K) Bar graph depicts the relative intensity of TRIM32 protein levels normalized to ATP5α in the indicated genotypes. N=3. (L) qPCR reveals that *tn* transcripts are indeed present in muscle carcasses upon expression of all transgenes, with mutant transgenes increased over control (*mef2/+*) or I. mRNA was normalized to *rp49* transcripts. N=3 biological replicates and 3 technical replicates for each genotype. Mean +/- SEM (*, $p < 0.05$; ***, $p < 0.005$). Scale bars: 50μm (A-D), 25μm (E-H).

Skeletal muscle fibers are multinucleated and the maintenance of myonuclear structure is essential for regulating the biomechanical properties of muscle tissue (FOLKER and BAYLIES 2013). Multiple nuclear envelope proteins are linked to cytoskeletal elements to mediate stress due to the mechanical forces transmitted during muscle contraction and relaxation. Disturbances in nucleo-cytoskeletal coupling in diseased muscles are often associated with nuclei clustering, irregular spacing and morphological changes (SKINNER and JOHNSON 2017). Lamins are structural components of the nuclear lamina that line the inner surface of the nuclear membrane. We recently identified proteins that physically interact with the NHL regions of TRIM32 using an unbiased proteomics approach (BAWA *et al.* 2020). Interestingly, in those data there was also an enrichment of nuclear envelope proteins, including *Drosophila* Lamin Dm_0/lamin B-type, Lamin C/lamin A-type and Barrier to autointegration factor (BAF) (**Table 4S2**). Therefore, to examine if nuclear defects are prominent in our disease-causing alleles, we dissected L3 larvae and immunostained with Lamin to visualize nuclear morphology in VL3 muscles. Myonuclei were flat and oval in *WT* (**Fig. 4S3A**), *tn-/-* (**Fig. 4S3B**), and *tn-/-; mef>TRIM32FL* (**Fig. 4S3C**) larval muscles. However, muscle expression of *TRIM32_R394H* (**Fig. 4S3D**), *TRIM32_D487N* (**Fig. 4S3E**), or *TRIM32_520fs* (**Fig. 4S3F**) in *tn* mutant muscles caused the nuclei to adopt a deformed, elongated shape with a majority of the myonuclei internalized within the myofiber and possessing a nuclear aspect ratio greater than 2 (**Fig. 4S5G**). Moreover, the spacing between nuclei, quantitated as the

internuclear distance, was altered in *tn* mutants and the *TRIM32* alleles, with the primary defect being aberrant nuclei clustering (**Fig. 4S5H**). Collectively, the abnormal nuclear architectures in muscles expressing mutated TRIM32 proteins may result from differential interactions with nuclear envelope proteins.

LGMD2H disease-causing alleles result in flight muscle degeneration

Loss of TRIM32 in multiple *tn* allelic combinations or upon muscle-specific *tn RNAi* is pupal lethal (LABEAU-DIMENNA *et al.* 2012a; DOMSCH *et al.* 2013; BAWA *et al.* 2020). Despite the dystrophic changes observed in larval muscle upon expression of our TRIM32 disease-causing mutations, these animals surprisingly survived to adulthood. Therefore, we were able to monitor the impact of aging on muscle structure and disease progression in the adult *Drosophila* indirect flight muscles (IFMs). The IFMs from adult flies were stained with phalloidin and TRIM32 antisera to analyze sarcomere structure and muscle morphology at days 1 through 9 post-eclosion. Adult flies expressing the *TRIM32_D487N* mutation exhibited normal sarcomeric structure at days 1,3 and 6 similar to *TRIM32FL* control flies (**Fig. 4.4A$_{1\text{-}3}$ and B$_{1\text{-}3}$**). However, defects with the D487N mutation became more pronounced by day 9 (**Fig. 4.4B$_4$**). In contrast, the *TRIM32_R394H* and *TRIM32_520fs* mutants displayed profound effects on myofibrillar arrangement starting at day 1 (**Fig. 4.4C$_1$,D$_1$**). These structural defects worsened by day 3 (**Fig. 4.4C$_2$,D$_2$**) and individual fibers appeared fragmented and were no longer ordered in parallel by days 6 and 9 (**Fig. 4.4C$_{3\text{-}4}$,D$_{3\text{-}4}$**). Dominant expression of *TRIM32FL* or *TRIM32_D487N* in a *WT* background resulted in IFMs with a normal myofibrillar arrangement (**Fig. 4S4A,B**), while the dominant effect of *R394H* could not be analyzed since these individuals died during the pupal stage. However, overexpression of the *TRIM32_520fs* mutation alone caused extensive damage to the myofibers (**Fig. 4S4C**). This latter result is somewhat surprising, since the *TRIM32_fs520* mutation showed a normal phenotype in

larval muscle. Nonetheless, these data together suggest that the muscle degeneration in mutant flies is age-dependent.

To further examine the relationship between IFM degeneration, TRIM32 expression and/or localization in each mutant genotype. TRIM32 localized to the Z-disc and M-line in the adult myofibers of TRIM32FL flies through day 9. (**Fig. 4.4A$_{1'-4'}$**). In *tn-/-; mef2>TRIM32_D487N* mutants, TRIM32 remained localized to the sarcomeres by days 1 and to a much lesser extent by day 3, however protein levels appeared reduced through day 9 (**Fig. 4.4B$_{1'-4'}$**). However, in *tn-/-; mef2> TRIM32_R394H* and *tn-/-; mef2> TRIM32_520fs* mutants, the sarcomeric structure lost integrity at day 1 and TRIM32 appeared diffuse along the degenerative myofibers with reduced expression through day 9 (**Fig. 4.4C$_{1-4'}$,D$_{1-4'}$**).

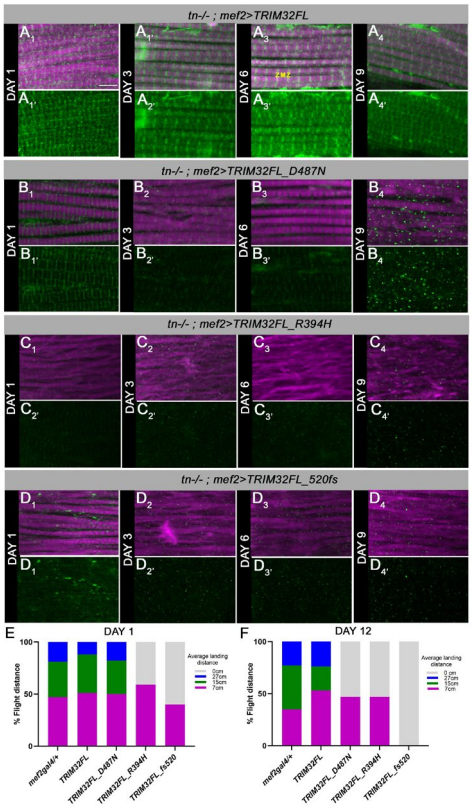

Figure 4.4: Human pathological mutations causes IFM defects and alters TRIM32 localization.

IFMs labeled with phalloidin (magenta) and TRIM32 (green) to visualize myofiber architecture. (A_1-A_4) Overexpression of *TRIM32FL* in a *tn-/-* mutant background results in flies with normal adult flight muscles. TRIM32 is localized at the Z-disc and M-line within the myofibers at all timepoints examined. ($B_{1'}$-$B_{4'}$). (B_1) Induction of the *D487N* mutation results in IFM's with *WT* morphology at day1. Myofibers show mild deterioration at day 3 (B_2) that continues to degenerate through day 6 (B_3) and day 9 (B_4). TRIM32 shows its normal sarcomere association at days 1-6 ($B_{1'}$-$B_{3'}$). By day 9 ($B_{4'}$), TRIM32 is no longer localized to sarcomeres, but appears in puncta. ($C_{1'}$-$D_{4'}$) In contrast, expression of the *R394H* and *520fs* mutations induced myofiber defects by day 1 (C_1,D_1) that progressively worsened as the flies aged (C_2-D_4). In addition to myofibrillar anomalies, TRIM32 was not localized in the myofibers of *R394H* ($C_{1'}$-$C_{4'}$) or *520fs* mutants ($D_{1'}$-$D_{4'}$) and its expression appeared reduced compared to *TRIM32FL* control IFM's. (E,F) Stacked bar graphs depicting flight ability of adult flies of the indicated genotypes at day 1 (E) or day 12 (F). Expression of all three mutations reduced flight ability. Scale bars: 10μm (A_1-$D_{4'}$).

We next tested the functional consequences of *TRIM32* disease mutations on flight ability. The total flight distance traveled by individual flies before landing was measured at days 1 and 12 after eclosion. Control (*mef2-Gal4/+*) and *TRIMFL* rescue flies retained the ability to fly long distances (~27 cm) at each time point (**Figs. 4.4E,F**). In contrast, *TRIM32* mutations showed reduced flight ability. The equivalent of the human *D487N* mutation exhibited normal flight at day 1, while 50% of these same flies lost their ability to traverse longer distances (>15 cm) by day 12. Consistent with IFM degeneration present by day 1, ~40-60% of flies expressing the *R394H* and *fs520* mutations were not able to fly. At day 12, this did not appreciably change for the *R394H* allele,

while the *fs520* flies were flightless. Consistent with a progressive loss of myofibrillar organization, we also observed an age-dependent decrease in flight ability

Structural changes associated with TRIM32 NHL domain mutations

Mutations may influence protein structure, stability and/or dynamics, ultimately leading to protein dysfunction. The observed reduction, but not complete absence, of protein levels corresponding to TRIM32 mutants **(Fig. 4.3I)** implies that these mutations allow for partial protein function. To further assess the consequences of these mutations, we modeled the structural and energetic changes of the NHL domain associated with the *R394H* and *D487N* amino acid substitutions. To estimate the change in the Gibbs free energy of protein folding (ddG), calculations were performed using Rosetta's cartesian ddG protocol (PARK *et al.* 2016) for the *Drosophila* TRIM32_NHL structure. The R394H-equivalent mutant (R1114) was slightly more destabilizing than the D487N-equivalent (1203) mutant (+7.36 kcal/mol vs +7.20 kcal/mol). The histidine that replaced the arginine in R394H/R1114 retained the positive charge, but due to its smaller size, it lost not only the salt bridge, but also a hydrogen bond network (**Fig. 4S5A,A'**). In contrast, the asparagine mutant in D487 was forced to present the hydrogen bond donating nitrogen of the amide toward the other donator atoms in the side chains of R1208 and Q1210 (**Fig. 4S5B,B'**). Since the cartesian ddG protocol sampling is limited to residues around the site of the mutation, we next used the relax protocol within Rosetta to generate an ensemble of structures to sample for differences in backbone conformations. Expectedly, there were perturbations in the backbone conformations around the sites of the mutations. For D487N (NHL3), most of the differences were in the vicinity of the mutation, while minor differences were observed in NHL 4 (**Fig. 4S5C**). Aside from the differences around the site of the R394H mutation (NHL1), several differences between the

ensembles of backbone conformations were seen in repeats of NHL 3 and NHL 4 far from the site of the mutation (**Fig. 4S5D**).

Looking at the average per-residue energies within the ensembles, there is a trend of higher energies around the mutated residue. For example, D487N has a significantly higher energy than the original aspartic acid amino acid residue [-1.15 vs -6.05 Rosetta Energy Units (REU), a full +4.90 difference]. A number of the residues surrounding those in contact with D487N have a smaller (0.2-0.4 REU) increase in energy, while most other surrounding residues find lower energy conformations (**Fig. 4.5A**). The R394H-equivalent mutant was different, in that histidine mutant exhibited a more modest increase in energy over the original arginine residue (-1.77 vs -4.16 REU, a difference of only +2.39 REU), while the residues finding higher or lower energies were spread around the entire protein, not just localized around the site of the mutation (**Fig. 4.5B**). In fact, residues with higher and lower energies were seen in NHLs repeats 3 and 4, where we observed the most change sin backbone conformation. These data, taken together, support our in vivo results that the R394H mutation is more destabilizing than D487N, possibly leading to structural changes that affect additional NHL repeats.

To confirm our modeling predictions using a biophysical approach, we utilized differential scanning calorimetry (DSC) to monitor changes in the thermal stability of TRIM32 mutants. Both WT (TRIM32NHL) and the TRIM32 point mutations (TRIM32NHL_R394H and TRIM32NHL_D487N) were fused to His_8MBP followed by a tobacco etch virus (TEV) cleavage site. In addition to MBP alone, we expressed and purified each of these fusion proteins followed by incubation with TEV to remove the MBP tag. Unlike the TRIM32NHL protein, both mutant proteins were insoluble upon cleavage of the MBP tag, suggesting that the mutation affects the stability of the NHL domain. Hence, for thermal unfolding analysis, we chose to compare the

TRIM32NHL and TRIM32 mutant proteins that retained the MBP fusion (**Fig. 4.5C**). Purified MBP-TRIM32NHL_D487N was prone to aggregation and not analyzed further. The heat capacity profile of MBP_TRIMNHL exhibited a single thermal transition with the mid-point temperature (T_m) around 54°C (**Fig. 4.5D, red trace**). The observed signal is a superposition of the thermal unfolding of TRIM32NHL and the MBP domain, which by itself unfolds with T_m~56°C (**Fig. 4.5D, black trace**). Strikingly, the DSC thermogram for MBP_TRIM32NHL_R394H exhibited two distinct signals, a shoulder around 55°C which likely corresponded to the MBP domain and a major peak at 51°C (**Fig 4.5D, green trace**). A clear decrease in T_m for the thermal unfolding of TRIM32NHL induced by the R394H mutation provides evidence that the mutation renders the protein conformation less stable, providing a likely explanation for the observed decrease in TRIM32_R394H protein levels and muscle degeneration.

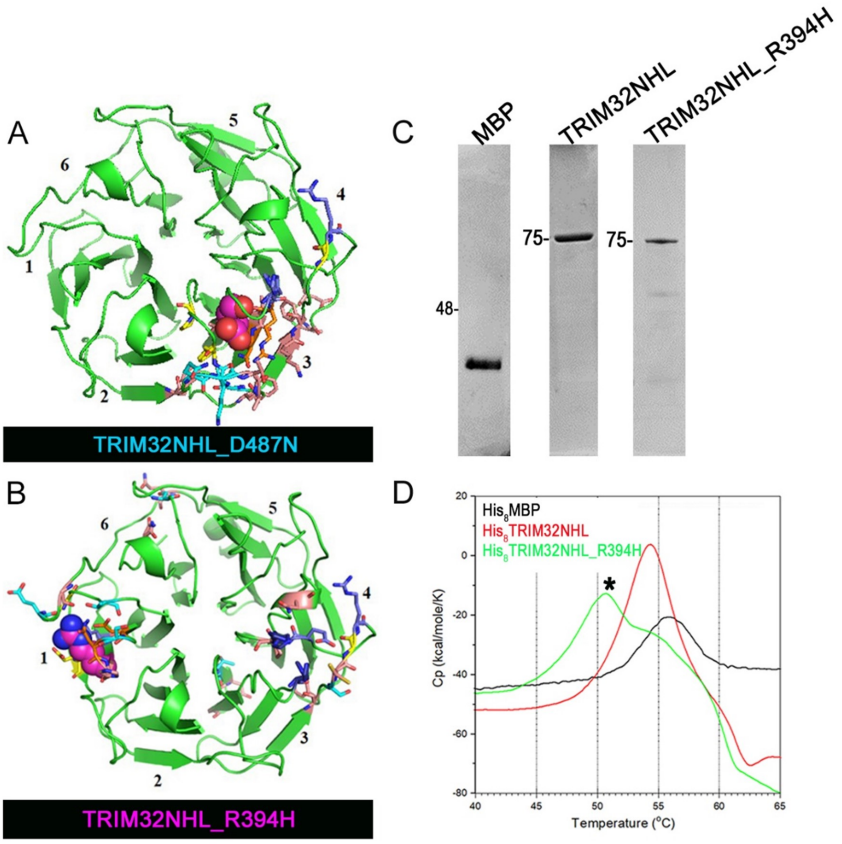

Figure 4.5: The R394H point mutation destabilizes the NHL structure.

(A,B) The average energy of each residue in the top 100 lowest energy members of each ensemble was calculated. The difference between the energies of the WT and D487N (A) or R394H (B) are shown. The site of mutation is shown in spheres. The mutated residues had at least a +2 REU increase in energy (magenta), while amino acids surrounding those residues have a small (0.2-0.4 REU) increase in energy (yellow), especially in D487N (A). Several other surrounding residues find lower energy conformations of 0.2-0.4 REU (cyan), 0.4-1 REU (violet), or even 1-2 REU (dark blue), evident in NHL domain 4 of R394H (B). (C) Coomassie-stained nickel-column purified fractions of $His_{(8)}$MBP, $His_{(8)}$MBP _TRIM32NHL, and the $His_{(8)}$MBP_TRIM32NHL_R394H mutant protein. (D) Thermal unfolding transitions measured for $His_{(8)}$MBP (black), $His_{(8)}$MBP _TRIM32NHL (red), and $His_{(8)}$MBP _TRIM32NHL_R394H (green) using Differential Scanning Calorimetry.

Tropomyosin protein levels are not altered in LGMD2H disease-causing alleles

Sarcomere maintenance requires a balance between protein synthesis and protein degradation. Thin filament associated proteins, such as Tropomyosin (TM), Troponin and actin, undergo proteasomal degradation essential for preventing accumulation of damaged proteins (CARLISLE *et*

al. 2017). Of the many muscle specific targets, TM is a known mammalian substrate of TRIM32 (COHEN *et al.* 2012). Furthermore, we recently showed that TRIM32 physically interacts with TM both *in vitro* and *in vivo* (BAWA *et al.* 2020). These results prompted us to investigate whether TM expression and/or localization is altered upon loss of TRIM32 domains or LGMD2H disease-causing alleles. We immunostained L3 larval muscles and examined the sarcomeric localization of TM. In *WT* (**Fig. S6A**) or *tn-/-*; *mef2>TRIM32FL* (**Fig. S6D**) control muscles, TM exhibited a normal sarcomeric distribution in the muscle. Consistent with our published results (LABEAU-DIMENNA *et al.* 2012a), TM was mislocalized and abnormally accumulated within *tn-/-* myofibers (**Fig. S6B**). We observed similar results in muscles expressing the Δ*RING* (**Fig. S6E**) and Δ*NHL* (**Fig. S6F**) deletions of TRIM32, whereby TM predominantly accumulated along the degenerative myofibers with aberrant localization defects in the unbundled muscles. We further assessed the accumulation of TM in *tn-/-*; *mef2>TRIM32_ΔRING* and *tn-/-*; *mef2>TRIM32ΔNHL* by analyzing total protein levels in whole L3 larvae. Western blot analysis showed elevated levels of TM in *tn* mutants (**Fig. S6C**) or upon deletion of the RING domain (**Fig. S6G**) compared to *WT* (**Fig. S6C**) or *TRIM32FL* rescued muscles (**Fig. S6G**). These data confirm that TM indeed is a substrate of *Drosophila* TRIM32 and the results further substantiate the functional conservation between human and fly TRIM32.

It was previously reported that TRIM32_D487N and R394H mutants lack the ability to ubiquitinate the TRIM32 substrate (LOCKE *et al.* 2009). Therefore, we wondered whether LGMD2H pathological mutations were also defective in regulating TM turnover. Upon immunostaining, we did not observe accumulation of TM in the myofibers of the *TRIM32 R394H, D487N* or *520fs* alleles and despite the presence of degenerative myofibers, TM was relatively well localized (**Fig. S6H-J**). In addition, immunoblotting for TM showed no changes in the overall

protein levels of TM (**Fig. S6K**). Taken together, our results provide evidence that unlike dysbindin (LOCKE *et al.* 2009), TM undergoes normal ubiquitination and proteasomal degradation, and is not implicated in disease progression, particularly with the investigated mutations.

TRIM32 pathological alleles cause elevated protein levels of costamere proteins

Integrins and Sarcoglycans are core components of costameric complexes that link the actin cytoskeleton with the extracellular matrix and are crucial for the maintenance of the sarcolemma during muscle contraction (ANASTASI *et al.* 2008). We previously reported that βPS integrin distribution at the sarcolemma was perturbed upon loss of TRIM32 (LABEAU-DIMENNA *et al.* 2012a). Consequently, we chose to investigate the correlation between point mutation-induced myofibrillar degeneration and disruption of the costameres in our LGMD2H model. *In vivo* staining of *WT* larval muscles with anti-βPS integrin revealed its normal association at the sarcolemma (**Fig. 4.6A,A'**). In contrast, βPS integrin distribution abnormally accumulated along the sarcolemma in TRIM32-deficient muscle (**Fig. 4.6B,B'**). Immunoblot analysis confirmed elevated βPS integrin protein levels in *tn* mutants (**Fig. 4.6C**). We next examined βPS integrin localization and protein levels in TRIM32 disease-causing alleles, with *tn-/-; mef2>TRIM32FL* serving as a control for properly localized βPS integrin protein (**Fig. 4.6D,D'**). However, expression of the *R394H* mutation showed a separate, distinct staining pattern, whereby βPS integrin abnormally accumulated in the degenerative muscles and appeared diffused at the sarcolemma (**Fig. 4.6E,E'**). Small regions of βPS integrin showed an aberrant sarcolemmal distribution in *tn-/-; mef2>TRIM32_D487N* (**Fig. 4.6F,F'**) or *tn-/-; mef2>TRIM32_fs520* muscles (**Fig. 4.6G,G'**). Western blot analysis confirmed a strong trend towards increased βPS integrin protein levels in the disease-causing alleles as compared to *TRIM32FL* larvae (**Fig. 4.6H**). These

observations strongly indicate the involvement of βPS integrin complexes in aggravating muscle defects associated with disease mutations.

We previously reported that the *in vivo* localization of Scgδ, highly expressed in skeletal and cardiac muscle (JUNG *et al.* 1996), was perturbed upon loss of *TRIM32* in larval muscles (LABEAU-DIMENNA *et al.* 2012b; LABEAU-DIMENNA *et al.* 2012a). To examine this further, we analyzed the total protein levels of Scgδ. Interestingly, there is ~50% increase in protein levels of Scgδ in *tn* mutants compared to the *WT* (**Fig. 4.6I**), suggesting that TRIM32 may regulate Scgδ protein levels through its E3 ligase activity. Since it is postulated that NHL repeats are essential for the recognition of TRIM32 substrates and that mutations in the NHL domain may disrupt protein-protein interactions, we also determined Scgδ protein levels in the pathological mutants. Immunoblot analysis confirmed upregulation of Scgδ protein levels upon expression of the *R394H*, *D487N*, or *fs520* mutations (**Fig. 4.6J**).

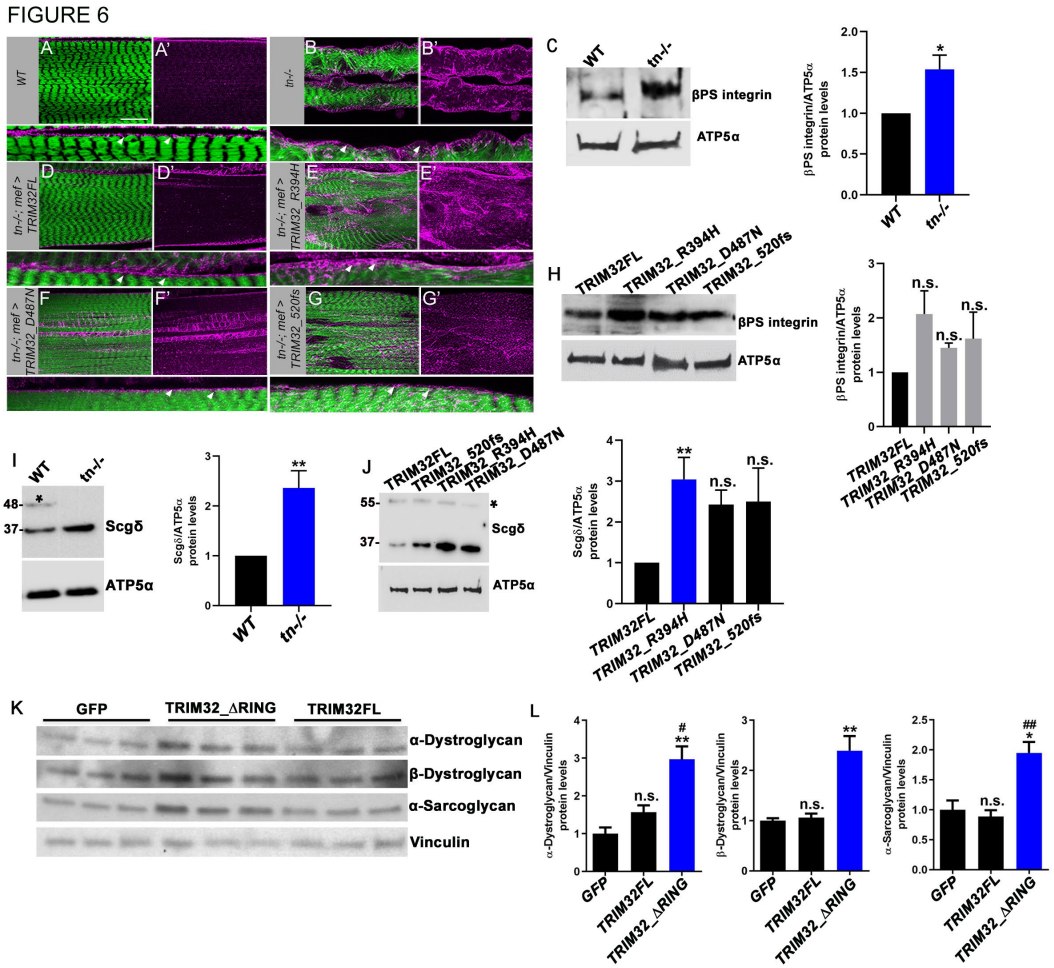

Figure 4.6: Costamere proteins abnormally accumulate upon loss of TRIM32 function in *Drosophila* or C2C12 cells.

(A-G') L3 larval muscles stained with phalloidin (green) and βPS integrin (magenta) to visualize muscle morphology. Horizontal panels are XZ confocal scans to show the sarcolemmal association of βPS integrin**.** (A,A') βPS integrin localizes normally at the sarcolemma in *WT* larval muscle (white arrowheads). (B,B') In *tn* mutants, βPS accumulates abnormally within the myofibers and appears diffused at the sarcolemma (white arrowheads). (C,C') Immunoblot analysis of L3 whole larvae reveal elevated βPS integrin protein levels in *tn* mutants. Bar graph representing quantification of βPS-integrin/ATP5α protein levels. D,D') Muscle rescue with *TRIM32FL* reverts the βPS localization defect to *WT*. (E,E') Transgenic expression of the *R394H* mutation causes βPS clustering within the degenerative myofibers and at the sarcolemma (white arrowheads). (F,F') βPS integrin is mostly normal at the sarcolemma of *D487N* mutants but increased within regions of muscle tissue. (G,G') Abnormal accumulation of βPS prominent within degenerative myofibers in *520fs* mutants. (H,H') Increased βPS integrin protein levels reported in *R394H* and *520fs* mutants. Quantification of βPS-integrin/ATP5α protein levels represented by a bar graph. (I) Western blot depicts significantly high levels of Scgδ protein in *tn* mutants. Bar graph projecting ratio of relative intensity of Scgδ/ATP5α. (J) Elevated Scgδ protein levels prominent in

R394H mutant as compared to TRIM32FL control animals. Bar graph projecting Scgδ/ATP5α protein levels. (K) Total lysates from C2C12 myoblasts transfected for 48 hours with the indicated plasmids were separated by SDS-PAGE. Immunoblotting was performed with antibodies against the indicated costamere protein components. Vinculin was used as loading control. (L) Bar graph depicts the relative intensity of costameric protein levels normalized to Vinculin N=3., Mean +/- SEM (*, p <0.05, **, p <0.01; ***, p < 0.001; n.s., non-significant). Scale bars: 10μm

To further confirm the evolutionary conservation of our results, we expressed GFP alone, GFP-tagged full length TRIM32 (TRIM32FL), or a version lacking the RING domain (TRIM32_ DRING) in murine C2C12 myoblasts and analyzed the protein levels using western blot. We found that expression of only the catalytically inactive TRIM32_ DRING, but not GFP or TRIM32FL, resulted in increased accumulation of α-Dystroglycan, β-Dystroglycans and α-Sarcoglycan in immunoblot analyses (**Fig. 6K,L**). Overall, these data indicate that the E3 ligase activity of TRIM32 is required for degradation of costamere components in mammals as in flies.

Discussion

It is unclear how loss of the single TRIM32 protein in muscle tissue initiates or promotes LGMD2H pathology. Interpretation of mouse TRIM32 models created to mimic LGMD2H pathology has proven complex, as both neurogenic and myopathic abnormalities are present in *TRIM32KO* or *TRIM32 D489N* knock-in mice (KUDRYASHOVA *et al.* 2009; KUDRYASHOVA *et al.* 2011). Moreover, loss of TRIM32 in satellite cells limits muscle regeneration (KUDRYASHOVA *et al.* 2012; NICKLAS *et al.* 2012), thereby promoting further tissue deterioration. Here we took advantage of the lack of satellite cells in *Drosophila* larval muscles to separate the muscle-intrinsic function of TRIM32 from its role in mammalian muscle regeneration. We confirmed that a decrease in neuronal TRIM32 does not contribute to muscle pathology, while the expression of myopathic mutations in larval and adult muscle lead to pathogenic defects with reduced TRIM32

protein levels. Most importantly, we have substantiated a role for costameric proteins in disease progression.

Drosophila and Human TRIM32 are evolutionary conserved

TRIM32 is a multidomain protein that consists of RING domains and NHL repeats that are structurally and functionally conserved between different species. At least twelve different molecules, consisting of either RNA or protein, have been shown to interact with NHL-containing proteins (TOCCHINI and CIOSK 2015). Moreover, mutations and/or deletions in the NHL region of TRIM family members are linked to diverse human diseases. In addition to LGMD2H caused by mutations in TRIM32, axonal neuropathy and gliomas, result from mutations in TRIM2 and TRIM3 respectively (BOULAY *et al.* 2009; YLIKALLIO *et al.* 2013). However, our understanding on how these repeats function in maintaining adequate protein-protein interactions, especially in muscle cytostructure, is limited.

Despite the moderate amino acid identity between *Drosophila* and human TRIM32, we demonstrate that structural homology of the entire NHL region is remarkably similar and serves as an ideal model to investigate the downstream consequences of these myopathic mutations. Previous modeling of the R394H and D487N mutations used the crystal structure of the related NHL-containing protein *Drosophila* Brat (SACCONE *et al.* 2008) as a template. Our domain mutation analysis, based upon the structure we solved for TRIM32, reveals alterations that not only impact local protein structure. For example, the R394H mutation located in NHL domain 1 causes backbone perturbations and residue energy changes in NHL domains 3 and 4, thus providing a molecular understanding for the destabilization of the R394H mutant relative to wild

type NHL by DSC. These results provide evidence that mutations exert debilitating effects on NHL structure and reduces protein levels, further contributing to disease progression.

LGMD2H disease causing mutations disprut larval and adult musculature

Similar to LGMD2H patients, the expression of disease-causing alleles (*R394H, D487N* and *520fs*) in *Drosophila* larval muscle causes muscle degeneration with reduced TRIM32 protein levels and locomotor defects (SERVIÁN-MORILLA *et al.* 2019). Domsch et.al reported that RNAi-mediated knockdown of TRIM32 disrupts adult myofiber architecture at day 7 and day 11 after *tn RNAi* induction post-eclosion (DOMSCH *et al.* 2013). In contrast, our genetic assays show that expression of the *R394H* and *520fs* mutations in IFMs cause severe damage to the myofibers by day 1 that continue to degenerate with age. Expression of the *D487N* mutation also triggered muscle deterioration but delayed compared to other mutations. It is also clear that TRIM32 protein levels correlated with protein destabilization and muscle degeneration. TRIM32 did not localize in the IFMs of *R394H* and *520fs* mutants, but remained relatively well localized in *D487N* mutant myofibers until day 3. In all destabilizing mutations, we observed variable accumulation of TRIM32 puncta. The presence of puncta, rather than the complete absence of protein, may indicate that TRIM32 no longer retains its correct sarcomeric association or possibly represents aggregated TRIM32 protein in response to the damage caused by the myopathic mutations. We believe that the differences in muscle degeneration and TRIM32 expression in different alleles partially explains why the onset and phenotype severity associated with LGMD2H patients is extremely variable.

Does components of the DGC and Integrin adhesion system play a critical role in LGMD2H disease progression?

Mutations in the DGC and integrin adhesion complex are associated with muscular dystrophies and cardiomyopathies (STRAUB *et al.* 1997; DURBEEJ *et al.* 1998; TAVERNA *et al.* 1998; DURBEEJ and CAMPBELL 2002; DAVIES and NOWAK 2006; JAKA *et al.* 2015). Deficiency of δ-sarcoglycan in mammalian skeletal muscle results in the absence of α-, β- and γ-sarcoglycan, suggesting that δ-sarcoglycan is a core component of sarcoglycan complex assembly (HACK *et al.* 2000). Similarly, integrin adhesion molecules at the costamere are indispensable for the development and maintenance of sarcomeric architecture. Work done in mice and fly showed that integrins play an important role in Z-disc formation (VOLK *et al.* 1990; FÄSSLER *et al.* 1996; SCHWANDER *et al.* 2003; SAMAREL 2005; SPARROW and SCHÖCK 2009). Our previous work revealed that TRIM32 is essential for costamere integrity, whereby βPS integrin, Talin, Spectrin, Vinculin, and Scgδ, abnormally accumulate along the sarcolemma (LABEAU-DIMENNA *et al.* 2012a). Our results here further support that loss of costamere stability may be involved in disease pathogenesis as the expression of TRIM32 mutations also phenocopy the mislocalization of βPS integrin and Scgδ. Similar data were obtained upon expression of a catalytically inactive version of TRIM32 in murine myoblasts, extending in mammals the novel role of TRIM32 in promoting the degradation of costamere components unraveled in *Drosophila*. Importantly, although TM protein is mislocalized upon loss of TRIM32, it retains its normal localization when pathogenic alleles are expressed in muscle tissue, suggesting that simply the abnormal accumulation of any muscle protein is insufficient to cause muscle degeneration.

Several studies have shown that upregulation of utrophin or integrin α7 partially compensates for the lack of dystrophin in *mdx* mice or in human DMD patients (YUCEL *et al.* 2018). Although the integrin adhesion complex (assayed by βPS integrin) and the DGC complex (assayed by Scgδ) are also upregulated upon loss of TRIM32, this buildup of costameric proteins at the sarcolemma compromises the attachment between the membrane and myofibrils, leading to muscle degeneration. Some or all of these costamere proteins may be substrates for TRIM32 E3 ligase activity. The abnormal accumulation of βPS integrin and Scgδ along the sarcolemma may result from the inability to be ubiquitinated and turned over by the proteasome and/or the inability to maintain its normal localization due to protein damage during muscle contraction.

There is conflicting data about whether LGMD2H mutations in the NHL domain of TRIM32 inhibit multimer formation or alter ubiquitination activity (LAZZARI and MERONI 2016). We speculate that disease-causing mutations elevate protein levels of at least a subset of costamere proteins, either by altering TRIM protein interactions or by abolishing the catalytic activity of TRIM32. However, additional work is required to understand and characterize the ubiquitination on these proteins by TRIM32. The structural and functional conservation of TRIM32, combined with the muscle-intrinsic *Drosophila* genetic model, will continue to provide novel insights into LGMD2H initiation and progression not currently available through study in other model organisms.

References

1. Adams, P.D., Grosse-Kunstleve, R.W., Hung, L.-W., Ioerger, T.R., McCoy, A.J., Moriarty, N.W., Read, R.J., Sacchettini, J.C., Sauter, N.K., and Terwilliger, T.C. (2002). PHENIX: Building New Software for Automated Crystallographic Structure Determination. Acta Cryst *D58*, 1948-1954.
2. Aditi, K., Shakarad, M.N., and Agrawal, N. (2016). Altered lipid metabolism in Drosophila model of Huntington's disease. Sci Rep *6*, 31411.
3. Ahmad, M., Keebaugh, E.S., Tariq, M., and Ja, W.W. (2018). Evolutionary responses of. Front Ecol Evol *6*.
4. Albor, A., El-Hizawi, S., Horn, E.J., Laederich, M., Frosk, P., Wrogemann, K., and Kulesz-Martin, M. (2006). The interaction of Piasy with Trim32, an E3-ubiquitin ligase mutated in limb-girdle muscular dystrophy type 2H, promotes Piasy degradation and regulates UVB-induced keratinocyte apoptosis through NFkappaB. J Biol Chem *281*, 25850-25866.
5. Arama, E., Dickman, D., Kimchie, Z., Shearn, A., and Lev, Z. (2000). Mutations in the beta-propeller domain of the Drosophila brain tumor (brat) protein induce neoplasm in the larval brain. Oncogene *19*, 3706-3716.
6. Bird, D.K., Yan, L., Vrotsos, K.M., Eliceiri, K.W., Vaughan, E.M., Keely, P.J., White, J.G., and Ramanujam, N. (2005). Metabolic mapping of MCF10A human breast cells via multiphoton fluorescence lifetime imaging of the coenzyme NADH. Cancer Res *65*, 8766-8773.
7. Borg, K., Stucka, R., Locke, M., Melin, E., Ahlberg, G., Klutzny, U., Hagen, M., Huebner, A., Lochmüller, H., Wrogemann, K.*, et al.* (2009). Intragenic deletion of TRIM32 in compound heterozygotes with sarcotubular myopathy/LGMD2H. Hum Mutat *30*, E831-844.
8. Brand, A.H., and Perrimon, N. (1993). Targeted gene expression as a means of altering cell fates and generating dominant phenotypes. Development *118*, 401-415.
9. Brooks, D.S., Vishal, K., Kawakami, J., Bouyain, S., and Geisbrecht, E.R. (2016). Optimization of wrMTrck to monitor Drosophila larval locomotor activity. J Insect Physiol *93-94*, 11-17.
10. Chiang, A.P., Beck, J.S., Yen, H.J., Tayeh, M.K., Scheetz, T.E., Swiderski, R.E., Nishimura, D.Y., Braun, T.A., Kim, K.Y., Huang, J.*, et al.* (2006). Homozygosity mapping with SNP arrays identifies TRIM32, an E3 ubiquitin ligase, as a Bardet-Biedl syndrome gene (BBS11). Proc Natl Acad Sci U S A *103*, 6287-6292.
11. Ciciliot, S., Rossi, A.C., Dyar, K.A., Blaauw, B., and Schiaffino, S. (2013). Muscle type and fiber type specificity in muscle wasting. Int J Biochem Cell Biol *45*, 2191-2199.
12. Cohen, S., Lee, D., Zhai, B., Gygi, S.P., and Goldberg, A.L. (2014). Trim32 reduces PI3K-Akt-FoxO signaling in muscle atrophy by promoting plakoglobin-PI3K dissociation. J Cell Biol *204*, 747-758.
13. Cohen, S., Zhai, B., Gygi, S.P., and Goldberg, A.L. (2012). Ubiquitylation by Trim32 causes coupled loss of desmin, Z-bands, and thin filaments in muscle atrophy. J Cell Biol *198*, 575-589.
14. Cossée, M., Lagier-Tourenne, C., Seguela, C., Mohr, M., Leturcq, F., Gundesli, H., Chelly, J., Tranchant, C., Koenig, M., and Mandel, J.L. (2009). Use of SNP array analysis to identify a novel TRIM32 mutation in limb-girdle muscular dystrophy type 2H. Neuromuscul Disord *19*, 255-260.

15. Cox, J., and Mann, M. (2012). 1D and 2D annotation enrichment: a statistical method integrating quantitative proteomics with complementary high-throughput data. BMC Bioinformatics *13 Suppl 16*, S12.
16. Demontis, F., and Perrimon, N. (2009). Integration of Insulin receptor/Foxo signaling and dMyc activity during muscle growth regulates body size in Drosophila. Development *136*, 983-993.
17. Denk, W., Strickler, J.H., and Webb, W.W. (1990). Two-photon laser scanning fluorescence microscopy. Science *248*, 73-76.
18. Domsch, K., Ezzeddine, N., and Nguyen, H.T. (2013). Abba is an essential TRIM/RBCC protein to maintain the integrity of sarcomeric cytoarchitecture. J Cell Sci *126*, 3314-3323.
19. Edwards, T.A., Wilkinson, B.D., Wharton, R.P., and Aggarwal, A.K. (2003). Model of the brain tumor-Pumilio translation repressor complex. Genes Dev *17*, 2508-2513.
20. Eichenlaub, T., Villadsen, R., Freitas, F.C.P., Andrejeva, D., Aldana, B.I., Nguyen, H.T., Petersen, O.W., Gorodkin, J., Herranz, H., and Cohen, S.M. (2018). Warburg Effect Metabolism Drives Neoplasia in a Drosophila Genetic Model of Epithelial Cancer. Curr Biol *28*, 3220-3228.e3226.
21. Frosk, P., Del Bigio, M.R., Wrogemann, K., and Greenberg, C.R. (2005). Hutterite brothers both affected with two forms of limb girdle muscular dystrophy: LGMD2H and LGMD2I. Eur J Hum Genet *13*, 978-982.
22. Geisbrecht, B.V., Bouyain, S., and Pop, M. (2006). An optimized system for expression and purification of secreted bacterial proteins. Protein Expr Purif *46*, 23-32.
23. Ghanbari, L., Carter, R.E., Rynes, M.L., Dominguez, J., Chen, G., Naik, A., Hu, J., Sagar, M.A.K., Haltom, L., Mossazghi, N.*, et al.* (2019). Cortex-wide neural interfacing via transparent polymer skulls. Nat Commun *10*, 1500.
24. Hartenstein, V., Spindler, S., Pereanu, W., and Fung, S. (2008). The development of the Drosophila larval brain. Adv Exp Med Biol *628*, 1-31.
25. Horn, E.J., Albor, A., Liu, Y., El-Hizawi, S., Vanderbeek, G.E., Babcock, M., Bowden, G.T., Hennings, H., Lozano, G., Weinberg, W.C.*, et al.* (2004). RING protein Trim32 associated with skin carcinogenesis has anti-apoptotic and E3-ubiquitin ligase properties. Carcinogenesis *25*, 157-167.
26. Hyun, S. (2013). Body size regulation and insulin-like growth factor signaling. Cell Mol Life Sci *70*, 2351-2365.
27. Ito, M., Migita, K., Matsumoto, S., Wakatsuki, K., Tanaka, T., Kunishige, T., Nakade, H., Nakatani, M., and Nakajima, Y. (2017). Overexpression of E3 ubiquitin ligase tripartite motif 32 correlates with a poor prognosis in patients with gastric cancer. Oncol Lett *13*, 3131-3138.
28. Izumi, H., and Kaneko, Y. (2014). Trim32 facilitates degradation of MYCN on spindle poles and induces asymmetric cell division in human neuroblastoma cells. Cancer Res *74*, 5620-5630.
29. Kano, S., Miyajima, N., Fukuda, S., and Hatakeyama, S. (2008). Tripartite motif protein 32 facilitates cell growth and migration via degradation of Abl-interactor 2. Cancer Res *68*, 5572-5580.
30. Kudryashova, E., Kramerova, I., and Spencer, M.J. (2012). Satellite cell senescence underlies myopathy in a mouse model of limb-girdle muscular dystrophy 2H. J Clin Invest *122*, 1764-1776.

31. Kudryashova, E., Kudryashov, D., Kramerova, I., and Spencer, M.J. (2005). Trim32 is a ubiquitin ligase mutated in limb girdle muscular dystrophy type 2H that binds to skeletal muscle myosin and ubiquitinates actin. J Mol Biol *354*, 413-424.
32. LaBeau-DiMenna, E.M., Clark, K.A., Bauman, K.D., Parker, D.S., Cripps, R.M., and Geisbrecht, E.R. (2012). Thin, a Trim32 ortholog, is essential for myofibril stability and is required for the integrity of the costamere in Drosophila. Proc Natl Acad Sci U S A *109*, 17983-17988.
33. Lazzari, E., El-Halawany, M.S., De March, M., Valentino, F., Cantatore, F., Migliore, C., Onesti, S., and Meroni, G. (2019). Analysis of the Zn-Binding Domains of TRIM32, the E3 Ubiquitin Ligase Mutated in Limb Girdle Muscular Dystrophy 2H. Cells *8*.
34. Lazzari, E., and Meroni, G. (2016). TRIM32 ubiquitin E3 ligase, one enzyme for several pathologies: From muscular dystrophy to tumours. Int J Biochem Cell Biol *79*, 469-477.
35. Lee, W.C., and Micchelli, C.A. (2013). Development and characterization of a chemically defined food for Drosophila. PLoS One *8*, e67308.
36. Li, H., Chawla, G., Hurlburt, A.J., Sterrett, M.C., Zaslaver, O., Cox, J., Karty, J.A., Rosebrock, A.P., Caudy, A.A., and Tennessen, J.M. (2017). Drosophila larvae synthesize the putative oncometabolite L-2-hydroxyglutarate during normal developmental growth. Proc Natl Acad Sci U S A *114*, 1353-1358.
37. Li, H., Rai, M., Buddika, K., Sterrett, M.C., Luhur, A., Mahmoudzadeh, N.H., Julick, C.R., Pletcher, R.C., Chawla, G., Gosney, C.J.*, et al.* (2019). Lactate dehydrogenase and glycerol-3-phosphate dehydrogenase cooperatively regulate growth and carbohydrate metabolism during. Development *146*.
38. Liberti, M.V., and Locasale, J.W. (2016). The Warburg Effect: How Does it Benefit Cancer Cells? Trends Biochem Sci *41*, 211-218.
39. Liu, J., Zhang, C., Wang, X.L., Ly, P., Belyi, V., Xu-Monette, Z.Y., Young, K.H., Hu, W., and Feng, Z. (2014). E3 ubiquitin ligase TRIM32 negatively regulates tumor suppressor p53 to promote tumorigenesis. Cell Death Differ *21*, 1792-1804.
40. Lloyd, A.C. (2013). The regulation of cell size. Cell *154*, 1194-1205.
41. Locke, M., Tinsley, C.L., Benson, M.A., and Blake, D.J. (2009). TRIM32 is an E3 ubiquitin ligase for dysbindin. Hum Mol Genet *18*, 2344-2358.
42. Lunt, S.Y., and Vander Heiden, M.G. (2011). Aerobic glycolysis: meeting the metabolic requirements of cell proliferation. Annu Rev Cell Dev Biol *27*, 441-464.
43. Martin, S.A., Souder, D.C., Miller, K.N., Clark, J.P., Sagar, A.K., Eliceiri, K.W., Puglielli, L., Beasley, T.M., and Anderson, R.M. (2018). GSK3β Regulates Brain Energy Metabolism. Cell Rep *23*, 1922-1931.e1924.
44. McCoy, A.J., Grosse-Kunstleve, R.W., Adams, P.D., Winn, M.D., Storoni, L.C., and Read, R.J. (2007). Phaser crystallographic software. J Appl Crystallogr *40*, 658-674.
45. Menard, L., Maughan, D., and Vigoreaux, J. (2014). The structural and functional coordination of glycolytic enzymes in muscle: evidence of a metabolon? Biology (Basel) *3*, 623-644.
46. Mokhonova, E.I., Avliyakulov, N.K., Kramerova, I., Kudryashova, E., Haykinson, M.J., and Spencer, M.J. (2015). The E3 ubiquitin ligase TRIM32 regulates myoblast proliferation by controlling turnover of NDRG2. Hum Mol Genet *24*, 2873-2883.
47. Mookerjee, S.A., and Brand, M.D. (2015). Measurement and Analysis of Extracellular Acid Production to Determine Glycolytic Rate. J Vis Exp, e53464.

48. Mookerjee, S.A., Goncalves, R.L.S., Gerencser, A.A., Nicholls, D.G., and Brand, M.D. (2015). The contributions of respiration and glycolysis to extracellular acid production. Biochim Biophys Acta *1847*, 171-181.
49. Nectoux, J., de Cid, R., Baulande, S., Leturcq, F., Urtizberea, J.A., Penisson-Besnier, I., Nadaj-Pakleza, A., Roudaut, C., Criqui, A., Orhant, L.*, et al.* (2015). Detection of TRIM32 deletions in LGMD patients analyzed by a combined strategy of CGH array and massively parallel sequencing. Eur J Hum Genet *23*, 929-934.
50. Neri, M., Selvatici, R., Scotton, C., Trabanelli, C., Armaroli, A., De Grandis, D., Levy, N., Gualandi, F., and Ferlini, A. (2013). A patient with limb girdle muscular dystrophy carries a TRIM32 deletion, detected by a novel CGH array, in compound heterozygosis with a nonsense mutation. Neuromuscul Disord *23*, 478-482.
51. Neville, K.E., Bosse, T.L., Klekos, M., Mills, J.F., Weicksel, S.E., Waters, J.S., and Tipping, M. (2018). A novel ex vivo method for measuring whole brain metabolism in model systems. J Neurosci Methods *296*, 32-43.
52. Nicklas, S., Otto, A., Wu, X., Miller, P., Stelzer, S., Wen, Y., Kuang, S., Wrogemann, K., Patel, K., Ding, H.*, et al.* (2012). TRIM32 regulates skeletal muscle stem cell differentiation and is necessary for normal adult muscle regeneration. PLoS One *7*, e30445.
53. Otwinowski, Z., and Minor, W. (1997). Processing of X-ray Diffraction Data Collected in Oscillation Mode. Methods Enzymol *276*, 307-326.
54. Pant, M., Sopariwala, D.H., Bal, N.C., Lowe, J., Delfín, D.A., Rafael-Fortney, J., and Periasamy, M. (2015). Metabolic dysfunction and altered mitochondrial dynamics in the utrophin-dystrophin deficient mouse model of duchenne muscular dystrophy. PLoS One *10*, e0123875.
55. Provenzano, P.P., Eliceiri, K.W., and Keely, P.J. (2009). Multiphoton microscopy and fluorescence lifetime imaging microscopy (FLIM) to monitor metastasis and the tumor microenvironment. Clin Exp Metastasis *26*, 357-370.
56. Ryu, Y.S., Lee, Y., Lee, K.W., Hwang, C.Y., Maeng, J.S., Kim, J.H., Seo, Y.S., You, K.H., Song, B., and Kwon, K.S. (2011). TRIM32 protein sensitizes cells to tumor necrosis factor (TNFα)-induced apoptosis via its RING domain-dependent E3 ligase activity against X-linked inhibitor of apoptosis (XIAP). J Biol Chem *286*, 25729-25738.
57. Schoser, B.G., Frosk, P., Engel, A.G., Klutzny, U., Lochmüller, H., and Wrogemann, K. (2005). Commonality of TRIM32 mutation in causing sarcotubular myopathy and LGMD2H. Ann Neurol *57*, 591-595.
58. Servián-Morilla, E., Cabrera-Serrano, M., Rivas-Infante, E., Carvajal, A., Lamont, P.J., Pelayo-Negro, A.L., Ravenscroft, G., Junckerstorff, R., Dyke, J.M., Fletcher, S.*, et al.* (2019). Altered myogenesis and premature senescence underlie human TRIM32-related myopathy. Acta Neuropathol Commun *7*, 30.
59. Skala, M.C., Riching, K.M., Gendron-Fitzpatrick, A., Eickhoff, J., Eliceiri, K.W., White, J.G., and Ramanujam, N. (2007). In vivo multiphoton microscopy of NADH and FAD redox states, fluorescence lifetimes, and cellular morphology in precancerous epithelia. Proc Natl Acad Sci U S A *104*, 19494-19499.
60. Sullivan, D.T., MacIntyre, R., Fuda, N., Fiori, J., Barrilla, J., and Ramizel, L. (2003). Analysis of glycolytic enzyme co-localization in Drosophila flight muscle. J Exp Biol *206*, 2031-2038.

61. Szaszák, M., Steven, P., Shima, K., Orzekowsky-Schröder, R., Hüttmann, G., König, I.R., Solbach, W., and Rupp, J. (2011). Fluorescence lifetime imaging unravels C. trachomatis metabolism and its crosstalk with the host cell. PLoS Pathog *7*, e1002108.
62. Tanner, L.B., Goglia, A.G., Wei, M.H., Sehgal, T., Parsons, L.R., Park, J.O., White, E., Toettcher, J.E., and Rabinowitz, J.D. (2018). Four Key Steps Control Glycolytic Flux in Mammalian Cells. Cell Syst *7*, 49-62.e48.
63. Tennessen, J.M., Baker, K.D., Lam, G., Evans, J., and Thummel, C.S. (2011). The Drosophila estrogen-related receptor directs a metabolic switch that supports developmental growth. Cell Metab *13*, 139-148.
64. Tennessen, J.M., Barry, W.E., Cox, J., and Thummel, C.S. (2014a). Methods for studying metabolism in Drosophila. Methods *68*, 105-115.
65. Tennessen, J.M., Bertagnolli, N.M., Evans, J., Sieber, M.H., Cox, J., and Thummel, C.S. (2014b). Coordinated metabolic transitions during Drosophila embryogenesis and the onset of aerobic glycolysis. G3 (Bethesda) *4*, 839-850.
66. TeSlaa, T., and Teitell, M.A. (2014). Techniques to monitor glycolysis. Methods Enzymol *542*, 91-114.
67. Tixier, V., Bataillé, L., Etard, C., Jagla, T., Weger, M., Daponte, J.P., Strähle, U., Dickmeis, T., and Jagla, K. (2013). Glycolysis supports embryonic muscle growth by promoting myoblast fusion. Proc Natl Acad Sci U S A *110*, 18982-18987.
68. Tocchini, C., and Ciosk, R. (2015). TRIM-NHL proteins in development and disease. Semin Cell Dev Biol *47-48*, 52-59.
69. Tyanova, S., Temu, T., Sinitcyn, P., Carlson, A., Hein, M.Y., Geiger, T., Mann, M., and Cox, J. (2016). The Perseus computational platform for comprehensive analysis of (prote)omics data. Nat Methods *13*, 731-740.
70. Volodin, A., Kosti, I., Goldberg, A.L., and Cohen, S. (2017). Myofibril breakdown during atrophy is a delayed response requiring the transcription factor PAX4 and desmin depolymerization. Proc Natl Acad Sci U S A *114*, E1375-E1384.
71. Wang, C.W., Purkayastha, A., Jones, K.T., Thaker, S.K., and Banerjee, U. (2016). In vivo genetic dissection of tumor growth and the Warburg effect. Elife *5*.
72. Watanabe, M., and Hatakeyama, S. (2017). TRIM proteins and diseases. J Biochem *161*, 135-144.
73. Yan, L., Rueden, C.T., White, J.G., and Eliceiri, K.W. (2006). Applications of combined spectral lifetime microscopy for biology. Biotechniques *41*, 249, 251, 253 passim.
74. Yaseen, M.A., Sutin, J., Wu, W., Fu, B., Uhlirova, H., Devor, A., Boas, D.A., and Sakadžić, S. (2017). Fluorescence lifetime microscopy of NADH distinguishes alterations in cerebral metabolism. Biomed Opt Express *8*, 2368-2385.
75. Zhao, T.T., Jin, F., Li, J.G., Xu, Y.Y., Dong, H.T., Liu, Q., Xing, P., Zhu, G.L., Xu, H., Yin, S.C.*, et al.* (2018). TRIM32 promotes proliferation and confers chemoresistance to breast cancer cells through activation of the NF-κB pathway. J Cancer *9*, 1349-1356.
76. Zhu, J., and Thompson, C.B. (2019). Metabolic regulation of cell growth and proliferation. Nat Rev Mol Cell Biol *20*, 436-450.
77. Zwart, P.H., Afonine, P.V., Grosse-Kunstleve, R.W., Hung, L.W., Ioerger, T.R., McCoy, A.J., McKee, E., Moriarty, N.W., Read, R.J., Sacchettini, J.C.*, et al.* (2008). Automated Structure Solution with the PHENIX Suite. Methods Mol Biol *426*, 419-435.

78. Ždralević, M., Marchiq, I., de Padua, M.M.C., Parks, S.K., and Pouysségur, J. (2017). Metabolic Plasiticy in Cancers-Distinct Role of Glycolytic Enzymes GPI, LDHs or Membrane Transporters MCTs. Front Oncol *7*, 313.

79. Ylikallio, E., R. Pöyhönen, M. Zimon, E. De Vriendt, T. Hilander *et al.*, 2013 Deficiency of the E3 ubiquitin ligase TRIM2 in early-onset axonal neuropathy. Hum Mol Genet 22**:** 2975-2983.
80. Yucel, N., A. C. Chang, J. W. Day, N. Rosenthal and H. M. Blau, 2018 Humanizing the mdx mouse model of DMD: the long and the short of it. NPJ Regen Med 3**:** 4.
81. Zhang, Y., 2008 I-TASSER server for protein 3D structure prediction. BMC Bioinformatics 9**:** 40

Chapter 5 - Moleskin, NUAK and TRIM32 function in promoting muscle homeostasis.

5.1 Introduction

Muscle homeostasis relies on the activity of satellite cells, recognition, and clearance of damaged proteins in myofibers, followed by cooperation of multiple myogenic signaling pathways. We have identified novel role for Moleskin, NUAK, and TRIM32 proteins in maintaining normal muscle structure and function. The summary of each project I contributed is described separately in the section below. I have provided technical assistance, designed, and executed experiments.

5.2 Adult Muscle Formation Requires *Drosophila* Moleskin for Proliferation of Wing Disc-Associated Muscle

The development of *Drosophila* DLM indirect flight muscle relies on a pool of adult muscle precursor (AMP) cells which are set aside in the embryo and remain undifferentiated in the wing disc until L1 larval stage. The proliferation of AMPs in the wing disc results in the generation of fusion competent myoblast cells critical for the formation of adult muscle fibers. Therefore, regulating and balancing the pool of AMPs is prime for muscle formation. We identified a new function for *moleskin (msk)* in maintaining adult myoblast pool size and DLM formation. Our lab previously reported that *msk* facilitates attachment of embryonic somatic musculature. Studies have reported vertebrate orthologue Importin-7 regulates myoblast

proliferation and differentiation. Therefore, we investigated the requirement of *Drosophila msk* in adult myogenesis. We show that loss of *msk* affects myoblast proliferation in the notum of the wing disc.

Further analysis revealed that reducing *msk* expression dramatically decreased the number of muscle fibers at both 20 hr and 24 hr APF (after puparium formation). Our genetic data validated the requirement of Msk in generating and maintain myoblast pool both in founder cells and fusing myoblasts. The transcriptional factor Vestigial (Vg) is highly expressed in the proximal myoblasts of the wing disc. Interestingly, loss of *msk* affected the presence of Vg a crucial element in IFM formation and development. Vg is a known transcriptional target of Wg signaling and our analysis show that introducing activated Armadillo a coactivator of Wg is a *msk* RNAi background partially rescued the myoblast number. This experiment tells us that *msk* either acts upstream or parallel to Arm/TCF transcriptional complex and regulate AMP pool size through Vg. Our findings suggest that msk regulates AMP pool size by either directly regulate the nuclear import of Arm and/ or T-cell factor (TCF) in response to Wg signaling or stabilizes Arm in the cytoplasm critical for myoblast amplification. Since *Drosophila* satellite cells are lineal descendent of AMPs and mimick the function of vertebrate satellite cells, it will be interesting to analyze if Msk can regulate myoblast pool during muscle injury and repair.

References

1. Anant, S., S. Roy, and K. VijayRaghavan, 1998 Twist and Notch negatively regulate adult muscle differentiation in Drosophila. Development 125: 1361–1369. Bate, M., 1990
2. The embryonic development of larval muscles in Drosophila. Development 110: 791–804. Bate, M., E. Rushton, and D. A. Currie, 1991 Cells with persistent twist expression are the embryonic precursors of adult muscles in Drosophila. Development 113: 79–89. Bejsovec, A., 2006
3. Flying at the head of the pack: Wnt biology in Drosophila. Oncogene 25: 7442–7449.
4. Benchabane, H., N. Xin, A. Tian, B. P. Hafler, K. Nguyen et al., 2011 Jerky/Earthbound facilitates cell-specific Wnt/Wingless signalling by modulating b-catenin-TCF activity. EMBO J. 30: 1444–1458.
5. Benmimoun, B., C. Polesello, L. Waltzer, and M. Haenlin, 2012 Dual role for insulin/TOR signaling in the control of hematopoietic progenitor maintenance in Drosophila. Development 139: 1713–1717.
6. Bernard, F., A. Lalouette, M. Gullaud, A. Y. Jeantet, R. Cossard et al., 2003 Control of apterous by vestigial drives indirect flight muscle development in Drosophila. Dev. Biol. 260: 391– 403.
7. Bernard, F., A. Dutriaux, J. Silber, and A. Lalouette, 2006 Notch pathway repression by vestigial is required to promote indirect flight muscle differentiation in Drosophila melanogaster. Dev. Biol. 295: 164–177.
8. Bernard, F., A. Krejci, B. Housden, B. Adryan, and S. J. Bray, 2010 Specificity of Notch pathway activation: twist controls the transcriptional output in adult muscle progenitors. Development 137: 2633–2642.
9. Bourouis, M., 2002 Targeted increase in shaggy activity levels blocks wingless signaling. Genesis 34: 99–102. Brack, A. S., I. M. Conboy, M. J. Conboy, J. Shen, and T. A. Rando, 2008 A temporal switch from notch to Wnt signaling in muscle stem cells is necessary for normal adult myogenesis. Cell Stem Cell 2: 50–59.
10. Brand, A. H., and N. Perrimon, 1993 Targeted gene expression as a means of altering cell fates and generating dominant phenotypes. Development 118: 401–415.
11. Breuninger, H., and M. Lenhard, 2010 Control of tissue and organ growth in plants. Curr. Top. Dev. Biol. 91: 185–220.
12. Bryantsev, A. L., P. W. Baker, T. L. Lovato, M. S. Jaramillo, and R. M. Cripps, 2012 Differential requirements for myocyte enhancer factor-2 during adult myogenesis in Drosophila. Dev. Biol. 361: 191–207.
13. Chen, T., E. Heller, S. Beronja, N. Oshimori, N. Stokes et al., 2012 An RNA interference screen uncovers a new molecule in stem cell self-renewal and long-term regeneration. Nature 485: 104–108.
14. Cripps, R. M., and E. N. Olson, 1998 Twist is required for muscle template splitting during adult Drosophila myogenesis. Dev. Biol. 203: 106–115.
15. Dutta, D., and K. VijayRaghavan, 2006 Metamorphosis and the formation of the adult musculature, pp. 125–142 in Muscle Development in Drosophila (Molecular Biology Intelligence Unit), edited by H. Sink. Springer Science+Business Media, New York.

16. Dutta, D., S. Anant, M. Ruiz-Gomez, M. Bate, and K. VijayRaghavan, 2004 Founder myoblasts and fibre number during adult myogenesis in Drosophila. Development 131: 3761–3772.
17. Egger, B., J. M. Chell, and A. H. Brand, 2008 Insights into neural stem cell biology from flies. Philos. Trans. R. Soc. Lond. B Biol. Sci. 363: 39–56.
18. Fassati, A., D. Görlich, I. Harrison, L. Zaytseva, and J. M. Mingot, 2003 Nuclear import of HIV-1 intracellular reverse transcription complexes is mediated by importin 7. EMBO J. 22: 3675– 3685.
19. Fernandes, J., M. Bate, and K. Vijayraghavan, 1991 Development of the indirect flight muscles of Drosophila. Development 113: 67–77.
20. Fernandes, J. J., K. B. Atreya, K. M. Desai, R. E. Hall, M. D. Patel et al., 2005 A dominant negative form of Rac1 affects myogenesis of adult thoracic muscles in Drosophila. Dev. Biol. 285: 11–27.
21. Figeac, N., M. Daczewska, C. Marcelle, and K. Jagla, 2007 Muscle stem cells and model systems for their investigation. Dev. Dyn. 236: 3332–3342.
22. Figeac, N., T. Jagla, R. Aradhya, J. P. Da Ponte, and K. Jagla, 2011 Specification and behavior of AMPs, muscle-committed transient Drosophila stem cells. Fly (Austin) 5: 7–9. Flores, K., and R. Seger, 2013 Stimulated nuclear import by b-like importins. F1000Prime Rep. 5: 41.
23. Freedman, N. D., and K. R. Yamamoto, 2004 Importin 7 and importin alpha/importin beta are nuclear import receptors for the glucocorticoid receptor. Mol. Biol. Cell 15: 2276–2286.
24. Gilboa, L., 2015 Organizing stem cell units in the Drosophila ovary. Curr. Opin. Genet. Dev. 32: 31–36.
25. Gonzalez, C., 2007 Spindle orientation, asymmetric division and tumour suppression in Drosophila stem cells. Nat. Rev. Genet. 8: 462–472.
26. Görlich, D., M. Dabrowski, F. R. Bischoff, U. Kutay, P. Bork et al., 1997 A novel class of RanGTP binding proteins. J. Cell Biol. 138: 65–80. Gunage, R. D., H. Reichert, and K. VijayRaghavan, 2014 Identification of a new stem cell population that generates Drosophila flight muscles. Elife 3: e03126
27. Homem, C. C., M. Repic, and J. A. Knoblich, 2015 Proliferation control in neural stem and progenitor cells. Nat. Rev. Neurosci. 16: 647–659.
28. Jäkel, S., W. Albig, U. Kutay, F. R. Bischoff, K. Schwamborn et al., 1999 The importin beta/importin 7 heterodimer is a functional nuclear import receptor for histone H1. EMBO J. 18: 2411–2423.
29. Jiang, H., and B. A. Edgar, 2012 Intestinal stem cell function in Drosophila and mice. Curr. Opin. Genet. Dev. 22: 354–360.
30. Kopec, S., 1923 The influence of the nervous system on the development and regeneration of muscles and integument in insects. J. Exp. Zool. 37: 14–25.
31. Lange, A. W., A. Sridharan, Y. Xu, B. R. Stripp, A. K. Perl et al., 2015 Hippo/Yap signaling controls epithelial progenitor cell proliferation and differentiation in the embryonic and adult lung. J. Mol. Cell Biol. 7: 35–47.
32. Liotta, D., J. Han, S. Elgar, C. Garvey, Z. Han et al., 2007 The Him gene reveals a balance of inputs controlling muscle differentiation in Drosophila. Curr. Biol. 17: 1409–1413.
33. Liu, Z. C., and E. R. Geisbrecht, 2011 Moleskin is essential for the formation of the myotendinous junction in Drosophila. Dev. Biol. 359: 176–189.

34. Liu, Z. C., N. Odell, and E. R. Geisbrecht, 2013 Drosophila importin-7 functions upstream of the Elmo signaling module to mediate the formation and stability of muscle attachments. J. Cell Sci. 126: 5210–5223.
35. Lorenzen, J. A., S. E. Baker, F. Denhez, M. B. Melnick, D. L. Brower et al., 2001 Nuclear import of activated D-ERK by DIM-7, an importin family member encoded by the gene moleskin. Development 128: 1403–1414.
36. Lovato, T. L., A. R. Benjamin, and R. M. Cripps, 2005 Transcription of Myocyte enhancer factor-2 in adult Drosophila myoblasts is induced by the steroid hormone ecdysone. Dev. Biol. 288: 612– 621.
37. Maqbool, T., C. Soler, T. Jagla, M. Daczewska, N. Lodha et al., 2006 Shaping leg muscles in Drosophila: role of ladybird, a conserved regulator of appendicular myogenesis. PLoS One 1: e122.
38. Marenda, D. R., A. D. Vrailas, A. B. Rodrigues, S. Cook, M. A. Powers et al., 2006 MAP kinase subcellular localization controls both pattern and proliferation in the developing Drosophila wing. Development 133: 43–51.
39. Mason, D. A., and D. S. Goldfarb, 2009 The nuclear transport machinery as a regulator of Drosophila development. Semin. Cell Dev. Biol. 20: 582–589.
40. McGuire, S. E., Z. Mao, and R. L. Davis, 2004 Spatiotemporal gene expression targeting with the TARGET and gene-switch systems in Drosophila. Sci. STKE 2004: pl6.
41. Micchelli, C. A., and N. Perrimon, 2006 Evidence that stem cells reside in the adult Drosophila midgut epithelium. Nature 439: 475–479.
42. Michailovici, I., H. A. Harrington, H. H. Azogui, Y. Yahalom-Ronen, A. Plotnikov et al., 2014 Nuclear to cytoplasmic shuttling of ERK promotes differentiation of muscle stem/progenitor cells. Development 141: 2611–2620.
43. Milán, M., S. Campuzano, and A. García-Bellido, 1997 Developmental parameters of cell death in the wing disc of Drosophila. Proc. Natl. Acad. Sci. USA 94: 5691–5696
44. Mukherjee, P., B. Gildor, B. Z. Shilo, K. VijayRaghavan, and E. D. Schejter, 2011 The actin nucleator WASp is required for myoblast fusion during adult Drosophila myogenesis. Development 138: 2347–2357.
45. Natalizio, A. H., and A. G. Matera, 2013 Identification and characterization of Drosophila Snurportin reveals a role for the import receptor Moleskin/importin-7 in snRNP biogenesis. Mol. Biol. Cell 24: 2932–2942.
46. Ranganayakulu, G., B. Zhao, A. Dokidis, J. D. Molkentin, E. N. Olson et al., 1995 A series of mutations in the D-MEF2 transcription factor reveal multiple functions in larval and adult myogenesis in Drosophila. Dev. Biol. 171: 169–181.
47. Roy, S., and K. VijayRaghavan, 1998 Patterning muscles using organizers: larval muscle templates and adult myoblasts actively interact to pattern the dorsal longitudinal flight muscles of Drosophila. J. Cell Biol. 141: 1135–1145.
48. Roy, S., and K. VijayRaghavan, 1999 Muscle pattern diversification in Drosophila: the story of imaginal myogenesis. Bioessays 21: 486–498.
49. Shim, J., S. Gururaja-Rao, and U. Banerjee, 2013 Nutritional regulation of stem and progenitor cells in Drosophila. Development 140: 4647–4656.
50. Soler, C., and M. V. Taylor, 2009 The Him gene inhibits the development of Drosophila flight muscles during metamorphosis. Mech. Dev. 126: 595–603.
51. Sudarsan, V., S. Anant, P. Guptan, K. VijayRaghavan, and H. Skaer, 2001 Myoblast diversification and ectodermal signaling in Drosophila. Dev. Cell 1: 829–839.

52. Swarup, S., and E. M. Verheyen, 2012 Wnt/Wingless signaling in Drosophila. Cold Spring Harb. Perspect. Biol. 4: a007930.
53. Takashima, S., M. Mkrtchyan, A. Younossi-Hartenstein, J. R. Merriam, and V. Hartenstein, 2008 The behaviour of Drosophila adult hindgut stem cells is controlled by Wnt and Hh signalling. Nature 454: 651–655.
54. Tumaneng, K., R. C. Russell, and K. L. Guan, 2012 Organ size control by Hippo and TOR pathways. Curr. Biol. 22: R368–R379.
55. Weitkunat, M., and F. Schnorrer, 2014 A guide to study Drosophila muscle biology. Methods 68: 2–14.
56. Xin, N., H. Benchabane, A. Tian, K. Nguyen, L. Klofas et al., 2011 Erect Wing facilitates context-dependent Wnt/Wingless signaling by recruiting the cell-specific Armadillo-TCF adaptor Earthbound to chromatin. Development 138: 4955–4967.

5.3 Thin is required for cell death in the *Drosophila* abdominal muscles by targeting DIAP1

During *Drosophila* metamorphosis, larval tissues undergo selective programmed cell death (PCD) essential to establish an adult body plan. It is reported that first pulse of ecdysone initiates larval to pupal transition and the second pulse triggers PCD around 12h APF (after puparium formation) which results in histolysis of old tissues to allow for new tissue growth before eclosion. The mid-gut histolysis is regulated by early ecdysone pulse followed by autophagy signaling. Salivary gland requires late ecdysone pulse and elimination are mediated by both cell death and autophagy genes. However, not much is known about the signaling pathways implicated in muscle remodeling during pupation. *Drosophila* generates two distinct sets of muscles during its life cycle. First set muscles are formed during embryogenesis for larval movement and the other set during pupal morphogenesis for adult behavior. Most of the larval muscles are histolyzed during metamorphosis and causes pupal remodeling to form adult-specific muscles. The muscles that undergo remodeling during the pupal transition are the dorsal internal oblique muscles (DIOMs) and the dorsal external oblique muscles (DEOMs). DIOMs do not undergo histolysis and persist until the adult stage, while PCD controls the elimination of DEOMs. On the contrary, DEOM1 histolysis is initiated at 8h APF and the muscles are lost at 12h APF. DEOM2 histolysis is completed by 24h APF.

We previously showed that TRIM32 is essential for myofibrillar stability and costamere integrity. In this study, we discovered a novel role of TRIM32 in regulating abdominal muscle breakdown. TRIM32 functions in a cell death pathway with Death-associated inhibitor of apoptosis 1 **(**DIAP1) and Death regulator Nedd2-like caspase (Dronc). Reducing TRIM32

expression results in a partial block in the degradation of DEOMs at 24h APF. Further analysis revealed that TRIM32 expression is not regulated by ecdysone. *In vivo* staining revealed overall reduced Caspase 3 (Dronc) protein in muscles with disrupted TRIM32 function. We also analyzed DIAP1 protein levels at different time points. *tnRNAi* DEOM*s* presented elevated levels of DIAP as compared to the control. Dronc and DIAP1 transcript levels in *tn* mutants were not altered.

Further muscle-specific overexpression of *DIAPI* or *p35* (baculovirus protein inhibits effector caspase) partially blocks the DEOM histolysis and no significant difference in DEOM1 histolysis was observed upon RNAi knockdown of *tn* alone and with the *DIAP1* and *p35* expression in the tn RNAi background. Muscle-specific Knockdown *Dark* and *Dronc* in *tn* RNAi background did not enhance the histolysis. DEOM1 histolysis was also blocked in *Dark* and *Dronc* mutants at 12h APF similar to *tn* mutant but to a lesser extent. In *tn* mutants, muscle degeneration was completely abolished. The data suggest that TRIM32 regulates muscle breakdown by acting through the DIAP1-Dronc pathway. mRNA levels of the cell death genes were normal in a *tn* mutant background, suggesting post-transcriptional regulation of these genes by TRIM32. Next, we did genetic rescue experiments to investigate the requirement of RING and NHL domain in muscle histolysis. We found that DEOM1 was intact after 24 APF in RING deletion mutant, and DEOM1 histolysis was rescued upon introducing TRIM32FL. DIAP1 elevated levels were also observed in the RING deletion mutant. Interestingly, DEOM1 histolysis was restored in NHL mutant, providing evidence that the RING domain is essential for muscle breakdown. Further western blot analysis showed increased DIAP1 protein levels in *tn* mutants at 8h APF compared to WT, suggesting that TRIM32 regulates DIAP1 protein turnover through proteasomal degradation.

DIAP1 binds Dronc and inhibits its activity. During apoptosis, Dronc gets cleaved into Pr1(processed form 1) and Pr2 (processed form 2) form. DIAP1 physically interacts with FL Dronc to prevent its cleavage into Pr2 active protein. In *tn* mutants, only Pr1 form was present, suggesting upregulation of DIAP1 in *tn RNAi* background prevents Dronc processing and activation. Our study discovered a new function of TRIM32 in muscle histolysis. The genetic and biochemical assays provide evidence that DIAP1 is a target of TRIM32 and regulates the caspase activity critical for initiating cell death.

References

1. Fuchs, Y. & Steller, H. Programmed cell death in animal development and disease. Cell 147, 742–758 (2011).
2. Fuchs, Y. & Steller, H. Live to die another way: modes of programmed cell death and the signals emanating from dying cells. Nat. Rev. Mol. Cell. Biol. 16, 329–344 (2015).
3. Denton, D., Aung-Htut, M. T. & Kumar, S. Developmentally programmed cell death in Drosophila. Biochim. Biophys. Acta 1833, 3499–3506 (2013).
4. Baehrecke, E. H. How death shapes life during development. Nat. Rev. Mol. Cell. Biol. 3, 779–787 (2002).
5. Jacobson, M. D., Weil, M. & Raff, M. C. Programmed cell death in animal development. Cell 88, 347–354 (1997).
6. Kerr, J. F., Wyllie, A. H. & Currie, A. R. Apoptosis: a basic biological phenomenon with wide-ranging implications in tissue kinetics. Br. J. Cancer 26, 239–257 (1972).
7. Yang, Z. & Klionsky, D. J. An overview of the molecular mechanism of autophagy. Curr. Top. Microbiol. Immunol. 335, 1–32 (2009).
8. Walker, N. I., Harmon, B. V., Gobé, G. C. & Kerr, J. F. Patterns of cell death. Methods Achiev. Exp. Pathol. 13, 18–54 (1988).
9. Nicolson, S., Denton, D. & Kumar, S. Ecdysone-mediated programmed cell death in Drosophila. Int. J. Dev. Biol. 59, 23–32 (2015).
10. Baehrecke, E. H. Ecdysone signaling cascade and regulation of Drosophila metamorphosis. Arch. Insect Biochem. Physiol. 33, 231–244 (1996).
11. Baehrecke, E. H. Autophagic programmed cell death in Drosophila. Cell Death Differ. 10, 940–945 (2003).
12. Thummel, C. S. Flies on steroids—Drosophila metamorphosis and the mechanisms of steroid hormone action. Trends Genet. 12, 306–310 (1996).
13. Jiang, C., Baehrecke, E. H. & Thummel, C. S. Steroid regulated programmed cell death during Drosophila metamorphosis. Development 124, 4673–4683 (1997).
14. Jiang, C., Lamblin, A. F., Steller, H. & Thummel, C. S. A steroid-triggered transcriptional hierarchy controls salivary gland cell death during Drosophila metamorphosis. Mol. Cell 5, 445–455 (2000).
15. Lee, C. Y., Simon, C. R., Woodard, C. T. & Baehrecke, E. H. Genetic mechanism for the stage- and tissue-specific regulation of steroid triggered programmed cell death in Drosophila. Dev. Biol. 252, 138–148 (2002).
16. DiBello, P. R., Withers, D. A., Bayer, C. A., Fristrom, J. W. & Guild, G. M. The Drosophila broad-complex encodes a family of related proteins containing zinc fingers. Genetics 129, 385–397 (1991).
17. Cakouros, D., Daish, T., Martin, D., Baehrecke, E. H. & Kumar, S. Ecdysoneinduced expression of the caspase DRONC during hormone-dependent programmed cell death in Drosophila is regulated by Broad-Complex. J. Cell Biol. 157, 985–995 (2002)
18. Burtis, K. C., Thummel, C. S., Jones, C. W., Karim, F. D. & Hogness, D. S. The Drosophila 74EF early puff contains E74, a complex ecdysone-inducible gene that encodes two ets-related proteins. Cell 61, 85–99 (1990).
19. Baehrecke, E. H. & Thummel, C. S. The Drosophila E93 gene from the 93F early puff displays stage- and tissue-specific regulation by 20-hydroxyecdysone. Dev. Biol. 171, 85–97 (1995).

20. Daish, T. J., Cakouros, D. & Kumar, S. Distinct promoter regions regulate spatial and temporal expression of the Drosophila caspase dronc. Cell Death Differ. 10, 1348–1356 (2003).
21. Kilpatrick, Z. E., Cakouros, D. & Kumar, S. Ecdysone-mediated up-regulation of the effector caspase DRICE is required for hormone-dependent apoptosis in Drosophila cells. J. Biol. Chem. 280, 11981–11986 (2005).
22. Berry, D. L. & Baehrecke, E. H. Growth arrest and autophagy are required for salivary gland cell degradation in Drosophila. Cell 131, 1137–1148 (2007).
23. Denton, D. et al. Autophagy, not apoptosis, is essential for midgut cell death in Drosophila. Curr. Biol. 19, 1741–1746 (2009).
24. Bate, M., Rushton, E. & Currie, D. A. Cells with persistent twist expression are the embryonic precursors of adult muscles in Drosophila. Development 113, 79–89 (1991).
25. Currie, D. A. & Bate, M. The development of adult abdominal muscles in Drosophila: myoblasts express twist and are associated with nerves. Development 113, 91–102 (1991).
26. Kimura, K. I. & Truman, J. W. Postmetamorphic cell death in the nervous and muscular systems of Drosophila melanogaster. J. Neurosci. 10, 403–401 (1990).
27. Wasser, M., Bte Osman, Z. & Chia, W. EAST and Chromator control the destruction and remodeling of muscles during Drosophila metamorphosis. Dev. Biol. 307, 380–393 (2007)
28. Zirin, J. et al. Ecdysone signaling at metamorphosis triggers apoptosis of Drosophila abdominal muscles. Dev. Biol. 383, 275–284 (2013).
29. Kuleesha, Y., Puah, W. C., Lin, F. & Wasser, M. FMAj: a tool for high content analysis of muscle dynamics in Drosophila metamorphosis. BMC Bioinforma. 15(Suppl. 16), S6 (2014).
30. Kuleesha, Y., Puah, W. C. & Wasser, M. Live imaging of muscle histolysis in Drosophila metamorphosis. BMC Dev. Biol. 16, 12 (2016).
31. Meier, P., Finch, A. & Evan, G. Apoptosis in development. Nature 407, 796–801 (2000).
32. Thornberry, N. A. Caspases: key mediators of apoptosis. Chem. Biol. 5, R97–R103 (1998).
33. McIlwain, D. R., Berger, T. & Mak, T. W. Caspase functions in cell death and disease. Cold Spring Harb. Perspect. Biol. 5, a008656 (2013).
34. Salvesen, G. S. & Duckett, C. S. IAP proteins: blocking the road to death's door. Nat. Rev. Mol. Cell. Biol. 3, 401–410 (2002).
35. Kocab, A. J. & Duckett, C. S. Inhibitor of apoptosis proteins as intracellular signaling intermediates. FEBS J. 283, 221–231 (2016).
36. Meier, P., Silke, J., Leevers, S. J. & Evan, G. I. The Drosophila caspase DRONC is regulated by DIAP1. EMBO J. 19, 598–611 (2000).
37. Daish, T. J., Mills, K. & Kumar, S. Drosophila caspase DRONC is required for specific developmental cell death pathways and stress-induced apoptosis. Dev. Cell 7, 909–915 (2004).
38. Waldhuber, M., Emoto, K. & Petritsch, C. The Drosophila caspase DRONC is required for metamorphosis and cell death in response to irradiation and developmental signals. Mech. Dev. 122, 914–927 (2005).
39. Wang, S. L., Hawkins, C. J., Yoo, S. J., Müller, H. A. & Hay, B. A. The Drosophila caspase inhibitor DIAP1 is essential for cell survival and is negatively regulated by HID. Cell 98, 453–463 (1999).
40. Yoo, S. J. et al. Hid, Rpr and Grim negatively regulate DIAP1 levels through distinct mechanisms. Nat. Cell Biol. 4, 416–424 (2002).

41. Goyal, L., McCall, K., Agapite, J., Hartwieg, E. & Steller, H. Induction of apoptosis by Drosophila reaper, hid and grim through inhibition of IAP function. EMBO J. 19, 589–597 (2000).
42. Ryoo, H. D., Bergmann, A., Gonen, H., Ciechanover, A. & Steller, H. Regulation of Drosophila IAP1 degradation and apoptosis by reaper and ubcD1. Nat. Cell Biol. 4, 432–438 (2002).
43. Hays, R., Wickline, L. & Cagan, R. Morgue mediates apoptosis in the Drosophila melanogaster retina by promoting degradation of DIAP1. Nat. Cell Biol. 4, 425–431 (2002).
44. Yu, X., Wang, L., Acehan, D., Wang, X. & Akey, C. W. Three-dimensional structure of a double apoptosome formed by the Drosophila Apaf-1 related killer. J. Mol. Biol. 355, 577–589 (2006).
45. Yuan, S. et al. Structure of the Drosophila apoptosome at 6.9 å resolution. Structure 19, 128–140 (2011).
46. Lazzari, E. & Meroni, G. TRIM32 ubiquitin E3 ligase, one enzyme for several pathologies: from muscular dystrophy to tumours. Int. J. Biochem. Cell Biol. 79, 469–477 (2016).
47. Shieh, P. B., Kudryashova, E. & Spencer, M. J. Limb-girdle muscular dystrophy 2H and the role of TRIM32. Handb. Clin. Neurol. 101, 125–133 (2011).
48. LaBeau-DiMenna, E. M. et al. Thin, a Trim32 ortholog, is essential for myofibril stability and is required for the integrity of the costamere in Drosophila. Proc. Natl Acad. Sci. USA 109, 17983–17988 (2012).
49. Brooks, D. S., Vishal, K., Kawakami, J., Bouyain, S. & Geisbrecht, E. R. Optimization of wrMTrck to monitor Drosophila larval locomotor activity. J. Insect Physiol. 93- 94, 11–17 (2016).
50. Yin, V. P. & Thummel, C. S. Mechanisms of steroid-triggered programmed cell death in Drosophila. Semin. Cell Dev. Biol. 16, 237–243 (2005).
51. Fan, Y. & Bergmann, A. The cleaved-Caspase-3 antibody is a marker of Caspase-9-like DRONC activity in Drosophila. Cell Death Differ. 17, 534–539 (2010).
52. Huh, J. R., Guo, M. & Hay, B. A. Compensatory proliferation induced by cell death in the Drosophila wing disc requires activity of the apical cell death caspase Dronc in a nonapoptotic role. Curr. Biol. 14, 1262–1266 (2004).
53. Srivastava, M. et al. ARK, the Apaf-1 related killer in Drosophila, requires diverse domains for its apoptotic activity. Cell Death Differ. 14, 92–102 (2007).
54. Xu, D., Li, Y., Arcaro, M., Lackey, M. & Bergmann, A. The CARD-carrying caspase Dronc is essential for most, but not all, developmental cell death in Drosophila. Development 132, 2125–2134 (2005).
55. Tocchini, C. & Ciosk, R. TRIM-NHL proteins in development and disease. Semin. Cell Dev. Biol. 47-48, 52–59 (2015).
56. Muro, I., Hay, B. A. & Clem, R. J. The Drosophila DIAP1 protein is required to prevent accumulation of a continuously generated, processed form of the apical caspase DRONC. J. Biol. Chem. 277, 49644–49650 (2002).
57. Muro, I., Monser, K. & Clem, R. J. Mechanism of Dronc activation in Drosophila cells. J. Cell Sci. 117, 5035–5041 (2004).
58. Lee, T. V. et al. Drosophila IAP1-mediated ubiquitylation controls activation of the initiator caspase DRONC independent of protein degradation. PLoS Genet. 7, e1002261 (2011).

59. Conradt, B. Genetic control of programmed cell death during animal development. Annu. Rev. Genet. 43, 493–523 (2009).
60. Frosk, P., Del Bigio, M. R., Wrogemann, K. & Greenberg, C. R. Hutterite brothers both affected with two forms of limb girdle muscular dystrophy: LGMD2H and LGMD2I. Eur. J. Hum. Genet. 13, 978–982 (2005).
61. Schoser, B. G. et al. Commonality of TRIM32 mutation in causing sarcotubular myopathy and LGMD2H. Ann. Neurol. 57, 591–595 (2005).
62. Borg, K. et al. Intragenic deletion of TRIM32 in compound heterozygotes with sarcotubular myopathy/LGMD2H. Hum. Mutat. 30, E831–E844 (2009).
63. Cossée, M. et al. Use of SNP array analysis to identify a novel TRIM32 mutation in limb-girdle muscular dystrophy type 2H. Neuromuscul. Disord. 19, 255–260 (2009).
64. Nectoux, J. et al. Detection of TRIM32 deletions in LGMD patients analyzed by a combined strategy of CGH array and massively parallel sequencing. Eur. J. Hum. Genet. 23, 929–934 (2015).
65. Neri, M. et al. A patient with limb girdle muscular dystrophy carries a TRIM32 deletion, detected by a novel CGH array, in compound heterozygosis with a nonsense mutation. Neuromuscul. Disord. 23, 478–482 (2013).
66. Saccone, V. et al. Mutations that impair interaction properties of TRIM32 associated with limb-girdle muscular dystrophy 2H. Hum. Mutat. 29, 240–247 (2008).
67. Cohen, S., Zhai, B., Gygi, S. P. & Goldberg, A. L. Ubiquitylation by Trim32 causes coupled loss of desmin, Z-bands, and thin filaments in muscle atrophy. J. Cell Biol. 198, 575–589 (2012).
68. Kudryashova, E., Kudryashov, D., Kramerova, I. & Spencer, M. J. Trim32 is a ubiquitin ligase mutated in limb girdle muscular dystrophy type 2H that binds to skeletal muscle myosin and ubiquitinates actin. J. Mol. Biol. 354, 413–424 (2005).
69. Locke, M., Tinsley, C. L., Benson, M. A. & Blake, D. J. TRIM32 is an E3 ubiquitin ligase for dysbindin. Hum. Mol. Genet. 18, 2344–2358 (2009).
70. Kudryashova, E., Kramerova, I. & Spencer, M. J. Satellite cell senescence underlies myopathy in a mouse model of limb-girdle muscular dystrophy 2H. J. Clin. Invest. 122, 1764–1776 (2012).
71. Liu, J. et al. E3 ubiquitin ligase TRIM32 negatively regulates tumor suppressor p53 to promote tumorigenesis. Cell Death Differ. 21, 1792–1804 (2014). 72. Lin, T. Y., Huang, C. H., Chou, W. G. & Juang, J. L. Abi enhances Abl-mediated CDC2 phosphorylation and inactivation. J. Biomed. Sci. 11, 902–910 (2004).
72. Ryu, Y. S. et al. TRIM32 protein sensitizes cells to tumor necrosis factor (TNFα)- induced apoptosis via its RING domain-dependent E3 ligase activity against Xlinked inhibitor of apoptosis (XIAP). J. Biol. Chem. 286, 25729–25738 (2011).
73. Qi, Y., Liu, H., Daniels, M. P., Zhang, G. & Xu, H. Loss of Drosophila i-AAA protease, dYME1L, causes abnormal mitochondria and apoptotic degeneration. Cell Death Differ. 23, 291–302 (2016).
74. Zirin, J., Nieuwenhuis, J. & Perrimon, N. Role of autophagy in glycogen breakdown and its relevance to chloroquine myopathy. PLoS Biol. 11, e1001708 (2013)
75. Wilson, R. et al. The DIAP1 RING finger mediates ubiquitination of Dronc and is indispensable for regulating apoptosis. Nat. Cell Biol. 4, 445–450 (2002).

76. Burgess, A. et al. Loss of human Greatwall results in G2 arrest and multiple mitotic defects due to deregulation of the cyclin B-Cdc2/PP2A balance. Proc. Natl Acad. Sci. USA 107, 12564–12569 (2010).
77. McCloy, R. A. et al. Partial inhibition of Cdk1 in G2 phase overrides the SAC and decouples mitotic events. Cell Cycle 13, 1400–1412 (2014).

5.4 *Drosophila* NUAK functions with Starvin/BAG3 in autophagic protein turnover

Abnormal accumulation of proteins within muscle fibers may result from impaired clearance of protein aggregates via UPS and or ALS. Under cellular stress chaperone-assisted selective autophagy (CASA) assists and facilitate disposal of damaged proteins. CASA complex is well conserved in mammals and *Drosophila*. The CASA complex comprises of molecular chaperones HSPA8/HSC70 and HSPB8/HSP22, co-chaperons BAG3 and STUB1/CHIP. In striated muscles, the CASA complex localizes at the Z-disks and serves as a mechanical sensor and recognizes damaged Filamin (Fil) protein and initiates its autophagic disposal. Mutations in CASA complex has been associated with myopathies and muscular dystrophies.

Our lab has identified a novel role for *Drosophila NUAK,* a serine threonine kinase in the autophagy-assisted protein clearance in muscle tissue. *NUAK* mutants exhibit degenerative muscles and defective larval locomotion. Loss of *NUAK* also limits new sarcomere addition however, the muscle defects are independent of growth. The myofibrillar defects include thinning muscles, muscle detachment and loss of sarcomeric patterning. Dark regions within the muscle devoid of F-actin were also observed. Transmission Electron Microscopy (TEM) micrographs revealed presence of damaged organelles and disintegrated Z-disc structure. Immunostaining showed accumulation of Filamin and CryAB in the *NUAK* mutant muscles. Further we used yeast two-hybrid screening approach (Y2H) to identify novel targets of *Drosophila* NUAK. Interestingly, Starvin and Filamin were identified as prey proteins and further analysis confirmed NUAK physically interacts with Starvin/BAG-3. We utilized GAL4/UAS system to analyze NUAK-Stv function in the muscle tissue. Knockdown of *stv* in *NUAK* heterozygous mutant background enhanced the muscle defects, providing evidence that *NUAK* and *stv* genetically

interact. Starvin/BAG-3 functions in autophagy pathway and Y2H approach identified clones of NUAK and HSC70 ATPase. BAG-3 is known to interact with HSC70 ATPase and accelerate the release of ADP and other client proteins. Further reducing *HSC70-4* expression *stv/+* background induced lethality and knockdown of *HSC70-4* alone in muscle caused extensive muscle damage and dark regions in the muscle showed Fil accumulation similar to *NUAK* and *Stv* mutants. The data together provides evidence that HSC70 ATPase is critical to prevent protein aggregation. Based on the genetic analysis we also observed increased number of p62(+) and ubiquitin puncta in *NUAK* and *stv* mutants. Immunoblot analysis also presented elevated p62 protein levels in both *NUAK* and *stv* L3 mutants. We also found that silencing Atg8a/LC3 core autophagy protein in muscles phenocopied the defects observed in *stv* and *NUAK* mutant. Further we also confirm that *Atg8a* genetically interacts with *NUAK* and *stv*. The biochemical analysis also exhibited accumulation of insoluble K63 linked Ubi and Filamin in *NUAK* mutants. For efficient clearance of protein aggregates fusion of autophagosomes with lysosome is crucial. Interestingly, we did not observe lysosomes in the aggregate region upon loss of *NUAK*. Taken together our study provides evidence that loss of *NUAK* results in protein aggregation in muscle tissue and perturbs sarcomeric structure and function. NUAK functions with Stv/BAG3 in facilitating autophagy mediated clearance of damaged proteins.

References

1. Jia B, Wu Y, Zhou Y. 14-3-3 and aggresome formation: implications in neurodegenerative diseases. Prion. 2014; 8(2). Epub 2014/02/18. https://doi.org/10.4161/pri.28123 PMID: 24549097; PubMed Central PMCID: PMC4189886.
2. Takalo M, Salminen A, Soininen H, Hiltunen M, Haapasalo A. Protein aggregation and degradation mechanisms in neurodegenerative diseases. Am J Neurodegener Dis. 2013; 2(1):1–14. Epub 2013/03/ 08. PMID: 23516262; PubMed Central PMCID: PMC3601466
3. Shamsi TN, Athar T, Parveen R, Fatima S. A review on protein misfolding, aggregation and strategies to prevent related ailments. Int J Biol Macromol. 2017; 105(Pt 1):993–1000. Epub 2017/07/23. https:// doi.org/10.1016/j.ijbiomac.2017.07.116 PMID: 28743576.
4. Klaips CL, Jayaraj GG, Hartl FU. Pathways of cellular proteostasis in aging and disease. J Cell Biol. 2018; 217(1):51–63. Epub 2017/11/10. https://doi.org/10.1083/jcb.201709072 PMID: 29127110; PubMed Central PMCID: PMC5748993.
5. Kaushik S, Cuervo AM. Chaperones in autophagy. Pharmacol Res. 2012; 66(6):484–93. Epub 2012/ 10/08. https://doi.org/10.1016/j.phrs.2012.10.002 PMID: 23059540; PubMed Central PMCID: PMC3502706.
6. Klimek C, Kathage B, Wo¨rdehoff J, Ho¨hfeld J. BAG3-mediated proteostasis at a glance. J Cell Sci. 2017; 130(17):2781–8. Epub 2017/08/14. https://doi.org/10.1242/jcs.203679 PMID: 28808089.
7. Stu¨rner E, Behl C. The Role of the Multifunctional BAG3 Protein in Cellular Protein Quality Control and in Disease. Front Mol Neurosci. 2017; 10:177. Epub 2017/06/21. https://doi.org/10.3389/fnmol.2017. 00177 PMID: 28680391; PubMed Central PMCID: PMC5478690.
8. Kettern N, Dreiseidler M, Tawo R, Ho¨hfeld J. Chaperone-assisted degradation: multiple paths to destruction. Biol Chem. 2010; 391(5):481–https://doi.org/10.1515/BC.2010.058 PMID: 20302520.
9. Ulbricht A, Ho¨hfeld J. Tension-induced autophagy: may the chaperone be with you. Autophagy. 2013; 9 (6):920–2. Epub 2013/03/21. https://doi.org/10.4161/auto.24213 PMID: 23518596; PubMed Central PMCID: PMC3672301.
10. Ulbricht A, Arndt V, Ho¨hfeld J. Chaperone-assisted proteostasis is essential for mechanotransduction in mammalian cells. Commun Integr Biol. 2013; 6(4):e24925. Epub 2013/06/11. https://doi.org/10.4161/ cib.24925 PMID: 23986815; PubMed Central PMCID: PMC3737759.
11. Arndt V, Dick N, Tawo R, Dreiseidler M, Wenzel D, Hesse M, et al. Chaperone-assisted selective autophagy is essential for muscle maintenance. Curr Biol. 2010; 20(2):143–8. Epub 2010/01/07. https://doi. org/10.1016/j.cub.2009.11.022 PMID: 20060297.
12. Ulbricht A, Eppler FJ, Tapia VE, van der Ven PF, Hampe N, Hersch N, et al. Cellular mechanotransduction relies on tension-induced and chaperone-assisted autophagy. Curr Biol. 2013; 23(5):430–5. Epub 2013/02/21. https://doi.org/10.1016/j.cub.2013.01.064 PMID: 23434281.
13. Ulbricht A, Gehlert S, Leciejewski B, Schiffer T, Bloch W, Ho¨hfeld J. Induction and adaptation of chaperone-assisted selective autophagy CASA in response to resistance exercise in human skeletal muscle. Autophagy. 2015; 11(3):538–46. https://doi.org/10.1080/15548627.2015.1017186 PMID: 25714469; PubMed Central PMCID: PMC4502687.

14. Fu¨rst DO, Goldfarb LG, Kley RA, Vorgerd M, Olive´ M, van der Ven PF. Filamin C-related myopathies: pathology and mechanisms. Acta Neuropathol. 2013; 125(1):33–46. Epub 2012/10/30. https://doi.org/ 10.1007/s00401-012-1054-9 PMID: 23109048; PubMed Central PMCID: PMC5127197.
15. Razinia Z, Ma¨kela¨ T, Yla¨nne J, Calderwood DA. Filamins in mechanosensing and signaling. Annu Rev Biophys. 2012; 41:227–46. Epub 2012/02/23. https://doi.org/10.1146/annurev-biophys-050511-102252 PMID: 22404683; PubMed Central PMCID: PMC5508560.
16. Gamerdinger M, Kaya AM, Wolfrum U, Clement AM, Behl C. BAG3 mediates chaperone-based aggresome-targeting and selective autophagy of misfolded proteins. EMBO Rep. 2011; 12(2):149–56. Epub 2011/01/21. https://doi.org/10.1038/embor.2010.203 PMID: 21252941; PubMed Central PMCID: PMC3049430.
17. Shaid S, Brandts CH, Serve H, Dikic I. Ubiquitination and selective autophagy. Cell Death Differ. 2013; 20(1):21–30. Epub 2012/06/22. https://doi.org/10.1038/cdd.2012.72 PMID: 22722335; PubMed Central PMCID: PMC3524631.
18. Tanaka Y, Guhde G, Suter A, Eskelinen EL, Hartmann D, Lu¨llmann-Rauch R, et al. Accumulation of autophagic vacuoles and cardiomyopathy in LAMP-2-deficient mice. Nature. 2000; 406(6798):902–6. https://doi.org/10.1038/35022595 PMID: 10972293.
19. Sun X, Gao L, Chien HY, Li WC, Zhao J. The regulation and function of the NUAK family. J Mol Endocrinol. 2013; 51(2):R15–22. https://doi.org/10.1530/JME-13-0063 PMID: 23873311.
20. Hawley SA, Boudeau J, Reid JL, Mustard KJ, Udd L, Ma¨kela¨ TP, et al. Complexes between the LKB1 tumor suppressor, STRAD alpha/beta and MO25 alpha/beta are upstream kinases in the AMP-activated protein kinase cascade. J Biol. 2003; 2(4):28. Epub 2003/09/24. https://doi.org/10.1186/1475- 4924-2-28 PMID: 14511394; PubMed Central PMCID: PMC333410.
21. Lefebvre DL, Rosen CF. Regulation of SNARK activity in response to cellular stresses. Biochim Biophys Acta. 2005; 1724(1–2):71–85. Epub 2005/04/08. https://doi.org/10.1016/j.bbagen.2005.03.015 PMID: 15893879.
22. Koh HJ, Toyoda T, Fujii N, Jung MM, Rathod A, Middelbeek RJ, et al. Sucrose nonfermenting AMPKrelated kinase (SNARK) mediates contraction-stimulated glucose transport in mouse skeletal muscle. Proc Natl Acad Sci U S A. 2010; 107(35):15541–6. https://doi.org/10.1073/pnas.1008131107 PMID: 20713714; PubMed Central PMCID: PMC2932588.
23. Lessard SJ, Rivas DA, So K, Koh HJ, Queiroz AL, Hirshman MF, et al. The AMPK-related kinase SNARK regulates muscle mass and myocyte survival. J Clin Invest. 2016; 126(2):560–70. https://doi. org/10.1172/JCI79197 PMID: 26690705; PubMed Central PMCID: PMC4731174.
24. Fisher JS, Ju JS, Oppelt PJ, Smith JL, Suzuki A, Esumi H. Muscle contractions, AICAR, and insulin cause phosphorylation of an AMPK-related kinase. Am J Physiol Endocrinol Metab. 2005; 289(6): E986–92. Epub 2005/07/19. https://doi.org/10.1152/ajpendo.00335.2004 PMID: 16030062; PubMed Central PMCID: PMC1350986.

25. Hirano M, Kiyonari H, Inoue A, Furushima K, Murata T, Suda Y, et al. A new serine/threonine protein kinase, Omphk1, essential to ventral body wall formation. Dev Dyn. 2006; 235(8):2229–37. https://doi. org/10.1002/dvdy.20823 PMID: 16715502.
26. Inazuka F, Sugiyama N, Tomita M, Abe T, Shioi G, Esumi H. Muscle-specific knock-out of NUAK family SNF1-like kinase 1 (NUAK1) prevents high fat diet-induced glucose intolerance. J Biol Chem. 2012; 287(20):16379–https://doi.org/10.1074/jbc.M111.302687 PMID: 22418434; PubMed Central PMCID: PMC3351321.
27. Tsuchihara K, Ogura T, Fujioka R, Fujii S, Kuga W, Saito M, et al. Susceptibility of Snark-deficient mice to azoxymethane-induced colorectal tumorigenesis and the formation of aberrant crypt foci. Cancer Sci. 2008; 99(4):677–82. Epub 2007/02/27. https://doi.org/10.1111/j.1349-7006.2008.00734.x PMID: 18307533.
28. Hoppe PE, Chau J, Flanagan KA, Reedy AR, Schriefer LA. Caenorhabditis elegans unc-82 encodes a serine/threonine kinase important for myosin filament organization in muscle during growth. Genetics. 2010; 184(1):79–90. https://doi.org/10.1534/genetics.109.110189 PMID: 19901071; PubMed Central PMCID: PMC2815932.
29. Schiller NR, Duchesneau CD, Lane LS, Reedy AR, Manzon ER, Hoppe PE. The Role of the UNC-82 Protein Kinase in Organizing Myosin Filaments in Striated Muscle of. Genetics. 2017; 205(3):1195– 213. Epub 2016/12/30. https://doi.org/10.1534/genetics.116.193029 PMID: 28040740; PubMed Central PMCID: PMC5340333.
30. Amin N, Khan A, St Johnston D, Tomlinson I, Martin S, Brenman J, et al. LKB1 regulates polarity remodeling and adherens junction formation in the Drosophila eye. Proc Natl Acad Sci U S A. 2009; 106 (22):8941–6. https://doi.org/10.1073/pnas.0812469106 PMID: 19443685; PubMed Central PMCID: PMC2690039.
31. Couderc JL, Richard G, Vachias C, Mirouse V. Drosophila LKB1 is required for the assembly of the polarized actin structure that allows spermatid individualization. PLoS One. 2017; 12(8):e0182279. Epub 2017/08/02. https://doi.org/10.1371/journal.pone.0182279 PMID: 28767695; PubMed Central PMCID: PMC5540607.
32. LaBeau-DiMenna EM, Clark KA, Bauman KD, Parker DS, Cripps RM, Geisbrecht ER. Thin, a Trim32 ortholog, is essential for myofibril stability and is required for the integrity of the costamere in Drosophila. Proc Natl Acad Sci U S A. 2012; 109(44):17983–8. https://doi.org/10.1073/pnas.1208408109 PMID: 23071324; PubMed Central PMCID: PMC3497806.
33. Clark KA, Bland JM, Beckerle MC. The Drosophila muscle LIM protein, Mlp84B, cooperates with D-titin to maintain muscle structural integrity. J Cell Sci. 2007; 120(Pt 12):2066–77. https://doi.org/10.1242/jcs. 000695 PMID: 17535853.
34. Green N, Odell N, Zych M, Clark C, Wang ZH, Biersmith B, et al. A Common Suite of Coagulation Proteins Function in Drosophila Muscle Attachment. Genetics. 2016. Epub 2016/08/31. https://doi.org/10. 1534/genetics.116.189787 PMID: 27585844; PubMed Central PMCID: PMC5105843.
35. Fogerty FJ, Fessler LI, Bunch TA, Yaron Y, Parker CG, Nelson RE, et al. Tiggrin, a novel Drosophila extracellular matrix protein that functions as a ligand for Drosophila alpha PS2 beta PS integrins. Development. 1994; 120(7):1747–58. PMID: 7924982.

36. Wang L, Evans J, Andrews HK, Beckstead RB, Thummel CS, Bashirullah A. A genetic screen identifies new regulators of steroid-triggered programmed cell death in Drosophila. Genetics. 2008; 180(1):269– 81. Epub 2008/08/30. https://doi.org/10.1534/genetics.108.092478 PMID: 18757938; PubMed Central PMCID: PMC2535680.
37. Bate M. The embryonic development of larval muscles in Drosophila. Development. 1990; 110(3):791– 804. PMID: 2100994.
38. Tatum EL, Beadle GW. DEVELOPMENT OF EYE COLORS IN DROSOPHILA: SOME PROPERTIES OF THE HORMONES CONCERNED. J Gen Physiol. 1938; 22(2):239–53. https://doi.org/10.1085/jgp. 22.2.239 PMID: 19873102; PubMed Central PMCID: PMC2141983.
39. Wo´jtowicz I, Jabłońska J, Zmojdzian M, Taghli-Lamallem O, Renaud Y, Junion G, et al. Drosophila small heat shock protein CryAB ensures structural integrity of developing muscles, and proper muscle and heart performance. Development. 2015; 142(5):994–1005. https://doi.org/10.1242/dev.115352 PMID: 25715399.
40. Zago´rska A, Deak M, Campbell DG, Banerjee S, Hirano M, Aizawa S, et al. New roles for the LKB1- NUAK pathway in controlling myosin phosphatase complexes and cell adhesion. Sci Signal. 2010; 3 (115):ra25. https://doi.org/10.1126/scisignal.2000616 PMID: 20354225.
41. Carrera AC, Alexandrov K, Roberts TM. The conserved lysine of the catalytic domain of protein kinases is actively involved in the phosphotransfer reaction and not required for anchoring ATP. Proc Natl Acad Sci U S A. 1993; 90(2):442–6. https://doi.org/10.1073/pnas.90.2.442 PMID: 8421674; PubMed Central PMCID: PMC45679.
42. Reimann L, Wiese H, Leber Y, Schwa¨ble AN, Fricke AL, Rohland A, et al. Myofibrillar Z-discs Are a Protein Phosphorylation Hot Spot with Protein Kinase C (PKCα) Modulating Protein Dynamics. Mol Cell Proteomics. 2017; 16(3):346–67. Epub 2016/12/27. https://doi.org/10.1074/mcp.M116.065425 PMID: 28028127; PubMed Central PMCID: PMC5340999.
43. Deshmukh A, Coffey VG, Zhong Z, Chibalin AV, Hawley JA, Zierath JR. Exercise-induced phosphorylation of the novel Akt substrates AS160 and filamin A in human skeletal muscle. Diabetes. 2006; 55 (6):1776–82. https://doi.org/10.2337/db05-1419 PMID: 16731842.
44. Murray JT, Campbell DG, Peggie M, Mora A, Alfonso M, Cohen P. Identification of filamin C as a new physiological substrate of PKBalpha using KESTREL. Biochem J. 2004; 384(Pt 3):489–94. https://doi. org/10.1042/BJ20041058 PMID: 15461588; PubMed Central PMCID: PMC1134134.
45. Brand AH, Perrimon N. Targeted gene expression as a means of altering cell fates and generating dominant phenotypes. Development. 1993; 118(2):401–15. PMID: 8223268.
46. Coulson M, Robert S, Saint R. Drosophila starvin encodes a tissue-specific BAG-domain protein required for larval food uptake. Genetics. 2005; 171(4):1799–812. Epub 2005/09/02. https://doi.org/10. 1534/genetics.105.043265 PMID: 16143622; PubMed Central PMCID: PMC1456105.
47. Rosati A, Graziano V, De Laurenzi V, Pascale M, Turco MC. BAG3: a multifaceted protein that regulates major cell pathways. Cell Death Dis. 2011; 2:e141. Epub 2011/04/07.

https://doi.org/10.1038/ cddis.2011.24 PMID: 21472004; PubMed Central PMCID: PMC3122056.
48. Knezevic T, Myers VD, Gordon J, Tilley DG, Sharp TE, Wang J, et al. BAG3: a new player in the heart failure paradigm. Heart Fail Rev. 2015; 20(4):423–34. https://doi.org/10.1007/s10741-015-9487-6 PMID: 25925243; PubMed Central PMCID: PMC4463985.
49. Behl C. BAG3 and friends: co-chaperones in selective autophagy during aging and disease. Autophagy. 2011; 7(7):795–8. https://doi.org/10.4161/auto.7.7.15844 PMID: 21681022.
50. Kabbage M, Dickman MB. The BAG proteins: a ubiquitous family of chaperone regulators. Cell Mol Life Sci. 2008; 65(9):1390–402. https://doi.org/10.1007/s00018-008-7535-2 PMID: 18264803.
51. Takayama S, Xie Z, Reed JC. An evolutionarily conserved family of Hsp70/Hsc70 molecular chaperone regulators. J Biol Chem. 1999; 274(2):781–6. https://doi.org/10.1074/jbc.274.2.781 PMID: 9873016.
52. Takayama S, Reed JC. Molecular chaperone targeting and regulation by BAG family proteins. Nat Cell Biol. 2001; 3(10):E237–41. https://doi.org/10.1038/ncb1001-e237 PMID: 11584289.
53. Lamark T, Johansen T. Aggrephagy: selective disposal of protein aggregates by macroautophagy. Int J Cell Biol. 2012; 2012:736905. Epub 2012/03/22. https://doi.org/10.1155/2012/736905 PMID: 22518139; PubMed Central PMCID: PMC3320095.
54. Lim J, Yue Z. Neuronal aggregates: formation, clearance, and spreading. Dev Cell. 2015; 32(4):491– 501. https://doi.org/10.1016/j.devcel.2015.02.002 PMID: 25710535; PubMed Central PMCID: PMC4376477.
55. Lee YK, Lee JA. Role of the mammalian ATG8/LC3 family in autophagy: differential and compensatory roles in the spatiotemporal regulation of autophagy. BMB Rep. 2016; 49(8):424–30. https://doi.org/10. 5483/BMBRep.2016.49.8.081 PMID: 27418283; PubMed Central PMCID: PMC5070729.
56. Abdollahzadeh I, Schwarten M, Gensch T, Willbold D, Weiergra¨ber OH. The Atg8 Family of ProteinsModulating Shape and Functionality of Autophagic Membranes. Front Genet. 2017; 8:109. Epub 2017/ 08/28. https://doi.org/10.3389/fgene.2017.00109 PMID: 28894458; PubMed Central PMCID: PMC5581321.
57. Erdi B, Nagy P, Zvara A, Varga A, Pircs K, Me´nesi D, et al. Loss of the starvation-induced gene Rack1 leads to glycogen deficiency and impaired autophagic responses in Drosophila. Autophagy. 2012; 8 (7):1124–35. Epub 2012/05/07. https://doi.org/10.4161/auto.20069 PMID: 22562043; PubMed Central PMCID: PMC3429548.
58. Chintapalli VR, Wang J, Dow JA. Using FlyAtlas to identify better Drosophila melanogaster models of human disease. Nat Genet. 2007; 39(6):715–20. https://doi.org/10.1038/ng2049 PMID: 17534367.
59. Vereshchagina N, Bennett D, Szo¨or B, Kirchner J, Gross S, Vissi E, et al. The essential role of PP1beta in Drosophila is to regulate nonmuscle myosin. Mol Biol Cell. 2004; 15(10):4395–405. Epub 2004/07/ 21. https://doi.org/10.1091/mbc.E04-02-0139 PMID: 15269282; PubMed Central PMCID: PMC519135.
60. Mizuno T, Tsutsui K, Nishida Y. Drosophila myosin phosphatase and its role in dorsal closure. Development. 2002; 129(5):1215–23. PMID: 11874917.

61. Kathage B, Gehlert S, Ulbricht A, Lu¨decke L, Tapia VE, Orfanos Z, et al. The cochaperone BAG3 coordinates protein synthesis and autophagy under mechanical strain through spatial regulation of mTORC1. Biochim Biophys Acta. 2017; 1864(1):62–75. Epub 2016/10/15. https://doi.org/10.1016/j. bbamcr.2016.10.007 PMID: 27756573.
62. Modarres HP, Mofradt MR. Filamin: a structural and functional biomolecule with important roles in cell biology, signaling and mechanics. Mol Cell Biomech. 2014; 11(1):39–65. PMID: 25330623.
63. Puissant A, Fenouille N, Auberger P. When autophagy meets cancer through p62/SQSTM1. Am J Cancer Res. 2012; 2(4):397–413. Epub 2012/06/28. PMID: 22860231; PubMed Central PMCID: PMC3410580.
64. Klionsky DJ, Abdelmohsen K, Abe A, Abedin MJ, Abeliovich H, Acevedo Arozena A, et al. Guidelines for the use and interpretation of assays for monitoring autophagy (3rd edition). Autophagy. 2016; 12 (1):1–222. https://doi.org/10.1080/15548627.2015.1100356 PMID: 26799652; PubMed Central PMCID: PMC4835977.
65. Dimauro I, Antonioni A, Mercatelli N, Caporossi D. The role of αB-crystallin in skeletal and cardiac muscle tissues. Cell Stress Chaperones. 2018; 23(4):491–505. Epub 2017/11/30. https://doi.org/10.1007/ s12192-017-0866-x PMID: 29190034; PubMed Central PMCID: PMC6045558
66. Fichna JP, Potulska-Chromik A, Miszta P, Redowicz MJ, Kaminska AM, Zekanowski C, et al. A novel dominant D109A CRYAB mutation in a family with myofibrillar myopathy affects αB-crystallin structure. BBA Clin. 2017; 7:1–7. Epub 2016/11/11. https://doi.org/10.1016/j.bbacli.2016.11.004 PMID: 27904835; PubMed Central PMCID: PMC5124346.
67. Markossian KA, Yudin IK, Kurganov BI. Mechanism of suppression of protein aggregation by α-crystallin. Int J Mol Sci. 2009; 10(3):1314–45. Epub 2009/03/19. https://doi.org/10.3390/ijms10031314 PMID: 19399251; PubMed Central PMCID: PMC2672032.
68. Fujita M, Mitsuhashi H, Isogai S, Nakata T, Kawakami A, Nonaka I, et al. Filamin C plays an essential role in the maintenance of the structural integrity of cardiac and skeletal muscles, revealed by the medaka mutant zacro. Dev Biol. 2012; 361(1):79–89. Epub 2011/10/14. https://doi.org/10.1016/j.ydbio. 2011.10.008 PMID: 22020047.
69. Min JN, Whaley RA, Sharpless NE, Lockyer P, Portbury AL, Patterson C. CHIP deficiency decreases longevity, with accelerated aging phenotypes accompanied by altered protein quality control. Mol Cell Biol. 2008; 28(12):4018–25. Epub 2008/04/14. https://doi.org/10.1128/MCB.00296-08 PMID: 18411298; PubMed Central PMCID: PMC2423116.
70. Morishima Y, Wang AM, Yu Z, Pratt WB, Osawa Y, Lieberman AP. CHIP deletion reveals functional redundancy of E3 ligases in promoting degradation of both signaling proteins and expanded glutamine proteins. Hum Mol Genet. 2008; 17(24):3942–52. Epub 2008/09/10. https://doi.org/10.1093/hmg/ ddn296 PMID: 18784277; PubMed Central PMCID: PMC2605787
71. Kley RA, Maerkens A, Leber Y, Theis V, Schreiner A, van der Ven PF, et al. A combined laser microdissection and mass spectrometry approach reveals new disease relevant proteins accumulating in aggregates of filaminopathy patients. Mol Cell Proteomics. 2013; 12(1):215–27. Epub 2012/10/31. https://doi. org/10.1074/mcp.M112.023176 PMID: 23115302; PubMed Central PMCID: PMC3536902.

72. Maerkens A, Kley RA, Olive´ M, Theis V, van der Ven PF, Reimann J, et al. Differential proteomic analysis of abnormal intramyoplasmic aggregates in desminopathy. J Proteomics. 2013; 90:14–27. Epub 2013/04/30. https://doi.org/10.1016/j.jprot.2013.04.026 PMID: 23639843; PubMed Central PMCID: PMC5120880.
73. Maerkens A, Olive´ M, Schreiner A, Feldkirchner S, Schessl J, Uszkoreit J, et al. New insights into the protein aggregation pathology in myotilinopathy by combined proteomic and immunolocalization analyses. Acta Neuropathol Commun. 2016; 4:8. Epub 2016/02/03. https://doi.org/10.1186/s40478-016- 0280-0 PMID: 26842778; PubMed Central PMCID: PMC4739336.
74. Olive´ M, Kley RA, Goldfarb LG. Myofibrillar myopathies: new developments. Curr Opin Neurol. 2013; 26 (5):527–35. https://doi.org/10.1097/WCO.0b013e328364d6b1 PMID: 23995273; PubMed Central PMCID: PMC5127196.
75. Be´hin A, Salort-Campana E, Wahbi K, Richard P, Carlier RY, Carlier P, et al. Myofibrillar myopathies: State of the art, present and future challenges. Rev Neurol (Paris). 2015; 171(10):715–29. Epub 2015/ 09/03. https://doi.org/10.1016/j.neurol.2015.06.002 PMID: 26342832.
76. Winter L, Goldmann WH. Biomechanical characterization of myofibrillar myopathies. Cell Biol Int. 2015; 39(4):361–3. Epub 2014/12/03. https://doi.org/10.1002/cbin.10384 PMID: 25264173.
77. Kley RA, Olive´ M, Schro¨der R. New aspects of myofibrillar myopathies. Curr Opin Neurol. 2016; 29 (5):628–34. https://doi.org/10.1097/WCO.0000000000000357 PMID: 27389816.
78. Batonnet-Pichon S, Behin A, Cabet E, Delort F, Vicart P, Lilienbaum A. Myofibrillar Myopathies: New Perspectives from Animal Models to Potential Therapeutic Approaches. J Neuromuscul Dis. 2017; 4 (1):1–15. https://doi.org/10.3233/JND-160203 PMID: 28269794; PubMed Central PMCID: PMC5345645.
79. Fichna JP, Maruszak A, Żekanowski C. Myofibrillar myopathy in the genomic context. J Appl Genet. 2018; 59(4):431–9. Epub 2018/09/10. https://doi.org/10.1007/s13353-018-0463-4 PMID: 30203143.
80. Schro¨der R. Protein aggregate myopathies: the many faces of an expanding disease group. Acta Neuropathol. 2013; 125(1):1–2. https://doi.org/10.1007/s00401-012-1071-8 PMID: 23224320.
81. Carra S, Boncoraglio A, Kanon B, Brunsting JF, Minoia M, Rana A, et al. Identification of the Drosophila ortholog of HSPB8: implication of HSPB8 loss of function in protein folding diseases. J Biol Chem. 2010; 285(48):37811–22. Epub 2010/09/21. https://doi.org/10.1074/jbc.M110.127498 PMID: 20858900; PubMed Central PMCID: PMC2988385.
82. Green N, Walker J, Bontrager A, Zych M, Geisbrecht ER. A tissue communication network coordinating innate immune response during muscle stress. J Cell Sci. 2018; 131(24). Epub 2018/12/18. https://doi. org/10.1242/jcs.217943 PMID: 30478194; PubMed Central PMCID: PMC6307882.
83. Geisbrecht ER, Haralalka S, Swanson SK, Florens L, Washburn MP, Abmayr SM. Drosophila ELMO/ CED-12 interacts with Myoblast city to direct myoblast fusion and ommatidial organization. Dev Biol. 2008; 314(1):137–49.

https://doi.org/10.1016/j.ydbio.2007.11.022 PMID: 18163987; PubMed Central PMCID: PMC2697615.
84. Sokol NS, Cooley L. Drosophila filamin encoded by the cheerio locus is a component of ovarian ring canals. Curr Biol. 1999; 9(21):1221–30. https://doi.org/10.1016/s0960-9822(99)80502-8 PMID: 10556087.
85. Friedrich MV, Schneider M, Timpl R, Baumgartner S. Perlecan domain V of Drosophila melanogaster. Sequence, recombinant analysis and tissue expression. Eur J Biochem. 2000; 267(11):3149–59. https://doi.org/10.1046/j.1432-1327.2000.01337.x PMID: 10824099.
86. Wang ZH, Clark C, Geisbrecht ER. Drosophila Clueless is involved in Parkin-dependent mitophagy by promoting VCP-mediated Marf degradation. Hum Mol Genet. 2016. https://doi.org/10.1093/hmg/ ddw067 PMID: 26931463.
87. Brooks DS, Vishal K, Kawakami J, Bouyain S, Geisbrecht ER. Optimization of wrMTrck to monitor Drosophila larval locomotor activity. J Insect Physiol. 2016; 93–94:11–7. Epub 2016/07/16. https://doi.org/ 10.1016/j.jinsphys.2016.07.007 PMID: 27430166.

Chapter 6 - Conclusions and Future Directions

Conclusions

Our work identified two independent functions of TRIM32 in regulating glycolytic flux and costameric proteins critical for muscle homeostasis (BAWA *et al.* 2020). TRIM32, an E3 ligase is a ubiquitously expressed protein associated with a plethora of biological functions (WULCZYN *et al.* 2011; LAZZARI and MERONI 2016). Humans with mutations in TRIM32 are independently affected with Bardet-Biedl syndrome 11 (BBS11) and Limb-girdle muscular dystrophy type 2H (LGMD2H) (CHIANG *et al.* 2006). While the primary function of TRIM32 is to regulate protein turnover, most of the research has been focused on identifying muscle-specific substrates responsible for the progression of the disease. The substrates identified so far do not improve our understanding of the pathology of the disease. Therefore, we utilized an unbiased *in vivo* proteomics approach to identify proteins/substrates that cooperate with TRIM32 in maintaining normal cellular physiology.

We have uncovered a novel function for TRIM32 in the maintenance of glycolysis, which assures the continual production of metabolic intermediates to produce macromolecules for cell growth. This mechanism is not specific for muscle tissue, as we find that highly glycolytic brains and tumors also require TRIM32 function. The data suggest that TRIM32-mediated defects in cell growth contribute to the observed muscle degeneration in LGMD2H patients. Since TRIM32 is also overexpressed in multiple cancer types, we propose that this upregulation promotes cell growth as a new paradigm for TRIM32-mediated tumorigenesis. These findings will not only be of interest to researchers in the fields of cell and developmental biology, metabolism, muscle biology, and cancer, but also to clinicians who treat muscle disease and cancer (BAWA *et al.* 2020).

Further, we show that LGMD2H disease-causing mutations in the NHL domain are molecularly and structurally conserved between fly and human TRIM32. Myogenic expression of LGMD2H alleles induce myofibril abnormalities and reduce TRIM32 protein levels. The abnormal accumulation of sarcomeric proteins has been reported in various myopathies such as nemaline myopathy, myosin storage myopathy and actin accumulation myopathy. Interestingly, apart from glycolytic proteins, Tropomyosin, a known mammalian TRIM32 substrate, was also identified in our proteomics screen. We show that Tropomyosin physically interacts with the NHL domain; however, the protein localization and levels are not altered in LGMD2H pathological mutants. Intriguingly, we also report for the first time that the protein levels of βPS integrin and Sarcoglycan δ (Scgδ), both core components of costameres, are elevated in TRIM32 disease-causing alleles. This abnormal accumulation of transmembrane proteins is likely to exacerbate muscle damage and disease progression.

Future Directions

How does loss of TRIM32 lead to a reduction in glycolytic enzymes?

Loss of *TRIM32* could result in increased substrate levels as a failure to add Ub chains by an E3 enzyme prevents protein turnover. Interestingly, our TRIM32 co-immunoprecipitation experiments show higher molecular weight forms of Ald and Pglym that cannot be explained by a single monoUb or polyUb chain, strongly suggesting a potential unidentified post-translational modification. Since we have been unable to detect polyUb chains on Ald or Pglym upon immunoprecipitation with TRIM32, it seems unlikely that TRIM32 is required for proteasomal turnover of these proteins. The surprising decrease in Ald and Pglym that we observe upon loss of

TRIM32 is consistent with observations that other glycolytic proteins (GAPDH and PyK) are also reduced in *TRIM32 KO* muscles. Far less attention has been paid to multiple substrates that are monoubiquitinated by TRIM32, including NDGR2, TRIM72, actin, Piasy, and Kv1.2. One reason may be that the fate of monoubiquitinated proteins (e.g., protein trafficking or stabilization) is less defined. Future experiments will be focused on assessing if TRIM32 can mono- or multi-monoubiquitinate glycolytic enzymes to regulate their subcellular localization and/or protein levels. Transgenic flies have been generated that contain an HA-tagged mutant form of Ub (UAS-HA-ubKO), in which all seven lysine (K) residues are mutated to arginine (R), to ensure only monoubiquitin formation. This reagent will be used to create monoubiquitinated proteins in normal muscle tissue (*mef2-Gal4>UAS-HA-ubKO*), muscles that overexpress TRIM32 (*mef2-Gal4>UAS-TRIM32 FL; UAS-HA-ubKO*), and *tn-/-* muscles (*tn-/-; mef2-Gal4>UAS-HAubKO*). Antibodies to Ald and Pglym will be assessed for both *in vivo* and *in vitro* Ub modifications: (1) proximity ligation assays (PLA) will be used to assess the subcellular localization of glycolytic proteins with Ub moieties (using anti-Ub or anti-HA); and (2) immunoprecipitations with anti-HA will allow for the isolation of ubiquitinated proteins followed by Western blotting with antiglycolytic enzymes and anti-Ub/anti-HA to assess the nature of the Ub modification. Monoubiquitinated proteins show up as a single band, while polyubiquitinated species appear as a ladder. The WT ub allele (UAS-HA-ubWT) that retains the ability to generate polyUb chains and will be tested in the same genetic backgrounds. The pulldowns will be scaled up and the resulting Ub modifications will be confirmed using MS. The experiments above will definitively determine which type of Ub modification exists on these proteins. It is possible that polyUb chains are attached to glycolytic proteins and the loss of Ald or Pglym proteins levels in *tn-/-* is due to autophagy-mediated protein clearance. A prediction of this model is that the adapter protein p62 would bind Ub and target these

tagged proteins for autophagosome clearance. Thus, RNAi knockdown of autophagy genes, p62 or the autophagosome protein Atg8 in a *tn-/-* background would lead to an increase in glycolytic proteins and restored sarcomeric localization. Alternatively, if we do not detect any ubiquitination, TRIM32 may be a scaffold for glycolytic complexes to regulate subcellular localization (**Fig 6.2AB**. Interestingly, high molecular weight forms of Ald and Pglym co-immunoprecipitated with TRIM32. We hypothesize TRIM32 may multi-monoubiquitinate glycolytic proteins and regulates protein levels (**Fig 6.2A**). Future experiment would focus on large-scale identification of ubiquitination sites on Ald and Pglym by mass spectrometry. Transgenic flies have been generated that contain an HA-tagged mutant form of Ub (*UAS-HA-ubKO*), in which all seven lysine (K) residues are mutated to arginine (R), to ensure only monoubiquitin formation. This reagent will be used to create monoubiquitinated proteins in normal muscle tissue (*mef2-Gal4>UAS-HA-ubKO*), muscles that overexpress TRIM32 (*mef2-Gal4>UAS-TRIM32 FL*; *UAS-HA-ubKO*), and *tn-/-* muscles (*tn-/-; mef2-Gal4>UAS-HAubKO*). Antibodies to Ald and Pglym will be assessed for both in vivo and in vitro Ub modifications: (1) proximity ligation assays (PLA) will be used to assess the subcellular localization of glycolytic proteins with Ub moieties (using anti-Ub or anti-HA); and (2) immunoprecipitations with anti-HA will allow for the isolation of ubiquitinated proteins followed by Western blotting with antiglycolytic enzymes and anti-Ub/anti-HA to assess the nature of the Ub modification. Monoubiquitinated proteins show up as a single band, while polyubiquitinated species appear as a ladder. The WT ub allele (*UAS-HA-ubWT*) that retains the ability to generate polyUb chains and will be tested in the same genetic backgrounds. The pulldowns will be scaled up and the resulting Ub modifications will be confirmed using MS.

What is the mechanism behind the misregulation of the DGC component? Does loss of Integrin adhesion complex proteins exacerbate LGMD2H disease progression?

Costamere proteins are crucial for the structural and functional integrity of muscle tissue. We followed up on previously published results where we reported mislocalized β-integrin and δ-sarcoglycan at the sarcolemma and within the myofibers in *tn-/-* mutants. Immunoblot analysis performed on LGMD2H pathological alleles showed elevated protein levels of β-integrin and δ-Sarcoglycan. Also, C2C12 myoblasts overexpressing catalytically inactive TRIM32 mutant demonstrated accumulation of α-Dystroglycan, β-Dystroglycan and α-Sarcoglycan (**Chapter 4**). Therefore, we hypothesize this abnormal increase in costameric protein levels is due to aberrant E3 ligase activity of TRIM32 and the inability of the substrate proteins to undergo proteasomal degradation. Future experiments will focus on validating the ubiquitination status on these proteins modulated by TRIM32. We have generated transgenic flies overexpressing TRIM32FL, TRIM32_ΔRING and TRIM32_ ΔNHL constructs and LGMD2H pathological alleles. First, we will examine the subcellular localization of DGC and integrin proteins in muscle tissue. Following *in vivo* analysis, total protein levels in deletion mutants will be analyzed. We will employ murine myoblast cells to confirm our findings. Next, in vitro and in vivo ubiquitination assays will be performed to validate the K48 polyubiquitin linkage on α, β-Dystroglycan, α, β-Sarcoglycan, and βPS-integrin. Since the RING domain is responsible for the catalytic activity and NHL repeats to recognize substrates, we expect to observe the accumulation of costameric proteins in deletion mutants and myopathic alleles. Murine myoblasts overexpressing deletion mutants and pathological alleles should also exhibit abnormal accumulation of proteins in vivo. Next, the ubiquitination assay will be performed to confirm the K48 mediated degradation of costameric

proteins by TRIM32. Further, we will either induce the expression of D87N, R394H, and 520fs mutants in C2C12 myoblasts or express and purify in *E. coli.* We will perform the ubiquitination reaction and evaluate which mutation(s) render TRIM32 incapable of adding polyubiquitin chains to the target protein (**Fig 6.1**).

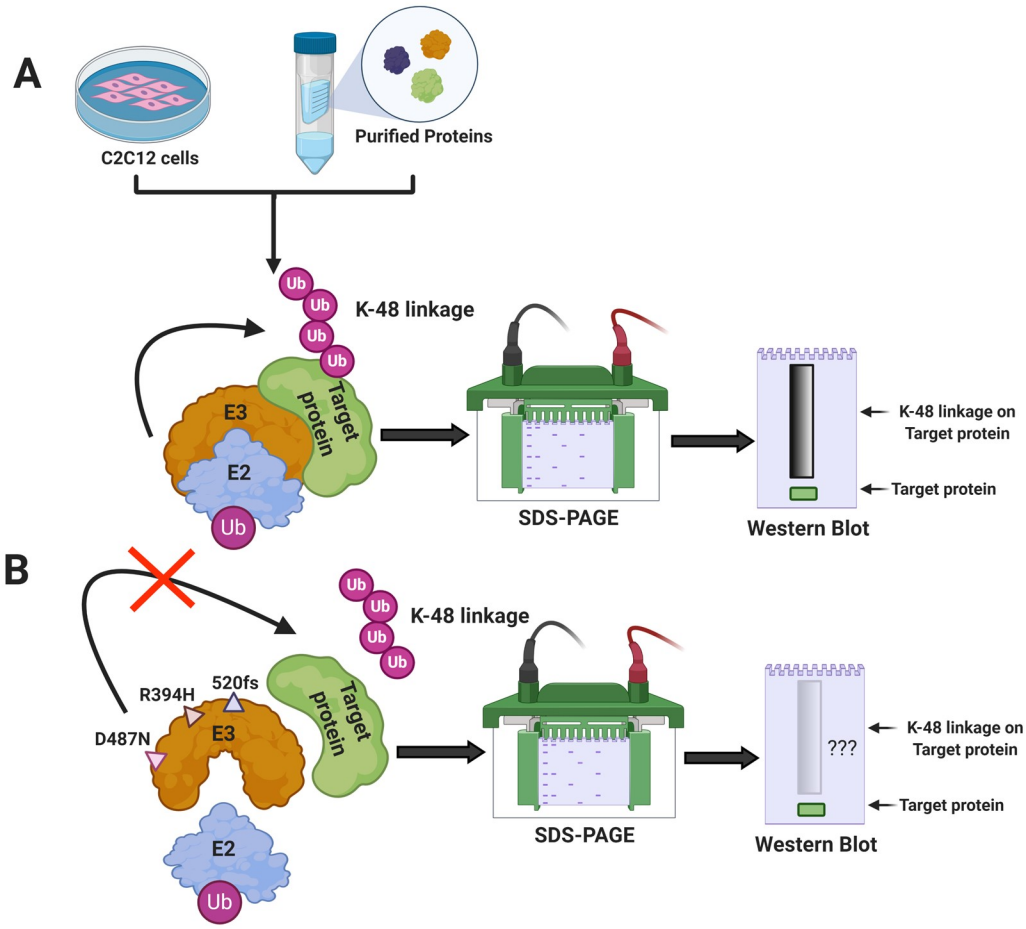

Figure 6.1: Schematic of in vitro/ in vivo ubiquitination assay.

(A) C2C12 myoblasts expressing E3 ligase and target protein. Alternatively, using *E. coli* system to express target and candidate proteins. Following protein expression in vitro/in vivo ubiquitination reaction will be performed to analyze the ubiquitination products generated by SDS-PAGE and western blot. (B) Illustration of pathological mutants examined to assess the impact of mutations on recruitment of ubiquitin moieties on the costameric proteins.

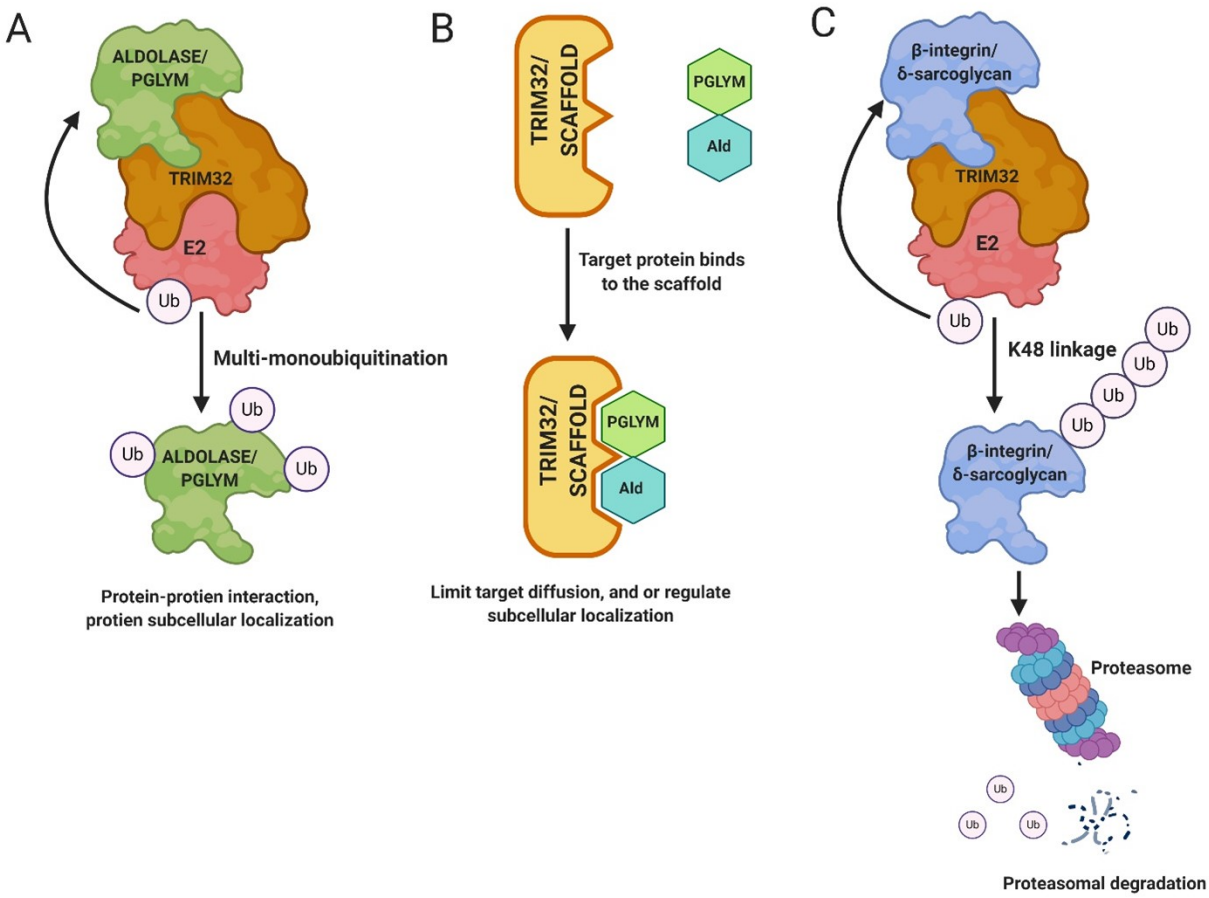

Figure 6.2: Proposed mechanisms of TRIM32 mediated regulation of glycolytic and costameric proteins.

(A) We hypothesize, TRIM32 adds a single ubiquitin molecule to multiple substrate (Aldolase/Pglym) residues, initiates protein interactions, and controls subcellular localization of Ald/Pglym within the muscle. (B) An alternate mechanism suggests TRIM32 could act as a scaffold protein and limit target diffusion. (C) Elevated costameric protein levels in *tn* mutants suggest that TRIM32 is an E3 ligase for transmembrane proteins and regulates protein turnover through proteasomal degradation.

References

1. Bawa, S., D. S. Brooks, K. E. Neville, M. Tipping, M. A. Sagar *et al.*, 2020 TRIM32 cooperates with glycolytic enzymes to promote cell growth. Elife 9.
2. Chiang, A. P., J. S. Beck, H. J. Yen, M. K. Tayeh, T. E. Scheetz *et al.*, 2006 Homozygosity mapping with SNP arrays identifies TRIM32, an E3 ubiquitin ligase, as a Bardet-Biedl syndrome gene (BBS11). Proc Natl Acad Sci U S A 103**:** 6287-6292.
3. Domsch, K., N. Ezzeddine and H. T. Nguyen, 2013 Abba is an essential TRIM/RBCC protein to maintain the integrity of sarcomeric cytoarchitecture. J Cell Sci 126**:** 3314-3323.
4. Guglieri, M., V. Straub, K. Bushby and H. Lochmüller, 2008 Limb-girdle muscular dystrophies. Curr Opin Neurol 21**:** 576-584.
5. Kudryashova, E., J. Wu, L. A. Havton and M. J. Spencer, 2009 Deficiency of the E3 ubiquitin ligase TRIM32 in mice leads to a myopathy with a neurogenic component. Hum Mol Genet 18**:** 1353-1367.
6. LaBeau-DiMenna, E. M., K. A. Clark, K. D. Bauman, D. S. Parker, R. M. Cripps *et al.*, 2012 Thin, a Trim32 ortholog, is essential for myofibril stability and is required for the integrity of the costamere in Drosophila. Proceedings of the National Academy of Sciences of the United States of America 109**:** 17983-17988.
7. Lazzari, E., and G. Meroni, 2016 TRIM32 ubiquitin E3 ligase, one enzyme for several pathologies: From muscular dystrophy to tumours. Int J Biochem Cell Biol 79**:** 469-477.
8. Mahmood, O. A., and X. M. Jiang, 2014 Limb-girdle muscular dystrophies: where next after six decades from the first proposal (Review). Mol Med Rep 9**:** 1515-1532.
9. Murphy, A. P., and V. Straub, 2015 The Classification, Natural History and Treatment of the Limb Girdle Muscular Dystrophies. J Neuromuscul Dis 2**:** S7-S19.
10. Sardiello, M., S. Cairo, B. Fontanella, A. Ballabio and G. Meroni, 2008 Genomic analysis of the TRIM family reveals two groups of genes with distinct evolutionary properties. BMC Evol Biol 8**:** 225.
11. Straub, V., J. A. Rafael, J. S. Chamberlain and K. P. Campbell, 1997 Animal models for muscular dystrophy show different patterns of sarcolemmal disruption. J Cell Biol 139**:** 375-385.
12. Tennessen, J. M., K. D. Baker, G. Lam, J. Evans and C. S. Thummel, 2011 The Drosophila estrogen-related receptor directs a metabolic switch that supports developmental growth. Cell Metab 13**:** 139-148.
13. Tocchini, C., and R. Ciosk, 2015 TRIM-NHL proteins in development and disease. Semin Cell Dev Biol 47-48**:** 52-59.
14. Wulczyn, F. G., E. Cuevas, E. Franzoni and A. Rybak, 2011 miRNAs Need a Trim : Regulation of miRNA Activity by Trim-NHL Proteins. Adv Exp Med Biol 700**:** 85-105.

Appendix A - Copyright Permissions

This appendix includes the copyright permissions for the work compiled in this dissertation.

PUBLISHED WORK Chapter 3- (BAWA *et al.* 2020)

eLIFE COPY RIGHT POLICY

eLife article is distributed under the terms of a Creative Commons Attribution License that permits unrestricted use and redistribution provided that the original author and source are credited.

OTHER IMAGES

FIGURE 1.3 falls under Creative Commons Attribution-NonCommercial-No Derivatives License (CC BY NC ND). Permission is not required for this non-commercial use.

FIGURE 2.1 and 2.7 is used with permission from Proceedings of the National Academy of Sciences of the United States of America (PNAS). See documentation on next page.

FIGURE 2.2 falls under Creative Commons CC BY license, which permits unrestricted use, distribution, and reproduction in any medium, provided the original work is properly cited. The work is cited according to the author's direction.

PP

PNAS Permissions <PNASPermissions@nas.edu>
Mon 10/12/2020 9:03 AM
To: Simran Bawa

Thank you for your message. Permission is granted for your use of the material as described in your request. Please include a complete citation for the original PNAS article when reusing its material. Because this material published after 2008, a copyright note is not needed. There is no charge for this material, either. Let us know if you have any questions.

Sincerely,

Kay McLaughlin for
Diane Sullenberger
PNAS Executive Editor

Appendix B - Chapter 3 Supplemental Materials

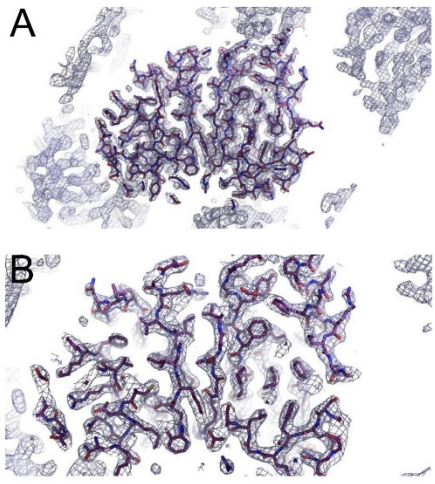

C

X-ray Diffraction Data Collection and Refinement Statistics

	TRIM32-C
Data Collection	
Space group	$P6_5$
Cell dimensions	
a, *b*, *c* (Å)	132.73 132.73 49.70
α, β, γ (°)	90.00 90.00 120.00
Resolution (Å)	43.45-2.60 (2.69-2.60)*
R_{merge}	0.128 (0.680)
$I / \sigma I$	14.4 (1.8)
Completeness (%)	99.0 (91.9)
Redundancy	7.2 (4.0)
Refinement	
Resolution (Å)	43.45-2.60
No. reflections	15,474
R_{work} / R_{free}	18.6/21.9
No. atoms	
Protein	2258
Ligand/ion	6
Water	85
B-factors	
Protein	37.86
Ligand/ion	26.70
Water	36.53
R.m.s. deviations	
Bond lengths (Å)	0.014
Bond angles (°)	1.502

*Values in parentheses are for the highest-resolution shell.

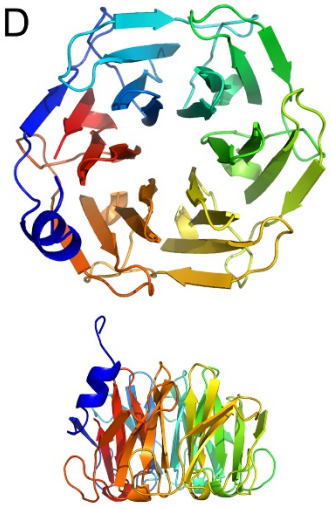

Fig 3.1–figure supplement 1. Crystal structure of the *Drosophila* TRIM32_NHL domain.

(A,B) Representative electron density maps. Two images showing regions of the final 2Fo-Fc electron density map (grey cage) corresponding to the NHL region of *Drosophila* TRIM32, contoured at 1.2 σ. The polypeptide is drawn in ball and stick convention (carbon atoms in purple). (C) Table of X-ray diffraction statistics. (D) Ribbon diagrams corresponding to the TRIM32_NHL domain are rendered in rainbow colors from red at the N-terminus to blue at the C-terminus. Top view (top panel) reveals six NHL repeats, each consisting of four antiparallel beta sheets that together are arranged toroidally around a central axis. Side view (bottom panel) shows that the NHL repeats form a compact structure with few extended loops.

A

Proteins identified via MS that co-purify with TRIM32-NHL

	Experiment #1 (1418)				Experiment #2 (1426.1)				Experiment #3 (1426.2)			
	Control[1]	TRIM32 _NHL[1]	FC[2]	T-test (p-value)	Control[1]	TRIM32 _NHL[1]	FC[2]	T-test (p-value)	Control[1]	TRIM32 _NHL[1]	FC[2]	T-test (p-value)
Bait												
Drosophila TRIM32	0.0	28.6	INF[3]	<0.0001	0.0	28.0	INF	<0.0001	0.0	14.6	INF	0.00054
Muscle proteins												
Tropomyosin-1 (Tm1)	2.0	55.6	27.6	<0.0001	12.6	42.0	3.3	0.00013	0.0	0.0	N/A	N/A
Tropomyosin-2 (Tm2)	5.0	36.6	7.3	<0.0001	13.6	56.0	4.1	<0.0001	12.3	51.0	4.1	<0.0001
Troponin C (TpnC73F)	0.0	13.3	INF	0.00027	0.0	17.3	INF	<0.0001	0.0	15.6	INF	<0.0001
Glycolytic enzymes												
Aldolase	18.6	44.0	2.4	0.0013	0.0	14.6	INF	<0.0001	0.0	7.6	INF	0.00033
Phosphoglycerate kinase	0.0	13.3	INF	0.00024	0.0	0.0	N/A	N/A	0.0	7.0	INF	0.00027
Pglym78	0.0	6.0	6.0	0.018	0.0	4.6	INF	0.0061	0.0	8.0	INF	0.00071
GAPDH	20.6	29.0	1.4	0.02	0.0	5.6	INF	0.0061	19.0	24.6	1.3	0.038
Pyruvate kinase	12.3	27.0	2.2	0.00015	0.0	0.0	N/A	N/A	4.0	18.6	3.8	0.0015

[1] Normalized total spectra
[2] Fold change (ratio of raw spectra in TRIM32_NHL pulldown/control pulldown)
[3] INF, Infinite (not detected in control pulldowns)

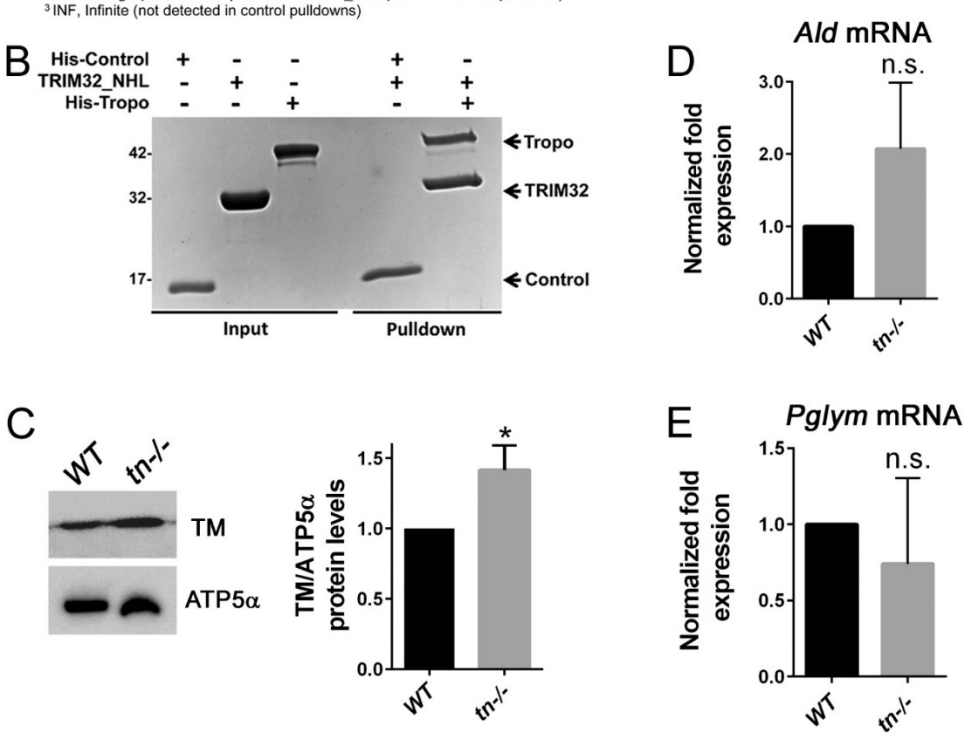

Fig 3.1–figure supplement 2. TRIM32 co-purifies with TM and other proteins.

(A) Summary of peptides that co-purify with the NHL domain of TRIM32. (B) *In vitro* binding assay shows that His-tagged TM, but not the His-tagged SCIN control protein, directly binds untagged TRIM32_NHL. (C) Western blot depicting overall protein levels in *WT* or *tn-/-* whole larvae quantitated relative to ATP5α. TM protein levels are increased in *tn-/-* mutants compared to *WT* controls. N=3 (D,E) qPCR shows there is no decrease in the mRNA levels of *Ald* (D) or *Pglym* (E) in *tn-/-* at the L3 stage. mRNA was normalized to *rp49* transcripts. N=3 biological replicates and 3 technical replicates for each genotype. Mean +/- SD (*, $p < 0.05$; n.s., not significant).

Figure 2 -figure supplement 1

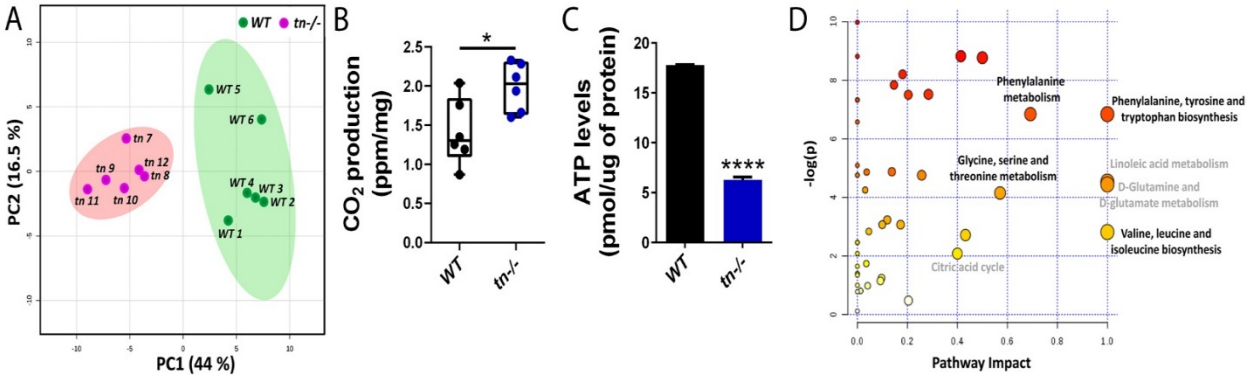

Fig 3.2 –figure supplement 1. Metabolite analysis upon loss of TRIM32.

(A) PCA analysis depicting metabolite variances between *WT* (green) and *tn-/-* (magenta) L3 larvae. PC1, principal component 1. PC2, principal component 2. (B) Scatter plot reveals CO_2 production is slightly elevated upon loss of TRIM32 in all tissues. (C) Bar graph depicts reduction in ATP levels in *tn-/-*L3 larvae. (D) Pathway analysis reveals a large proportion of amino acid biosynthetic pathways are impacted upon loss of TRIM32. P-value significance is plotted on the y-axis (yellow to red depict increased p-values). More metabolites affected in a particular pathway increase from left to right along the x-axis. Mean +/- SD (****, $p<0.001$; *, $p< 0.05$).

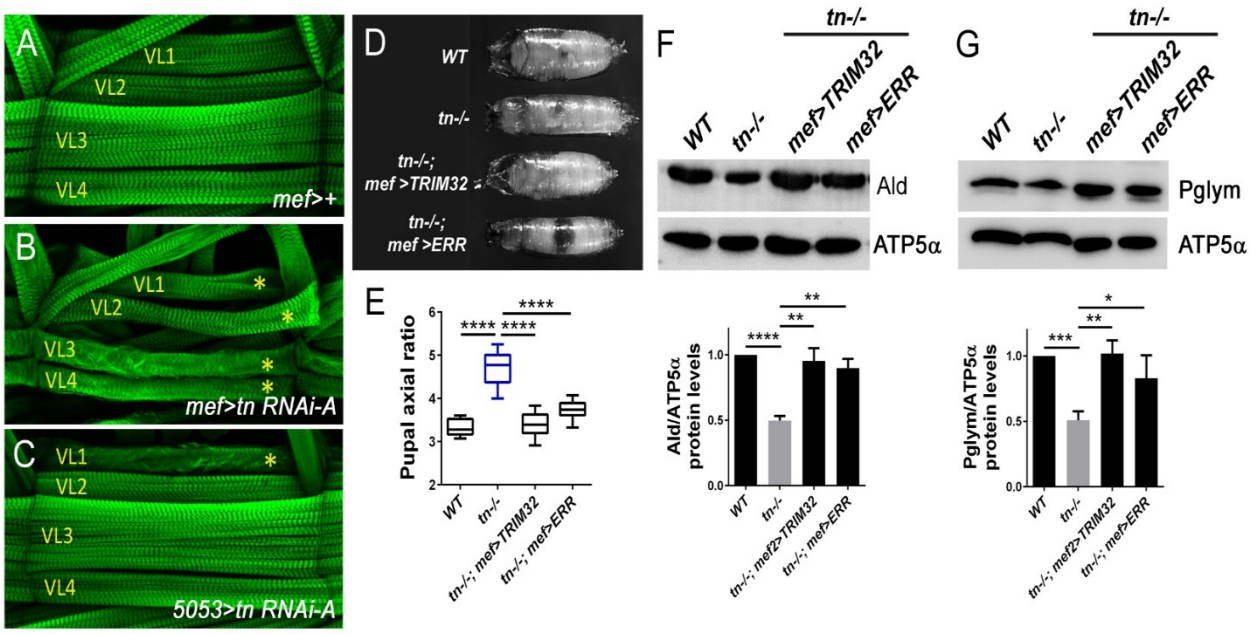

Fig 3.2 –figure supplement 2. Muscle growth defects are cell autonomous and can be rescued upon stabilization of glycolytic enzyme levels.

(A-C) Phalloidin-labeled VL1-4 muscles in a representative hemisegment of the indicated genotypes. (A) *mef2*>+ control muscles appear *WT*. (B,C) RNAi knockdown of *tn* in all muscles with *mef2*-Gal4 (B) or only muscle VL1 using the *5053*-Gal4 driver (C) show a reduction in muscle size (asterisk). (D,E) The inability to contract body wall muscles in *tn-/-* causes elongated pupae. Muscle-specific expression of TRIM32 or ERR restores muscle contraction. (D) Representative pupal cases of the indicated genotypes. (E) Quantitation of pupal axial ratios represented by a box and whisker plot. (F,G) Western blots showing the relative amounts of Ald or Pglym protein relative to the ATP5α loading control. Both Ald and Pglym protein levels are stabilized upon TRIM32 or ERR expression in muscle tissue compared to *tn-/-*. Mean +/- SD (****, p<0.001; ***, p< 0.01; **, p< 0.05; *, p< 0.01).

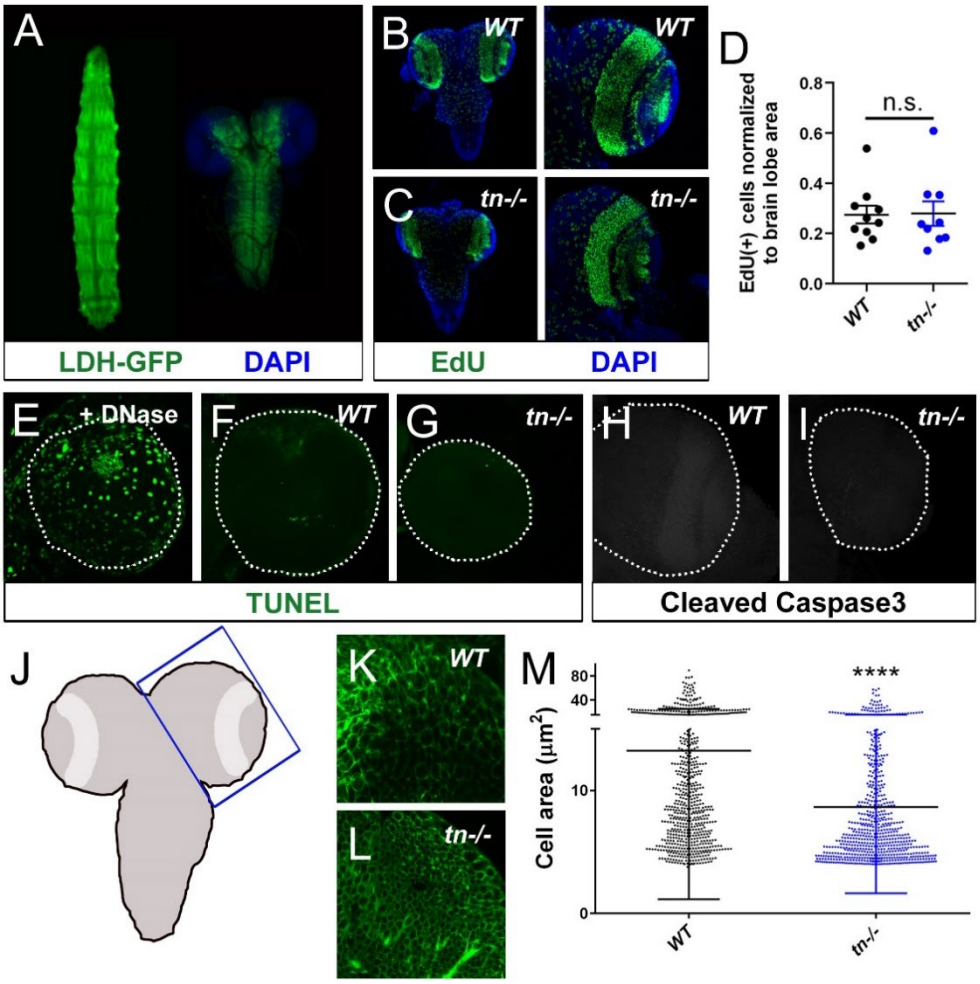

Fig. 3.4–figure supplement 1. Cell proliferation or cell death are not affected in *tn-/-*.

(A) Endogenous LDH-GFP (green) expression in the somatic muscles of whole larvae (left) and isolated larval brains (right). DAPI (blue) is used to visualize the entire brain lobe. (B,C) EdU incorporation (green) in whole larval brains (left panels) or individual brain lobes (right panels) reveals no difference in the proliferative capacity of neuroblasts. DAPI (blue) demarcates the outlines of each tissue. (D) Scatter plot depicting the average number of EdU(+) cells normalized to the brain lobe area. (E-I) Individual brain lobes (white dotted outline) visualized with TUNEL (E-G) or cleaved caspase3 immunostaining (H,I) to assay apoptotic cells. There is no difference in the number of TUNEL(+) or Caspase3(+) cells in *WT* or *tn-/-*. Tissue treated with DNase served as a positive control for TUNEL labeling (E). (J-M) Analysis of cell size in the larval brain lobe. (J) Schematic of larval brain. Blue box indicates region of brain lobe images. (K,L) Representative micrograph of phalloidin-stained cells in the lobe region of *WT* (K) or *tn-/-* brains (L). (M) Quantification reveals various sizes of neuroblasts in brain lobe tissue. Overall cell size is reduced upon loss of TRIM32. Mean +/- SD (****, $p<0.001$). N≥300 cells in 10 independent brain lobes of each genotype.

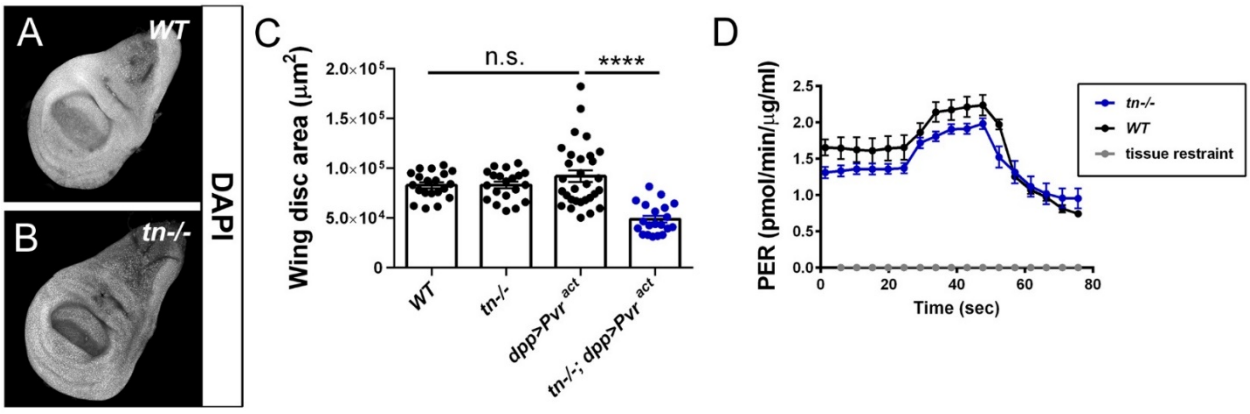

Fig 3.5 –figure supplement 1. Wing disc size and glycolysis are not altered in *tn-/-*.

(A,B) Isolated L3 wing discs are the same size when isolated from *WT* (A) or *tn-/-* (B) L3 larvae. (C) Scatter plot depicting the relative wing disc area in the indicated genotypes. (D) PER, a measure of the glycolytic rate, between *WT* and *tn-/-* wing discs appear similar. Mean +/- SD. (****, p< 0.001; *, p< 0.05; n.s., not significant).

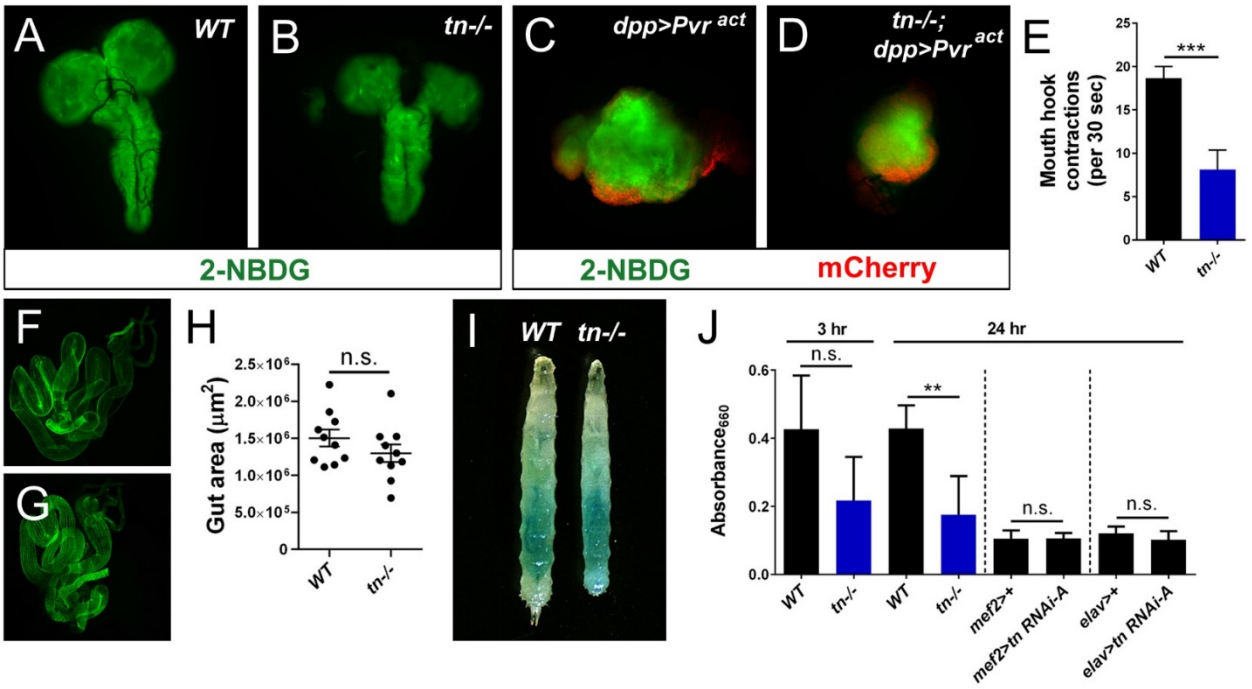

Fig 3.5 –figure supplement 2. Glucose uptake and feeding behavior upon whole animal or tissue-specific loss of TRIM32.

(A-D) Incubation of the fluorescent glucose analog 2-NBDG with isolated larval brains (A,B) or *Pvr*^{act} tumors (C,D) from L2 larvae show no visible difference in glucose uptake. (E) Mount hook contractions, a proxy for feeding behavior, is decreased in *tn-/-* larvae. (F,G) Isolated L3 midguts from *WT* (F) or *tn-/-* (G) stained with phalloidin. (H) Quantitation of total midgut area is not significantly different between *WT* and *tn-/-*. (I) L3 larvae after feeding dye for 24 hrs. (J) Bar graph shows measured absorbance readings from L3 isolated midguts after for 3 hrs or 24 hrs of feeding. *tn-/-* show differential food intake, while tissue-specific knockdown of TRIM32 in muscle or brain after 24 hrs does not alter food intake.

Table 1: **X-ray Diffraction Data Collection and Refinement Statistics**
Figure 1-source data file 1

	TRIM32-C
Data Collection	
Space group	$P\,6_5$
Cell dimensions	
a, *b*, *c* (Å)	132.73 132.73 49.70
α, β, γ (°)	90.00 90.00 120.00
Resolution (Å)	43.45-2.60 (2.69-2.60)*
R_{merge}	0.128 (0.680)
$I / \sigma I$	14.4 (1.8)
Completeness (%)	99.0 (91.9)
Redundancy	7.2 (4.0)
Refinement	
Resolution (Å)	43.45-2.60
No. reflections	15,474
R_{work} / R_{free}	18.6/21.9
No. atoms	
Protein	2258
Ligand/ion	6
Water	85
B-factors	
Protein	37.86
Ligand/ion	26.70
Water	36.53
R.m.s. deviations	
Bond lengths (Å)	0.014
Bond angles (°)	1.502

*Values in parentheses are for the highest-resolution shell.

Table 2 : Proteins identified via MS that co-purify with TRIM32-NHL

	Experiment #1 (1418)				Experiment #2 (1426.1)				Experiment #3 (1426.2)			
	Control [1]	TRIM32_NHL [1]	FC [2]	T-test (p-value)	Control [1]	TRIM32_NHL [1]	FC [2]	T-test (p-value)	Control [1]	TRIM32_NHL [1]	FC [2]	T-test (p-value)
Bait												
Drosophila TRIM32	0.0	28.6	INF[3]	<0.0001	0.0	28.0	INF	<0.0001	0.0	14.6	INF	0.00054
Muscle proteins												
Tropomyosin-1 (Tm1)	2.0	55.6	27.6	<0.0001	12.6	42.0	3.3	0.00013	0.0	0.0	N/A	N/A
Tropomyosin-2 (Tm2)	5.0	36.6	7.3	<0.0001	13.6	56.0	4.1	<0.0001	12.3	51.0	4.1	<0.0001
Troponin C (TpnC73F)	0.0	13.3	INF	0.00027	0.0	17.3	INF	<0.0001	0.0	15.6	INF	<0.0001
Glycolytic enzymes												
Aldolase	18.6	44.0	2.4	0.0013	0.0	14.6	INF	<0.0001	0.0	7.6	INF	0.00033
Phosphoglycerate kinase	0.0	13.3	INF	0.00024	0.0	0.0	N/A	N/A	0.0	7.0	INF	0.00027
Pglym78	0.0	6.0	6.0	0.018	0.0	4.6	INF	0.0061	0.0	8.0	INF	0.00071
GAPDH	20.6	29.0	1.4	0.02	0.0	5.6	INF	0.0061	19.0	24.6	1.3	0.038
Pyruvate kinase	12.3	27.0	2.2	0.00015	0.0	0.0	N/A	N/A	4.0	18.6	3.8	0.0015

[1] Normalized total spectra
[2] Fold change (ratio of raw spectra in TRIM32_NHL pulldown/control pulldown)
[3] INF, Infinite (not detected in control pulldowns)

Appendix C - Chapter 4 Supplemental Materials

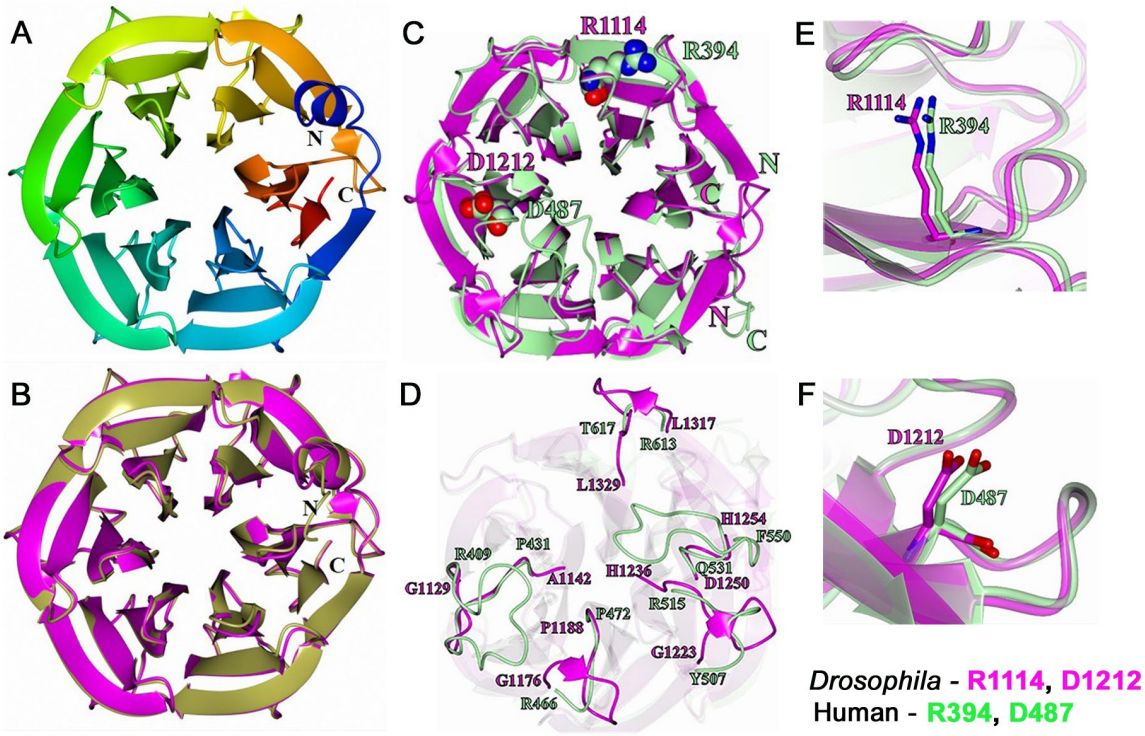

Figure S1. Structural conservation between the NHL domain of *Drosophila* and human TRIM32.

(A) Blend through coloring from the N-terminus (blue) to the C-terminus (red). (B) Superposition of the high resolution structure (magenta) with PDB 6D69 (gold). (C) Comparison of *Drosophila* TRIM32_NHL (magenta) with the top model of the human TRIM32_NHL structure modeled using I-TASSER (green). Superposition showing the secondary structure elements as ribbons. The R394/R1114 and D487/D1203 residues are rendered as spheres. Superposition showing the secondary structure elements as ribbons. The R394/R1114 and D487/D1212 residues are rendered as spheres. (D) The major differences are observed in loops between secondary structure elements. (E,F) Comparison of the conformation of R394/R1114 (E) and D487/D1212 (F) in each structure.

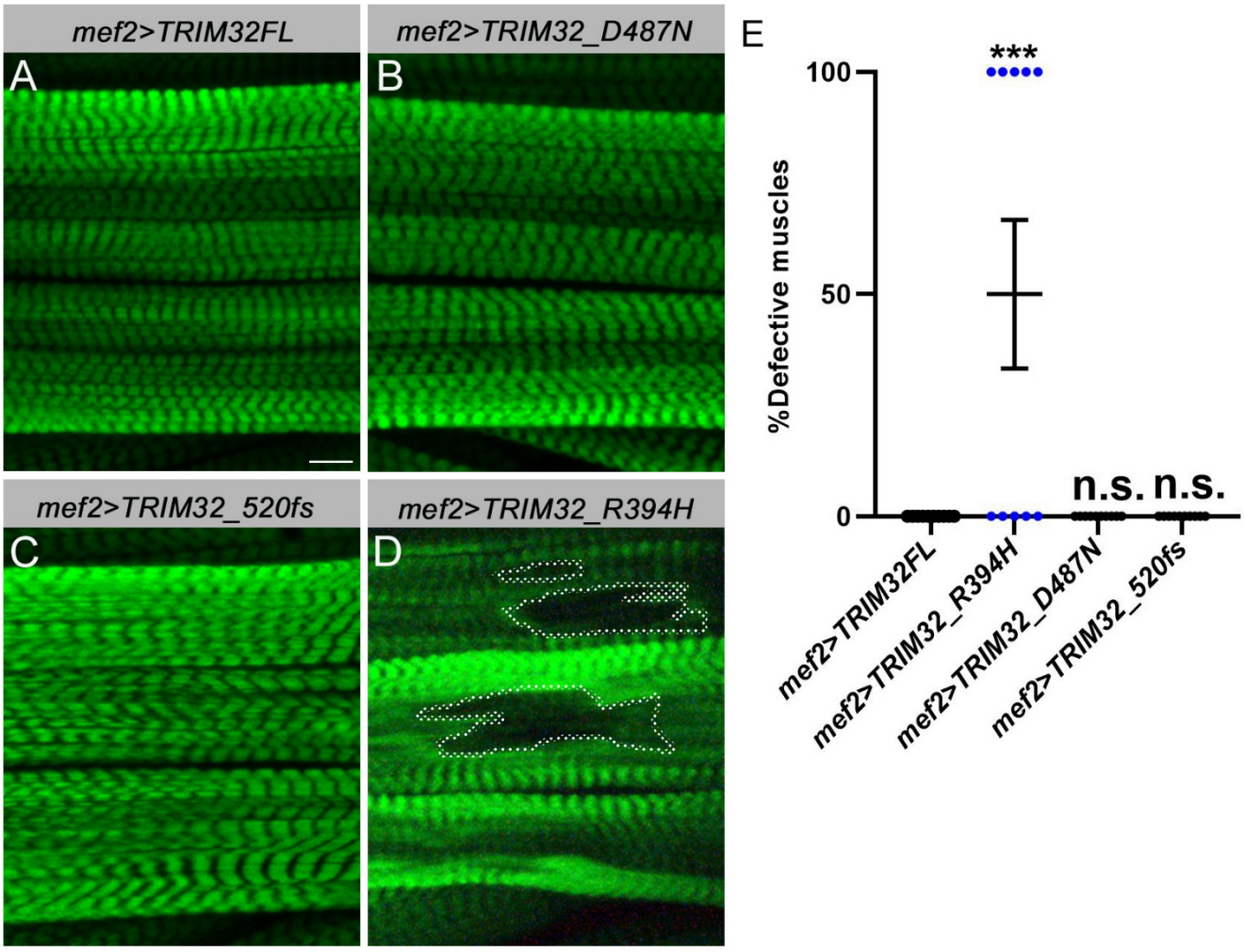

Figure S2. Muscle expression of the *R394H* mutation causes dominant muscle defects.

(A-D) Phalloidin staining of L3 larval muscles. Overexpression of *TRIM32FL* (A), or the *D487N* (B) and *520fs* (C) mutations in a *WT* background using *mef2*-Gal4 does not affect muscle morphology. (D) However, expression of the *R394H* mutation induces muscle damage. (E) Bar graph representing percent muscle defects. N=10, Mean +/- SEM (***, p <0.005; n.s., non-significant). Scale bar: 50µm (A-D)

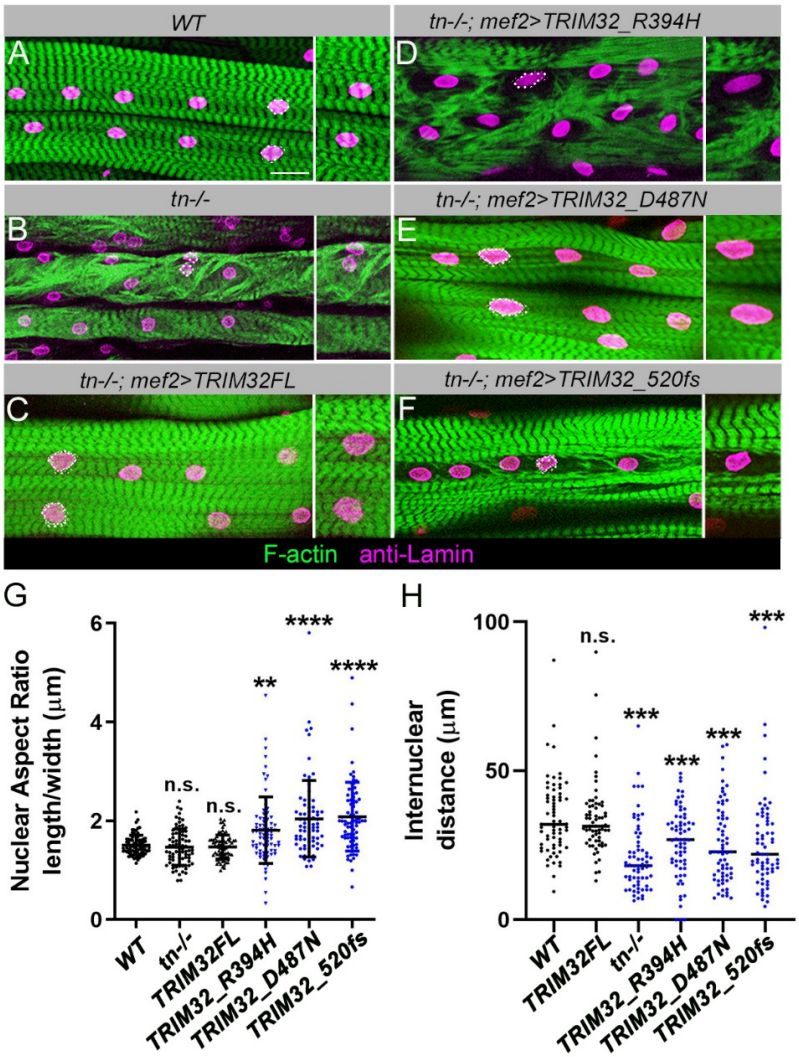

Figure S3. Changes in nuclear morphology prominent in human pathological mutations.

A-F) L3 larval muscles stained for F-actin and nuclei labeled with anti-Lamin to visualize morphological changes. In *WT* (A), *tn-/-* (B) and (C) *TRIM32* rescue larvae (*tn-/-;mef2>TRIM32FL*), theVL3 muscles exhibit round-shaped nuclei. The nuclei in *R394H* (D), *D487N* (E) and *520fs* (F) mutants exhibit a distorted and/or elongated nuclear architecture that were more prominent between degenerative myofibers. (G) Scatter plot depicting the nuclear aspect ratio (length/width) in the indicated genotypes. (H) Nuclear positioning is altered in *tn-/-*

and LGMD2H disease causing mutants. Mean +/- SEM (**, p<0.01; ***, p<0.005; ****, p<0.001; n.s., non-significant). Scale bars: 50µm (A-F)

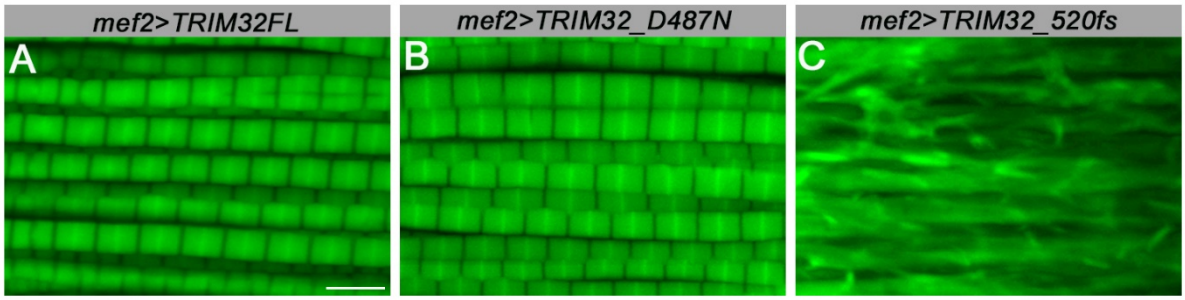

Figure S4. Dominant expression of the *520fs* mutation alters the adult IFM musculature. (A,B) Overexpression of *TRIM32FL* (A) or the *D487N* (B) mutation in an otherwise *WT* background results in flies with normal myofiber morphology stained with phalloidin. (C) Muscle specific expression of the *520fs* mutation causes extensive damage to the IFMs and induces muscle degeneration. Scale bars: 10µm (A-C)

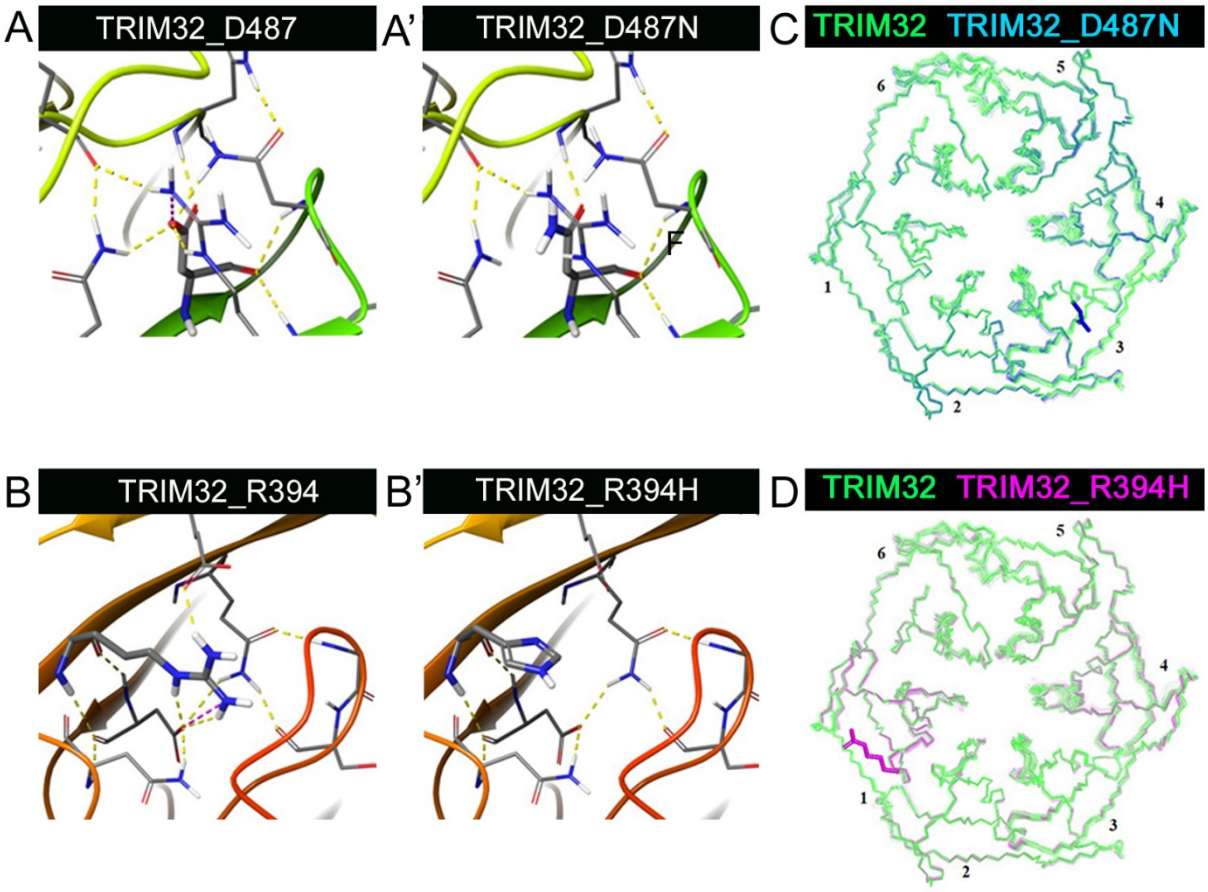

Figure S5. Comparison of hydrogen bond interactions and backbone conformations in TRIM32_NHL vs point mutants.

(A) D487 (sticks) participates in a hydrogen bond network (yellow dashes) and salt bridge interaction (magenta dashes) with nearby residues. (A') N487 (sticks) disrupts the hydrogen bond network and loses the salt bridge interaction. (B) R394 (sticks) participates in a hydrogen bond network (yellow dashes) and salt bridge interaction (magenta dashes) with nearby residues. (B') H394 (sticks) disrupts the hydrogen bond network and loses the salt bridge interaction. (C) The ensembles of the WT (green) and D487N (blue) Trim are shown. D487 is represented as sticks. Many regions overlap, as shown with primarily green lines, whereas other regions, particularly in the NHL repeats adjacent to the site of the mutations, have distinct separation between green and blue, suggesting sampling of slightly different backbones. The NHL repeats are numbered. (D) The ensembles of the WT (green) and R394H (magenta) Trim are shown. R394 is represented as sticks. Many regions overlap, as shown with primarily green lines, whereas the distinct separation between green and magenta suggests sampling of slightly different backbone conformations not limited to the adjacent NHL repeats. The NHL repeats are numbered.

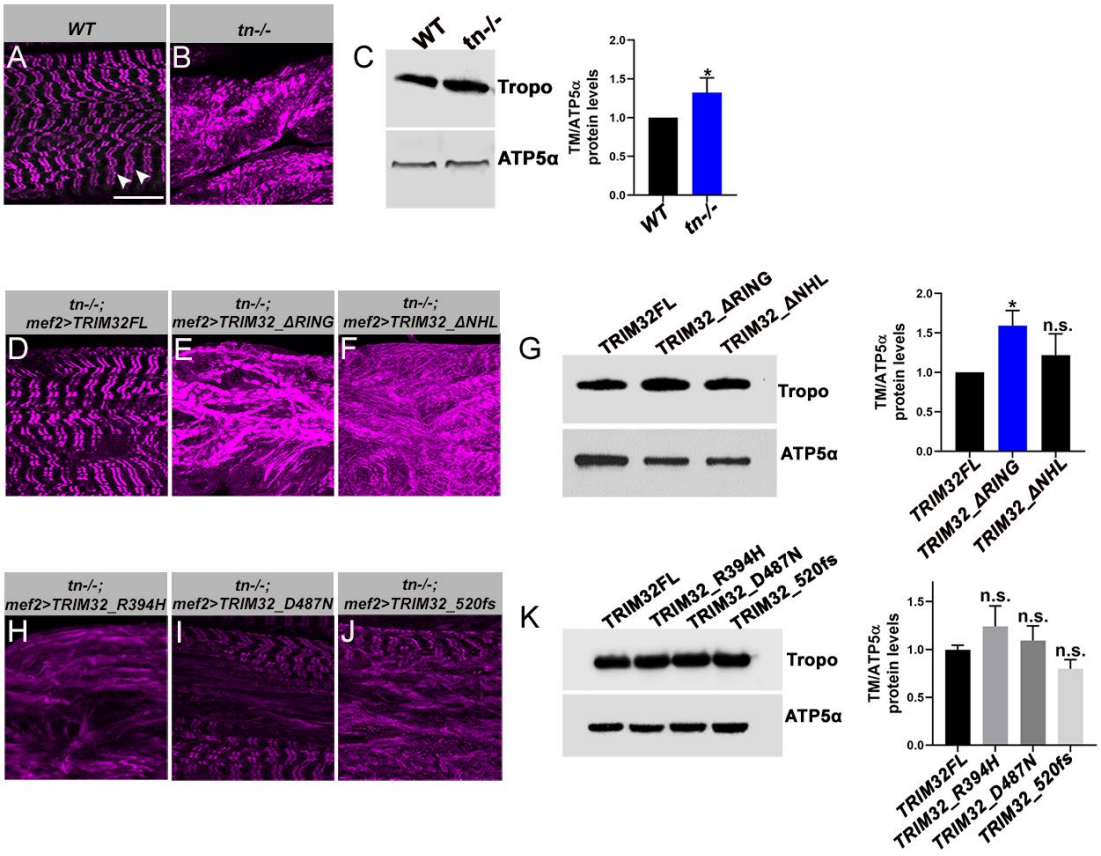

Figure S6. TM protein levels and sarcomere association is normal in LGMD2H disease-causing mutations.

(A,B,E-G,I,-K) VL3 muscles of *WT*, *tn-/-*, *TRIM32* deletion mutants and LGMD2H myopathic mutants stained with anti-TM. (A) TM is normally found in thin filaments surrounding the Z-disc (white arrowheads). (B) In *tn-/-* muscle, TM protein is present, but no longer retains its sarcomeric localization. (C) Overall TM protein levels are increased in *tn-/-* mutants compared to *WT* controls, N=4. (D) TM is localized within the sarcomeres in *tn-/-*;*mef2>TRIM32FL* larve. In Δ*RING* (E) and Δ*NHL* (F) deletion mutants, TM abnormally accumulates within the unbundled myofibers. (G) Western blot depicting elevated protein levels of TM in Δ*RING* and Δ*NHL* deletion mutants. Bar graph shows the amount of TM protein relative to ATP5α used as loading control, N=3. Expression of the LGMD2H disease-causing alleles *R394H* (H) , *D487N* (I) and *520fs* (J) displayed relatively well localized TM in the myofibers despite the muscle defects. (K) Overall protein levels of TM are not changed in human disease alleles. Relative TM levels quantified relative to ATP5α, N=3. Mean +/- SEM (*, p <0.05; n.s., not significant) (C- t-test, G&K- one-way Anova). Scale bars: 25μm (A,B,D-FH-J)

Table 3: **Crystallographic data for Trim32 NHL**

	dTrim32 NHL
Data Collection	
Unit-cell parameters (Å, º)	*a*=42.63, *b*=51.92, *c*=105.12
Space group	$P2_12_12_1$
Resolution (Å)[1]	46.55-1.30 (1.32-1.30)
Wavelength (Å)	1.0000
Temperature (K)	100
Observed reflections	376,145
Unique reflections	58,203
$\langle I/\sigma(I)\rangle$[1]	10.7 (1.8)
Completeness (%)[1]	99.9 (99.9)
Multiplicity[1]	6.5 (6.6)
R_{merge} (%)[1, 2]	8.3 (99.1)
R_{meas} (%)[1, 4]	9.0 (107.7)
R_{pim} (%)[1, 4]	3.5 (41.7)
$CC_{1/2}$ [1, 5]	0.998 (0.650)
Refinement	
Resolution (Å) [1]	33.11-1.30
Reflections (working/test)[1]	55,123/2,995
R_{factor} / R_{free} (%)[1,3]	13.8/17.4
No. of atoms	2,277/247
(Protein/ Water)	
Model Quality	
R.m.s deviations	
Bond lengths (Å)	0.008
Bond angles (º)	1.004
Mean *B*-factor (Å^2)	
All Atoms	17.5
Protein	16.1
Water	29.0
Coordinate error	0.13
(maximum likelihood) (Å)	
Ramachandran Plot	
Most favored (%)	96.5
Additionally allowed (%)	3.2

1) Values in parenthesis are for the highest resolution shell.
2) $R_{merge} = \Box_{hkl}\Box_i |I_i(hkl) - \langle I(hkl)\rangle| / \Box_{hkl}\Box_i I_i(hkl)$, where $I_i(hkl)$ is the intensity measured for the *i*th reflection and $\langle I(hkl)\rangle$ is the average intensity of all reflections with indices hkl.
3) $R_{factor} = \Box_{hkl} ||F_{obs}(hkl)| - |F_{calc}(hkl)|| / \Box_{hkl}|F_{obs}(hkl)|$; Rfree is calculated in an

identical manner using 5% of randomly selected reflections that were not included in the refinement.

4) R_{meas} = redundancy-independent (multiplicity-weighted) R_{merge}(EVANS 2006; EVANS 2011). R_{pim} = precision-indicating (multiplicity-weighted) R_{merge}(DIEDERICHS and KARPLUS 1997; WEISS 2001).
5) $CC_{1/2}$ is the correlation coefficient of the mean intensities between two random half-sets of data (EVANS 2012; KARPLUS and DIEDERICHS 2012).

Table 4: Nuclear envelope proteins identified by mass spectrometry using TRIM32_NHL as bait.

	Experiment 1				**Experiment 2**				**Experiment 3**			
	Control[1]	TRIM32 _NHL[2]	Fold-Change	T-test (p-value)	Control	TRIM32 _NHL	Fold-Change	T-test (p-value)	Control	TRIM32 _NHL	Fold-Change	T-test (p-value)
***Drosophila* TRIM32_NHL**	**0.0**	**28.6**	**INF[3]**	**<0.00010**	**INF**	**28.0**	**INF**	**<0.00010**	**0.0**	**14.6**	**INF**	**0.00054**
Lamin Dm_0	0.0	55	INF	<0.00010	INF	65	INF	<0.00010	0.0	60.0	INF	<0.00010
Lamin C	4.9	70.7	46	<0.00010	3.38	74.1	INF	<0.00010	0.0	62.2	INF	<0.00010
Barrier-to-autointegration factor	0.0	62.2	INF	<0.00010	0.0	57.8	INF	<0.00010	0.0	62.2	INF	<0.00010

[1] Control is GST alone
[2] GST-TRIM32_NHL
[3] INF = infinite (not detected in control)

Table 5: Statistics Summary

Panel	Graph type	N value	Statistical test used	Precision	p-value
Figure 1, G and H	Scatter plot	N≥20	Unpaired t-test	Mean +/- SEM	p<0.05
Figure 2F	Scatter plot	N≥13	One-Way ANOVA Kruskal-Wallis test	Mean +/- SEM	p<0.05
Figure 2g	Box and Whisker plot	N≥13	One-Way ANOVA Kruskal-Wallis test	Min to Max	P<0.001
Figure 3K	Bar graph	Pool of 5 larvae per genotype (N=3 biological replicates and N=3 technical replicates)	One-Way ANOVA Dunnett's multiple comparison test	Mean +/- SEM	p<0.05
Figure 3L	Bar graph		N/A	Mean +/- SEM	N/A
Figure 6, C and I	Bar graph	Pool of 5 larvae per genotype (N=3 biological replicates and N=3 technical replicates)	Unpaired t-test	Mean +/- SEM	p<0.05
Figure 6, H and J	Bar graph	Pool of 5 larvae per genotype (N=3 biological replicates and N=3 technical replicates)	One-Way ANOVA Kruskal-Wallis test	Mean +/- SEM	p<0.05
Figure 6L	Bar graph	Pool of 3 larvae per genotype (N=3 biological replicates and N=3 technical replicates)	One-Way ANOVA Turkey's multiple comparison test	Mean +/- SEM	p<0.05
Figure S2E	Scatter plot	N=10	One-Way ANOVA Kruskal-Wallis test	Mean +/- SEM	p<0.05
Figure S3, G and H	Scatter plot	N≥30	One-Way ANOVA Kruskal-Wallis test	Mean +/- SEM	p<0.001
Figure S6C	Bar graph	Pool of 5 larvae per genotype (N=3 biological replicates and N=3 technical replicates)	Unpaired t-test	Mean +/- SEM	p<0.05
Figure S6, G and K	Bar graph	Pool of 5 larvae per genotype (N=3 biological replicates and N=3 technical replicates)	One-Way ANOVA Kruskal-Wallis test	Mean +/- SEM	p<0.05

SUPPLEMENTAL REFERENCES

1. Kabsch, W., *Automatic indexing of rotation diffraction patterns.* Journal of Applied Crystallography, 1988. **21**(1): p. 67-72.
2. Kabsch, W., *Xds.* Acta Crystallogr D Biol Crystallogr, 2010. **66**(Pt 2): p. 125-32.
3. Vonrhein, C., et al., *Data processing and analysis with the autoPROC toolbox.* Acta Crystallogr D Biol Crystallogr, 2011. **67**(Pt 4): p. 293-302.
4. Evans, P.R., *An introduction to data reduction: space-group determination, scaling and intensity statistics.* Acta Crystallogr D Biol Crystallogr, 2011. **67**(Pt 4): p. 282-92.
5. McCoy, A.J., et al., *Phaser crystallographic software.* J. Appl. Cryst., 2007. **40**: p. 658-674.
6. Adams, P.D., et al., *PHENIX: a comprehensive Python-based system for macromolecular structure solution.* Acta Crystallogr D Biol Crystallogr, 2010. **66**(Pt 2): p. 213-21.
7. Emsley, P., et al., *Features and development of Coot.* Acta Crystallogr D Biol Crystallogr, 2010. **66**(Pt 4): p. 486-501.
8. Chen, V.B., et al., *MolProbity: all-atom structure validation for macromolecular crystallography.* Acta Crystallogr D Biol Crystallogr, 2010. **66**(Pt 1): p. 12-21.
9. Potterton, L., et al., *Developments in the CCP4 molecular-graphics project.* Acta Crystallogr D Biol Crystallogr, 2004. **60**(Pt 12 Pt 1): p. 2288-94.
10. Krissinel, E., *Enhanced fold recognition using efficient short fragment clustering.* Journal of Molecular Biochemistry, 2012. **1**(2): p. 76-85.
11. Winn, M.D., et al., *Overview of the CCP4 suite and current developments.* Acta Crystallogr D Biol Crystallogr, 2011. **67**(Pt 4): p. 235-42.
12. Roy, A., A. Kucukural, and Y. Zhang, *I-TASSER: a unified platform for automated protein structure and function prediction.* Nat Protoc, 2010. **5**(4): p. 725-38.
13. Zhang, Y., *I-TASSER server for protein 3D structure prediction.* BMC Bioinformatics, 2008. **9**: p. 40.
14. Evans, P., *Scaling and assessment of data quality.* Acta Crystallogr D Biol Crystallogr, 2006. **62**(Pt 1): p. 72-82.
15. Diederichs, K. and P.A. Karplus, *Improved R-factors for diffraction data analysis in macromolecular crystallography.* Nat Struct Biol, 1997. **4**(4): p. 269-75.
16. Weiss, M.S., *Global indicators of X-ray data quality.* Journal of Applied Crystallography, 2001. **34**: p. 130-135.
17. Karplus, P.A. and K. Diederichs, *Linking crystallographic model and data quality.* Science, 2012. **336**(6084): p. 1030-3.
18. Evans, P., *Biochemistry. Resolving some old problems in protein crystallography.* Science, 2012. **336**(6084): p. 986-7.